Functional Dissection of Transport Processes during Glycopeptide Antibiotic Production

Dissertation

der Mathematisch-Naturwissenschaftlichen Fakultät
der Eberhard Karls Universität Tübingen
zur Erlangung des Grades eines
Doktors der Naturwissenschaften
(Dr. rer. nat.)

vorgelegt von
Nicola Gericke
aus Celle

Leonberg
2025

Gedruckt mit Genehmigung der Mathematisch-Naturwissenschaftlichen Fakultät der Eberhard Karls Universität Tübingen.

Tag der mündlichen Qualifikation:	10.07.2025
Dekan:	Prof. Dr. Thilo Stehle
1. Berichterstatter/-in:	Prof. Samuel Wagner, PhD
2. Berichterstatter/-in:	Prof. Dr. Harald Groß

Table of Contents

Abbreviations

AA	amino acid
A. balhimycina	*Amycolatopsis balhimycina*
ABC	ATP-binding cassette
Act	actinorhodin
A. japonicum	*Amycolatopsis japonicum (japonica)*
A. keratiniphila	*Amycolatopsis keratiniphila*
AMR	antimicrobial resistance
Apr	apramycin
ATP	adenosine triphosphate
Å	Ångström
BGC	biosynthetic gene cluster
BN	blue native
B. subtilis	*Bacillus subtilis*
βHt	β-hydroxytyrosine
Cam	chloramphenicol
Cb	carbenicillin
CH	coupling helix
CL	cardiolipin
CM	crude membranes
CSR	cluster-situated regulator
°C	degree Celsius
Da	dalton
D-Ala-D-Ala	D-alanyl-D-alanine
D-Ala-D-Lac	D-alanyl-D-lactate
ddH_2O	double-distilled water
ΔG	gibbs free energy change
DNA	deoxyribonucleic acid
Dpg	3,5-dihydroxyphenylglycine
E	elution
EB	elution buffer
E. coli	*Escherichia coli*
EDDS	[S,S]-ethylenediamine-disuccinc acid
EDTA	ethylenediaminetetraacetic acid
eGFP	enhanced green fluorescent protein
EH	elbow helix
Ery	erythromycin
FMM	functional membrane microdomains
FT	flow-through
et al.	*et alia*
GlcNAc	N-acetylglucosamine
GPA	glycopeptide antibiotic

GRP	GPA related peptides
Hpg	hydroxyphenylglycine
HPLC	high-performance liquid chromatography
I	input
IF	inward-facing
IM	inner membrane
IMAC	immobilized metal affinity chromatography
IPTG	isopropyl β-d-1-thiogalactopyranoside
Kan	kanamycin
L. lactis	*Lactococcus lactis*
LB	lysogeny broth
LFQ	label-free quantification
LTA	lipoteichoic acids
mAU	milli arbitrary unit
MDR	multidrug resistance
MFS	major facilitator superfamily
MM	molecular mass
MRSA	methicillin-resistant *Staphylococcus aureus*
MS	mass spectrometry
MurNAc	N-acetylmuramic acid
Nal	nalidixic acid
NBD	nucleotide binding domain
NRPS	non-ribosomal peptide synthetases
NS	non-solubilized
OD_{600}	optical density at 600 nm
ODU	optical density units
OF	outward-facing
OM	outer membrane
ORF	open reading frame
PAGE	polyacrylamide gel electrophoresis
PBP	penicillin binding protein
PCR	polymerase chain reaction
PE	phosphatidylethanolamine
PI	phosphatidylinositol
PKS	polyketide synthase
PVDF	polyvinylidene difluoride
Red	undecylprodigiosin
RFU	relative fluorescence units
Rha	L-rhamnose
RNA	ribonucleic acid
rpm	revolutions per minute
S	solubilized
SARP	Streptomyces antibiotic regulatory protein

S. aureus	*Staphylococcus aureus*
SBD	substrate binding domain
SDS	sodium dodecyl sulphate
SEC	size exclusion chromatography
SEC-MALS	SEC with multi-angle light scattering
Sec	secretase translocon
S. lividans	*Streptomyces lividans*
SMA	polystyrene-co-maleic acid
SMALP	SMA lipid particles
S. peucetius	*Streptomyces peucetius*
SPFH	Stomatin, Prohibitin, Flotillin, HflK/C protein family
Spp.	several species
SRP	signal recognition particle
T7Lys	T7 lysozyme
T7RNAP	T7 RNA polymerase
TB	terrific broth
TEV	*Tobacco Etch Virus*
TMD	transmembrane domain
TMS	transmembrane segment
Tsr	thiostrepton
UDP	undecaprenyl pyrophosphate
UV	ultraviolet
UZ	ultracentrifugation
v/v	volume/volume
W	wash
WC	whole cells
WT	wild-type
WTA	wall teichoic acids
w/v	weight/volume
w/w	weight/weight

The one letter code of AA was used in this thesis.

Zusammenfassung

Glykopeptid Antibiotika (GPA) - wie Vancomycin oder Teicoplanin- sind Naturstoffe, die zur Bekämpfung bakterieller Infektionen durch Hemmung der Zellwandbiosynthese eingesetzt werden. Viele Mitglieder der Gattungen *Amycolatopsis* und *Streptomyces* innerhalb des Stammes der Actinomycetota produzieren GPAs als Teil ihres Sekundärstoffwechsels. GPAs bestehen in der Regel aus einem Heptapeptidgrundgerüst mit einer Vielzahl unterschiedlicher Modifikationen, einschließlich Glykosylierung, Halogenierung oder Acylierung, die ihre biologische Aktivität modulieren. Das Grundgerüst besteht aus verschiedenen proteinogenen und nicht-proteinogenen Aminosäuren, deren Zusammensetzung die Grundlage für die allgemeine Einteilung der GPAs in fünf Untergruppen bildet. Die Biosynthese erfolgt durch nicht-ribosomale Peptidsynthetasen (NRPS) und modifizierende Enzyme. Diese sind in einem biosynthetischen Gencluster (BGC) kodiert, zusammen mit Enzymen, welche die Bereitstellung von Vorläufermolekülen, Resistenz und Export vermitteln. Obwohl die Biosynthese einiger BGCs gut untersucht ist, ist noch wenig über ihren Export bekannt.

Ich habe mehrere GPA Transporter charakterisiert und durch bioinformatische Analyse und Strukturvorhersage als Typ IV ABC Transporter identifiziert. Trotz der starken Ähnlichkeit in Sequenz und Struktur zeigte die phylogenetische Analyse, dass die GPA Transporter Unterschiede aufweisen, welche auch durch die Vielfalt ihrer vorhergesagten Substrate widerspiegelt wird. Dies wurde durch ein *in vivo* Export Assay bestätigt, welches zeigte, dass Tba, der Transporter des Typ I GPA Balhimycin, Tri, der mutmaßlichen Transporter des Typ III GPA Ristomycin, und Tva, der mutmaßliche Transporter des Typ I GPA Vancomycin eine selektive Spezifität für ihre jeweiligen Substrate aufweisen, die auf der Zusammensetzung des Grundgerüsts und nicht auf Modifikationen beruht. Darüber hinaus zeigte die Analyse der lokalen zellulären Umgebung von Tba in *Amycolatopsis balhimycina*, dass sich viele biosynthetische Enzyme in unmittelbarer Nähe des Transporters befinden und möglicherweise ein Mikrokompartiment bilden. Die Co-Immunpräzipitation von biosynthetischen Enzymen mit dem Transporter Tba unterstützt diese Hypothese und deutet darauf hin, dass es sogar spezifische Protein-Protein-Wechselwirkungen gibt. Es ist denkbar, dass diese Wechselwirkungen für die transportabhängige Biosynthese von Balhimycin entscheidend sind. Um die Bindungs- und Transportkinetik von Tba und Tri *in vitro* zu charakterisieren, habe ich auch ihre Expression und Reinigung in *E. coli* optimiert. Aufgrund von Herausforderungen, z.B. bei der Erzielung hoher Expressionslevels, falscher Membraninsertion, Proteolyse und ineffizienter Detergenzextraktion, wurde jedoch der Expressionswirt gewechselt. Es zeigte sich, dass der natürliche Wirt von Tba, *Amycolatopsis balhimycina*, oder ein eng verwandter Organismus, *Streptomyces lividans*, für die Expression der GPA Transporter Tba und Tri besser geeignet waren als der üblicherweise verwendete Wirt *Escherichia coli*.

Zusammenfassend erweitern diese Ergebnisse das begrenzte Wissen über den GPA Export und zeigen, dass GPA Transporter funktionell in den Biosyntheseprozess ihrer Substrate integriert sind. Diese Arbeit bildet die Grundlage für weitere Studien an GPA Transportern, die unser Wissen über die Substratspezifität von Transportproteinen erheblich erweitern können. Darüber hinaus könnte eine detaillierte Analyse der Wechselwirkungen zwischen Tba und den biosynthetischen Enzymen Aufschluss über die Rolle von membranassoziierten bakteriellen

Mikrokompartimenten geben. Ein besseres Verständnis des Transportprozesses wird auch dazu beitragen, die mikrobielle Produktion von GPAs in industriellen Umgebungen zu optimieren, um den Export von medizinisch relevanten GPAs zu erhöhen.

Summary

Glycopeptide antibiotics (GPAs) - such as vancomycin or teicoplanin - are valuable natural products that have been used to fight bacterial infections by inhibiting cell wall biosynthesis. Numerous members of the genera *Amycolatopsis* and *Streptomyces* within the phylum of Actinomycetota produce GPAs as part of their secondary metabolism. GPAs usually consist of a heptapeptide backbone decorated with a variety of different modifications, including glycosylation, halogenation, or acylation, which modulate their biological activity. The backbone consists of various proteinogenic and non-proteinogenic amino acids, the composition of which provides the basis for the general classification of GPAs into five subgroups. Biosynthesis is carried out by non-ribosomal peptide synthetases (NRPS) and modifying enzymes. These are encoded in a biosynthetic gene cluster (BGC) together with enzymes that mediate the supply of precursor building blocks, resistance, and export. Although the biosynthesis of some GPAs has been well studied, the nature of their export is still poorly understood.

Here, I characterized several GPA transporters and identified them as type IV ABC transporters using bioinformatic analysis and structure prediction. Despite high similarity in sequence and structure, phylogenetic analysis suggested that GPA transporters do exhibit differences, reflecting the diversity of their predicted substrates. This was confirmed using an *in vivo* export assay, which showed that Tba, the transporter of the type I GPA balhimycin, Tri, the putative transporter of the type III GPA ristomycin, and Tva, the putative transporter of the type I GPA vancomycin, exhibit selective specificity for their cognate substrates based on backbone composition rather than modifications. Moreover, analysis of the local cellular environment of Tba in *Amycolatopsis balhimycina* showed that many biosynthetic enzymes are in close proximity to the transporter and potentially form a microcompartment. Co-immunoprecipitation of biosynthetic enzymes with the transporter Tba supports this hypothesis and indicates that there are even specific protein-protein interactions. It is conceivable that these interactions are crucial for the transport-dependent biosynthesis of balhimycin. To characterize the binding and transport kinetics of Tba and Tri *in vitro,* I also optimized their expression and purification in *E. coli.* Due to challenges, e.g., in achieving high expression levels, incorrect membrane insertion, proteolysis, and inefficient detergent extraction, the expression host was changed. It became apparent that the native host of Tba, *Amycolatopsis balhimycina*, or a closely related organism, *Streptomyces lividans*, was more suitable for the expression of the GPA transporters Tba and Tri than the commonly used host *Escherichia coli*.

In conclusion, these findings add to the limited knowledge of GPA export and demonstrate that GPA transporters are functionally integrated into the biosynthetic process of their cognate substrates. This work provides the basis for further single-protein studies of GPA ABC transporters, which can significantly broaden our knowledge of the substrate specificity of transport proteins. In addition, a detailed analysis of the interactions between Tba and the biosynthetic enzymes could shed light on the role of membrane-associated bacterial microcompartments. A better understanding of the transport process will furthermore help to

optimize the microbial production of GPAs in an industrial setting to increase the export of medically relevant GPAs.

1 Introduction

Nearly one century after Alexander Fleming's serendipitous discovery of penicillin revolutionized medicine [1], the rise of antimicrobial resistance (AMR) has emerged as a major global health crisis. In 2019, an estimated 4.95 million deaths worldwide were related with AMR, with 929,000 deaths directly attributed to infections caused by the six leading pathogens: *Escherichia coli*, *Staphylococcus aureus*, *Klebsiella pneumoniae*, *Streptococcus pneumoniae*, *Acinetobacter baumannii*, and *Pseudomonas aeruginosa* [2]. In the past, infections caused by these and other pathogens were easily treatable. However, the overuse and misuse of antibiotics, alongside environmental contaminants, have accelerated both the natural evolution of resistance mechanisms and the transfer of resistance genes to previously susceptible organisms [3]. The increasing prevalence of AMR is now challenging healthcare systems worldwide on an unprecedented scale.

1.1 The bacterial cell wall: a common antibiotic target

Antibiotics typically target essential bacterial structures or interfere with biosynthetic pathways that are critical for cell survival and proliferation. Common targets include peptidoglycan biosynthesis (cell wall), cell membrane(s), protein biosynthesis (translation), DNA replication, RNA synthesis (transcription), and folate biosynthesis [4]. However, to reach their cytoplasmic targets, antibiotics have to cross the cell envelope, the outermost barrier of bacterial cells. This makes the cell envelope itself a particularly attractive target for antibiotics, and many compounds have been discovered that disrupt either the cell wall biosynthesis or the integrity of bacterial membranes [5].

The cell envelope of most Gram-negative bacteria consists of an outer membrane (OM), a thin layer of peptidoglycan, and a cytoplasmic inner membrane (IM). Gram-positive bacteria lack the OM but possess a thick multilayer of peptidoglycan. Peptidoglycan is found exclusively in bacteria and is composed of long glycan strands formed by alternating β-1,4-linked N-acetylglucosamine (GlcNAc) and N-acetylmuramic acid (MurNAc) subunits. These strands are cross-linked by pentapeptides attached to the carboxyl group of muramic acid, providing a stable and rigid structure that maintains cell shape by counteracting the cytoplasmic turgor pressure [6,7]. Despite its rigidity, peptidoglycan is porous enough to allow the diffusion of small molecules such as nutrients and metabolites [7,8]. The cell wall also serves as a scaffold for the attachment of proteins and polymers. In many Gram-positive bacteria, lipoteichoic acids (LTA) and wall teichoic acids (WTA) are characteristic components [9]. Extensive studies in *Staphylococcus aureus* (*S. aureus*) have revealed diverse functions for LTA and WTA. These include protection against environmental stressors and antimicrobial peptides [10,11], coordination of enzymatic activities like autolysins [12], which are crucial for cell wall turnover, and they also play a key role in binding and adhesion processes involved in biofilm formation or pathogenicity [13,14].

Cell wall biogenesis is a complex process that begins with the cytoplasmic synthesis of the individual glycan building blocks. Initially, a MurNAc-(pentapeptide)-GlcNAc molecule is synthesized and attached to undecaprenyl pyrophosphate (UDP) [15]. The resulting structure, known as lipid II, is subsequently flipped across the cytoplasmic membrane, where penicillin binding proteins (PBPs) incorporate it into the growing cell wall through trans glycosylation and trans peptidation reactions [7]. PBPs are so named because they are the targets of penicillin and other β-lactam antibiotics [16]. Other antibiotics target different stages of cell wall biosynthesis. Glycopeptide antibiotics (GPAs), for example, bind directly to the terminal D-alanyl-D-alanine (D-Ala-D-Ala) residues of the pentapeptide, blocking trans peptidation and trans glycosylation [17]. GPAs are discussed in more detail in a later chapter. Bacitracin, a cyclic dodecyl peptide antibiotic, forms complexes with UDP and inhibits lipid II synthesis [18], while fosfomycin, which can cross the cell membrane by using host transporters, disrupts an early enzymatic step in UDP-MurNAc biosynthesis [19].

In fact, the complexity of the steps in cell wall biosynthesis is mirrored by the multitude of antibiotics produced by bacteria and fungi, reflecting the evolutionary ingenuity of nature in developing inhibitors of these essential processes. Besides being a target, the bacterial cell envelope is also a hurdle to cross for antibiotics, since these usually have to be exported by antibiotic producer cells and in some cases reimported into the target cell. This necessity makes interactions of antibiotics with the cell wall, membranes, and transport proteins indispensable.

1.2 Biological membranes and membrane proteins

The fundamental structure of biological membranes consists of amphipathic lipid molecules with a hydrophilic head and hydrophobic tail. In aqueous environments, these lipids naturally assemble into a ~30 Å bilayer structure, with the hydrophobic tails facing inward and hydrophilic heads facing outward, creating an interface with the surrounding aqueous phase [20,21]. This bilayer forms the essential outer boundary of all unicellular organisms, cells, and cellular compartments and is impermeable to large hydrophilic molecules and ions [22,23]. The primary lipid types include glycerophospholipids, sphingolipids, and sterols [24]. However, the exact chemical composition varies depending on the organism, the specific function of the membrane, and environmental conditions [25,26]. A useful analogy is to think of membranes as rivers, each with unique characteristics, like depth, speed, and obstacles. The "water" of the membrane - the lipid bilayer - does not flow uniformly, some areas move swiftly, while others are more static, shaped by surrounding molecular interactions. Similarly, different lipid species influence the fluidity and physicochemical properties of the membrane [27].

For many years, the dominant view on membrane dynamics was that described by Singer and Nicolson in their fluid mosaic model, which regarded membranes as two-dimensional structures with random lateral diffusion of all components and minimal organization [28]. However, this model was challenged by the discovery of lipid microdomains, rich in cholesterol and sphingolipids, which form functional membrane subunits essential for certain trafficking

and signal transduction processes within eukaryotic cells [29]. These so-called lipid rafts are accompanied by membrane-bound scaffolding proteins, known as Flotillins [30]. Flotillins are evolutionarily well-conserved members of the Stomatin, Prohibitin, Flotillin, HflK/C (SPFH) protein family, which serve as marker proteins for lipid rafts and are thought to be involved in recruiting and organizing the proteins within these functional subunits [31,32]. Despite the absence of cholesterol in most bacterial membranes, similar domains known as functional membrane microdomains (FMMs) have been identified, along with flotillin homologs [33].
Membranes play a critical role in mediating interactions with the external environment, a function primarily facilitated by membrane proteins. Additionally, glycation of both proteins and lipids contributes to interaction and signaling pathways [34]. Membrane proteins confer selective permeability to biological membranes by transporting large molecules and ions across the lipid bilayer, thereby maintaining electrochemical gradients essential for fundamental cellular functions, including energy metabolism [35].

1.2.1 **Insertion and folding of membrane proteins in bacteria**

Integral membrane proteins are classified into two structural types: α-helix bundles and β-barrels [36]. α-helix bundles consist of one or more α-helices containing mainly hydrophobic residues. They can be long membrane-spanning helices (~20 amino acids) or short, kinked helices bent at various angles [37]. In contrast, β-barrel proteins are composed of several antiparallel β-sheets with alternating hydrophobic and polar residues that fold into a barrel-like structure [38]. These β-barrel proteins are exclusively found in the OM of Gram-negative bacteria, chloroplasts, and mitochondria and account for about 2-3% of the open reading frames (ORF) in Gram-negative bacteria [38]. In comparison, about 20-30% of the ORFs in genomes of various organisms encode α-helical membrane proteins [39]. Since the membrane proteins discussed in this thesis have an α-helical structure, only these will be addressed in the following section and will simply be referred to as membrane proteins.

Many studies on membrane protein biogenesis have been conducted in *Escherichia coli* (*E. coli)*, and therefore the following description focuses on this model organism. However, the proteins and mechanisms involved show a high degree of conservation in many other prokaryotes and are likely to be generalizable to some extent. The majority of membrane proteins are targeted and inserted into the cytoplasmic membrane co-translationally [40]. This process typically involves the signal recognition particle (SRP), which binds to hydrophobic stretches at the N-terminus of nascent polypeptide chains as they emerge from the ribosome exit tunnel [40] and directs the complex to the membrane, where this is recognized by the SRP receptor FtsY [41]. Here, the hydrophobic domains of the polypeptide chain are inserted into the membrane by the secretase (Sec) translocon [42]. The Sec translocon is a heterotrimeric protein complex [43] composed of SecY, SecE, and SecG subunits [44–46]. It facilitates either the translocation of hydrophilic polypeptides across the membrane or the integration of polypeptides with long hydrophobic regions into the lipid bilayer through a lateral exit gate [43,47]. Another insertion pathway involves the insertase YidC, a member of the Oxa1/Alb3/YidC family of membrane insertases [48]. YidC can insert membrane proteins independently [49] or assist as a chaperone in the insertion and folding of membrane proteins by the Sec translocon. For

instance, YidC facilitates the proper folding by stabilizing essential helix-helix interactions of the lactose permease LacY after the Sec-dependent insertion in the *E. coli* membrane [50,51]. Some membrane proteins are also targeted post-translationally to the cytoplasmic membrane, which usually requires the assistance of chaperones to prevent aggregation [52,53]. These chaperones can also be involved in the folding and assembly of membrane proteins into their tertiary and quaternary structures within the lipid bilayer. The folding of cytosolic proteins is primarily driven by the hydrophobic effect [54], which is less relevant in the anisotropic environment of membrane proteins. Instead, folding of the latter is guided by helix-helix or helix-lipid interactions, which are stabilized by van der Waals forces, ionic interactions, or hydrogen bonds [34].

1.2.2 Challenges and strategies for membrane protein overexpression in bacteria

Recombinant overexpression and protein production are among the most important tools for obtaining proteins to study their structure and function. Since many membrane proteins are present in low abundance in their native environment, overexpression is often required to achieve sufficient protein yields for subsequent analyses, such as *in vitro* assays or structure determination [55]. Various overexpression systems are available, including prokaryotic systems, like *E. coli* or *Lactococcus lactis* (*L. lactis*) [56], eukaryotic systems such as *Saccaromyces cerevisiae* [57] or baculovirus infected insect cells [58], and cell free systems [59]. The choice of the expression system is dependent on the characteristics of the protein being studied. *E. coli* is a particularly popular and well-studied host for recombinant protein production due to its fast and inexpensive growth to high cell densities [60,61], easy genetic manipulation strategies, and the availability of a wide variety of expression vectors [62,63]. The most common strategies and major challenges in the expression and purification of (membrane) proteins using *E. coli* are outlined below.

E. coli BL21(DE3) and its derivatives are commonly used for overexpression of recombinant genes. These strains lack the Lon protease and the membrane protease OmpT, which reduces protein degradation, and express the T7 RNA polymerase (T7RNAP) from the λ-lysogen DE3 under the control of a *lacUV5* promoter [64]. Thus, this system allows isopropyl-ß-D-1-thiogalactopyranoside (IPTG)-inducible expression of the T7RNAP, resulting in high transcription rates of target genes regulated by the T7*lac* promoter [64]. Although strong overexpression can lead to high protein yields, it significantly impacts the metabolism of the producing cell and often causes toxic effects [65]. This so-called metabolic burden manifests as altered growth rates, reduced protein stability of both native and recombinant proteins, genetic instability, and abnormal cell size [65].The burden is largely driven by the drain of specific amino acids and charged tRNAs during recombinant protein synthesis, particularly when genes from foreign organisms with a different codon usage than the *E. coli* host are expressed [65,66]. These effects ultimately lead to protein misfolding and trigger various stress responses, including the stringent response [67,68] and the heat shock (σ^{32}-induced) response [68,69].

However, the recombinant overexpression of membrane protein-encoding genes adds an additional layer of complexity to the metabolic burden. Despite a ≈10-20% higher abundance of SecY, SecE, and SecG during membrane protein overexpression, the Sec translocon, which facilitates the insertion of most integral membrane proteins in *E. coli*, easily reaches its

capacity and becomes saturated [70]. This saturation impairs not only the insertion of recombinant but also native membrane proteins, leading to extensive protein aggregation within the cell [70]. The limited capacity of the Sec translocon is therefore considered to be the major bottleneck during membrane protein overexpression that restricts efficient recombinant protein production and high yields. Other bottlenecks that contribute to the metabolic burden and limit high yields of recombinant proteins include the limited availability of *E. coli*-specific chaperones such as DnaK, proteolytic degradation (e.g., by the membrane protein-specific protease FtsH), an altered energy metabolism due to changes in membrane organization, and the absence of endogenous biogenesis factors, such as specific chaperones that are not present in *E. coli* [65,70].

Over the past decades, various strategies have been developed to optimize the expression and production of membrane proteins in *E. coli* and overcome the major bottlenecks. These include the elimination of codon bias by codon optimization of the host strain or heterologous genes, modifying the target protein by the addition of signal sequences, N- or C-terminal fusion proteins (e.g., GFP, MBP, SUMO), and short tags (e.g., StrepII, 6xHis), as well as optimizing the host strain [56,71]. It has been shown that host strain optimization, specifically slowing down the translation rate of the T7RNAP, increases the quality of the recombinant membrane proteins significantly and leads to higher protein yields [72–74]. Popular examples include the so-called Walker strains, *E. coli* C41(DE3) and C43(DE3), which carry a mutation in the *lacUV5* promoter, reducing T7RNAP levels [73]. Another example is *E. coli* Mutant56(DE3), which has a mutation in T7RNAP that weakens its binding to the T7*lac* promoter [74]. Additionally, *E. coli* Lemo21(DE3) encodes the T7 lysozyme (T7Lys), the natural inhibitor of the T7RNAP, under the control of a rhamnose-inducible promoter, thereby allowing rhamnose-dependent fine-tuning of T7RNAP levels [72].
In addition to the challenges of overexpression and production, the purification of recombinant membrane proteins presents significant difficulties. Unlike most cytosolic proteins, membrane proteins are usually insoluble in aqueous solutions and often exhibit instability due to their amphiphilic nature [75]. Detergents are commonly used to extract and stabilize them from their native membrane. However, the efficiency of this process is hard to predict and typically requires empirical optimization [75]. Alternatively, membrane proteins can be extracted without detergents using SMA copolymers (polystyrene-co-maleic acid), which penetrate the membrane, isolate small membrane fragments, and form so-called SMA lipid particles (SMALPs) [76]. While this method offers a more native-like environment by co-extracting also adjacent lipids, the functional integrity of the extracted proteins is not always guaranteed and must be evaluated in every case.

1.3 ABC transporters

Adenosine 5'-triphosphate (ATP)-binding cassette (ABC) transporters represent a group of integral membrane proteins that form one of the largest protein super families present across all domains of life. They mediate the ATP-driven translocation of chemically diverse substrates, e.g., polysaccharides, amino acids, lipids, toxins, and antibiotics across biological

membranes [77–80]. Due to their broad substrate range, ABC transporters play a crucial role in numerous biological processes. Dysfunctions of ABC transporters have been implicated in various human diseases, such as cystic fibrosis [81] or macular degeneration [82]. A notable function is the export of toxic substances and antibiotics by multidrug resistance (MDR) transporters, e.g., in bacteria [83,84] or in human cancer cells [85–87], which is a major cause of chemotherapy resistance.

1.3.1 **Structure of ABC transporters**

ABC transporters share a common architecture with two cytoplasmic nucleotide-binding domains (NBD) and two transmembrane domains (TMD), which together form two half transporters with a substrate translocation pathway along their mirror axis [77,78]. The organization of these domains can vary: bacterial and archaeal systems typically consist of single domains or dimers, whereas eukaryotic transporters are often composed of a single polypeptide chain [77,80]. However, exceptions do exist.

The NBDs belong to the highly conserved P-loop nucleotide-binding protein family and dimerize in a "head-to-tail" arrangement, bringing together all essential motifs for ATP hydrolysis at the dimer interface and thereby forming two ATP-binding sites [88–90]. TMDs exhibit greater structural variability and are believed to have evolved independently from NBDs. The prevailing hypothesis suggests that ancient motor domains fused with various transmembrane-spanning systems, resulting in a variety of different proteins. Recently, a new universal nomenclature for the ABC transporter superfamily was proposed. This classification organizes transporters into seven subgroups based on structural data, membrane topology, and the phylogenetic relationships of their TMD, rather than focusing on their physiological function, transport direction, or origin [91]. Transporters with type I-III folds are exclusively importers, while those with type IV-VII folds primarily function as exporters. However, other roles, such as regulation, extraction, or mechanotransmission, have also been discovered [91].

One of the first full protein crystal structures (3.0 Å) of an ABC transporter was that of the type IV transporter Sav1866 from *S. aureus*, which exports several anticancer drugs, including doxorubicin and vinblastine [83]. It is a homodimer consisting of a 6+6 transmembrane helix (TMH) organization featuring a domain swap from TMH4 and TMH5 to the opposite half transporter [83] and a short N-terminal “elbow helix” (EH) at the cytosolic membrane interface that may contribute to stabilizing the transporter [80] (Fig. 1). Two intracellular coupling helices (CHs), located between TMH2/3 and TMH4/5 within a distinct groove of the NBD, ensure interdomain communication between the NBD and TMD and are essential for mechanochemical coupling [83,92] (Fig. 1). The presence of at least one CH is a common feature of all ABC transporters.

The structural characteristics of type IV ABC transporters differ from those of the other subgroups, particularly in their membrane topology. Furthermore, some ABC transporters possess accessory domains that are not universally present within the protein family. These include extracellular or periplasmic substrate binding domains (SBDs), which are commonly found in bacterial importers (types I and II) and essential for high-affinity uptake of nutrients. An example is BtuCDF, which mediates the uptake of vitamin B_{12} in *E. coli* [93]. In some eukaryotic ABC transporters, a non-conserved additional transmembrane domain (TMD0) has

been found, located N-terminally and connected to the TMD by a short peptide called the lasso peptide (L_0). Its function is not fully understood, but it is believed to play a regulatory role in subcellular localization or interaction with other proteins [94,95]. There are numerous examples of additional domains or extensions in ABC transporters that perform tasks other than transport. One of the most intriguing examples is represented by SUR1 and SUR2, which no longer have a transport function but are solely responsible for modulating the ATP-sensitive potassium channel $K_{IR}6.x$ [96].

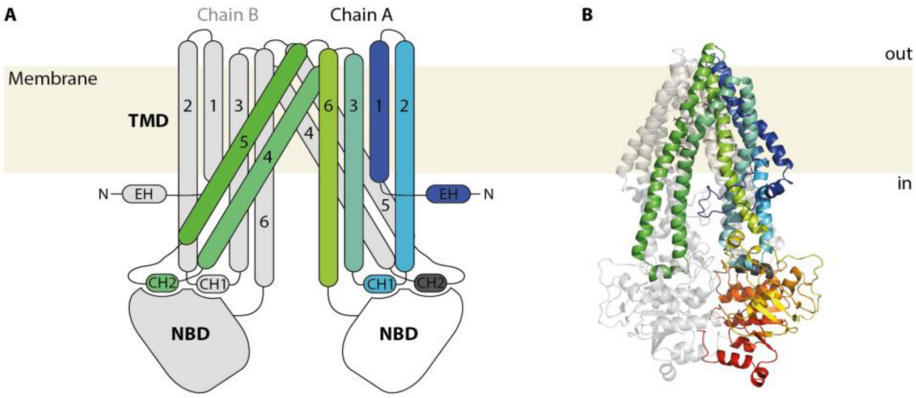

Figure 1 | Type IV ABC transporters.
(A) Schematic topology of a type IV ABC transporter homodimer. The structural elements of the TMD of chain A are displayed in colors, while those of chain B are displayed in gray. (**B**) Representative ribbon structure of the type IV ABC transporter Tba (homodimer). TMH of chain A are colored as in A. The NBD of chain A is colored in orange, yellow, and red. (Adapted from publication 1 [97]) **Abbreviations:** TMD: transmembrane domain; TMH: transmembrane helix; NBD: nucleotide binding domain; EH: elbow helix; CH: coupling helix.

1.3.2 Transport mechanism and substrate selectivity of ABC transporters

The transport mechanism of ABC transporters can be outlined in five main events: ATP-Mg^{2+} binding, ATP hydrolysis, ADP/P_i release, substrate binding, and substrate translocation [79,80]. However, a unified mechanism for the entire transport cycle has only been described for reactions occurring at the NBD. These reactions are driven by seven highly conserved motifs characteristic of the P-loop ATPase family [79,80]. ATP coordination occurs at the Walker A motif (P-loop), which binds the β and γ phosphate and coordinates Mg^{2+}, and at the A-loop, which interacts with the adenine ring through an aromatic residue [88,98]. The head-to-tail orientation of the NBDs enables the ABC signature motif (C-loop) from the opposite NBD to contribute to ATP binding. This interaction drives ATP-induced dimerization, resulting in a closed, sandwich-like dimer conformation of the NBDs that creates two possible ATP binding sites [99]. The Walker B motif is involved in Mg^{2+} coordination and is responsible for polarizing the attacking water molecule during hydrolysis by providing the catalytic base [88,100]. Here, the catalytic glutamate (E) is essential for ATP hydrolysis, and mutation to glutamine (Q) results in a catalytically inactive transporter [100]. The histidine (H) of the H-switch stabilizes transition states during hydrolysis [101], while the Q-loop is a Mg^{2+} ligand and is in contact with the coupling helix and therefore essential for the interaction with the TMD [101,102]. The D-loop plays a role in positioning

the attacking water molecule, interdomain communication, and transport direction [99,103,104]. ATP-binding-induced dimerization is considered to be the key step in the catalytic cycle of any ABC transporter, providing the power stroke for substrate translocation, while subsequent ATP hydrolysis and ADP/P_i release cause the NBDs to separate and reset the transporter to its initial state [105].

Although ATP binding and hydrolysis are highly conserved across ABC transporters, the precise coupling of these processes to the major conformational changes in the TMD and substrate translocation is still not fully understood for all transporters, and no universally applicable model has been formulated so far. Based on distinct structural conformations resolved in recent years, the 'alternating access' model has emerged as the most prominent one [83,106,107]. This model proposes that access to the substrate-translocation cavity is gated and available from only one side of the membrane at a time, resulting in two main conformations: inward-facing (IF) and outward-facing (OF), between which the transporter alternates through several possible intermediate states. The mechanochemical coupling was recently demonstrated quantitatively for the MDR transporter TmrAB (type IV) from *Thermus thermophilus*, where a single power stroke generated by the binding of one ATP molecule is sufficient to drive the IF-to-OF transition and substrate translocation [105,108]. A different model, the 'outward-only' model, has been proposed for the lipid-bound oligosaccharide flippase PglK from *Campylobacter jejuni*, in which substrates enter the outward-facing cavity directly from the inner leaflet of the membrane [109]. These examples highlight the absence of a universally applicable transport mechanism for all ABC transporters. Instead, the mechanism is influenced by the chemical nature of the specific substrate, which varies in size, charge, and hydrophobicity. Several examples demonstrate that ABC transporters specifically adapted to their substrates. For example, structural analysis of the amino acid ABC transporter Art$(QN)_2$ from *Thermoanaerobacter tengcongensis* revealed that it forms a negatively charged substrate tunnel that selectively binds the positively charged amino acids histidine, arginine, and lysine [110]. Homologous transporters appear to employ a similar substrate selection mechanism [110]. Another example is provided by the *E. coli* ABC transporter McjD, which exclusively binds the lassopeptide MccJ25 through van der Waals interactions and hydrogen bonds, while failing to recognize structurally identical lassopeptides with a different amino acid composition [111]. Interestingly, some MDR transporters exhibit a remarkable polyspecificity towards different substrates, challenging the notion of specific adaptation seen in their substrate-specific relatives. For example, the mammaliam MDR transporter P-gp exports hundreds of chemically different substrates[112,113]. Hydrophobic substrates can enter the inner substrate binding pocket of the transporter via the inner leaflet of the cytoplasmic membrane, while others enter from the cytoplasmic side [112,113]. The polyspecificity of P-gp is mainly attributed to a large substrate-binding pocket containing multiple binding sites, which exhibit a positive cooperative binding effect [112,114]. In many cases, however, the lack of structural data with bound ligands hinders the precise elucidation of the substrate specificity of ABC transporters.

1.4 Actinomycetota: a reservoir of natural product producers

Actinomycetota (Actinobacteria) is a diverse phylum within the bacterial domain consisting of Gram-positive bacteria with guanine + cytosine (G+C) rich DNA (ø ~60 mol%) that colonize a multiplicity of environments and are particularly abundant in terrestrial and aquatic ecosystems [115,116]. In soil ecosystems they play a crucial role, for instance, by degrading complex organic molecules like chitin or cellulose, performing nitrogen fixation, or helping stabilize pH levels [117]. Some members of the phylum are pathogenic, causing severe diseases in humans and plants, such as *Mycobacterium tuberculosis* [118], *Corynebacterium diphtheriae* [119], and *Streptomyces scabies* [120]. Others are recognized as valuable producers of natural products, with significant medical and industrial potential [121].
Natural products are secondary metabolites that are typically not essential for vegetative growth but can enhance nutrient access and thus offer competitive advantages to their producing organisms or symbiotic partners [122]. These compounds include antibiotics, which are critically important in human medicine, especially considering the growing threat of antimicrobial resistance (AMR). Enzymes involved in the production of natural products are typically encoded in biosynthetic gene clusters (BGC). Comparative genomic analyses within the Actinomycetota phylum revealed an immense potential for BGCs related to natural products and antibiotics that have not yet been identified by traditional methods [123,124]. However, advances in next-generation sequencing and genome mining techniques promise to accelerate the identification and characterization of new natural products and BGCs [125].

1.4.1 The genus *Amycolatopsis*

The genus *Amycolatopsis* was formulated in 1986 [126], and its members typically exhibit non-motile filamentous growth, form various types of mycelium, and can sometimes sporulate [115]. Within the phylum Actinomycetota, the genus *Amycolatopsis*, along with other genera such as *Streptomyces* or *Actinoplanes*, is particularly notable for the production of diverse secondary metabolites, with *Streptomyces* alone accounting for approximately 70-80% of these compounds [127]. These metabolites have diverse structures and functions, and many have already found medical and industrial applications.
An example is the chelating agent [S,S]-ethylenediamine-disuccinc acid (EDDS), produced by *A. japonicum* MG417-CF17 [128] under zinc-deficient conditions [129]. Optimized strains have boosted EDDS production, offering a biodegradable alternative to ethylenediamine-tetraacetic acid (EDTA) in biotechnology [130]. Another example is the xylanase and cellulase producer *Amycolatopsis* sp. GDS, which has the potential to degrade difficult-to-process biomass wastes such as wheat straw [131]. There are numerous other examples; however, the most well-known natural products synthesized by *Amycolatopsis* species are antibiotics. Notable examples include rifamycin, a polyketide precursor of the antibiotic rifampicin produced by *A. mediterranei* [132], and vancomycin, a glycopeptide antibiotic (GPA) produced by *A. orientalis* [133]. Vancomycin is commonly used to treat patients with infections caused by Gram-positive pathogens, such as methicillin-resistant *S. aureus* (MRSA) [134]. It was the first GPA discovered [135], and since then, the identification of new *Amycolatopsis* species has often

coincided with the discovery and research of new GPAs. However, GPAs are not exclusively produced by *Amycolatopsis* strains.

A particularly well-studied example is *A. balhimycina*, the producer of the vancomycin-like GPA balhimycin [136]. It is a non-motile, terrestrial, aerobic bacterium first isolated from a soil sample in India. The bacterium forms substrate mycelium but lacks aerial mycelium and is unable to form spores [136]. The cell wall of *A. balhimycina* contains meso-diaminopimelic acid, along with the diagnostic sugars arabinose and galactose, while mycolic acids are absent [137]. Analysis of the lipid composition revealed that the most abundant phospholipids are phosphatidylethanolamine (PE), hydroxy-phosphatidylethanolamine, diphosphatidylglycerol (cardiolipin, CL), and phosphatidylinositol (PI), with iso-C16:0 being the major fatty acid component [137]. Whole genome sequencing of *A. balhimycina* revealed a circular genome of 10.56 Mb, with 8,585 predicted open reading frames (ORFs) and a high G+C content of 69.9% [138]. Depending on the growth medium, the cells appear light yellow to orange [137].

The GPA balhimycin is very similar to vancomycin, an important antibiotic of last resort in human medicine. Although balhimycin has shown bactericidal activity against various Gram-positive bacteria [136], it induces blood platelet apoptosis and is therefore not an ideal candidate for clinical use [139]. However, *A. balhimycina* has historically been more genetically accessible than other GPA producers and has therefore become a model organism for studying GPA biosynthesis.

1.4.2 **Glycopeptide antibiotics**

GPAs are heptapeptides composed of both proteinogenic and non-proteinogenic amino acids, with various modifications such as glycosylation, halogenation, or acylation [140]. The most prevalent non-proteinogenic amino acids are β-hydroxytyrosine (βHt), 4-hydroxyphenylglycine (Hpg), and 3,5-dihydroxyphenylglycine (Dpg). The oxidative cross-links between the aromatic side chains result in a multicyclic and cup-shaped structure of the GPA [141,142], which is important for its interaction with the molecular target, the cell wall precursor lipid II [17]. By binding to the terminal D-alanyl-D-alanine (D-Ala-D-Ala) of lipid II, GPAs block transpeptidation and trans glycosylation of the peptidoglycan layer and thereby prevent cell wall biosynthesis [17].

GPAs are classified into five subtypes based on their backbone composition (Fig. 2) [143]. Types I-IV, commonly referred to as true GPAs [144], differ mainly in their backbone composition [143]. The differences lie in the amino acid positions AA-1 and AA-3, where either aliphatic (type I) (Fig. 2A-B) or aromatic (type II-IV) (Fig. 2C-E) amino acids are incorporated. In type III (Fig. 2D) and IV (Fig. 2E), these aromatic residues are oxidatively cross-linked, forming an additional ring system. Type IV differs from type III in other unique modifications, such as in teicoplanin, where a fatty acid side chain is attached to the sugar modification. Type V GPAs (Fig. 2F), or glycopeptide-related peptides (GRPs), are more distantly related and exhibit significant variations in their backbone composition [145]. They contain 7 to 10 amino acids, and lack the characteristic glycosylation pattern seen in true GPAs. Additionally, some GRPs have been found to inhibit cell growth by binding to autolysins rather than targeting lipid II [144].

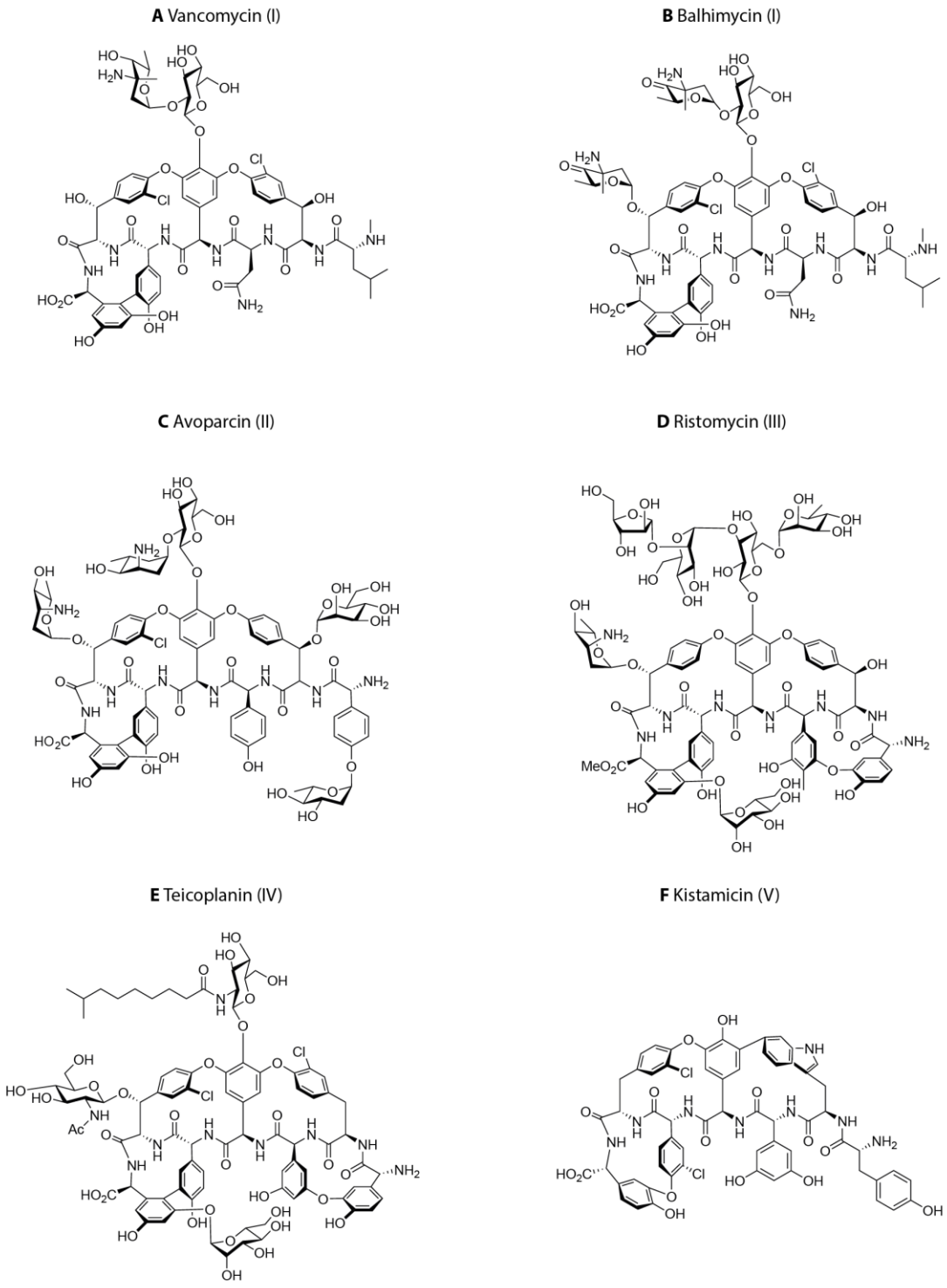

Figure 2 | Representative structures of GPA types I-V.
Structures of GPA types exemplified by (**A**) type I GPA vancomycin, (**B**) type I GPA balhimycin, (**C**) type II GPA avoparcin, (**D**) type III GPA ristomycin, (**E**) type IV GPA teicoplanin, and (**F**) type V GPA kistamicin.

1.4.3 **Biosynthesis of glycopeptide antibiotics**

The biosynthesis of glycopeptides occurs in three main steps: (1) the supply of precursors, including the non-proteinogenic amino acids, (2) the assembly of the peptide backbone by non-ribosomal peptide synthetases (NRPS), and (3) the modification of the heptapeptide (Fig. 3) [146]. This section focuses on the biosynthesis of the type-I GPA balhimycin in *A. balhimycina*. The majority of enzymes involved in the production of fully modified balhimycin are encoded within the corresponding BGC (Fig. 3A) [147,148].

The supply of non-proteinogenic amino acid precursors (Fig. 3A) is linked to the primary metabolism via the shikimate pathway [149], which is essential for aromatic amino acid biosynthesis, like tyrosine, phenylalanine, and tryptophan [150]. To enhance the production of GPA building blocks, *A. balhimycina* expresses two isoenzymes for key reactions in the shikimate pathway: the prephenate dehydrogenase (Pdh) and the 3-deoxy-D-arabino-heptulosonate-7-phosphate synthase (Dahp), which streamline the production towards the GPA precursors [149,151]. βHt is synthesized directly from tyrosine by the NRPS BpsD, the monooxygenase OxyD [152,153], and the prehydrolase Bhp [154]. The precursor of Hpg is hydroxyphenylpyruvate, which is the direct precursor of tyrosine. Hpg is synthesized by the hydroxymandelate synthase HmaS, the hydroxymandelate oxidase Hmo, and the p-hydroxyphenylglycine transaminase Pgat [155]. Dpg is synthesized from malonyl-CoA by the polyketide synthase (PKS) DpgABCD and Pgat, which is also involved in the synthesis of Hpg and uses tyrosine as an amino donor in both cases [155,156].

The amino acids are connected by a multi modular NRPS complex. In *A. balhimycina* the NRPS consists of three enzymes: BpsA, BpsB, and BpsC, which collectively encode seven modules in a 3-3-1 arrangement (Fig. 3B) [157]. Each module activates one amino acid and incorporates it into the growing peptide chain with the amino acid sequence of Leu-βHt-Asn-Hpg-Hpg-βHt-Dpg (Fig. 2B) [157]. The conserved NRPS domain structure includes an adenylation (A) domain for substrate recognition and activation, a thiolation (T) domain that binds intermediates as thioesters, and a condensation (C) domain responsible for peptide bond formation [158]. The thioesterase (TE) domain in the final module terminates synthesis. Some modules contain an epimerization (E) domain, which configures the correct stereochemistry of amino acids [158]. In *A. balhimycina* the E domain is present in modules 2, 4, and 5, and module 7 contains an X domain, which is believed to be a degenerated E or C domain [157]. In *Actinoplanes teichomyceticus*, the producer of the type-IV GPA teicoplanin, this domain recruits P450 monooxygenases for oxidative crosslinking of aromatic side chains [159]. *A. balhimycina* encodes three oxygenases: OxyA, OxyB, and OxyC which convert the linear balhimycin precursor peptide into a cyclized aglycone. The reactions follow a distinct order (B>A>C) while the peptide remains bound to the NRPS [141,160,161]. OxyB and OxyA form diaryl ether bonds (C-O-C) between AA4 and AA6, as well as AA2 and AA4, respectively, while OxyC catalyzes a C-C bond between AA5 and AA7 [141,160,161]. The cyclized aglycone is the first biologically active compound [147]. However, various tailoring enzymes further modify the heptapeptide (Fig. 3A) and enhance its activity by increasing its solubility and facilitating back-to-back dimer formation, which in turn may increase substrate affinity [162,163].

Balhimycin carries sugar modifications on AA4 and AA6. Similar to crosslinking reactions, glycosylation occurs in a defined order by regiospecific glycosyltransferases [142]. First, BgtfB attaches a glucose molecule to AA4 (Hpg), followed by BgtfA adding oxo-vancosamine to AA6 (βHt). Finally, BgtfC attaches another *oxo*-vancosamine to the glucose moiety on AA4, though this last step occurs with low efficiency. Vancosamine biosynthesis is catalyzed by DvaABCDE, while glucose is derived from the primary metabolism [148,164]. Chlorination of βHt residues at positions AA2 and AA6 is catalyzed by the halogenase BhaA while the peptide is still bound to the NRPS [165]. N-methylation of AA1 (Leu) is performed by the methyltransferase Bmt as one of the final steps in biosynthesis [160,166].

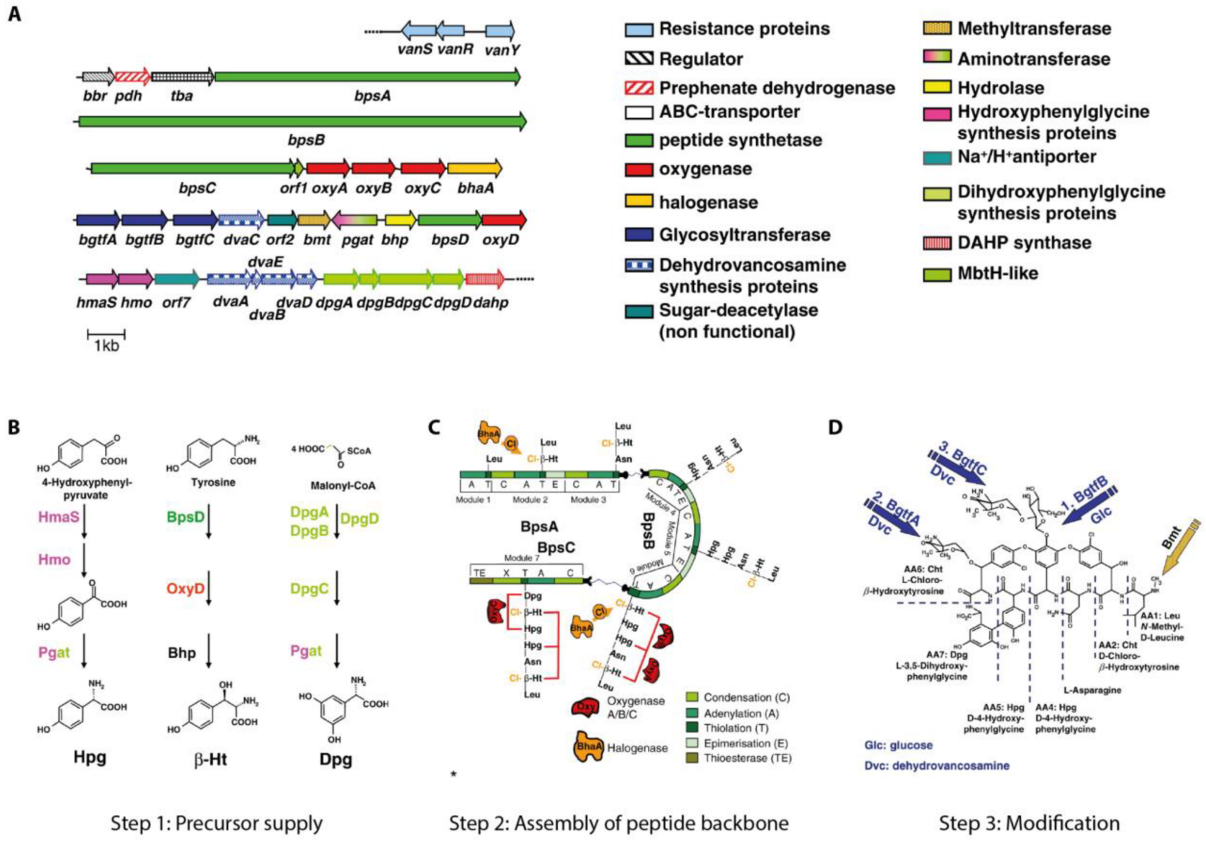

Figure 3 | Balhimycin biosynthetic gene cluster and biosynthesis steps.
(A) Balhimycin BGC with description of the gene functions. (**B**) Step 1: Synthesis of the relevant amino acid precursors Hpg, βHt, and Dpg. (**C**) Step 2: Biosynthesis of the heptapeptide backbone of balhimycin at the NRPS enzymes BpsA, BpsB, and BpsC. (**D**) Step 3: Modification reactions on the balhimycin precursor (Figure modified from Stegmann et al. [146]). **Abbreviations:** BGC: biosynthetic gene cluster; Leu: leucine; βHt: β-hydroxytyrosine; Asn: asparagine; Hpg: 4-hydroxyphenylglycine; Dpg: 3,5-dihydroxyphenylglycine; NRPS: non-ribosomal peptide synthetase.

1.4.4 **Export of glycopeptide antibiotics**

Typically, exporters encoded in the BGC of natural products are ABC transporters or major facilitator superfamily (MFS) transporters [167]. In addition to their primary transport function, these transporters may have bifunctional roles, such as detoxification in case of toxic compounds, or they play a critical role in the biosynthesis process, contributing to the maturation or final modification of their substrate [167]. The ABC transporter Tba, co-encoded within the balhimycin BGC, is crucial for the export of the final antibiotic [168]. In its absence, no extracellular balhimycin is detected, confirming its essential role in secretion. However, the lack of Tba does not affect the growth of *A. balhimycina*, indicating that Tba is not involved in the organism's self-resistance to its own glycopeptide antibiotic. In certain antibiotic-producing organisms, transporters provide the primary mechanism of self-resistance by exporting the compound, thereby reducing its intracellular concentration and preventing potential cellular damage [169].

1.4.5 **Regulation of GPA biosynthesis**

The production of secondary metabolites is crucial for the producing organism, as it provides a selective advantage in its natural habitat, but it is also energetically demanding. Strict regulatory mechanisms that respond to different stimuli are therefore essential to enable producers to rapidly adjust biosynthesis as required. The activation of the balhimycin BGC in *A. balhimycina* and subsequent antibiotic production depends on the cluster-situated regulator (CSR) Bbr, which specifically binds to five promotor sites within the BGC [170]. The promoter regions are located upstream of the *bbr* gene, the ABC transporter gene *tba*, the P450 monooxygenase gene *oxyA*, the *dvaA* gene, which encodes a protein that is involved in dehydrovancosamine synthesis, and *orf7*, which encodes a putative sodium-proton antiporter whose role in balhimycin biosynthesis remains unknown [170]. The genes located between the five promoter regions are thought to be co-transcribed as part of an operon [170]; however, the involvement of additional pathway-specific or global regulators is conceivable. The balhimycin BGC contains two additional regulatory genes encoding a two-component system (TCS), VanR and VanS, which are involved in the balhimycin resistance mechanism [148,171].
Other producers, such as *Nonomuraea* sp. ATCC39727, which synthesizes A40926 [172], and *Actinoplanes teichomyceticus* (*A. teichomyceticus*) [173], the producer of teicoplanin, encode a StrR-like regulator, similar to Bbr, a LuxR-like family regulator, and two proteins that form a TCS similar to VanRS [172–176]. Additionally, *A. teichomyceticus* encodes a Streptomyces antibiotic regulatory protein (SARP) [173,177]. The StrR-like regulators - Bbr (balhimycin), Dbv4 (A40926), and Tei15* (teicoplanin) - are direct positive regulators of their respective BGCs, whereas the LuxR-like regulators are thought to regulate the GPA production positively via indirect effects [172–176]. Interestingly, high phosphate levels inhibit *dbv4* transcription, preventing the biosynthesis of A40926 in *Nonomuraea* sp. ATCC39727 [178]. To my knowledge, this is the only experimentally validated external stimulus that regulates GPA biosynthesis. However, phosphate limitation is known to activate the biosynthesis of other antibiotics in members of the Actinomycetota phylum. For example, in *Streptomyces coelicolor (S. coelicolor)*, the two-component system (TCS) PhoRP acts as a master regulator, activating CSRs, which, in turn,

trigger the biosynthesis of actinorhodin (Act) and undecylprodigiosin (Red) [179–181]. Furthermore, the global nitrogen metabolism regulator GlnR is directly involved in regulating Act and Red biosynthesis, as well as avermectin and oligomycin biosynthesis in *Streptomyces avermitilis* [182,183]. This shows that nitrogen availability, in addition to phosphate, can influence the regulation of antibiotic BGCs in Actinomycetota. In *S. coelicolor*, Act biosynthetic intermediates have been shown to control the expression of the corresponding exporter genes through feedback regulation [184]. Another regulatory mechanism is glucose catabolite repression, e.g, in *Streptomyces lividans* (Act) [185], *Streptomyces venezuelae* (chloramphenicol) [186], or *Saccharopolyspora erythraea* (erythromycin) [187].
These examples demonstrate the diversity of regulatory mechanisms for antibiotic biosynthesis in Actinomycetota. However, in the context of GPA biosynthesis, only CSRs have been identified. However, it has not yet been shown that these were allosterically activated by the GPA itself. The only external stimulus identified was a low phosphate level for the biosynthesis of A40926 in *Nonomuraea sp. ATCC39727*. However, it is likely that the CSR of the balhimycin BGC, Bbr, is also activated by external stimuli, as GPA production has mainly been observed in R5 medium [e.g,168 and personal lab experience]. Other global regulators, or feedback regulatory mechanisms, may also be involved in the regulation of GPA biosynthesis but have not yet been characterized in detail.

1.4.6 **Self-resistance of *A. balhimycina***

Self-resistance in *A. balhimycina* is achieved by target modification, specifically the constitutive production of a modified lipid II molecule featuring a D-ala-D-lactate (D-ala-D-lac) terminus instead of the typical D-ala-D-ala [188]. This alteration significantly reduces the binding affinity of type-I GPAs to their target by approximately 1000-fold due to the loss of a critical hydrogen bond [189]. The enzymes responsible for the modification, VanH, VanA, and VanX, whose homologs also confer resistance to some target organisms, are encoded outside the balhimycin BGC [188]. In contrast, enzymes involved in the cell wall remodeling upon activation of the balhimycin BGC, namely VanRSY, are encoded within the BGC [171,188].

2 Research objective

The objective of this work was the systematic investigation of the ABC transporter Tba from *A. balhimycina*, the natural producer of the type I GPA balhimycin, along with homologous transporters from other GPA-producing organisms. The primary goal was a comprehensive functional analysis of Tba within its cellular context to elucidate its specific role in antibiotic production and biosynthesis. The relationship to the substrates as well as the co-encoded enzymes involved in biosynthesis were studied to gain inisghts into how antibiotic transporters are integrated into the biosynthetic process of their respective substrates. To address these questions, two key aspects were addressed: (1) the specificity of GPA-associated ABC transporters and (2) potential interactions of Tba with the balhimycin biosynthetic machinery.

By exploring the fundamentals of GPA biosynthesis and secretion, as well as elucidation how the respective transporters are integrated in this process in the natural producers, we can optimize existing resources and develop new approaches for the biotechnological advancement of antimicrobials.

3 List of publications and personal contribution

1. Nicola Gericke*, Dardan Beqaj*, Thales Kronenberger, Andreas Kulik, Athina Gavriilidou, Mirita Franz-Wachtel, Ulrich Schoppmeier, Theresa Harbig, Johanna Rapp, Iwan Grin, Nadine Ziemert, Hannes Link, Kay Nieselt, Boris Macek, Wolfgang Wohlleben, Evi Stegmann, Samuel Wagner. (2025) **Unveiling the substrate specificity of the ABC transporter Tba and its role in glycopeptide biosynthesis, ISCIENCE (2025)**

   DOI: https://doi.org/10.1016/j.isci.2025.112135.

   **Nicola Gericke and Dardan Beqaj contributed equally to this publication*

All experiments in this publication were planned and designed by me, Nicola Gericke, Dardan Beqaj, Evi Stegmann, Wolfgang Wohlleben, and Samuel Wagner.

I, Nicola Gericke, performed the *in silico* analysis of transporter sequences and phylogenetic analysis resulting in **Figure 1**, **Figure S1**, **Figure S2**, **Figure S3**, and **Figure S12**. I analyzed the AlphaFold2 models of all transporters manually and contributed to **Figure 3B**. Athina Gavriilidou and Nadine Ziemert identified the biosynthetic gene clusters and provided the transporter sequences, contributing to Figure 1 and Figure S3. Iwan Grin performed pairwise comparison of transporter sequences, and Athina Gavriilidou performed hierarchical clustering of the transporter sequences, contributing to Figure S2. Iwan Grin automated AlphaFold2 usage, contributing to Figure 3B. Thales Kronenberger performed all MD simulations, resulting in Figure 3 and Figure S7.

I, Nicola Gericke, and Dardan Beqaj constructed all plasmids and *A. balhimycina* strains, performed all *in vivo* experiments, and analyzed all corresponding data, resulting in **Figure 2**, **Figure 4**, **Figure S4**, **Figure S5**, **Figure S6**, **Figure S8**, **Figure S10**. Andreas Kulik performed all HPLC-MS measurements of balhimycin, contributing to Figure 2, Figure 4, Figure S4, Figure S6, Figure S8, and Figure S11. Ulrich Schoppmeier did statistical analysis of the *in vivo* balhimycin export assay, contributing to Figure 2 and Figure 4.

I, Nicola Gericke, and Dardan Beqaj performed the transcriptomics experiment and final analysis, resulting in **Figure 5A** and **Figure S9A**. Raw data generation and primary analysis for transcriptomics were performed by Kay Nieselt and Theresa Harbig, contributing to Figure S9A.

I, Nicola Gericke, and Dardan Beqaj performed the metabolomics experiment and final analysis, resulting in **Figure 5B** and **Figure S9B**. Raw data generation and primary analysis for transcriptomics were performed by Hannes Link and Johanna Rapp, contributing to Figure S9B.

I, Nicola Gericke, and Dardan Beqaj performed the proteomics experiment and final analysis, resulting in **Figure 6** and **Figure S11**. Raw data generation and primary analysis for proteomics were performed by Mirita Franz-Wachtel and Boris Macek.

I, Nicola Gericke, and Dardan Beqaj participated in development of the study, drafting the manuscript, and writing of the paper.

4 Results

4.1 Advancing GPA ABC transporter purification: from *E. coli* to the native environment

In this chapter, I will present a series of selected experiments describing the rational optimization process of the overexpression and purification conditions of the GPA ABC transporters Tba (*A. balhimycina*) and Tri (*A. japonicum*), with the aim of obtaining stable and functional proteins in sufficient quantities for *in vitro* analyses. Tba and Tri are homologous proteins that share 78% sequence identity (Fig. S2 - Publication 1) and transport a type I GPA (balhimycin) and a type III GPA (ristomycin), respectively. I will discuss different expression conditions, affinity tags, and detergents, as well as the use of unconventional expression hosts in this chapter.

4.1.1 GFP-based expression and solubility screen for Tri and Tba in *E. coli* Lemo21(DE3)

For the initial step of optimization of the expression, solubility, and purification of the ABC GPA transporters, enhanced GFP (eGFP), hereafter referred to as GFP, was C-terminally fused to Tri and Tba on a high copy number vector. GFP is a soluble protein shown to facilitate the overexpression and purification of membrane proteins by serving as a folding indicator that is only fluorescent in the cytoplasm, but not in inclusion bodies [190]. Overexpression of membrane proteins often leads to the formation of inclusion bodies instead of correct localization in the cytoplasmic membrane due to saturation of the Sec translocon [70], which is responsible for the insertion of most integral membrane proteins in bacteria [42]. In addition, the fluorescent signal allows easy tracking of the membrane protein-GFP fusion at later stages of the purification process [190]. Here, *E. coli* Lemo21(DE3) (Lemo21) was used as a heterologous host for a screen of various overexpression conditions (growth medium, growth temperature, with and without induction with IPTG, induction time, and rhamnose concentration). Representative examples of the screened conditions are depicted below (Fig. 4). GFP was used as a control for a cytosolic protein, and the integral membrane flavocytochrome YedZ with six transmembrane segments (TMS), C-terminally fused to GFP (YedZ-GFP) [70,191], was used as a control for a membrane protein. The expression host used in this screen, Lemo21, was optimized for membrane protein overexpression and is a derivative of *E. coli* BL21(DE3) (BL21), which supports high expression rates by transcription with the T7 RNA polymerase (T7RNAP). Lemo21 additionally encodes the natural inhibitor of the T7RNAP, the T7 lysozyme (T7Lys), under the control of a rhamnose-inducible promoter [72]. The addition of different concentrations of rhamnose can counteract the saturation of the Sec translocon and thereby increase the yield of membrane proteins.

Here, the relative fluorescence intensity of whole cells after growth was measured to identify a suitable rhamnose concentration for each protein used in this screen (Fig. 4A-D). The addition of rhamnose into the growth medium led to an almost complete loss of relative fluorescence intensity in cells expressing the soluble protein GFP (Fig. 4A), whereas cells

expressing the membrane proteins YedZ-GFP (Fig. 4A), Tri-GFP, or Tba-GFP (Fig. 4B) still showed an intensity that was at least half as high as in the control without rhamnose. In the case of Tri-GFP, the addition of 100 µM rhamnose resulted in an increased signal (Fig. 4B, yellow), suggesting that slowing down expression upon the addition of rhamnose does lead to more protein.

It was then tested whether the relative fluorescence intensity could be increased by culturing the bacteria in Terrific Broth (TB) medium instead of Lysogeny Broth (LB) medium and using longer induction times (Fig. 4C+D). TB medium is known to promote high cell densities by prolonging the exponential growth phase and often results in higher cell densities than other nutrient-rich media, thereby indirectly increasing the yield of recombinantly expressed proteins [192]. Expression of Tri-GFP in TB medium and 12 h induction led to at least 4-fold higher relative intensities at all rhamnose concentrations compared to growth in LB medium and 5 h induction, indicating more protein (Fig. 4C). This effect was less pronounced for Tba-GFP (Fig. 4C). Next, the influence of reducing the growth temperature from 30°C to 25°C was examined (Fig. 4C). As lower temperatures reduce the metabolic rate of the cell, the saturation of the Sec translocon may also be reduced. The relative fluorescence intensity of the cells expressing *tri-gfp* was significantly lower at 25°C than at 30°C and was approx. $1x10^4$ for all rhamnose concentrations. In cells expressing *tba-gfp*, the lower growth temperature resulted in higher relative fluorescence intensities, with the highest value of approx. $4.25\ x10^4$ being observed upon addition of 50 µM rhamnose. The highest relative fluorescence intensity for Tri-GFP was obtained after induction at 30°C for 12 h and the addition of 100 µM rhamnose (Fig. 4C, left), and for Tba-GFP after induction at 25°C for 15 h and 50 µM rhamnose (Fig. 4D, right). The results emphasize that the addition of rhamnose affects expression differently and needs to be tested individually for every protein and condition. Furthermore, the analysis of relative fluorescence alone does not provide sufficient information on whether the proteins are being stably expressed. This was analyzed by immunodetection after SDS-PAGE of whole cells (Fig. 4E+F). Tri-GFP and Tba-GFP have calculated molecular weights of 100.9 kDa and 101 kDa, respectively, but were detected, with anti-GFP antibodies, at approx. 90 kDa in both conditions (30°C and 12 h induction; 25°C and 15 h induction). This so-called gel shift has been observed for many membrane proteins and is caused by the altered detergent binding capacity of proteins with different amino acid composition and tertiary structures compared to the marker proteins, which are usually soluble and globular [193].

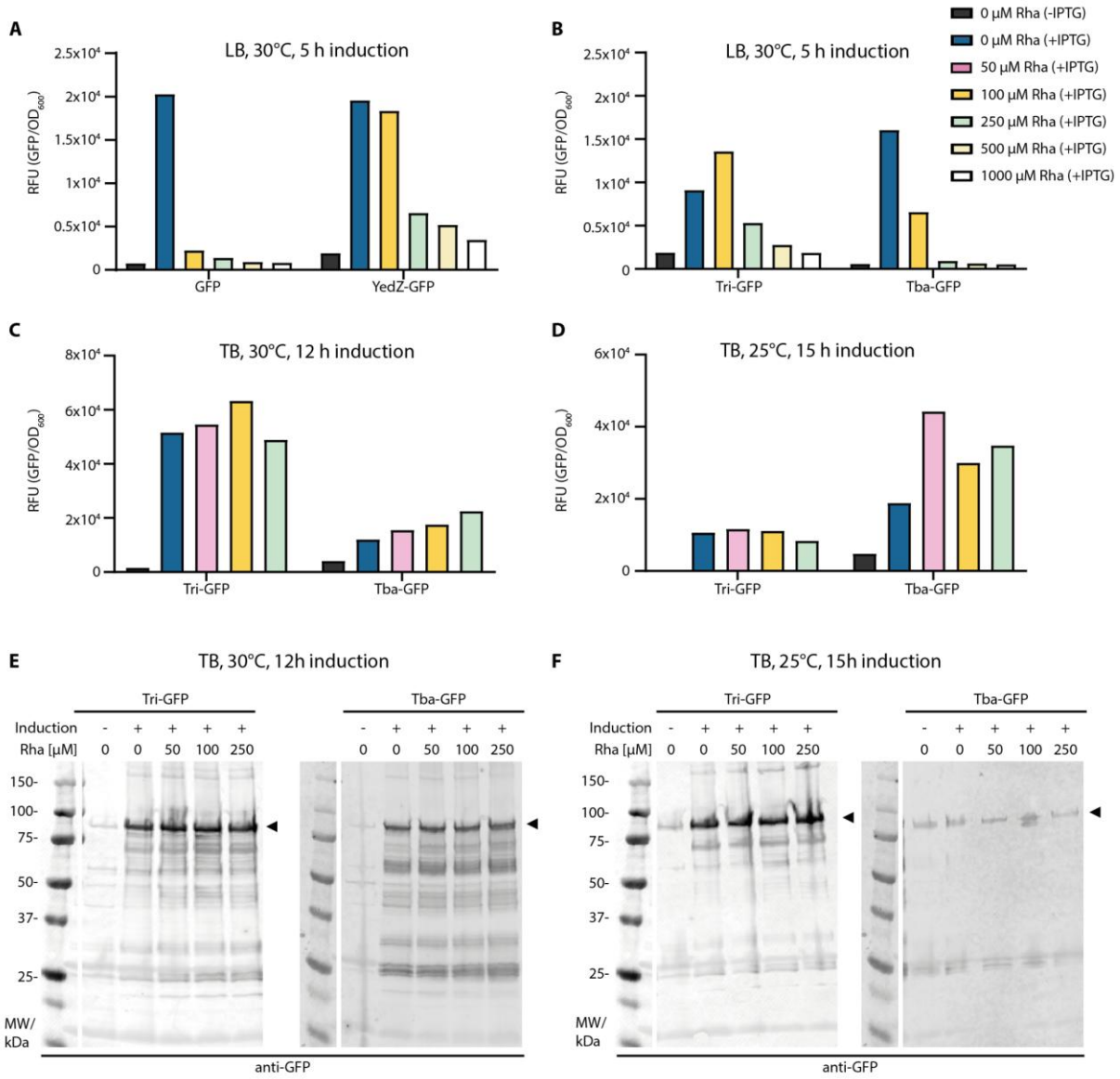

Figure 4 | Screen of overexpression conditions of tri-gfp and tba-gfp using *E. coli* Lemo21(DE3) as heterologous host.

Overexpression screen of *tri-gfp* and *tba-gfp* under different growth conditions (growth medium, growth temperature, with and without IPTG induction, varying induction time, and rhamnose concentrations) in Lemo21 in small scale (12 ml culture volume). (**A**) RFU of Lemo21 expressing the cytosolic or membrane control *gfp* or *yedZ-gfp*, respectively, in LB medium at 30°C before and after 5 h of induction with IPTG (0.04 µM) and different concentrations of rhamnose (legend). GFP fluorescence intensity was normalized to the cell growth (OD_{600}) and presented as RFU. (**B**) RFU of Lemo21 expressing *tri-gfp* (*A. japonicum*) or *tba-gfp (A. balhimycina)*, respectively, in LB medium at 30°C before and after 5 h of induction with IPTG (0.04 µM) and different concentrations of rhamnose. (**C**) RFU of Lemo21 expressing *tri-gfp* or *tba-gfp*, respectively, in LB medium at 30°C before and after 12 h of induction or (**D**) 25°C after 15 h of induction with IPTG (0.4 µM) and different concentrations of rhamnose. (**E**) Immunoblotting (anti-GFP) after SDS-PAGE of whole cells (0.1 ODU) from condition C and (**F**) condition D. The black arrowheads indicate the bands corresponding to Tri-GFP or Tba-GFP. **Repetitions:** A single experiment was performed using the parameters described. However, they are representative of other experiments with only slight variations in induction time. **Abbreviations:** RFU: relative fluorescence unit; Rha: L-rhamnose; IPTG: Isopropyl-ß-D-1-thiogalactopyranoside; ODU: optical density unit.

Interestingly, Tba-GFP was detected at the highest intensity after 12 h of induction at 30°C (Fig. 4 E+F, right), although the relative fluorescence intensities were higher at 25°C after 15 h at all rhamnose concentrations (Fig. 4 D, right). This discrepancy suggests that the stability of full-length Tba-GFP is superior at 30°C after 12 h induction than at 25°C and 15 h induction (Fig. 4 E+F, right), since the determination of relative fluorescence involves the measurement of the total GFP signal, including N-terminally degraded GFP transporter fusions or cleaved GFP. A band corresponding to the size of GFP (≈26 kDa) was detected in both conditions (Fig. 4 E+F, right). The influence of rhamnose, seen by fluorescence measurement, was not visible by immunodetection. Tri-GFP was detected with similar intensities under all temperature and rhamnose conditions (Fig. 4 E+F, left) and did not clearly correlate with the relative fluorescence intensities (Fig. 4 C+D; left). Overall, however, fewer bands below 90 kDa were detected after expression of Tri-GFP at 25°C than at 30°C, indicating less degradation (Fig. 4 E+F, left). The expression of Tba-GFP and Tri-GFP in Lemo21 was differentially affected by the addition of rhamnose. However, immunodetection of the proteins produced indicated that, compared to Tba-GFP, Tri-GFP was present in higher amounts in the cells under all conditions tested.

Since Tri-GFP was detected more strongly than Tba-GFP in the previous overexpression screen (Fig. 4), a solubility screen was initially carried out with Tri-GFP only (Fig. 5). Due to their amphipathic properties, membrane proteins are usually insoluble in water and require extraction from the cytoplasmic membrane with detergents and stabilization in aqueous buffers to prevent aggregation. Determining which detergent is most suitable for the extraction and stabilization of which protein is an empirical process. Therefore, the main objective of the solubility screen was to test whether Tri-GFP can be extracted from the cytoplasmic membrane of Lemo21 and stabilized by one of the commonly used detergents LMNG, DMNG, DDM, or DM. Detailed characteristics of the detergents are provided in Table 3 (Chapter 7.12).

Cells expressing Tri-GFP were harvested after growth at 25°C for 12 hours in TB medium supplemented with 250 µM rhamnose. After mechanical lysis, the lysate was cleared of cell debris by centrifugation and separated by ultracentrifugation into two fractions: the supernatant containing soluble proteins and the pellet containing crude membranes (CM) including integral membrane proteins. Relative fluorescence intensity was detectable after lysis but significantly reduced to approximately a quarter of the initial signal after separation of the CM from the cytosolic components of the cells, indicating that the majority of GFP was present in the cytoplasm (Fig. 5A). The crude membranes were divided into four equal parts and solubilized in 1% (w/v) LMNG, DMNG, DDM, or DM, respectively. Afterwards, the mixture was separated into a solubilized (S) and non-solubilized (NS) fraction by ultracentrifugation. In all four conditions tested, the majority of the GFP fluorescent signal was measured in the non-solubilized fraction (Fig. 5B). This indicates that only small amounts of Tri-GFP were correctly extracted from the cytoplasmic membrane. This was more pronounced when the crude membranes were solubilized with DDM or DM and may be due to the different strength of the detergents. Immunodetection of the solubilized and non-solubilized fractions confirmed the presence of Tri-GFP mainly in the non-solubilized fraction (Fig. 5D).

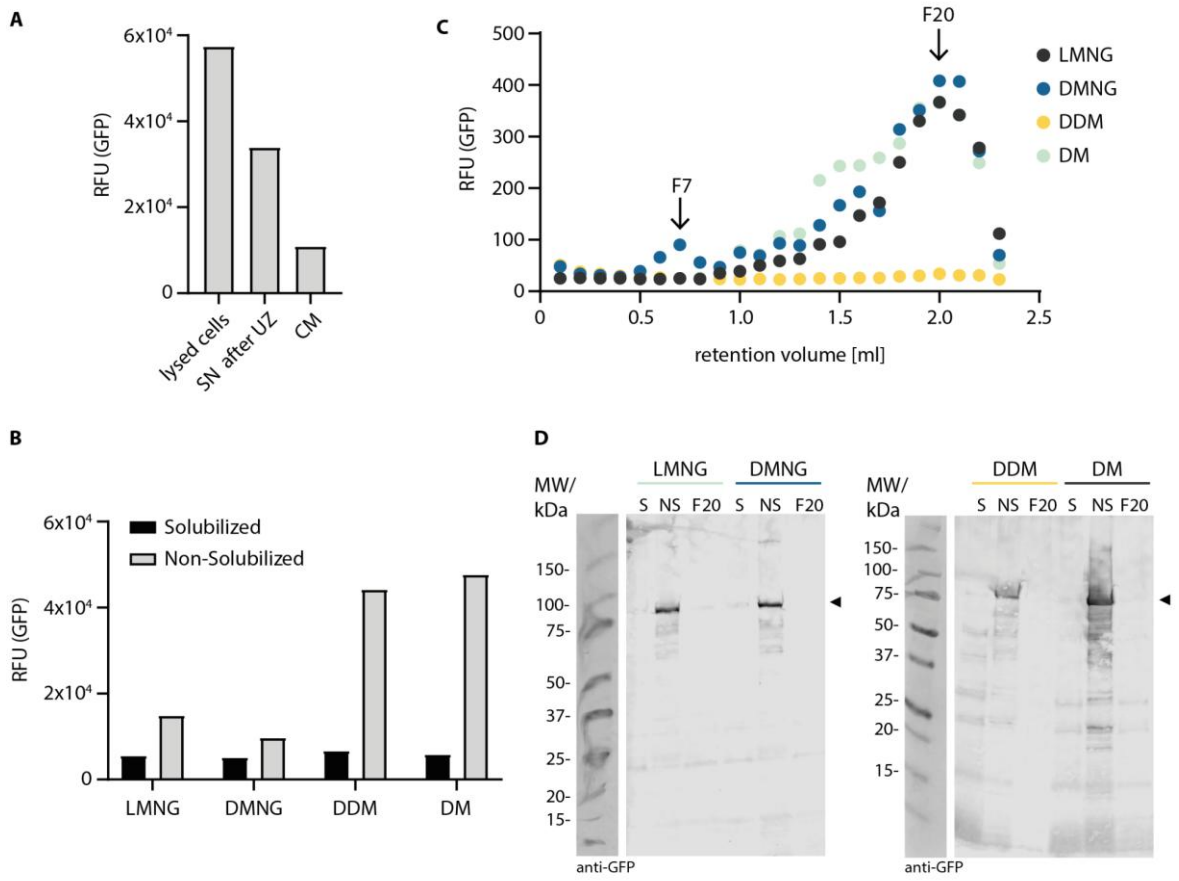

Figure 5 | Solubility screen of Tri-GFP using *E. coli* Lemo21(DE3).
Solubility screen of Tri-GFP expressed in Lemo21 at 30°C before induction and 25°C after induction for 15 h with 250 µM rhamnose. (**A**) RFU of 0.1 ODU of lysed cells, the cytosolic fraction after ultracentrifugation (SN after UZ), and crude membranes (CM). (**B**) RFU of comparable amounts of solubilized and non-solubilized fractions after solubilization with 1% (w/v) of LMNG, DMNG, DDM, or DM are shown in black and gray, respectively. (**C**) RFU of every fraction after SEC (Column: Superose 6 Increase 3.2/300). (**D**) Immunoblotting (anti-GFP) after SDS-PAGE of solubilized (S) and non-solubilized (NS) fractions after solubilization and F20 after SEC. The black arrowhead indicates the bands corresponding to Tri-GFP. **Repetitions:** A single experiment was performed using the parameters described. **Abbreviations:** F7: fraction 7 after SEC; F20: fraction 20 after SEC.

The solubilized membranes were further separated by size exclusion chromatography (SEC) (Column: Superose 6 Increase 3.2/300), and the individual fractions were examined for GFP fluorescence (Fig. 5C). The highest fluorescence intensity was obtained after a retention volume of 2 ml (F20) for LMNG, DMNG, and DM-solubilized samples, whereas no signal was detected for DDM-solubilized samples (Fig. 5C). A second peak was detected for DMNG-solubilized samples at 0.7 ml (F7). According to the manufacturer's function test [194], a retention volume of 2 ml corresponds to proteins with a molecular weight of 13.7 kDa. However, this was tested using soluble globular proteins and does not directly apply to membrane proteins, which typically exhibit a higher apparent molecular weight due to the surrounding detergent micelle. Therefore, the primary peak observed at 2.0 ml likely does not represent the full transporter Tri-GFP but instead corresponds to a degradation product or cleaved GFP, as the GFP signal remains detectable. Immunoblotting by anti-GFP antibodies confirmed that Tri-

GFP is not present in F20 after SEC (Fig. 5D). Therefore, none of the detergents used extracted full-length Tri-GFP. However, additional bands below 90 kDa were visible in both F20 and the two fractions after solubilization, suggesting N-terminal degradation of Tri-GFP.

These results reveal that a large fraction of the functional GFP was present in the cytoplasm and was not part of membrane-integrated Tri-GFP. It is possible that the entire C-terminus, including GFP, was cleaved off the transporter. Furthermore, they also show that the detergents were unable to extract and stabilize large amounts of Tri-GFP from the membrane, which may be due to the detergents being not suitable but also to the fact that there was little Tri-GFP present in the cytoplasmic membrane. It is also likely that the small amount that was present has been further degraded.

4.1.2 Investigating the subcellular localization of Tri-GFP and Tba-GFP in *E. coli* Lemo21(DE3)

Tri-GFP could not be extracted from the cytoplasmic membrane of Lemo21 with the detergents LMNG, DMNG, DDM, or DM. (Fig. 5). It is therefore unclear whether the transporter was correctly inserted into the cytoplasmic membrane. This was analyzed by membrane fractionation of the crude membranes of Lemo21 expressing *tri-gfp*, *tba-gfp*, or the membrane protein control *yedZ-gfp*. Expression was induced with IPTG in TB medium supplemented with 250 µM, 100 µM, or 50 µM rhamnose, and cells were harvested after 15, 12, and 15 h, respectively. After preparation of the crude membranes, they were applied to a 30-53% (w/w) sucrose density gradient, separated by ultracentrifugation, and subsequently fractionated in 12 equal fractions. These were then analyzed by SDS-PAGE followed by Coomassie staining and immunodetection. The *E. coli* inner membrane (IM) protein leader peptidase Lep was used as a marker for the IM and detected using specific antibodies [195]. All three Coomassie-stained SDS-PAGE gels showed a similar pattern with a smear in the fractions 3-4 and 8-9 in the upper part of the gel, indicating a high number of proteins (Fig. 6A-C). As the proteins are mainly present in the membranes, the smear fractions correspond to the two membranes. The inner membrane usually equilibrates at lower sucrose concentrations than the outer membrane [196]. Therefore, the earlier smear fractions correspond to the inner membrane, and inner membrane proteins are expected to colocalize. However, the IM marker Lep was not exclusively detectable in the inner membrane fractions in all three conditions, which may indicate technical errors in the experiment. The two transporters, Tri-GFP (Fig. 6A) and Tba-GFP (Fig. 6B), were also not only detected in the fractions assigned to the inner membrane, similar to the inner membrane protein YedZ-GFP (Fig. 6C). In addition, the GFP fluorescence of each fraction was measured and analyzed to identify whether functional GFP was associated with one of the two suggested membrane fractions (Fig. 6D). However, only fractions of cells expressing *yedZ-GFP* showed a GFP signal in the suggested IM, while the fractions of cells expressing *tba-GFP* revealed no GFP fluorescence, and the ones expressing *tri-gfp* showed a maximum signal in fraction 8 (OM) (Fig. 6D). Despite technical problems, these results indicate that neither Tri-GFP nor Tba-GFP is present in the membrane with a functional C-terminal GFP. It is possible that the GFP tag was cleaved off or that heavy intramembrane aggregation

occurred, and consequently equilibrated with higher sucrose concentrations. Therefore, it was not possible to confirm the localization of Tri-GFP and Tba-GFP in the inner membrane of Lemo21.

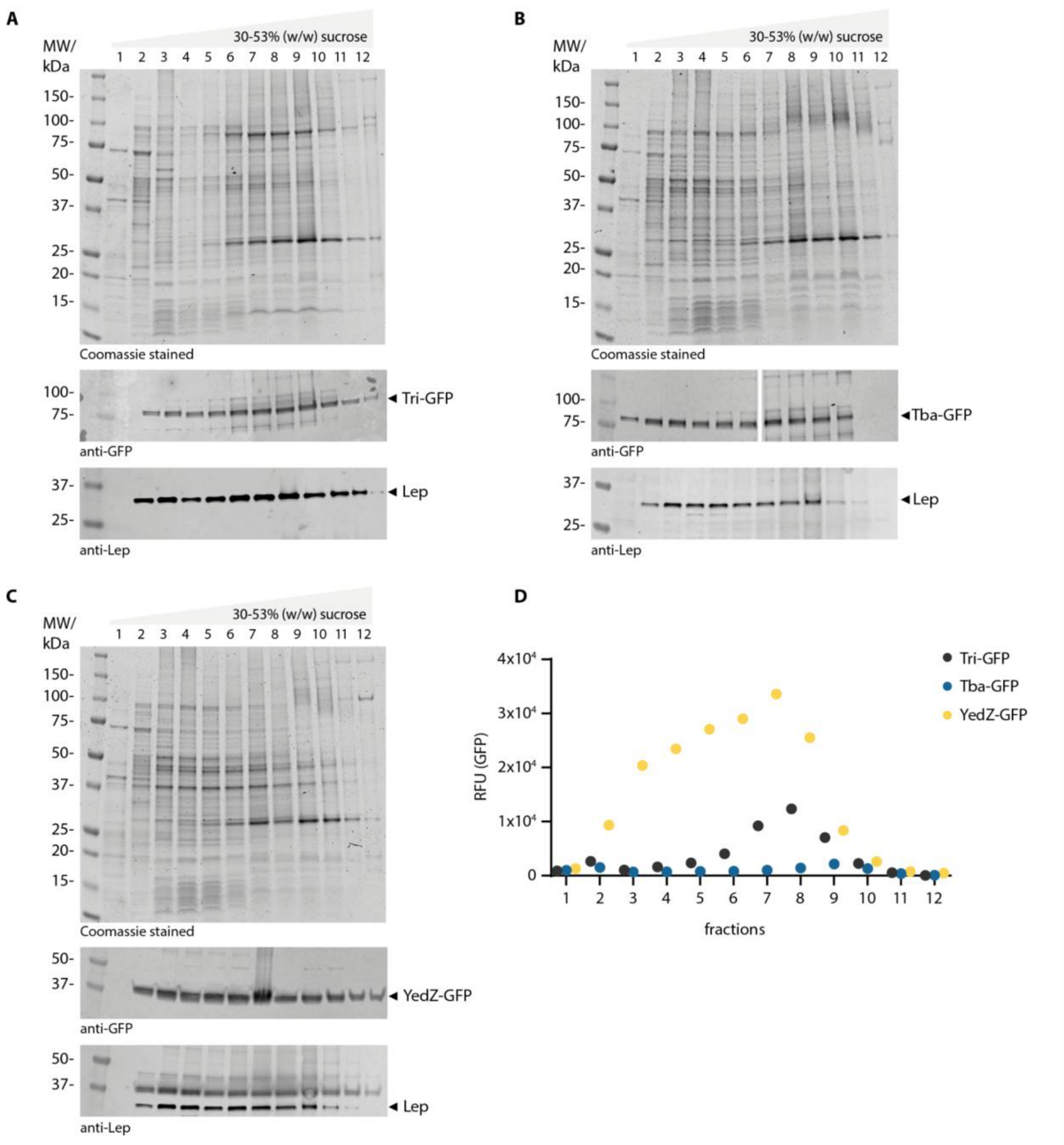

Figure 6 | Membrane localization of Tri-GFP and Tba-GFP in *E. coli* Lemo21(DE3).
Membrane fractionation (12 fractions) of (**A**) Lemo21+tri-gfp (**B**) Lemo21+tba-gfp and (**C**) Lemo21+yedZ-gfp (control) crude membranes separated in a 30-53% (w/w) sucrose gradient. Coomassie staining (top), immunoblot (anti-GFP) (middle), and immunoblot (anti-Lep) (control) (bottom) after SDS-PAGE of every fraction. (**D**) RFU of fractions 1-12 after membrane fractionation. Three individual experiments were performed and one representative example is shown here. **Repetitions:** A single experiment was performed using the parameters described.

The majority of the fluorescence signal of cells expressing Tri-GFP was detected in the cytoplasm after lysis and ultracentrifugation (Fig. 5), and Tri-GFP as well as Tba-GFP were not clearly localized in the inner membrane after membrane fractionation (Fig. 6). It was therefore investigated whether the proteins were present in cytoplasmic aggregates. Lemo21 cells expressing *tri-gfp*, *tba-gfp*, *yedZ-gfp* or *gfp,* under the above-mentioned conditions, were lysed, and the membranes were pelleted together with cytoplasmic aggregates. The membranes were then removed by multiple washes with 2% (w/v) of the mild detergents NP-40. The remaining cytoplasmic aggregates were analyzed by immunodetection (Fig. 7A) and Coomassie staining (Fig. 7B) after SDS-PAGE. The membrane protein control YedZ-GFP was detectable in cytoplasmic aggregates with anti-GFP antibodies and Coomassie staining, whereas soluble GFP was barely detectable by immunodetection and Coomassie staining (Fig. 7), indicating that YedZ-GFP is present in cytoplasmic aggregates. This is consistent with the literature, which shows that YedZ-GFP is present in both the inner membrane and cytoplasmic aggregates when overexpressed [70]. Both Tri-GFP and Tba-GFP were detected with anti-GFP antibodies, with Tri-GFP showing a stronger signal. However, neither protein was visible after Coomassie staining, indicating that both transporter-GFP fusion proteins are only present at low levels in cytoplasmic aggregates.

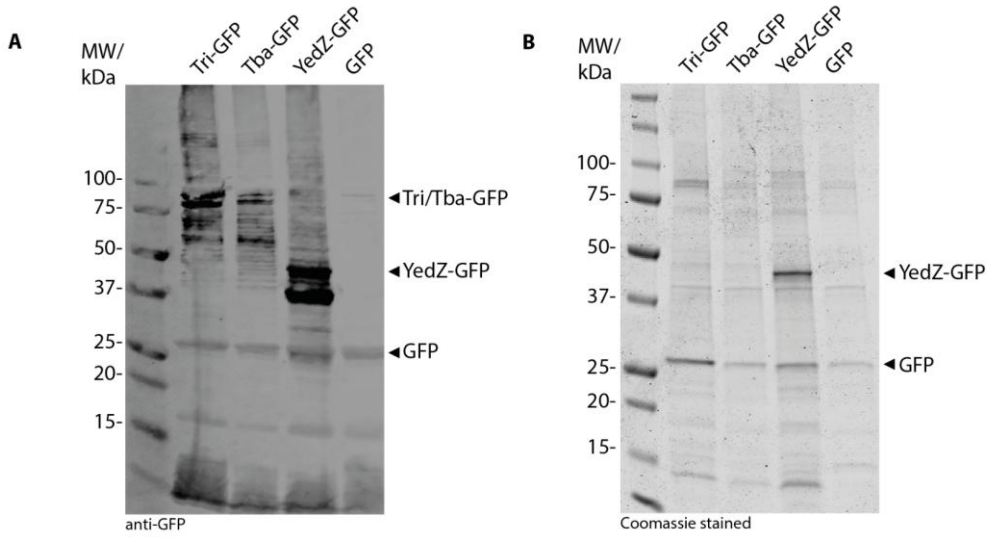

Figure 7 | Intracellular aggregation of Tri-GFP and Tba-GFP in *E. coli* Lemo21(DE3).
Immunoblotting (anti-GFP) (**A**) and Coomassie staining (**B**) after SDS-PAGE of 7 ODU of purified intracellular aggregates of Lemo21 overexpressing *tri-gfp*, *tba-gfp*, *yedZ-gfp* (control), and *gfp* (control). A single experiment was performed using the parameters described. **Repetitions:** A single experiment was performed using the parameters described.

Tri-GFP and Tba-GFP were both not clearly localized in the IM of Lemo21 and also not present in large amounts in cytoplasmic aggregates. Therefore, the localization of the proteins was still unclear and was further investigated using epifluorescence microscopy of the GFP tag (Fig. 8). For microscopy, Lemo21 expressing *tri-gfp*, *tba-gfp*, *yedZ-gfp*, and *gfp* were cultivated under the above-mentioned conditions but harvested in the exponential growth phase. The cells expressing cytosolic *gfp* showed a homogeneous GFP signal throughout the entire cell (Fig. 8A), while the signal for the cells expressing *yedZ-gfp* was stronger at the cell border

(Fig. 8B). This exemplified the cytosolic localization of GFP and the localization at the cytoplasmic membrane of YedZ-GFP. Tri-GFP and Tba-GFP showed a weaker signal compared to the controls and were not detected at the cytoplasmic membrane. Tri-GFP appeared to be distributed over the whole cell, comparable to GFP (Fig. 8C), and Tba-GFP formed several distinct foci across the cell, of varying size (Fig. 8D).

In conclusion, the localization experiments indicated that both Tri-GFP and Tba-GFP were not correctly localized at the IM of Lemo21 upon overexpression, as was demonstrated for the control YedZ-GFP. This argues against Lemo21 as an expression host under the conditions tested for these proteins.

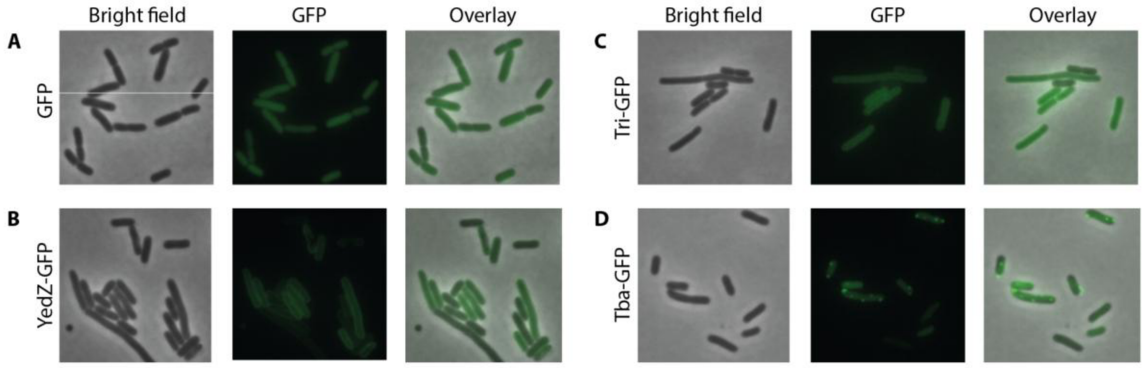

Figure 8 | Localization of Tri-GFP and Tba-GFP using epifluorescence microscopy in *E. coli* Lemo21(DE3).
Subcellular localization of (**A**) GFP, (**B**) YedZ-GFP, (**C**) Tri-GFP, and (**D**) Tba-GFP (green) in Lemo21 by epifluorescence microscopy. Cells were expressed in TB medium supplemented with 0, 50, 250, or 100 µM rhamnose and harvested in the exponential growth phase. **Repetitions:** Two independent experiments were performed using the parameters described. At least three different images were taken from each sample, and the images shown are representative of the entire sample.

4.1.3 Exploring overexpression of *tri* and *tba* in *E. coli* Mutant56(DE3)

Previous attempts have been made to express Tri-GFP and Tba-GFP in Lemo21. Although expression was confirmed by fluorescence measurement and immunodetection, it was not possible to extract the proteins stably from the membrane. Epifluorescence microscopy localization studies showed that neither Tri-GFP nor Tba-GFP was localized at the cytoplasmic membrane of Lemo21 (Fig. 8). Consequently, the expression host was changed to *E. coli* Mutant56(DE3) (Mt56). Mt56, like Lemo21, is a BL21 derivative and has a single amino acid substitution in the T7RNAP that weakens the binding property to the T7*lac* promoter, thereby slowing down gene expression and counteracting saturation of the Sec translocon [74].

Different growth temperatures (30°C, 25°C, and 18°C), and induction times were screened and analyzed by the relative fluorescence intensity of whole cells and epifluorescence microscopy (Fig. 9). The highest relative fluorescence intensity of Mt56 expressing *tri-gfp* and *yedZ-gfp* was measured after induction at 30°C, while it decreased at lower temperatures (Fig. 9A). The relative fluorescence intensity of cells expressing cytosolic *gfp* and *tba-gfp* was barely measurable, indicating that the proteins were not produced under these conditions (Fig. 9A).

Epifluorescence microscopy analysis was therefore only performed for cells expressing *tri-GFP* and the control *yedZ-gfp* (Fig. 9B). Tri-GFP was localized differently depending on the growth temperature. While at 30°C and 25°C the GFP signal is homogeneously distributed throughout the cell, at 18°C the transporter appeared to be localized at the border of the cell, as in the YedZ-GFP control (Fig. 9B). Although this suggests that Tri-GFP is localized in the cytoplasmic membrane upon expression at 18°C and 15 h induction, it does not necessarily provide evidence that Tri-GFP is correctly integrated.

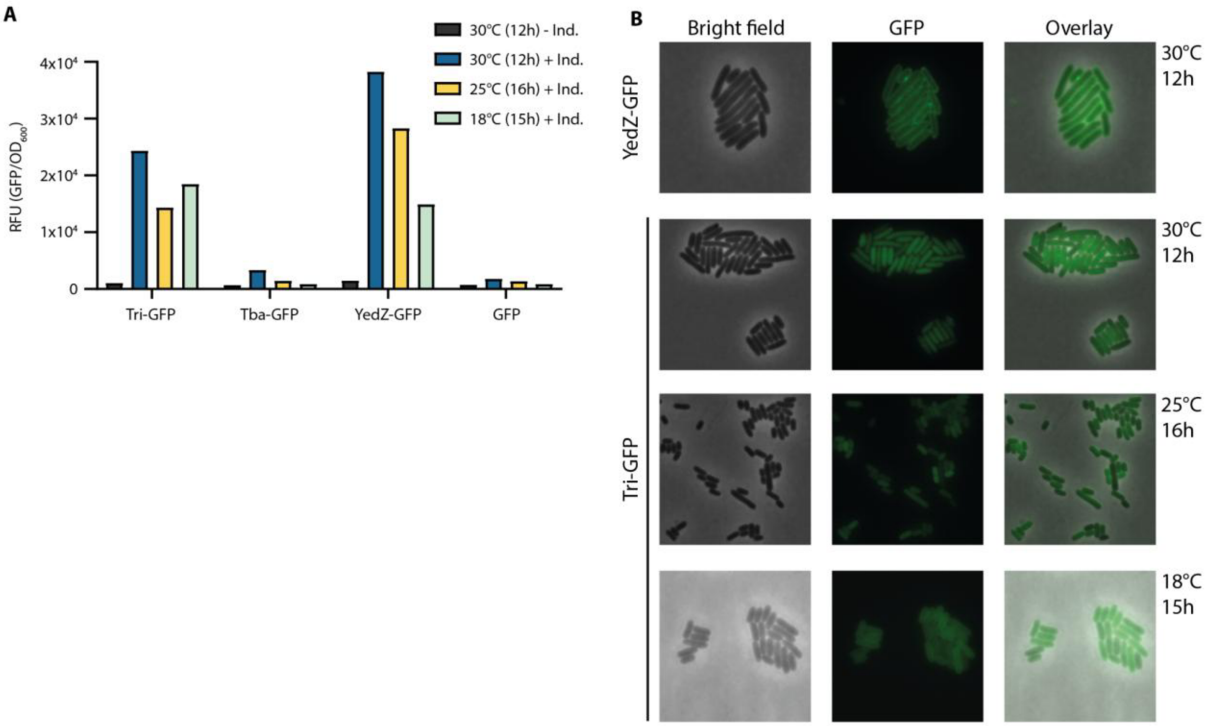

Figure 9 | Overexpression and solubilization of Tri-GFP and Tba-GFP (*E. coli* Mutant56(DE3)). Overexpression screen of *tri-gfp* and *tba-gfp* under different growth conditions (growth temperature, +/- induction (0.04 µM IPTG), induction time) in Mt56. (**A**) RFU of Mt56 expressing *tri-gfp*, *tba-gfp*, *yedZ-gfp*, and *gfp* at different temperatures and induction times, with or without induction with IPTG. GFP fluorescence intensity was normalized to the cell growth (OD_{600}) and presented as RFU. (**B**) Subcellular localization of YedZ-GFP and Tri-GFP (green) in Mt56 at different conditions by epifluorescence microscopy. **Repetitions:** A single experiment was performed using the parameters described. However, they are representative of two more independent experiments with only slight variations in induction time. At least three different images were taken from each sample, and the images shown are representative of the entire sample. **Abbreviations**: Ind.: Induction with IPTG.

The localization of Tri-GFP was further investigated by membrane fractionation (Fig. 10) of Mt56 expressing *tri-gfp* at 18°C and 15 h induction. The characteristic smear bands of the outer and inner membrane were visible in the upper part of the Coomassie-stained SDS-PAGE gel in fractions 3-4 and 10-11 (Fig. 10A). The anti-GFP antibodies detected Tri-GFP in fractions 3-5 and to a much lesser extent in the fractions with higher sucrose concentrations, suggesting that Tri-GFP is partially localized within the IM (Fig. 10A). None of the bands detected after Coomassie-staining correlated to the intensity profile of Tri-GFP found by immunodetection (Fig. 10A). Analysis of GFP fluorescence signals of each fraction after fractionation showed the highest signal in fractions 2-3 and a lower one at higher sucrose concentrations. However,

a peak was visible in fraction 10 with approximately one third of the intensity of fraction 2 (Fig. 10B). In contrast to the previous membrane fractions of Lemo21 (Fig. 6), which expressed *tri-gfp*, in Mt56 a correlation between the measured relative fluorescence intensity (Fig. 10B) and the immunodetection of Tri-GFP in the suggested IM fraction was observed for the first time. This indicates correct localization of Tri-GFP in the IM of Mt56 under these conditions.

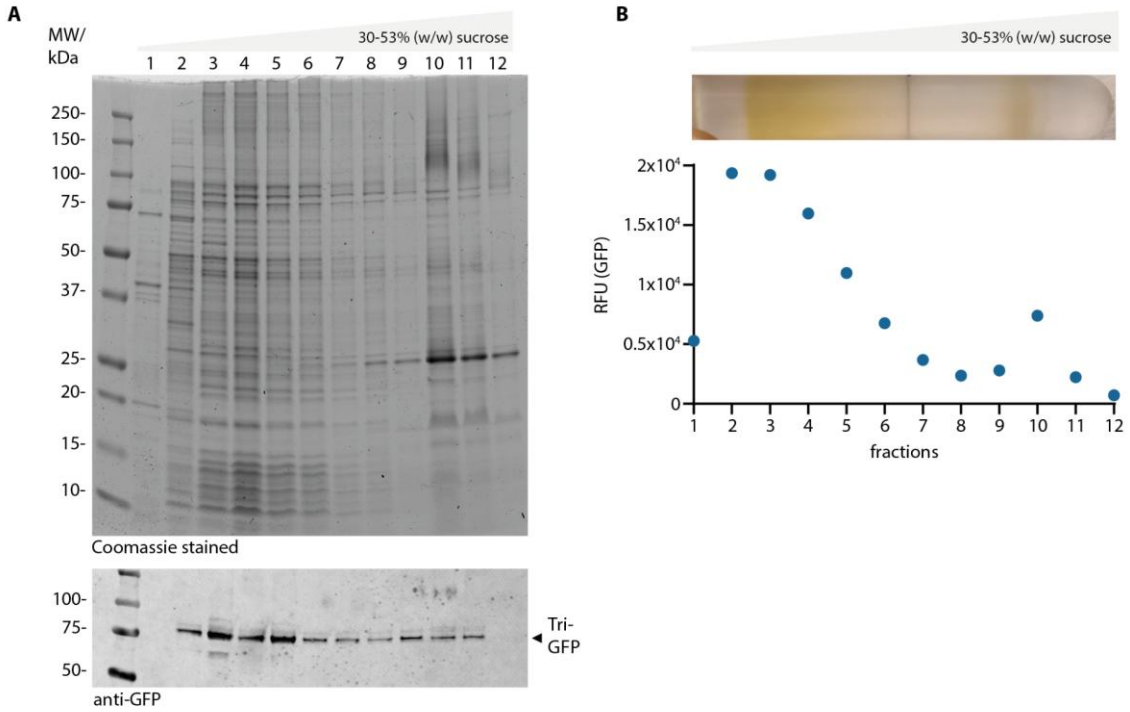

Figure 10 | Membrane localization of Tri-GFP in *E. coli* Mutant56(DE3).
Membrane fractionation (12 fractions) of crude membranes of Mt56+*tri-gfp* separated in a 30-53% (w/w) sucrose gradient. (**A**) Coomassie staining (top) and immunoblot (anti-GFP) (bottom) after SDS-PAGE of every fraction. (**B**) Picture of crude membranes separated in sucrose gradient (top) and RFU of every fraction after fractionation (bottom). **Repetitions:** Three individual experiments were performed using the parameters described. However, only one representative example is shown here.

Tri-GFP could be extracted from the cytoplasmic membrane using 1% (w/v) LMNG and DDM at different protein concentrations (Fig. 11). Relative fluorescence intensity of the solubilized and non-solubilized fractions was measured. For both detergents used, the intensity of the solubilized samples increased with higher protein concentrations and reached a maximum at 12 mg/ml. The ratio of solubilized to non-solubilized also showed a tendency to increase with higher protein concentration in both conditions. However, the total intensity of the DDM-solubilized samples was higher than that of the LMNG-solubilized samples. The solubilization of the cytoplasmic membrane of Mt56 and extraction of Tri-GFP was successful with both detergents. However, 1% (w/v) DDM resulted in a higher relative fluorescence intensity, indicating that more protein was extracted compared to 1% (w/v) LMNG. Therefore, from now on 1% (w/v) DDM was used to solubilize Tri-GFP.

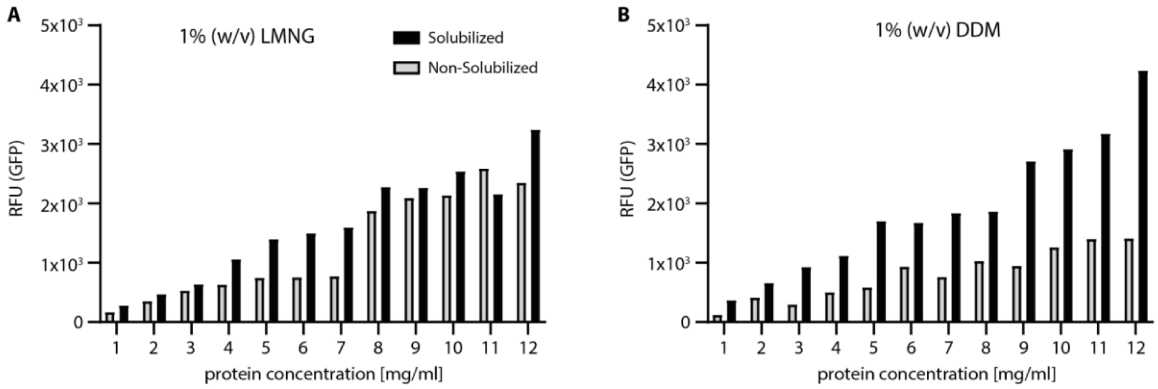

Figure 11 | Solubilization of Tri-GFP with LMNG and DDM (*E. coli* Mutant56(DE3)).
RFU of soluble (black) and non-soluble (gray) fractions after solubilization of crude membranes of Mt56 expressing *tri-gfp* with 1% (w/v) LMNG (**A**) or DDM (**B**) at different protein concentrations. **Repetitions:** A single experiment was performed using the parameters described.

After optimization of the expression and solubilization conditions of Tri-GFP in Mt56 (Figs. 9-11), the purification conditions were optimized. Mt56 expressing *tri-gfp* were grown at 18°C and induced for 72 h to potentially increase the yield of protein (Fig. 12). Solubilization was carried out with 1% (w/v) DDM at a protein concentration of the crude membranes of 9.5 mg/ml. The relative fluorescence intensity decreased during cell disruption and solubilization (Fig. 12A). Most of the fluorescence signal was already lost after preparation of the crude membranes, as in the previous purification from Lemo21 (Fig. 5). Nevertheless, the solubilized fraction was used for an immobilized metal affinity chromatography (IMAC). Here, the entire material was loaded onto a Ni^{2+} resin containing column. Since there is an 8xHis tag at the C-terminus of Tri-GFP, the fusion proteins should bind to the resin, and other proteins should not bind and accumulate in the flow-through (FT). Then, the proteins that have specifically bound to the column can be eluted with an imidazole-containing buffer. An additional washing step using a 10 mM imidazole-containing buffer was included to increase the purity of the elution fractions. A high elution peak (≈2300 mAu) was detected in the UV chromatogram after IMAC at 20% (w/v) elution buffer (EB), corresponding to an imidazole concentration of 100 mM (Fig.12B). A second smaller peak (≈400 mAu) was detected at 100% EB (500 mM imidazole) (Fig. 12B). This demonstrates that the majority of the bound proteins eluted at 20% (w/v) EB. Tri-GFP was detected by immunodetection at approximately 75 kDa in elution fractions E1-E7 (20% EB) but not in E8-E10 (100% EB) (Fig. 12C, top). Additional strong bands at 70 kDa, 50 kDa, and 27 kDa were also detected in the E2-E4 fractions, suggesting degradation of Tri-GFP (Fig. 12C, top). Tri-GFP was not detectable with the same intensity profile by Coomassie staining (Fig. 12C, bottom). Additional strong bands at 75 kDa, 70 kDa, and 50 kDa, as well as some weaker bands below 50 kDa, were visible in almost all fractions after Coomassie staining (Fig. 12C, bottom). This may be due to the high non-specific binding capacity of the Ni^{2+} resin to proteins with consecutive histidine residues.

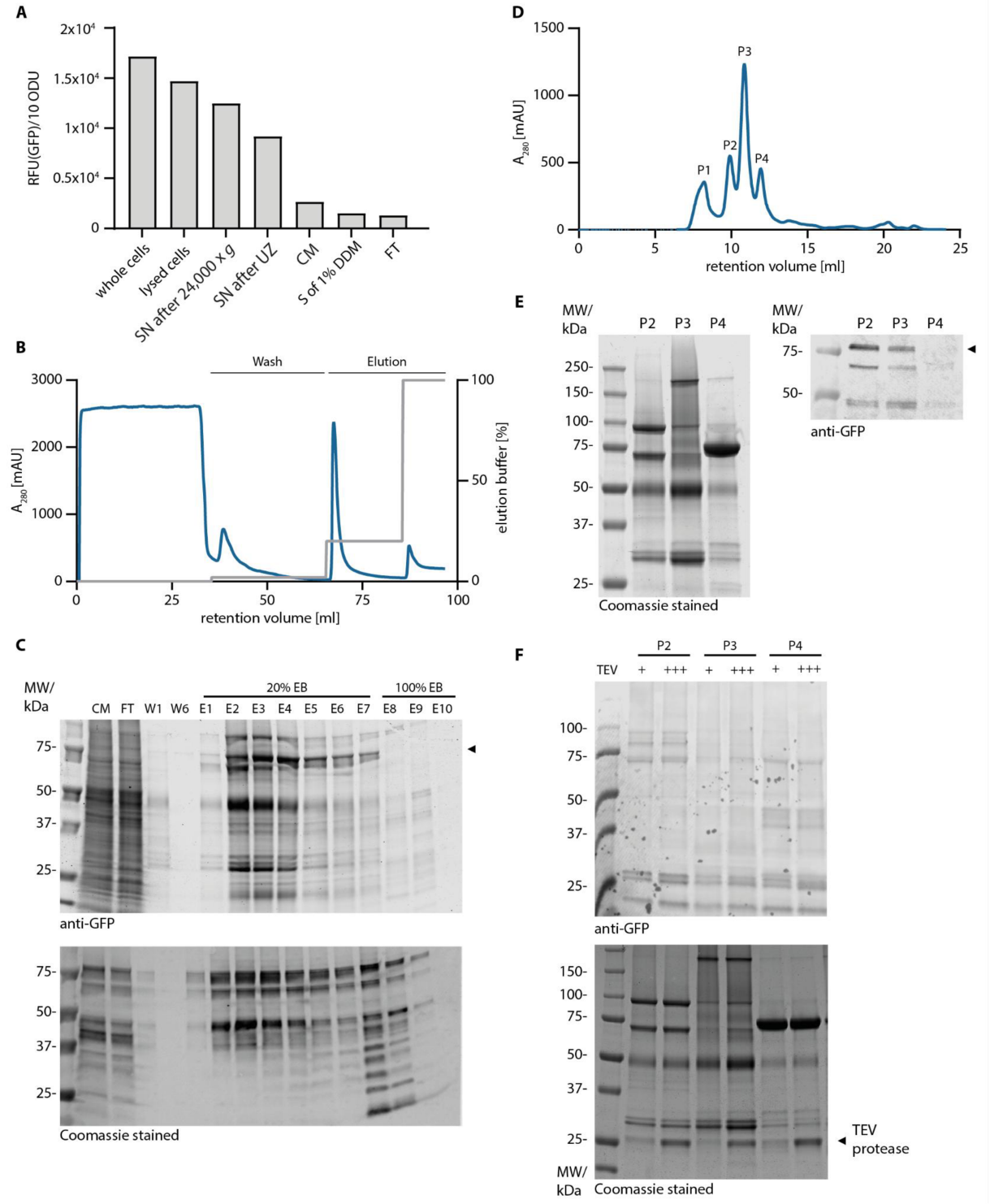

Figure 12 | Purification of Tri-GFP (*E. coli* Mutant56(DE3)).
Purification of Tri-GFP expressed by Mt56 at 30°C before induction and 18°C after induction for 72 h. (**A**) RFU/10 ODU of whole cells, lysed cells, the supernatant after low-speed centrifugation (S after 24,000 x g) and ultracentrifugation (SN after UZ), crude membranes (CM), solubilized IMAC input (S of 1% (w/v) DDM), and flow-through of the IMAC (FT). (**B**) UV (A_{280}) chromatogram after IMAC (blue) and concentration of elution buffer (EB) (gray). (**C**) Immunoblotting (anti-GFP) (top) and Coomassie staining (bottom) after SDS-PAGE of CM and IMAC fractions (FT, wash (W), elution (E)). Tri-GFP is marked by the black arrowhead. (**D**) UV (A_{280}) chromatogram after SEC (Column: Superdex 200 Increase 10/300 GL) (blue). (**E**) Coomassie staining (left) and immunoblotting (anti-GFP) (right) after SDS-PAGE of SEC peaks 1-3. Tri-GFP is marked by the black arrowhead. (**F**) Immunoblotting (anti-GFP) (top) and

Coomassie staining (bottom) after SDS-PAGE of SEC peaks 1-3 after TEV digest (1 µg TEV/100 µg protein (+) or 10 µg TEV/100 µg protein (+++)). Tri-GFP is marked by the black arrowhead. **Repetitions:** A single experiment was performed using the parameters described. However, they are representative of five more experiments with only slight variations in elution buffer concentration and length of the wash and elution steps. TEV digest was only performed once. **Abbreviations**: IMAC: immobilized metal affinity chromatography. A single experiment was performed using the parameters described.

The IMAC elution fractions E1-E7 were pooled and separated by SEC (Column: Superdex 200 Increase 10/300 GL) to remove impurities of non-specifically bound proteins (Fig. 12D). The corresponding UV chromatogram showed four peaks. P1 is typically the void peak containing large protein aggregates. P3 was the highest peak with approximately 1350 mAU. Tri-GFP was detected by immunodetection in P2 and P3 together with two protein fragments of approximately 70 kDa and 50 kDa in size (Fig 12E, left). These were also detectable after IMAC (Fig. 12C) and most likely represent N-terminal degradation products of Tri-GFP, as they were detected by anti-GFP antibodies. However, Coomassie staining revealed the presence of many other proteins in all three peaks (P2-P4) (Fig. 12E, right). The intensity and size of the individual bands did not allow direct assignment of any of the bands to those detected with anti-GFP antibodies.

Next, the peak fractions of P2-P3 were treated with the tobacco etch virus (TEV) protease, which is able to proteolytically cleave the C-terminal GFP-His tag from the transporter at the designated cleavage site between Tri and GFP (Fig. 12F). The TEV digest was tested with two different TEV/protein ratios: 1 µg TEV/100 µg protein or 10 µg TEV/100 µg protein. However, immunodetection and Coomassie staining before and after digestion showed a similar band pattern for both conditions, indicating that the removal of GFP-His was not successful (Fig. 12F). The removal of the C-terminal GFP-His should have resulted in a band shift visible on the gels. This led to the conclusion that this purification did not result in a significant enrichment of Tri-GFP and therefore did not allow further *in vitro* experiments, but rather to an accumulation of impurities.

Despite optimization of expression and solubilization protocols, Tri-GFP could not be successfully purified in large quantities. To address potential membrane insertion or solubility problems caused by the large C-terminal GFP, further expression and purification efforts were performed using an N-terminal 8xHis tag only. Tri-His was expressed in Lemo21 and Mt56 at 18°C at different induction times and rhamnose concentrations (Fig. 13A). In the absence of the GFP tag, evaluation of the different conditions was only possible using immunodetection of the 8xHis tag. *Tri-his* was expressed in both Lemo21 and Mt56 and was detectable after 18, 43, and 67 h after induction in whole cells and crude membranes and at each rhamnose concentration (Fig. 13A). The lowest intensity was detected after 67 h and 1 mM rhamnose in Lemo21 and 67 h in Mt56 (Fig. 13A). Although the expression intensity after 18 h and 43 h was stronger in Lemo21, Mt56 was selected for a solubilization screen based on the previously observed, better membrane localization data. It was tested how well Tri-His could be extracted from the membrane of Mt56 by 1% (w/v) LMNG or DDM. The extraction efficacy of DDM and LMNG was analyzed based on immunodetection of Tri-His in the solubilized and non-solubilized fractions by immunodetection (Fig. 13B). Both detergents were able to extract Tri-

His from the cytoplasmic membrane of Mt56, but a weak band was also visible in the non-solubilized fractions for all protein concentrations tested. On the basis of immunodetection, it was not possible to clearly assess which detergent extracts Tri-his better, so I decided to use the milder detergent LMNG [197], that possibly preserve the native conformations of the proteins, for further experiments.

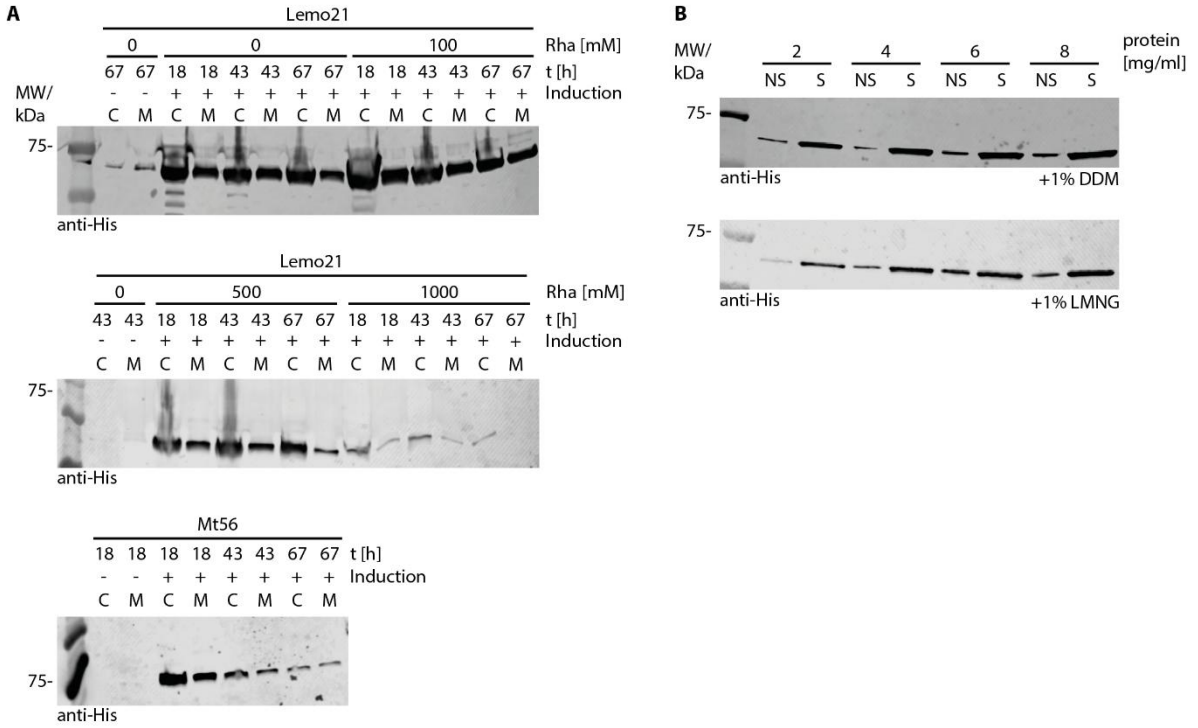

Figure 13 | Overexpression and solubilization of Tri-His in *E. coli* Mutant56(DE3).
(**A**) Immunodetection (anti-His) of Tri-His after SDS-PAGE of whole cells (C) (0.1 ODU) and crude membranes (M) (0.5 ODU) under different growth conditions in TB medium, in Lemo21 or Mt56 at 18°C. (**B**) Immunodetection (anti-His) of solubilized (S) and non-solubilized (NS) fractions after solubilization of crude membranes with 1% (w/v) DDM (top) or LMNG (bottom) with different protein concentrations. **Repetitions:** A single experiment was performed using the parameters described. **Abbreviations**: t: time. A single experiment was performed using the parameters described.

The next step was the purification of Tri-His from Mt56 (Fig. 14). For this, expression was induced in a 3L culture in TB medium at 18°C for 18 hours. After lysis, removal of cell debris, and solubilization with 1% (w/v) LMNG, the solubilized fraction was used for IMAC, which resulted in a large elution peak at 50% (v/v) EB (250 mM imidazole) at approximately 3000 mAU (Fig. 14A, top). Tri-His was detectable in four of the five elution fractions (Fig. 14A, middle). Additionally, a strong band at 50 kDa was detected, which is most likely a degradation product (Fig. 14A, middle). However, after Coomassie staining numerous other bands were visible, indicating the presence of non-specific impurities (Fig. 14A; bottom). Therefore, a second IMAC was performed to reduce the amount of impurities and further purify Tri-His (Fig. 14B). Here, an additional elution step was performed with 10% (v/v) EB (50 mM imidazole) to remove weakly bound proteins from the resin before elution of Tri-His with 50%

(v/v) EB. The UV chromatogram of the second IMAC resulted in two elution peaks, at 10% and 50% (v/v) EB, respectively (Fig. 14B, top). Tri-GFP was detectable in all peak elution fractions at 50% (v/v) EB by immunodetection (Fig. 14B, middle), and a corresponding band was also visible after Coomassie staining (Fig. 14B, bottom). After Coomassie staining of these fractions, fewer bands were visible overall (Fig. 14B, bottom). This and the elution peak in the UV chromatogram at 10% (v/v) EB indicate that the amount of non-specific protein contaminants was reduced after the second IMAC. The fractions of the elution peak at 50% (v/v) EB were then pooled and concentrated using a centrifugal filter with a cutoff of 30 kDa and separated by SEC (Column: Superdex 200 Increase 10/300 GL) (Fig 14C). The SEC resulted in a prominent void peak (P1) of 120 mAU and a second smaller peak (P2) of 10 mAU (Fig. 14C; top). P2 appears at a retention volume of 11 ml which, according to the manufacturer's function test, corresponds to a size of approximately 300 kDa [198]. Analysis with His-specific antibodies showed that Tri-His was present in both peaks, with a stronger signal in the second peak (Fig. 14C; bottom). The difference may be due to the protein being associated with the detergent micelles. In summary, despite successful purification of Tri-His and removal of some impurities, the total amount of protein, as measured by the height of the elution peak (P2) after SEC, was very low. Therefore, this purification approach was not suitable for purifying large quantities of Tri-His for *in vitro* analysis.

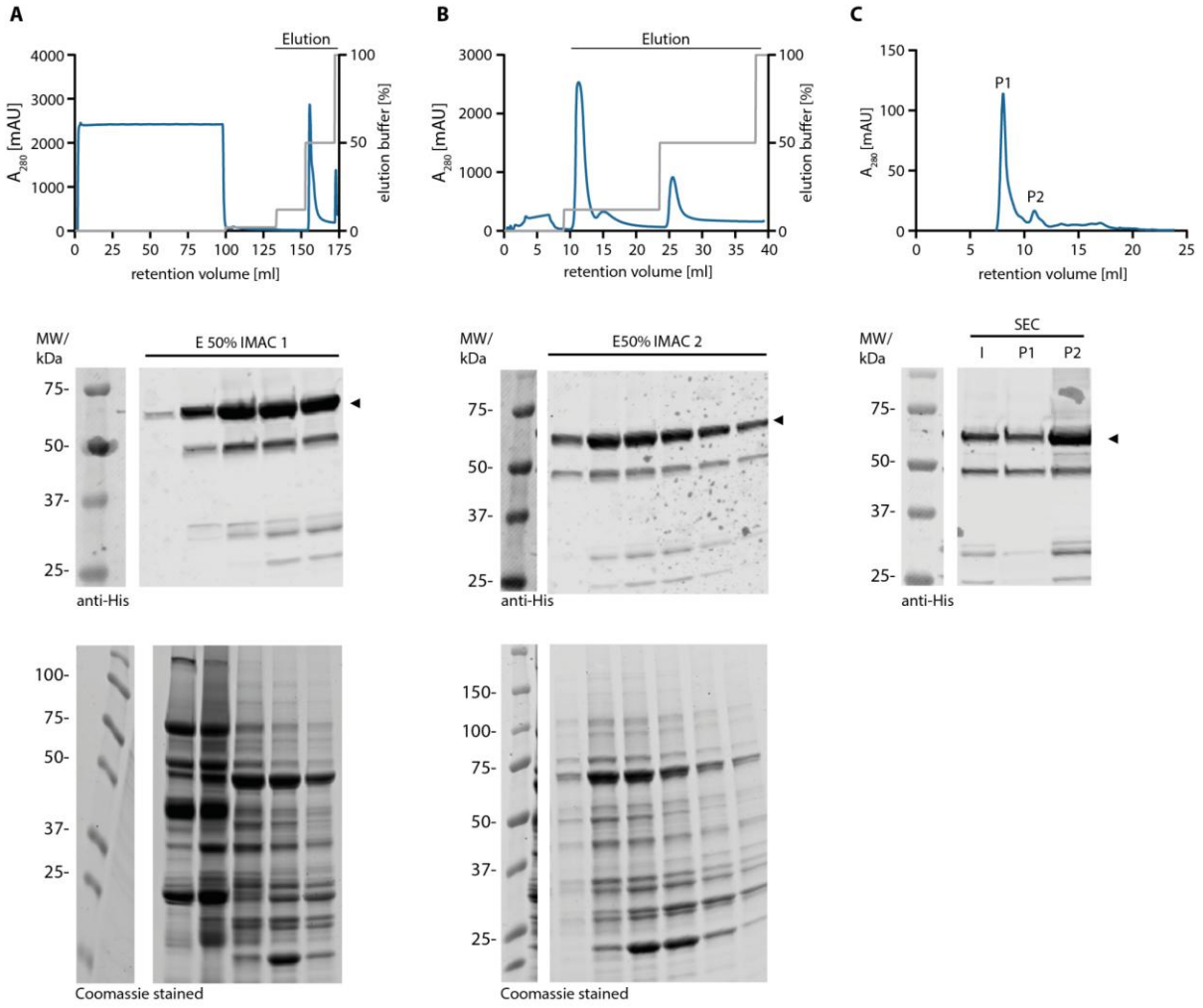

Figure 14 | Purification of Tri-His (*E. coli* Mutant56(DE3)).
Purification of Tri-His expressed by Mt56 at 30°C before induction and 18°C after induction for 18 h in TB medium. (**A**) UV (A_{280}) chromatogram after IMAC1 (blue) and concentration of elution buffer (EB) (gray) (top). Immunodetection (anti-His) (middle) and Coomassie staining (bottom) after SDS-PAGE of elution (E) fractions of IMAC1. Tri-His is marked by the black arrowhead. (**B**) UV (A_{280}) chromatogram after IMAC2 (blue) and concentration of elution buffer (gray) (top). Immunodetection (anti-His) (middle) and Coomassie staining (bottom) after SDS-PAGE of E fractions after IMAC2. Tri-His is marked by the black arrowhead. (**C**) UV (A_{280}) chromatogram after SEC (Column: Superdex 200 Increase 10/300 GL) (blue) (top). Immunodetection (anti-His) (bottom) after SDS-PAGE of input (I) and flow-through (FT) after concentration using Amicon-30 kDa, and I and E fractions after SEC. **Repetitions:** A single experiment was performed using the parameters described. However, they are representative of four more experiments with only slight variations in elution buffer concentration and length of the wash and elution steps.

4.1.4 **Evaluating a solubility-enhancing tag: SUMO**

Initial overexpression experiments and protein localization analysis of Tri and Tba showed promising results, particularly at low temperatures. However, solubilization efforts using different detergents and protein concentrations were inconclusive, and Tri and Tba were only partially extracted from the cytoplasmic membrane, regardless of the affinity tag. This may be due to the transporters being localized at the membrane but not correctly inserted and folded, causing them to aggregate after extraction, or because the detergents tested were not ideal for these specific proteins.
To further improve expression and solubilization, I tested an N-terminal SUMO (small ubiquitin-like modifier) tag. SUMO is an approximately 100 amino acid-long eukaryotic protein involved in regulatory processes that has been used to improve the expression and solubility of recombinant proteins and can be cleaved specifically by the SUMO protease 1 [199]. Although N-terminal tagging is uncommon for membrane proteins, since their targeting and insertion into the cytoplasmic membrane is typically based on the recognition of hydrophobic sequences in the N-terminal region, the SUMO fusion has also been reported to improve the expression and solubility of some membrane proteins [200]. To enable detection and affinity purification, the SUMO tag was fused to an N-terminal 6xHis tag.

In the first step, the expression of *sumo-tri* and *sumo-tba* was tested in *E. coli* strains Lemo21 and Mt56 and assessed by immunodetection of the N-terminal 6xHis tag in whole cells (Fig. 15A+B). Expression of *sumo-tri* was strongest in Lemo21 at 18°C and without the addition of rhamnose (Fig. 15A). Weaker expression was observed in Lemo21 at 30°C. Expression was very low in Mt56 at 30°C and not detectable at 18°C (Fig. 15A). Similarly, with the GFP and 6xHis tags previously tested, expression was detectable at all temperatures tested (30°C, 25°C, and 18°C) (Figs. 4, 9, 13), but the only condition at which membrane localization was clearly shown was 18°C and 15 h induction in Lemo21 (Figs. 8-10). *Sumo-tba* was most strongly expressed in Lemo21 at 30°C, without the addition of rhamnose (Fig. 15B). Lower temperatures and expression in Mt56, however, resulted in very low or no expression (Fig. 15B). Expression was also detected more strongly at 30°C with the GFP tag tested previously (Fig. 4).
The following solubilization test was carried out only for *sumo-tri* expressed in Lemo21 at 18°C without the addition of rhamnose due to the higher levels of protein detected by immunodetection. In addition to the previously used non-ionic detergents LMNG, DMNG, DM, and DDM, five other non-ionic detergents (CYMAL-4, CYMAL-6, GDN, UD, and OG) and three zwitterionic detergents (LDAO, CHAPS, and FC-12) were included. All detergents used and their relative properties are listed in Table 3 (Chapter 7.12). Solubilization was performed as previously described by incubating the crude membranes (5 mg/ml protein concentration) with 1% (w/v) of the respective detergent. The solubilized fraction was then separated from the non-solubilized fraction by ultracentrifugation and analyzed by Coomassie staining after SDS-PAGE (Fig. 15C).

SUMO-Tri was detected at approximately 75 kDa in the crude membranes (CM) (Fig. 15C). A band of similar height and intensity was visible for all detergents used. Only after solubilization

with FC-12 was a significantly stronger band visible (Fig. 15C). The zwitterionic detergent FC-12 is relatively harsh but has been used successfully to extract and stabilize membrane proteins [201]. However, it can also lead to denaturation of protein structures and is known to extract proteins that are already aggregated or misfolded within the membrane [202].

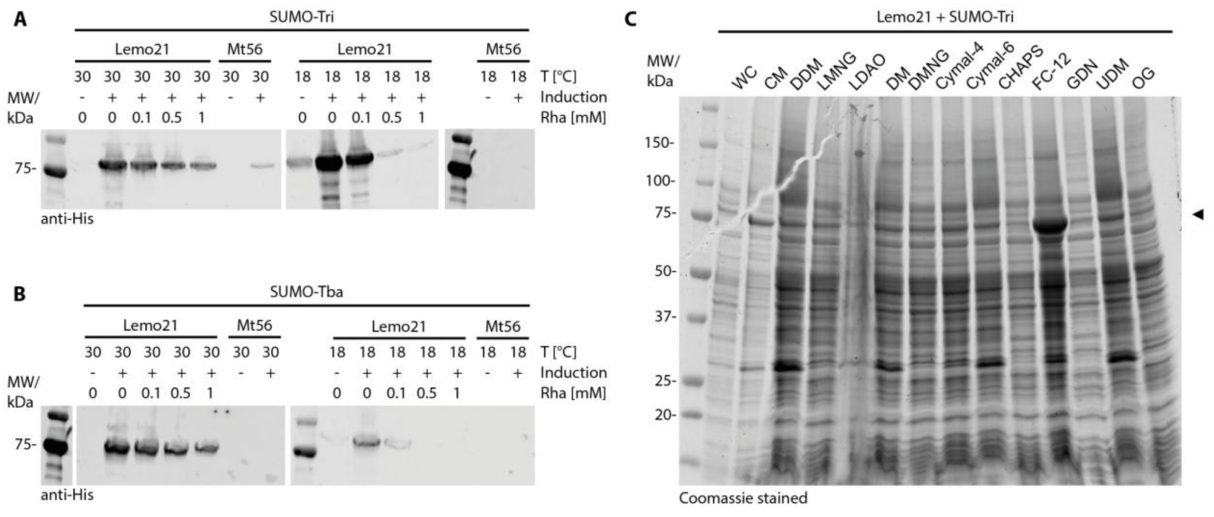

Figure 15 | Overexpression and solubilization screen of SUMO-Tri and SUMO-Tba.
(**A**) Immunodetection (anti-His) of SUMO-Tri and (**B**) SUMO-Tba after SDS-PAGE of whole cells (0.1 ODU) under different growth conditions in Lemo21 and Mt56. (**C**) Coomassie staining after SDS-PAGE of whole cells (WC; 0.1 ODU), crude membranes (CM; 0.5 ODU), and solubilized crude membranes by 1% (w/v) of detergents (depicted in figure) from Lemo21 expressing sumo-tri at 30°C before induction and 18°C after induction without the addition of rhamnose. SUMO-Tri is marked by the black arrowhead. **Repetitions:** A single experiment was performed using the parameters described. **Abbreviations:** T: temperature.

Although the solubilization screen showed that large amounts of SUMO Tri can be solubilized with FC-12, it was not possible to assess whether the protein is functional and correctly folded (Fig. 15C). I therefore tested the solubilization and subsequent purification of SUMO-Tri using FC-12 in comparison with a milder non-ionic detergent, DDM (Fig. 16). Purification was performed as described in the previous section. Briefly, the cells were harvested, lysed by mechanical lysis, cleared from cell debris, and separated into the cytosolic fraction and crude membranes. The crude membranes were then solubilized with 1% (w/v) detergent (6 mg/ml protein concentration), and the soluble fraction was used for IMAC. Immunodetection confirmed that *sumo-tri* was expressed and the majority of the protein was present in the crude membranes (CM), compared to the cytosolic fraction after ultracentrifugation (SN after UZ) (Fig. 16A). However, the chromatograms of the two IMACs performed showed no peak for FC-12-solubilized and only a very small peak for DDM-solubilized samples (Fig. 16B). This means that only very little DDM-solubilized protein was eluted and no FC-12-solubilized protein. SUMO Tri was not detectable by immunodetection in the peak fraction (P1-DDM) but in both flow-through fractions (FT) after IMAC (Fig. 16A). This indicates that the amount of protein in P1-DDM is very low or that some other proteins not specifically bound to the column were eluted. The intensity of the band in the FC-12 flow-through is stronger than in the DDM flow-through, confirming that it solubilized significantly more protein than DDM, in agreement with the results of the solubilization screen described above (Fig. 15B).

The solubilized fractions and the flow-through after IMAC were additionally analyzed using Blue Native PAGE (BN-PAGE), a technique suitable for examining native protein complexes (Fig. 16C). In the FC-12-solubilized fraction and corresponding flow-through, a diffuse band at approximately 200 kDa was visible, whereas in the DDM-solubilized sample and flow-through, only a smear above 1,236 kDa was detected (Fig. 16C). This suggests that solubilization with DDM resulted in aggregation of SUMO-Tri, while solubilization with FC-12 resulted in extraction of a protein complex of approximately 200 kDa. The ABC transporter SUMO-Tri forms a homodimer with a calculated molecular weight of 141.7 kDa. However, running behavior of protein complexes in the BN-PAGE is influenced by the surrounding detergent micelle that results in a higher molecular weight band. The detected band may therefore be a homodimer of SUMO-Tri.

In summary, FC-12 was the only detergent that successfully extracted SUMO-Tri in a potentially correct oligomeric state, whereas DDM led to visible aggregation. Unfortunately, none of the FC-12 solubilized SUMO-Tri bound to the Ni^{2+} resin during IMAC. Possible explanations include that the 6xHis tag was covered by the detergent micelle and was therefore not able to bind to the resin.

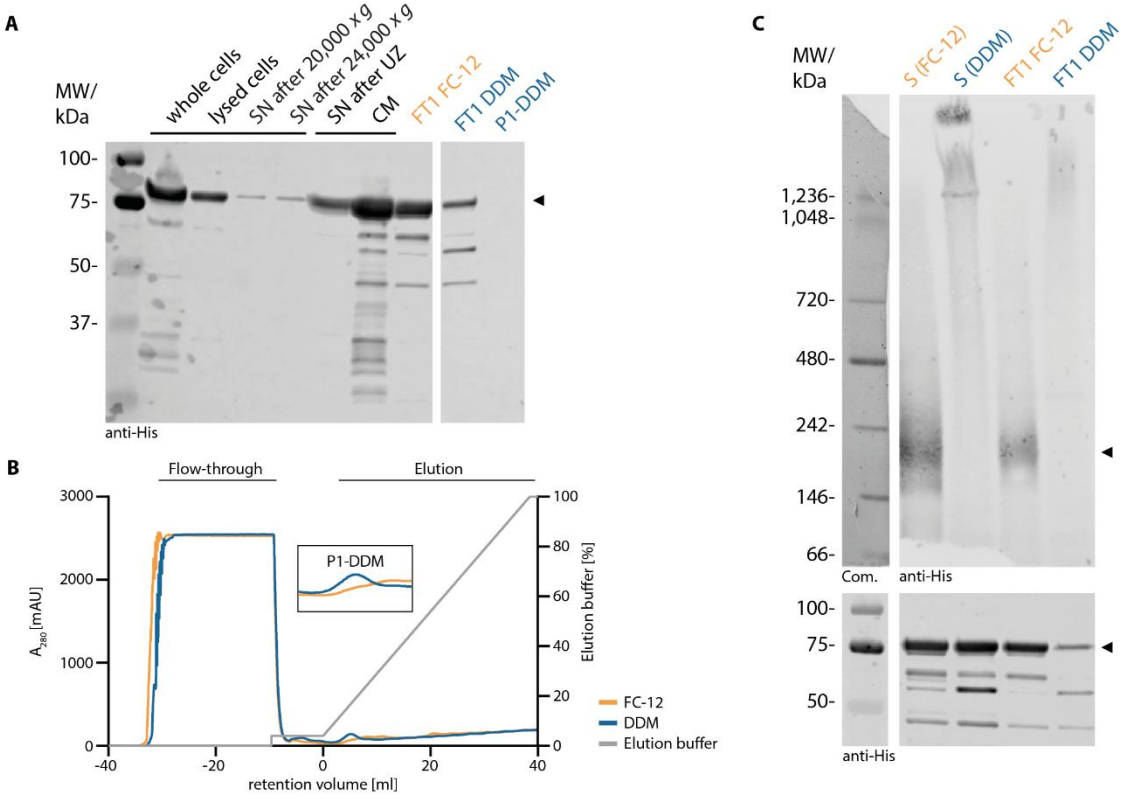

Figure 16 | Purification of SUMO-Tri (*E. coli* Lemo21(DE3)).
Purification of SUMO-Tri expressed in Lemo21 at 30°C before induction and 18°C after induction for 18 h without the addition of rhamnose. Solubilized crude membranes with 1% (w/v) DDM or FC-12. (**A**) Immunodetection (anti-His) after SDS-PAGE of whole cells (0.1 ODU), lysed cells (0.1 ODU), the supernatant after low-speed centrifugations (S after 20,000/24,000 x *g*) (0.1 ODU), the supernatant after ultracentrifugation (SN after UZ) (0.5 ODU), crude membranes (CM) (0.5 ODU), flow-through (FT) after every IMAC, and one peak fraction (0.5 ODU). SUMO-Tri is marked by the black arrowhead. (**B**) UV (A_{280}) chromatogram after IMAC1 with FC-12 (orange) or DDM (blue) solubilized samples. Concentration of the elution buffer is shown in gray. Zoom of P1-DDM is shown in the black box. (**C**) Immunodetection (anti-His) after BN-PAGE (top) and SDS-PAGE (bottom) of solubilized fractions and FT after IMAC (20 µg). **Repetitions:** A single experiment was performed using the parameters described.

4.1.5 **Unconventional expression hosts and switching to the native environment**

The attempts to purify the ABC transporters, Tri and Tba, using different *E. coli* expression hosts only resulted in inefficient purification of Tri. Both transporters originate from bacteria of the genus *Amycolatopsis*. These are Gram-positive bacteria belonging to the phylum Actinomycetota. It is conceivable that the composition of the cytoplasmic membranes of *A. balhimycina* and *A. japonicum* offers some features that favor the insertion and stability of Tba and Tri that are not present in *E. coli*, since they are phylogenetically very distant. To explore this hypothesis, I tested two different expression hosts from the phylum Actinomycetota. On the one hand, for the expression of *tba-3xflag*, I used *Streptomyces lividans* T7 [203], which offers the advantage of T7-based overexpression and stable plasmid maintenance. On the other hand, I used the native organism *A. balhimycina*, in which Tba-3xFLAG was chromosomally integrated into the *ϕC31* attachment site under the control of a strong constitutive promoter (*ermE*p)*.

To test the expression of Tba-3xFLAG in *S. lividans* T7, a 2-day-old preculture in TSB medium was used to inoculate the expression culture, which was incubated for 3 days and Tba-3xFLAG overexpression was induced from the beginning with different concentrations of thiostrepton (Tsr). The cells were then harvested, lysed by mechanical and chemical lysis, cleared from cell debris by centrifugation (10,000 x *g*), and the crude membrane was prepared and analyzed by immunodetection (Fig. 17A). *Tba-3xflag* was expressed under all conditions, but reached its maximum expression level at 6.25 mM Tsr. Thereafter a solubilization screen was carried out using seven different detergents: LMNG, DMNG, DDM, DM, FC-12, GDN and CHAPS. The solubilization was performed after crude membrane preparation (5 mg/ml protein concentration) using 1% (w/v) of the respective detergent and assessed by immunodetection after SDS-PAGE (Fig. 17B) and BN-PAGE (Fig. 17C).

Immunodetection after SDS-PAGE detected Tba-3xFLAG as a strong band in almost every non-soluble sample (NS) and in the samples solubilized with LMNG, DMNG, GDN and CHPAS strong bands in the solubilized fraction (S) were also detected (Fig. 17B). This suggests that these four detergents may be suitable for the extraction of Tba-3xFLAG but not DDM, DM, and FC-12. Immunodetection after BN-PAGE revealed a diffuse band at approximately 350 kDa for LMNG- and DMNG-solubilized samples, indicating extraction of a protein complex (Fig. 17C). For GDN- and CHAPS-solubilized samples, a strong smear was detected from the top of the gel until approximately 480 kDa and 400 kDa (Fig. 17C), respectively, likely representing partial aggregation. In contrast, DDM, DM, and FC-12-solubilized samples did not give any strong band detectable by immunodetection, but only a faint signal above 1,236 kDa (Fig. 17C). Based on these findings, the following affinity purification of Tba-3xFLAG from *S. lividans T7* was performed using induction with 6.25 mM Tsr and membrane solubilization with 1% (w/v) DMNG (Fig. 17D). To this end, the solubilized membrane was mixed and incubated with anti-FLAG antibodies covalently bound to agarose in a batch mode for binding. Non-binding proteins were removed by centrifugation after binding and several washing steps. Tba-3xFLAG was then eluted by the addition of an excess amount of purified 3xFLAG peptide. Tba-3xFLAG was detectable by immunodetection after lysis and remained present until

solubilization (Fig. 17D). However, a significant amount was also present in the supernatant after ultracentrifugation (SN after UZ) and in the non-solubilized fraction after solubilization (Fig. 17D). This suggests further optimization of solubilization conditions is required. Nevertheless, the subsequent FLAG affinity purification resulted in a strong enrichment of Tba-3xFLAG in the elution fraction (E) (Fig. 17D; left). This was also visible by Coomassie staining (Fig. 17D; right). The Coomassie-stained SDS-PAGE gel also showed an additional band below Tba-3xFLAG at about 70 kDa (Fig. 17D; right). This could be a degradation product. However, it is striking that this purification turned out to be highly specific and showed only minimal impurities from non-specifically purified proteins. The total yield of protein in the elution fraction was approximately 370 µg.

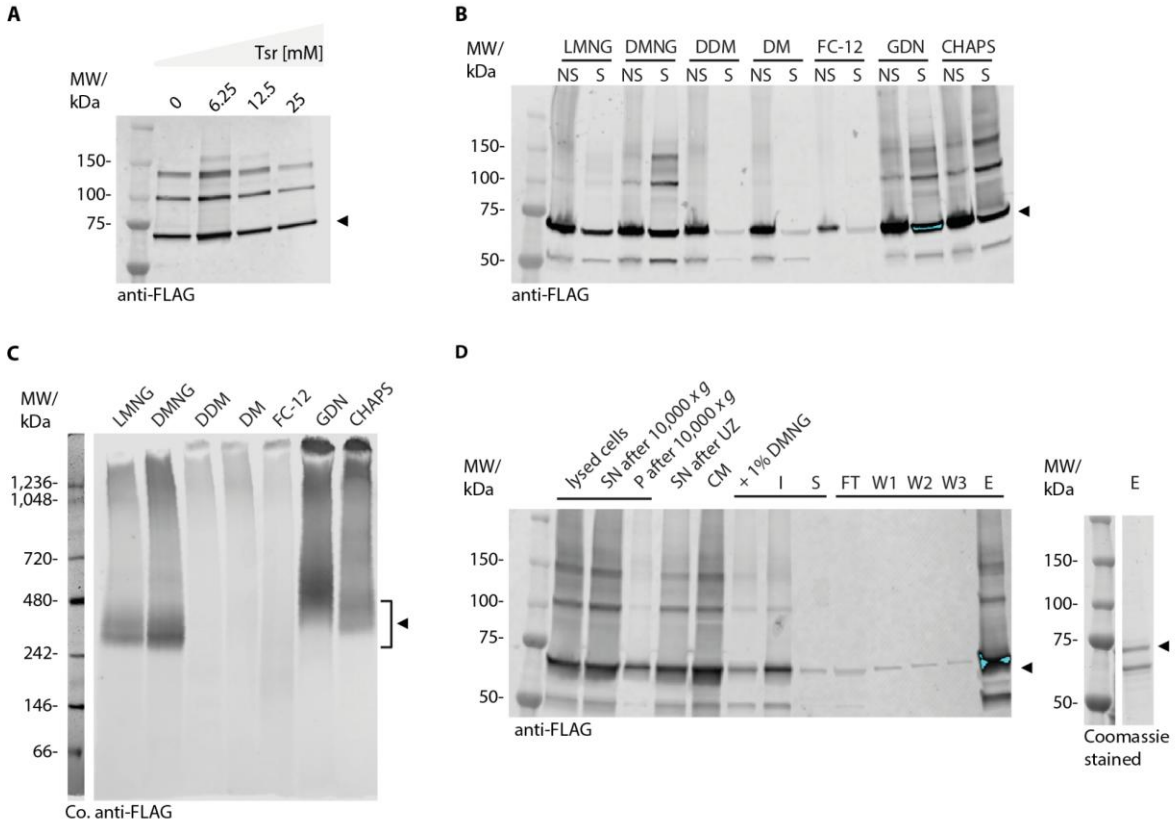

Figure 17 | Overexpression, solubilization, and purification of Tba-3xFLAG (*S. lividans* T7). (**A**) Immunodetection (anti-FLAG) of Tba-3xFLAG in crude membrane (15 µg) of *S. lividans* T7 expressing *tba-3xflag* at different thiostrepton (Tsr) concentrations. Tba-3xFLAG is marked by the black arrowhead. (**B**) Immunodetection (anti-FLAG) of Tba-3xFLAG after SDS-PAGE of solubilized (S) and non-solubilized (I) fractions after solubilization with 1% (w/v) of detergent (depicted in figure). (**C**) Immunodetection (anti-FLAG) of Tba-3xFLAG after BN-PAGE of solubilized (S) fractions after solubilization with 1% (w/v) of detergent (depicted in figure). (**D**) Immunodetection (anti-FLAG) (left) and Coomassie staining (right) of lysed cells; supernatant and pellet after low-speed centrifugation (S/P after 10,000 *x* g); supernatant after ultracentrifugation (SN after UZ); crude membrane (CM), solubilized fraction (+ 1% (w/v) DMNG); non-soluble (NS) fraction; soluble (S) fraction; and affinity chromatography fractions (flow-through (FT); wash (W); elution (E)). **Repetitions:** A single experiment was performed using the parameters described.

Finally, the purification of Tba-3xFLAG from *A. balhimycina*, the native host of Tba, was tested. The bacteria were cultivated under balhimycin-producing conditions for 3 days in R5 medium. Since Tba-3xFLAG is under the control of a constitutive promoter, induction of expression was not necessary. The affinity purification procedure using conjugated 3xFLAG antibodies was performed as described for *S. lividans* T7, with the only difference that LMNG was used instead of DMNG for solubilization.

Affinity purification again resulted in minimal non-specific binding, as most proteins were present in the flow-through (FT), and Tba-3xFLAG was detected mainly in the elution fraction (E) by immunodetection (Fig. 18A) and Coomassie staining (Fig. 18A). The elution fraction was then concentrated using a centrifugal filter with a cut-off of 30 kDa (Amicon) and subjected to SEC (Column: Superdex 200 Increase 10/300 GL). The corresponding chromatogram revealed three peaks, P1-P3 (Fig. 18B). P1 (void peak) and P2 had similar heights of approximately 20 mAu, while P3 was significantly higher with approximately 90 mAU (Fig. 18C). BN-PAGE confirmed that Tba-3xFLAG was exclusively present in P2, forming a band with a size of approximately 300-400 kDa (Fig. 18D). Therefore, P3 most likely contained the FLAG peptide that was used for elution. Interestingly, Tba-3xFLAG was detected at different heights after SDS-PAGE of the elution fraction (E) following affinity purification by immunodetection (Fig. 18A) and Coomassie staining (Fig. 18B). To investigate this, mass spectrometry (MS) was performed on all three bands of this fraction. Tba-3xFLAG was identified in fractions E1–E3 with the highest intensity of all proteins detected (Fig. 18E). Surprisingly, proteins involved in the balhimycin biosynthesis were co-purified and detected by MS, including the NRPS enzymes BpsB and BpsC, the halogenase BhaA, and the glycosyltransferase BgtfA (Fig. 18F). In addition, other transporters, proteins of the bacterial respiratory chain, the primary metabolism, cytoplasmic chaperones, and ribosomal subunits were identified, mainly in E1 and E2. A Paraslipin was found in E2 and a flotillin-like protein in E3, both belonging to the Stomatin, Prohibitin, Flotillin, and HflK/C (SPFH) protein family [31]. The co-purification of proteins suggests possible interactions with the bait protein Tba-3xFLAG. However, this would require further verification by means of additional experiments.

Switching the expression host to a near-native or native system and using the 3xFLAG affinity tag clearly resulted in a cleaner purification with minimal impurities of additional proteins compared to the previously tested *E. coli* system in combination with a GFP, His, or SUMO tag. Under these conditions, solubilization using mild detergents proved feasible, suggesting that the extracted protein is likely to be in the correct oligomeric state. Although protein yields remained low, the purified material was of high-purity. Both expression hosts proved to be promising, indicating that future efforts should focus on optimizing expression levels to enhance the overall yield.

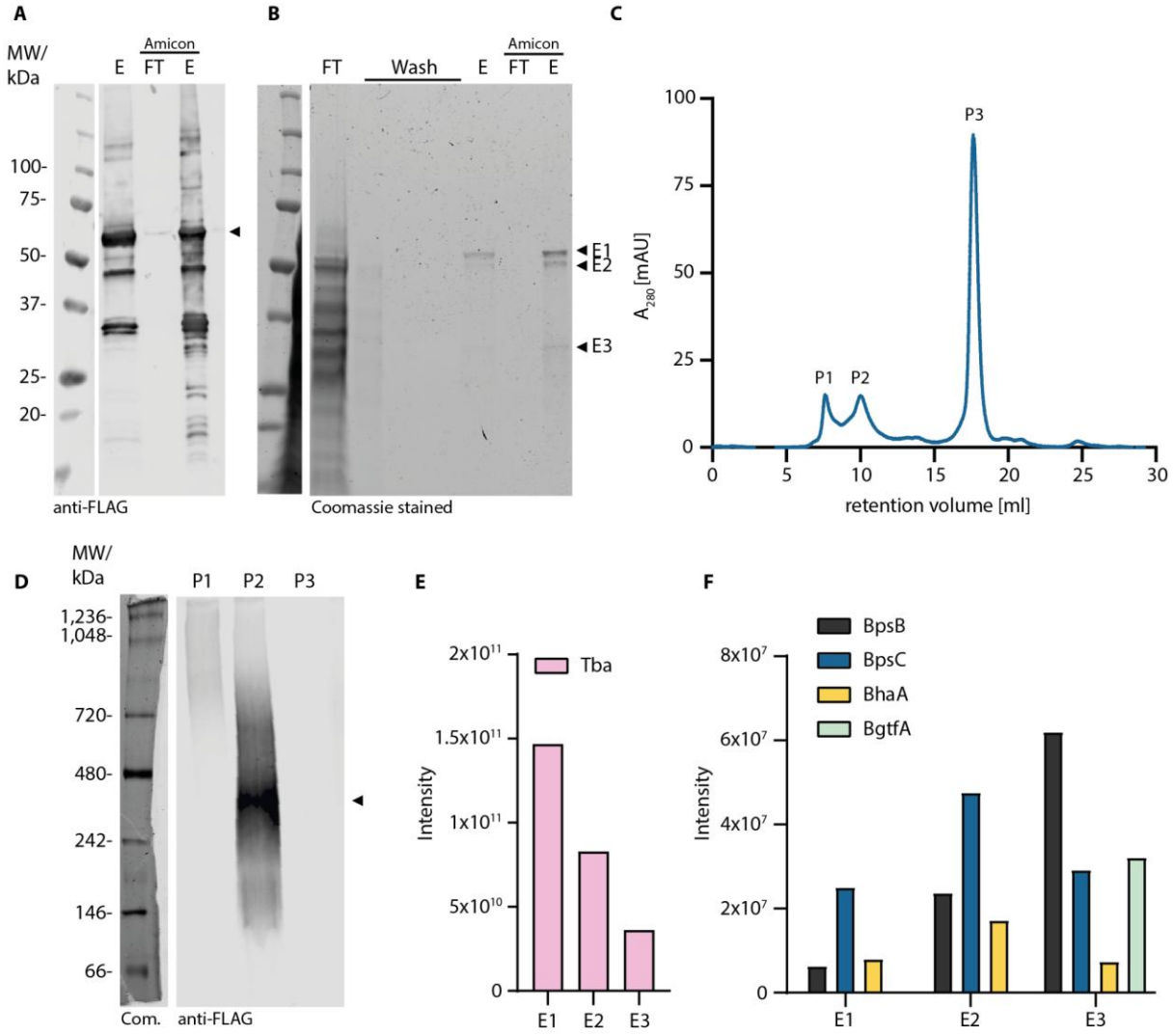

Figure 18 | Purification of Tba-3xFLAG (*A. balhimycina*).
Affinity purification (FLAG) followed by SEC (Column: Superdex 200 Increase 10/300 GL) of Tba-3xFLAG expressed in *A. balhimycina*. (**A**) Immunodetection (anti-FLAG) and (**B**) Coomassie staining (right) after SDS-PAGE of flow-through (FT), wash (W), and elution (E) fractions after affinity purification, and FT and E after concentration using Amicon-30 kDa. (**C**) UV (A_{280}) chromatogram after SEC with concentrated E fractions. (**D**) Immunodetection (anti-FLAG) after BN-PAGE of SEC peaks 1-3 (15 µl of each peak). (**E**) LFQ intensities of Tba-3xFLAG of E bands 1-3. (**F**) LFQ intensities of BpsB, BpsC, BhaA, and BgtfA of E bands 1-3. **Repetitions:** A single experiment was performed using the parameters described. **Abbreviations:** LFQ: Label-free quantification.

4.2 Publication 1: Unveiling the substrate specificity of the ABC transporter Tba and its role in glycopeptide biosynthesis

Gericke, N., Beqaj, D., Kronenberger, T., Kulik, A., Gavriilidou, A., Franz-Wachtel, M., Schoppmeier, U., Harbig, T., Rapp, J., Grin, I., Ziemert, N., Link, H., Nieselt, K., Macek, B., Wohlleben, W., Stegmann, E., Wagner, S., Unveiling the substrate specificity of the ABC transporter Tba and its role in glycopeptide biosynthesis, ISCIENCE (2025)

DOI: *https://doi.org/10.1016/j.isci.2025.112135*.

This chapter is a publictaion Therefore, the reference numbers used in this chapter (4.2) correspond to the bibliography in this chapter and not to the general bibliography of this work. Furthermore, the numbering of the figures and tables does not correspond to the numbering of figures and tables in the other chapters of this work. An overview of all figures and tables in this thesis can be found in the "List of Figures" and "List of Tables".

iScience

Article

Unveiling the substrate specificity of the ABC transporter Tba and its role in glycopeptide biosynthesis

Graphical abstract

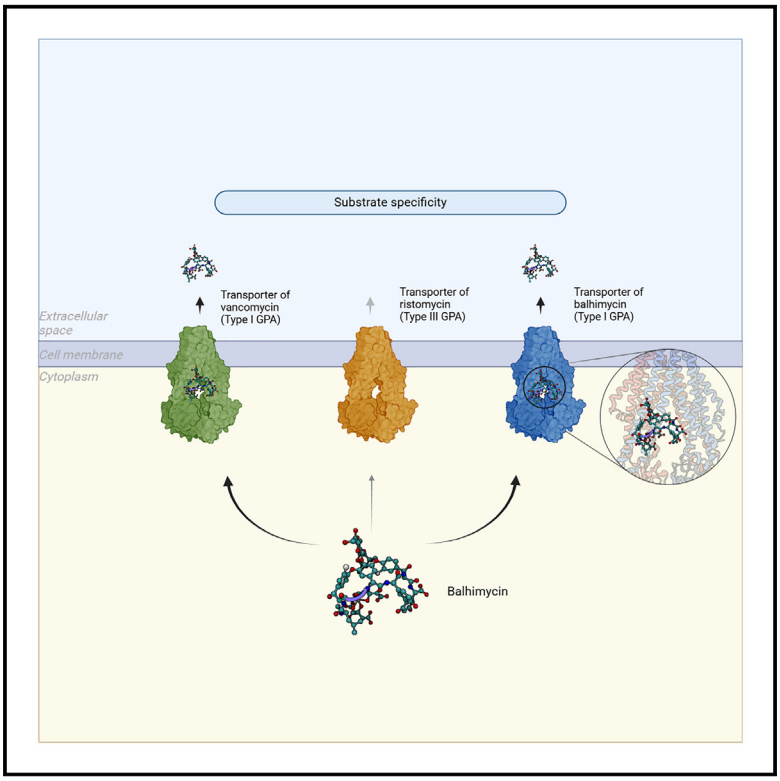

Authors

Nicola Gericke, Dardan Beqaj, Thales Kronenberger, ..., Wolfgang Wohlleben, Evi Stegmann, Samuel Wagner

Correspondence

evi.stegmann@uni-tuebingen.de (E.S.), samuel.wagner@med.uni-tuebingen.de (S.W.)

In brief

Biosynthesis; Biochemistry; Chemical synthesis

Highlights

- Tba recognizes balhimycin's backbone, rather than its attached modifications
- The biosynthesis of balhimycin is dependent on a functional ABC transporter
- Proximity labeling suggests Tba interacts with the biosynthetic machinery

Gericke et al., 2025, iScience *28*, 112135
April 18, 2025
https://doi.org/10.1016/j.isci.2025.112135

CellPress

iScience

CellPress
OPEN ACCESS

Article

Unveiling the substrate specificity of the ABC transporter Tba and its role in glycopeptide biosynthesis

Nicola Gericke,[1,11] Dardan Beqaj,[2,11] Thales Kronenberger,[1,3,4] Andreas Kulik,[2] Athina Gavriilidou,[5] Mirita Franz-Wachtel,[6] Ulrich Schoppmeier,[1,7] Theresa Harbig,[8] Johanna Rapp,[7,9] Iwan Grin,[1] Nadine Ziemert,[3,5] Hannes Link,[7,9] Kay Nieselt,[8] Boris Macek,[6] Wolfgang Wohlleben,[3,7,10] Evi Stegmann,[2,3,7,12,*] and Samuel Wagner[1,3,7,*]

[1]Cellular and Molecular Microbiology, Interfaculty Institute of Microbiology and Infection Medicine (IMIT), University of Tübingen, Elfriede-Aulhorn-Str. 6, 72076 Tübingen, Germany

[2]Microbial Active Compounds, Interfaculty Institute of Microbiology and Infection Medicine (IMIT), University of Tübingen, Auf der Morgenstelle 28, 72076 Tübingen, Germany

[3]Partner-Site: DZIF Tübingen, Elfriede-Aulhorn-Str. 6/Auf der Morgenstelle 28, 72076 Tübingen, Germany

[4]School of Pharmacy, Faculty of Health Sciences, University of Eastern Finland, Yliopistonrinne 3, 70211 Kuopio, Finland

[5]Translational Genome Mining for Natural Products, Interfaculty Institute of Microbiology and Infection Medicine Tübingen (IMIT), University of Tübingen, Auf der Morgenstelle 24, 72076 Tübingen, Germany

[6]Proteome Center Tübingen, Institute of Cell Biology, University of Tübingen, Auf der Morgenstelle 15, 72076 Tübingen, Germany

[7]Excellence Cluster "Controlling Microbes to Fight Infections" (CMFI), University of Tübingen, 72076 Tübingen, Germany

[8]Interfaculty Institute for Bioinformatics and Medical Informatics (IBMI), University of Tübingen, Sand 14, 72076 Tübingen, Germany

[9]Bacterial Metabolomics, Interfaculty Institute of Microbiology and Infection Medicine (IMIT), University of Tübingen, Auf der Morgenstelle 28, 72076 Tübingen, Germany

[10]Microbiology/Biotechnology, Interfaculty Institute of Microbiology and Infection Medicine (IMIT), University of Tübingen, Auf der Morgenstelle 28, 72076 Tübingen, Germany

[11]These authors contributed equally

[12]Lead contact

*Correspondence: evi.stegmann@uni-tuebingen.de (E.S.), samuel.wagner@med.uni-tuebingen.de (S.W.)

https://doi.org/10.1016/j.isci.2025.112135

SUMMARY

Glycopeptide antibiotics (GPA) such as vancomycin are essential last-resort antibiotics produced by actinomycetes. Their biosynthesis is encoded within biosynthetic gene clusters, also harboring genes for regulation, and transport. Diverse types of GPAs have been characterized that differ in peptide backbone composition and modification patterns. However, little is known about the ATP-binding cassette (ABC) transporters facilitating GPA export. Employing a multifaceted approach, we investigated the substrate specificity of GPA ABC-transporters toward the type-I GPA balhimycin. Phylogenetic analysis suggested and *trans*-complementation experiments confirmed that balhimycin is exported only by the related type I GPA transporters Tba and Tva (transporter of vancomycin). Molecular dynamics simulations and mutagenesis experiments showed that Tba exhibits specificity toward the peptide backbone rather than the modifications. Unexpectedly, deletion or functional inactivation of Tba halted balhimycin biosynthesis. Combined with proximity biotinylation experiments, this suggested that the interaction of the active transporter with the biosynthetic machinery is required for biosynthesis.

INTRODUCTION

Glycopeptide antibiotics (GPAs) belong to a diverse class of bioactive compounds synthesized by various actinomycetes. Notable examples include vancomycin and teicoplanin, which are clinically used to treat infections caused by multidrug-resistant gram-positive bacterial pathogens.[1]

Based on their backbone composition, GPAs have been classified into five structural subclasses. Type I-IV GPAs are commonly referred to as ''true'' GPAs.[2] They share a similar backbone composition, featuring type-specific amino acids (aa) at positions aa1 and aa3 with either aliphatic (l) or aromatic (II, III, IV) side chains. However, the modification pattern of the backbone varies between GPAs within the same type.[3] Type V GPAs have recently been classified as glycopeptide-related peptides (GRPs) due to significant differences in structural, phylogenetic, and functional features.[4] GPA backbones are synthesized by non-ribosomal peptide synthetases (NRPS)[5] from both proteinogenic and non-proteinogenic aa. During peptide assembly the aromatic side chains are halogenated and cross-linked by dedicated enzymes, resulting in the antibiotic's characteristic multicyclic and cup-shaped structure.[6–8] Following peptide assembly, additional diversifications such as glycosylation, acylation, methylation, and sulfonation occur.[9] The enzymes

responsible for these modifications are typically encoded within biosynthetic gene clusters (BGCs).

The export of GPAs represents the last step in their biosynthesis process. To date, only one transporter associated with GPAs, the transporter of the type I (vancomycin type) GPA balhimycin (Tba) in *Amycolatopsis balhimycina* has been functionally characterized.[10] This ATP-binding cassette (ABC) transporter specifically mediates the export of balhimycin and is not involved in self-resistance.[10,11] ABC transporters form a large superfamily of integral membrane proteins and are known to facilitate ATP-driven transport of various substrates across the cytoplasmic membrane. However, they may fulfill other roles in addition to transport.[12] ABC transporters can be associated with accessory domains,[13] play a vital role in the biosynthesis of their substrates,[14,15] or be involved in producer's self-immunity.[16,17] The latter is particularly relevant to ABC transporters within BGCs encoding compounds with antimicrobial activity.

Considering the paucity of data on how the processes of biosynthesis and export of GPAs are coordinated, we performed a comprehensive investigation of the specificity and functional roles of GPA-associated transporters, with a particular emphasis on the ABC transporter of balhimycin, Tba. Phylogenetic analysis, molecular dynamics simulation (MD simulation), and transport assays revealed that the specificity of Tba toward GPAs of the same type as balhimycin is dictated by the peptide backbone rather than the sugar modifications. Unexpectedly, deletion or functional inactivation of Tba did not lead to intracellular accumulation of balhimycin, suggesting a regulatory role of the transporter in balhimycin biosynthesis. This notion was supported by the observation that the transporter is in close proximity to the biosynthetic machinery.

RESULTS

Bioinformatic analysis and phylogenetic reconstitution of GPA ABC transporters suggest type-associated specificity

Members of the ABC transporter family share a similar architecture consisting of two cytoplasmic nucleotide binding domains (NBD) responsible for ATP binding and hydrolysis, coupled with two transmembrane domains (TMD) forming the substrate translocation pathway at their mirror axis.[18] Based on these features, we searched for putative ABC transporter genes in 89 GPA and GRP BGCs from producers of various families such as *Pseudonocardiaceae*, *Streptosporangiaceae*, *Micromonosporaceae*, *Streptomycetaceae*, and *Nocardiaceae.* Our analysis identified a single gene encoding a putative transporter in each BGC (Table S1).

Analysis of transmembrane topology based on prediction of the membrane integration propensity of segments of the protein sequence,[19] revealed six hydrophobic regions in the N-terminal half of all scanned proteins (exemplary in Figure S1). Furthermore, typical motifs for functional NBDs -Walker A, Walker B, and ABC signature motif (C-loop) as well as A-, Q-, D loop, and H-switch[18]- were identified in the C-terminal half of every protein. These findings strongly suggest that the GPA BGCs encode a homodimeric ABC transporter with six transmembrane (TM) helices per TMD, wherein each half-transporter consists of one TMD and one NBD, similar to Tba.[10] All transporters shared an aa sequence identity of more than 50% (Figure S2). Notably, sequence identities between transporters from putative type I-IV GPA BGCs were substantially higher than those to the transporters of GRP BGCs (Figure S2). Transporters with the highest similarity to Tba (88% sequence identity) were identified in *Amycolatopsis orientalis* DSM 40400, *Amycolatopsis keratiniphila* HCCB10007, and *Amycolatopsis regifaucium* DSM45072. These strains harbor BGCs for vancomycin (the first two)[20,21] and decaplanin,[22] both of which, like balhimycin, are type I GPAs.

To determine the substrate spectrum of the identified transporters, we investigated their evolutionary relationship with GPAs. Using all 89 transporter sequences, we generated a phylogenetic tree employing the maximum likelihood algorithm (Figure S3), with an unrelated ABC transporter (Abc30) from *A. balhimycina* serving as an outgroup. By correlating the transporters with the GPA known GPA/GRP types I-V[4] potentially encoded by the BGCs that also encode the respective transporter, we have categorized them according to these, creating a classification based on their substrates (in colors, Figure S3). Type V (GRP) transporters form a distinct cluster separate from all type I-IV transporters in the phylogenetic tree, indicating an earlier evolutionary divergence and significant differences in their putative substrates. Consequently, our focus was exclusively on type I-IV GPA transporters. Consistent with the high sequence identity, phylogenetic analysis of only type I-IV GPAs did not reveal distinct and widely separated clades, but a rough grouping of transporters associated with the export of GPAs of the same type, indicating an underlying specificity for them (in colors, Figure 1). Transporters exporting GPAs of the same type but with different modification patterns tended to cluster closely together (Figure 1). For example, balhimycin, decaplanin, and vancomycin, which share a type I backbone but vary in glycosylation patterns, formed a distinct clade (Bootstrap >81.6%). These findings indicate that the evolutionary trajectory of the transporters follows that of the BGCs, as these also build clades based on GPA type.[23] They also suggest that the specificity of the transporters may be associated with the peptide backbone rather than its modifications.

GPA-associated ABC transporters demonstrate specificity in exporting their native substrates

In silico analyses and phylogenetic reconstitution of putative ABC transporters of GPAs suggested a significant degree of similarity among them. To empirically confirm their substrate specificity, we developed an *in vivo* system based on *trans* complementation of an *A. balhimycina* Δ*tba* mutant. To this end, we constructed the *A. balhimycina* Δ*tba* deletion and evaluated balhimycin export using high-performance liquid chromatography-mass spectrometry (HPLC-MS). Specifically, we quantified balhimycin in culture supernatants and mycelium extracts obtained from a 96-h culture of *A. balhimycina* wildtype and *A. balhimycina* Δ*tba* under balhimycin-producing conditions. The HPLC-MS results confirmed the presence of balhimycin in both strains, with prominent peaks corresponding to fully glycosylated (*m/z* 1587.49 $[M+H]^+$), double-glycosylated (*m/z* 1446.41 $[M+H]^+$), and mono-glycosylated (*m/z* 1305.34 $[M+H]^+$) derivatives in each sample (Figures 2A, 2B and S4). Since accurate

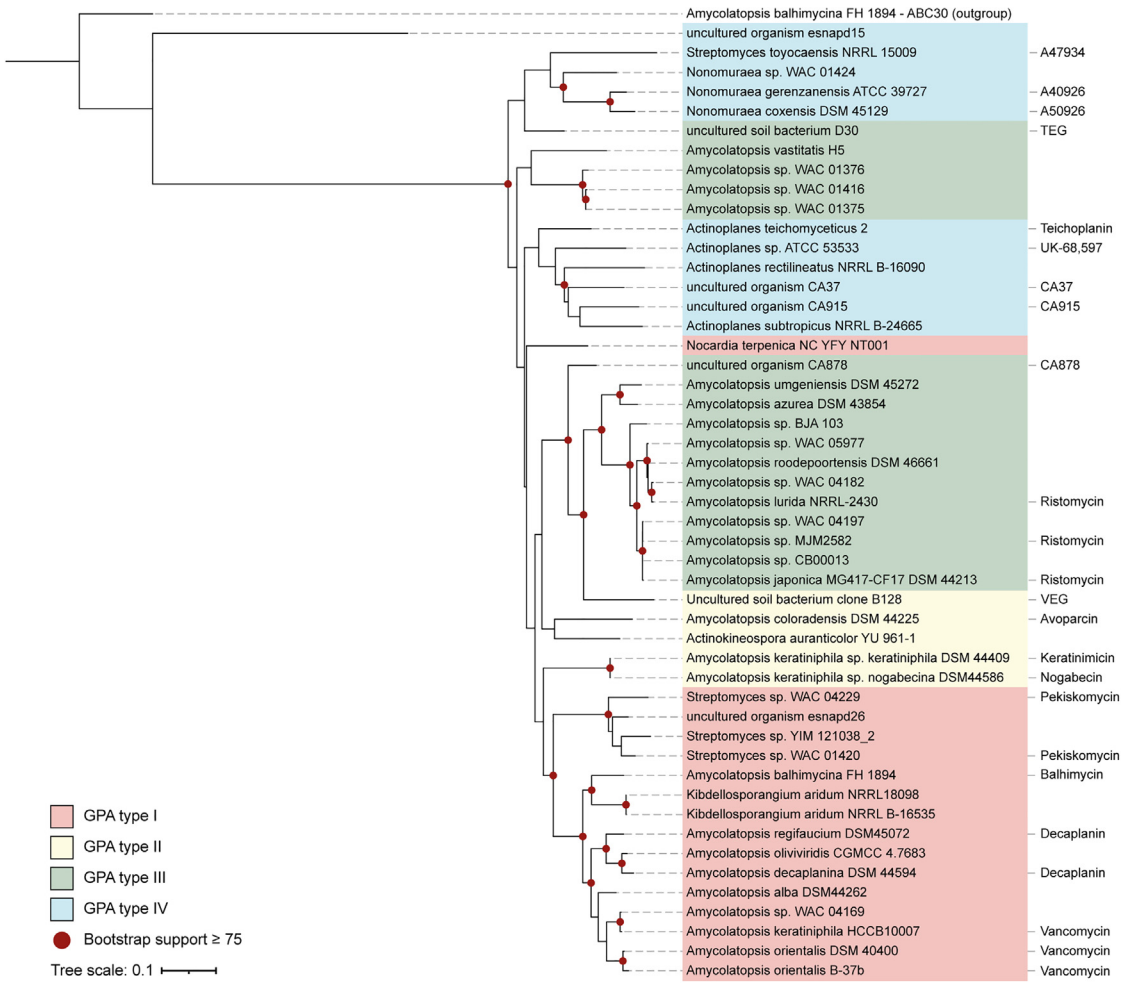

Figure 1. Evolutionary relationship within the group of GPA ABC transporters

Phylogenetic tree (maximum likelihood (LG + F + G) algorithm with 1,000 bootstrap repetitions) of ABC transporters encoded in BGCs of GPAs. Nodes with bootstrap support ≥75% are marked by red dots on the branches. The tree was rooted using a putative ABC transporter encoded in an uncharacterized BGC in A. balhimycina (Abc30). The strain from which the BGC and thus the associated ABC transporter originates is indicated in the tree. (Predicted) GPA types are labeled accordingly: type I (red), type II (yellow), type III (green), type IV (blue). Known and predicted GPAs are mentioned behind the branches.

protein concentrations of the produced transporter could not be measured due to purification constraints, we relied on HPLC-MS results for quantification, normalizing to dry cellular weight for better comparability (Figures 2C and 2D).

The extracellular amount of balhimycin in *A. balhimycina* Δ*tba* was significantly reduced in comparison to *A. balhimycina* wildtype, by a factor of 50 (Figure 2C), in accordance with previous results.[10] Unexpectedly, the level of balhimycin that accumulated intracellularly in *A. balhimycina* Δ*tba* was approximately 70-fold lower than the level of balhimycin exported by *A. balhimycina* wildtype, indicating impaired biosynthesis. To confirm that the reduction of balhimycin in *A. balhimycina* Δ*tba* resulted solely from the deletion of *tba*, we complemented the mutant with the native *tba* gene and with tba^{3xFLAG} under the control of a strong constitutive promoter (*ermE*p*).[24] Each gene was integrated into the genome at an ectopic locus, specifically the *ΦC31* attachment site. The expression of *tba* with a 3xFLAG epitope tag enabled us to verify the production and dimerization of the transporter via immunoblot analysis. Both complementations restored balhimycin export function in *A. balhimycina* Δ*tba* (Figure 2C), although not to wildtype levels, possibly due to the integration of the gene at a non-native locus. Statistical analysis revealed no significant difference between the amount of balhimycin exported by Tba or Tba^{3xFLAG} (Table S4), suggesting that the C-terminal epitope tag did not affect the export function of Tba.

To investigate the substrate specificity of Tba, we complemented *A. balhimycina* Δ*tba* with genes coding for putative GPA transporters and a non-GPA transporter. We used transporters encoded in the BGC of vancomycin (Tva) from *A. keratiniphila* HCCB10007 and ristomycin (Tri) from *A. japonica* MG417-CF17 DSM 44213, both with a 3xFLAG epitope tag. Vancomycin (type I) differs from balhimycin only in the glycosylation pattern (Figure 3A), while ristomycin (type III)

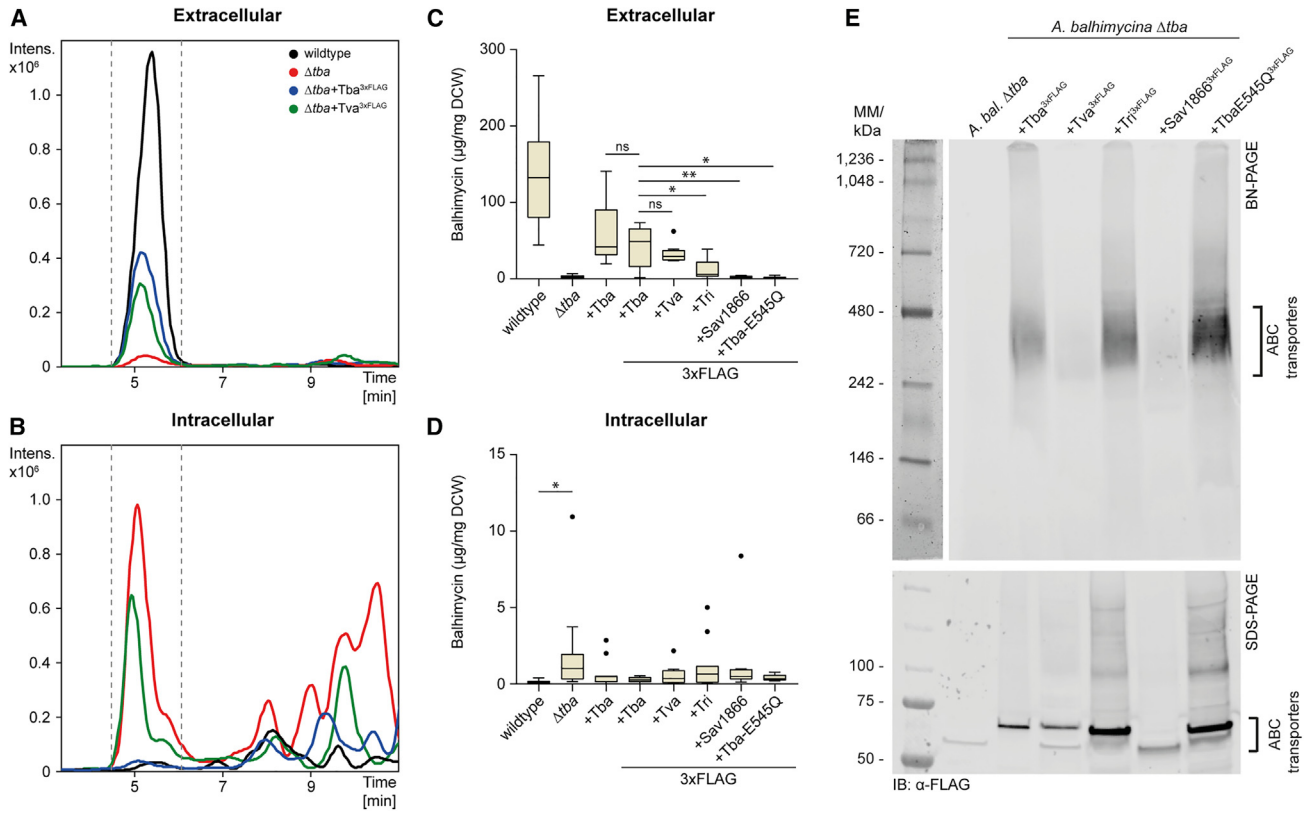

Figure 2. Analysis of complementation efficiency of *A. balhimycina* Δ*tba* using HPLC-MS detection of balhimycin

(A and B) Raw (not normalized) HPLC-MS chromatograms of the culture supernatants (A) and mycelium extracts (B) of *A. balhimycina* wildtype (black), Δ*tba* (red), Δ*tba*+*tba*^{3xFLAG} (blue), and Δ*tba*+*tva*^{3xFLAG} (green). The peaks (retention time 5–5.5 min) represent the extracted ion chromatogram (EIC) of the protonated balhimycin mass *m/z* 1446.41 $[M+H]^+$ (positive mode, smoothed 10.63–10.76 GA) (Figure S4).

(C and D) Quantification of extracellular (C) and intracellular (D) levels of balhimycin in *A. balhimycina* and respective mutant strains based on HPLC-MS data. Values were normalized to the dry cell weight (DCW). All data are shown in boxplot representation. Error bars indicate standard deviations. Statistical outliers are displayed as dots. Statistically significant differences are highlighted with asterisks ($p < 0.05$ (*); $p < 0.01$ (**)) (“Wilcoxon signed-rank test” and “Benjamini-Hochberg procedure”) (Table S2).

(E) Immunoblotting after BN- (top) and SDS-page (bottom) of solubilized crude membranes of *A. balhimycina* Δ*tba* and respective mutant strains. Detection with 3xFLAG specific antibodies.

differs in the aa composition of the backbone and has a higher degree of glycosylation compared to balhimycin (Figure S5). All complemented mutants were compared with *A. balhimycina* Δ*tba*+*tba*^{3xFLAG} instead of the wildtype, ensuring a consistent starting point for analysis. Our results showed significant differences in the export of balhimycin by the ABC transporters used. Tva^{3xFLAG} exhibited a similar export to Tba^{3xFLAG}, with no significant difference ($p > 0.05$). In contrast, Tri^{3xFLAG} exported significantly less ($p = 0.03$) balhimycin than Tba^{3xFLAG}. Intracellularly, we observed only a slight accumulation of balhimycin in presence of Tva^{3xFLAG} or Tri^{3xFLAG} compared to Tba^{3xFLAG}, but similar to *A. balhimycina* Δ*tba*, it was only detectable at very low levels (<1% of wildtype production). For complementation with a gene encoding a non-GPA ABC transporter, we selected the unrelated but well characterized multidrug transporter Sav1866 from *Staphylococcus aureus*,[25] which shares only 33% sequence identity with Tba. In our assay, no export by Sav1866^{3xFLAG} was detected mirroring the findings from *A. balhimycina* Δ*tba*. Additionally, no significant intracellular accumulation was detectable.

The presence of the 3xFLAG epitope tag allowed us to verify proper production and insertion of the transporters into the membrane. This validation was crucial, particularly for transporters exhibiting minimal or no balhimycin export. All ABC transporters were detectable in the membrane fraction by immunodetection after SDS-PAGE (Figure 2E). Furthermore, BN-PAGE analysis following membrane solubilization with the nonionic detergent LMNG demonstrated that each transporter was detectable at the expected size (Figure 2E), indicating that neither aggregation nor incorrect dimerization significantly contributed to the reduced transport activity. However, the varying intensity of the bands indicated that the transporters differ in their accumulation levels in the membrane. For precise protein quantification, alternative methods should be considered in future studies to enable more accurate normalization and comparison of different transporters.

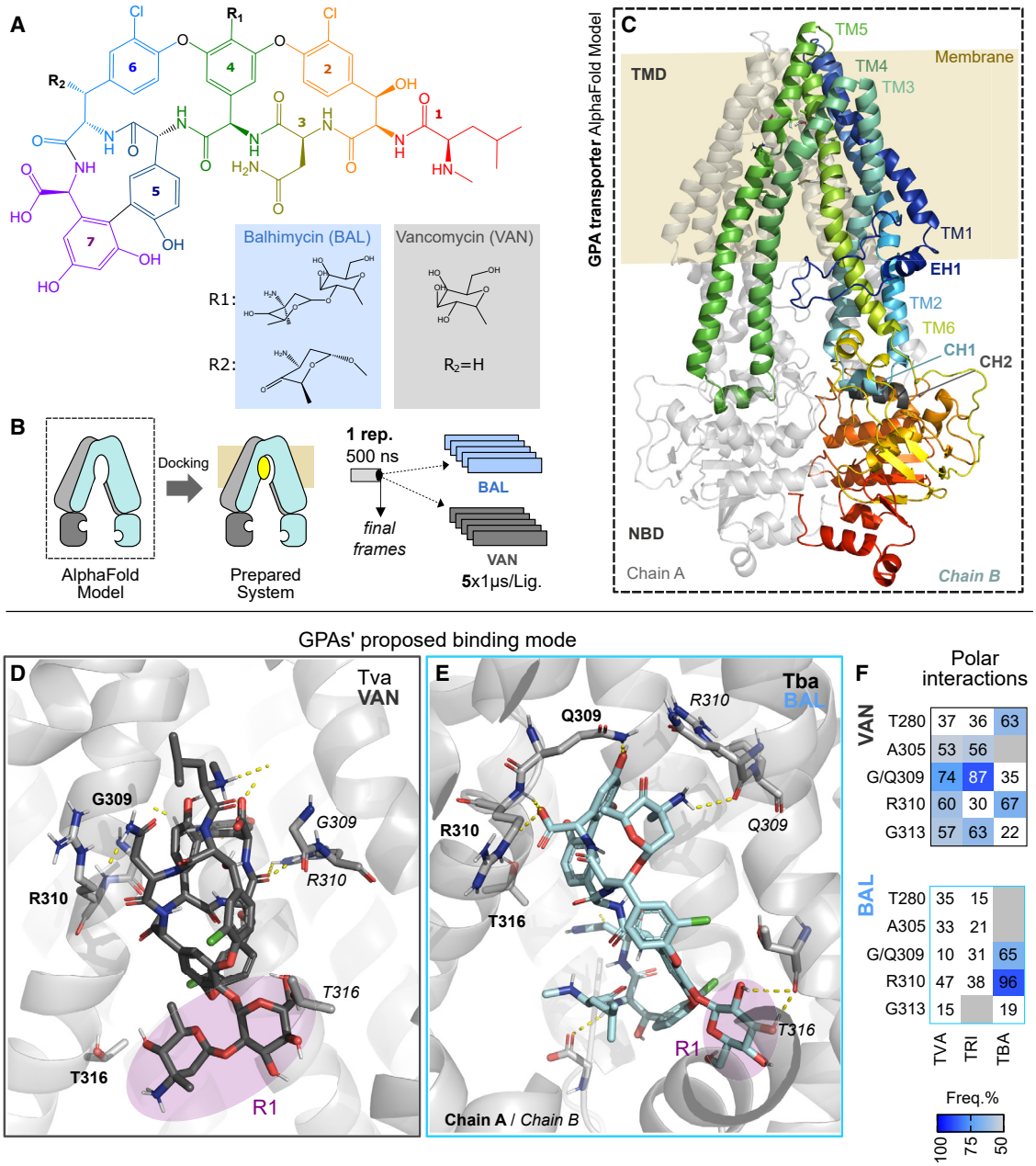

Figure 3. GPA binding mode on GPA transporter

(A) 2D schematic representation of the GPAs exemplified by balhimycin and vancomycin, highlighting the individual portions and the insertion points for the sugar moieties.

(B) Overview of the modeling pipeline (described in Star Methods 13).

(C) 3D representation of a type IV GPA transporter, showing its six transmembrane (TM) helices (colored from dark blue to green) and the coupling (CH 1 and 2) and elbow (EH) helices.

(D and E) Proposed binding mode for relevant GPAs, generated from representative conformations from the MD simulation for the transporter Tva bound to vancomycin (D) and Tba (E) bound to balhimycin. R1 substituent is highlighted in purple. Hydrogen bonds are depicted as yellow dashed lines.

(F) heatmap representations of the hydrogen bond interaction frequencies in the analyzed trajectory. Numbering based on Tva sequence.

Altogether, the results of the *trans* complementation assay indicate that only the transporter gene from the BGC of a type I GPA, vancomycin, could complement *A. balhimycina* Δ*tba*, whereas the transporter gene from the BGC of a type III GPA, ristomycin could not. Given that vancomycin and balhimycin differ solely in their glycosylation pattern, we speculated that sugars may not play a pivotal role in binding to the ABC transporter, a hypothesis that we set out to validate.

The specificity of the ABC transporter depends on the GPA backbone, rather than the sugar moieties

To further confirm the sugar independence and evaluate potential interaction between GPAs and ABCs, we applied a molecular modeling pipeline encompassing docking and long MD simulations (Figure 3B). We used AlphaFold2[26] to generate structural models of all 89 ABC transporters. The predicted structures were nearly identical with differences only in the unstructured N-terminal region. The models contained all the previously described structural elements of type IV ABC transporters (Figures 3C and S12).[27] Models featured a short N-terminal cytosolic helix (elbow helix, (Figures 3C and S12), a conserved TMD core comprising six TM helices, of which two perform a domain swap with those of the other half-transporter, and two coupling helices (i.e., CH1+2), responsible for the interaction of the TMD.[27]

We docked the type I GPAs vancomycin and balhimycin (Figure 3A) within a predicted binding cavity in the center of the inward-open TMD core (Figure 3D). These proposed binding modes underwent MD simulations and had their protein-ligand interaction frequencies monitored along the trajectory. Representative structures from the simulations displayed conserved interactions between the GPAs' backbone and residues from the TMD core pocket, specifically, GPA aa at position 4–7 (Figures 3D and 3E) interacting with F269 (aa 6, numbering as in Figures 3A–3F, R310 (aa 5 and 7), G309, and G313 (aa 4). Interestingly, no significant differences were observed in the interaction pattern for aa 1–3, which are primarily responsible for the classification of the GPAs. We highlight this as a limitation of our current binding model. Additionally, in the proposed binding mode the R1 sugar moieties of GPAs point to the cytoplasm (Figures 3D and 3E). Based on that, we suggest that the sugar would contribute more to the compound solubility than to the binding energy.

In vivo validation of binding interactions between tba and balhimycin confirms binding of the peptide backbone

Our MD simulation suggested that the transporter's binding affinity toward the GPA substrates relies on interactions with the backbone. Notably, our model points to polar contacts between specific TMD residues and the GPA backbone, prompting us to validate the effect of mutations on transport efficiency.

To address this, we constructed mutants of *A. balhimycina* to probe the impact of Tba mutations on the transport process. Specifically, we introduced mutations in the TMD of the transporter Tba^{3xFLAG} at residues Q309 (G309 in Tva), R310 (conserved in all studied transporters), and T316 (conserved in GPA I-III transporters and located at the base of the substrate binding pocket), substituting them with either glycine or alanine (designated Q309G, R310A, and T316A, respectively). Complementation of *A. balhimycina* Δ*tba* with these constructs resulted in three recombinant strains carrying the individual mutations. Interestingly, only the T316A substitution significantly decreased the export level compared to the transporter Tba^{3xFLAG}, emphasizing the critical role of T316 in the export process. Similar to a strain lacking Tba (Figures 2C and 2D), the *A. balhimycina* recombinant strain carrying the TbaT316A mutant slightly accumulated intracellular balhimycin, however, approximately 85-fold lower than the exported level by the wildtype. In contrast, the Q309G and R310A substitutions neither reduced the extracellular balhimycin levels nor had an effect on intracellular levels. (Figures 4A and 4B; Table S2; Figure S6A). Although T316 is not directly involved in balhimycin binding according to our model, its location on the cytoplasmic side of the putative substrate binding pocket suggests a role in pocket formation and stabilization. Importantly, we ruled out that the reduction in export levels was due to protein misfolding, as TbaT316A^{3xFLAG} was detected at the correct size by SDS-PAGE and BN-PAGE, albeit at lower accumulation levels than the wildtype protein (Figure 4C).

Our MD simulations suggest that the R1 sugar moieties do not interfere with binding (Figure S7), prompting us to assess the effects of GPA modifications on transport efficiency. In particular, we aimed to determine if non-glycosylated and non-chlorinated balhimycin could be exported by Tba. To investigate this, we used an *A. balhimycina* mutant lacking the halogenase gene *bhaA*, responsible for chlorination of the β-hydroxytyrosine residues at aa 2 and 6 of the balhimycin backbone[28] (Figure 3A), and a mutant lacking the glycosyltransferase gene *bgtfB*, responsible for attaching the first sugar moiety to the hydroxyphenylglycine residue at AA4 (R1, Figure 3A). The deletion of *bgtfB* results in the production of a non-glycosylated heptapeptide, as glycosylation occurs stepwise in a defined order. Missing the first glycosylation step prevents the attachment of subsequent sugars.[29] In addition, we included a double mutant lacking both genes, *bhaA* and *bgtfB*. By analyzing the supernatants via HPLC-MS we identified the peaks of the corresponding final products of each mutant and used the intensities for subsequent quantification. The HPLC-MS analysis of culture supernatants from *A. balhimycina* Δ*bhaA* showed peaks corresponding to masses of *m/z* 1237.5 $[M+H]^+$ and *m/z* 1377.49 $[M+H]^+$ (Figure S6B; Table S3), assignable to balhimycin without chlorine and with either one or two sugar moieties, respectively. In the culture supernatant of *A. balhimycina* Δ*bgtfB*, a peak with a corresponding mass of *m/z* 1142.28 $[M+H]^+$ (Figure S6B; Table S3) was identified as chlorinated balhimycin lacking all sugar moieties. The double mutant exhibited peaks with prominent masses of *m/z* 1074.36 $[M+H]^+$ and *m/z* 1088.38 $[M+H]^+$, corresponding to balhimycin without chlorine atoms and sugar moieties, and the same molecule with an additional methyl group, respectively (Figure S6B; Table S3). All data were confirmed by comparing the UV-spectra derived from the diode array detector (DAD) with in-house databases (Figure S8).

Interestingly, the absence of sugar modifications on the balhimycin peptide backbone led to a significant increase in exported balhimycin derivatives, approximately 5.5-fold higher in *A. balhimycina* Δ*bgtfB* as compared to the glycosylated balhimycin in the wildtype (Figure 4D). However, the biological activity decreased in the absence of the sugars, as we confirmed by exposing the indicator strain *Bacillus subtilis* DSM10 to the culture supernatants of the *A. balhimycina* mutants (Figure 4E). Moreover, we observed an even higher export of balhimycin derivatives in the *A. balhimycina* double mutant Δ*bhaA*Δ*bgtfB*. The biological activity of the balhimycin derivative produced by this mutant was totally abolished (Figure 4E), which confirms the importance of these modifications in the mode of action of

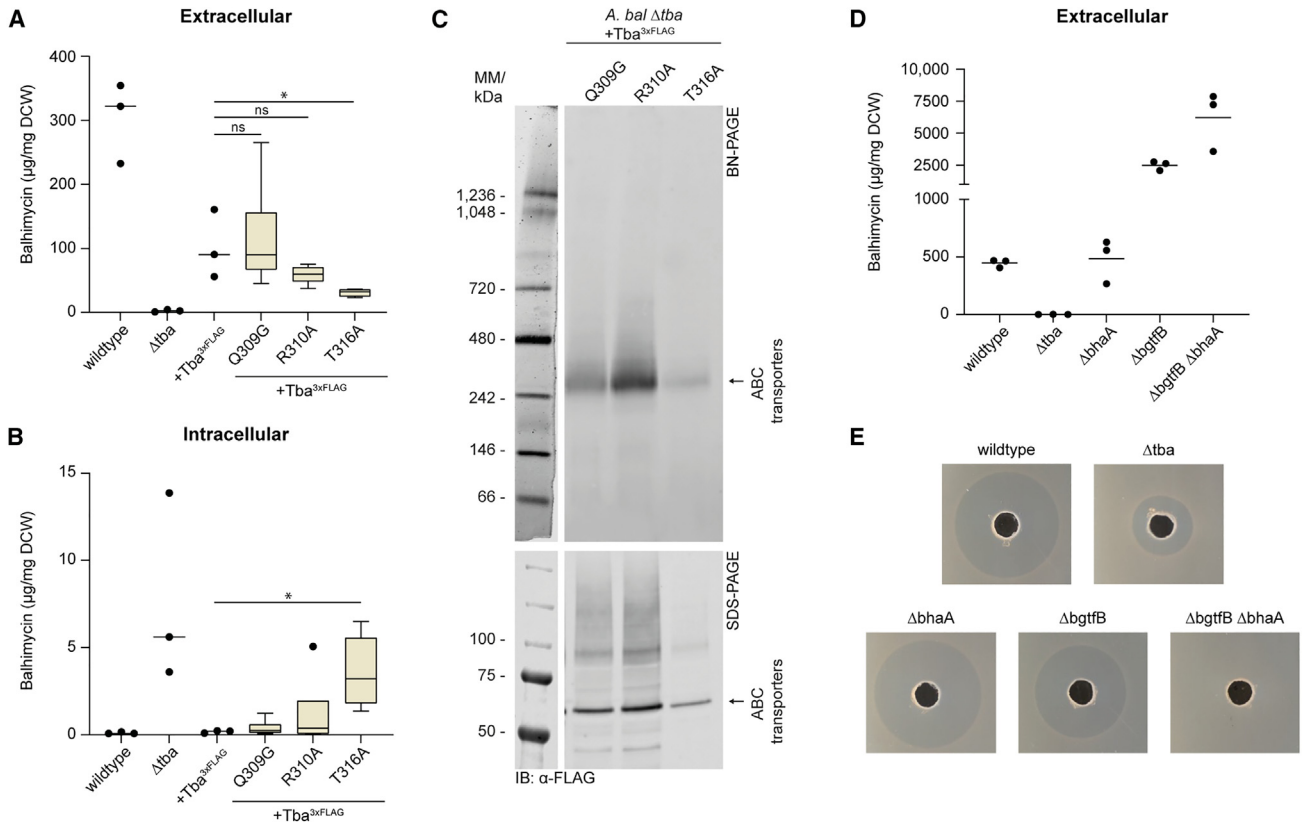

Figure 4. Analysis of transport specificity of the balhimycin transporter Tba

(A and B) Quantification of extracellular (A) and intracellular (B) levels of balhimycin in *A. balhimycina* and respective mutant strains based on HPLC-MS data (Figure S6A). Values were normalized to the dry cell weight (DCW). Data are shown in boxplot representation or by individual data points (+median) if $n \leq 3$. Error bars indicate standard deviations. Statistical outliers are displayed as dots as well. Statistically significant differences compared to +Tba^{3xFLAG} are highlighted with asterisks ($p < 0.05$ (*)) ("Wilcoxon signed-rank test" and "Benjamini-Hochberg Procedure") (Table S2).

(C) Immunoblotting after BN- (up) and SDS-page (down) of solubilized crude membranes of *A. balhimycina* transporter mutant strains. Detection with 3xFLAG specific antibodies.

(D) Quantification of extracellular levels of balhimycin in *A. balhimycina* and respective mutant strains based on HPLC-MS data (Figure S6B). Values were normalized to the DCW. Data are shown by individual data points (+median).

(E) Bioassay on *B. subtilis* DSM10 indicator plates using culture supernatant of the indicated *A. balhimycina* strains.

balhimycin. In *A. balhimycina* Δ*bhaA* the balhimycin derivative lacking chlorine atoms appeared to be exported at the same levels as fully modified balhimycin in the wildtype strain (Figure 4D), and didn't exhibit any decrease in inhibitory activity. This indicates that chlorine atoms do not interfere with the transport process.

The ABC transporter tba interacts with the GPA biosynthetic machinery at the membrane

The low intracellular balhimycin levels in the *A. balhimycina* Δ*tba* mutant and in the mutant strain producing the export-defective transporter TbaT316A^{3xFLAG} (Figures 2D and 4B) were unexpected. We anticipated intracellular accumulation of balhimycin following transporter deletion or inactivation, considering that *A. balhimycina* produces intrinsically resistant cell wall precursors. To confirm that active transport through Tba is required for the biosynthesis of balhimycin to occur, we constructed a mutant expressing TbaE545Q^{3xFLAG}, a variant that carries a point mutation in the NBD, leading to a catalytically inactive protein unable to hydrolyze ATP. In this mutant, we could only detect negligible amounts of balhimycin both intracellularly and extracellularly (Figures 2C and 2D). This shows that TbaE545Q^{3xFLAG} is indeed unable to export balhimycin. Furthermore, the mere presence of the transporter is not sufficient to promote balhimycin biosynthesis, which would lead to its intracellular accumulation. Thus, it appears that a regulatory mechanism responsible for the arrest of balhimycin biosynthesis is triggered by the lack of active transport. When not actively exported, balhimycin could negatively regulate the transcription of the biosynthetic genes, thereby decreasing biosynthesis. We conducted a differential expression analysis of the transcriptome of *A. balhimycina* wildtype and *A. balhimycina* Δ*tba* to test this hypothesis (Figures 5A and S9A). We included in our investigation the *A. balhimycina* Δ*bbr* mutant lacking the StrR-like regulator gene *bbr*. Bbr is known to activate the transcription of the BGC genes.[30] No significant difference in BGC expression was observed between the wildtype and *A. balhimycina* Δ*tba* after 48 h of cultivation. However, a clear downregulation was apparent in *A. balhimycina* Δ*bbr* (Figure 5A).

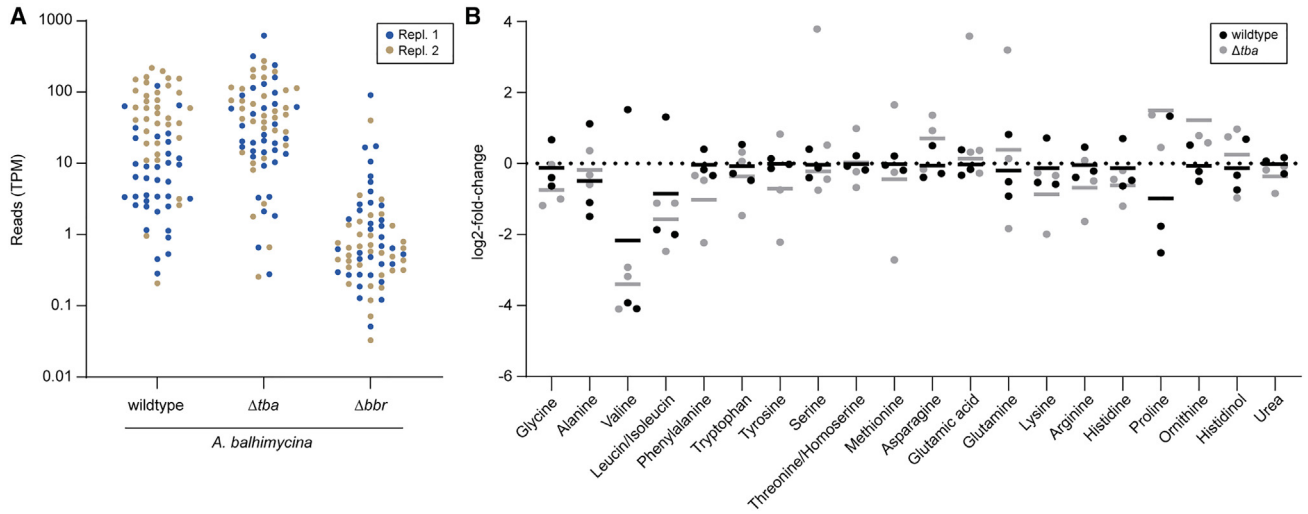

Figure 5. Transcriptome and metabolome analysis of *A. balhimycina* Δ*tba*

(A) Display of transcription of every gene within the balhimycin BGC in *A. balhimycina* wildtype, Δ*tba*, and Δ*bbr* in transcripts per million (TPM). Two individual replicates are shown in beige and blue, respectively.

(B) Amino acids levels after 48 h measured by LC-MS/MS and normalized to the dry cell weight (DCW). *A. balhimycina* wildtype (black) and Δ*tba* (gray) are displayed as log2 fold changes in comparison to a 13C internal standard.

This result shows that the absence of Tba does not affect the transcription of the genes in the BGC.

Since we observed no effect at the transcriptional level, we explored the possibility of biosynthesis inhibition due to the accumulation of precursors or intermediates of balhimycin biosynthesis acting as feedback inhibitors. By measuring the levels of aa and different balhimycin intermediates in *A. balhimycina* wildtype and Δ*tba* at the same time point (48 h) using LC-MS/MS and flow-injection mass spectrometry, respectively, we observed neither a significant increase or decrease in relevant aa (leucine, asparagine, and tyrosine) involved in balhimycin biosynthesis (Figure 5B), nor accumulation of intermediates (Figures S9B and S10).

Both transcriptome and metabolome analyses have remained inconclusive regarding the cause of the inhibition of balhimycin biosynthesis in the absence of the transporter. To explore the possibility that the transporter might interact with the biosynthetic machinery and thereby exert a direct regulatory function, we sought to identify the proteins localized in the vicinity of the transporter. To address this question, we employed a proximity dependent biotinylation approach using the recently developed and promiscuous biotin ligase TurboID (TID).[31] Fusing TID to any protein of interest results in short-range (∼10 nm) biotinylation of primary amines on lysine residues of proximal proteins, thereby allowing the identification of the microenvironment of specific proteins[32] (Figure 6A). We successfully established this method in *A. balhimycina DSM 44591* by using Tba as a bait protein for proximity studies (Figure 6B). We generated a recombinant strain by introducing a Tba^{TID} fusion construct into *A. balhimycina* Δ*tba* and confirmed that production of Tba^{TID} restored balhimycin export (Figure S11A). In order to detect biotinylation that is specific for Tba^{TID}, we constructed two control strains of *A. balhimycina*. One strain produces TID as a cytosolic protein, while the other strain produces a GPA-unrelated transporter of *A. balhimycina*, Abc30, fused to TID. To enrich and identify the proteins biotinylated by Tba^{TID} we performed pull-downs with streptavidin beads (Figure S11B), followed by HPLC-MS/MS analysis. This yielded 563 proteins after processing the data. To ensure robust statistical analysis, we excluded hits identified in only one replicate. Intriguingly, comparison between the Tba^{TID} and control strains revealed a clear enrichment of balhimycin biosynthetic enzymes. These included NRPSs (BpsB, and BpsC), modification enzymes (OxyC, BhaA, BgtfAB, and Bmt), and enzymes involved in precursor supply (Pgat, BpsD, OxyD, HmaS, DvaB, and DvaC). The presence of these biosynthetic enzymes in close proximity to the Tba transporter suggests that an active transporter might "stimulate" the production of balhimycin via interaction with the biosynthetic machinery, a hypothesis that awaits confirmation in follow-up studies.

DISCUSSION

Our in-depth study of GPA-related ABC transporters provides valuable new insights into their evolutionary relationships, substrate specificity, and regulatory functions in GPA biosynthesis. The phylogeny of these transporters is consistent with the evolutionary trajectory of their respective substrates, as proposed by Hansen et al. and Waglechner et al. It is suggested that type I GPAs evolved from type IV GPAs.[23,33] Consequently, our analysis implies that the putative ABC transporters of type IV GPAs are more ancestral than those of type I GPAs. Notably, transporters encoded by BGCs of the same GPA type often cluster together. This clustering suggests that their specificity is likely to be determined by differences in the aa composition of the GPA backbone rather than by variations in modifications, as GPAs of the same type can exhibit different modification patterns.

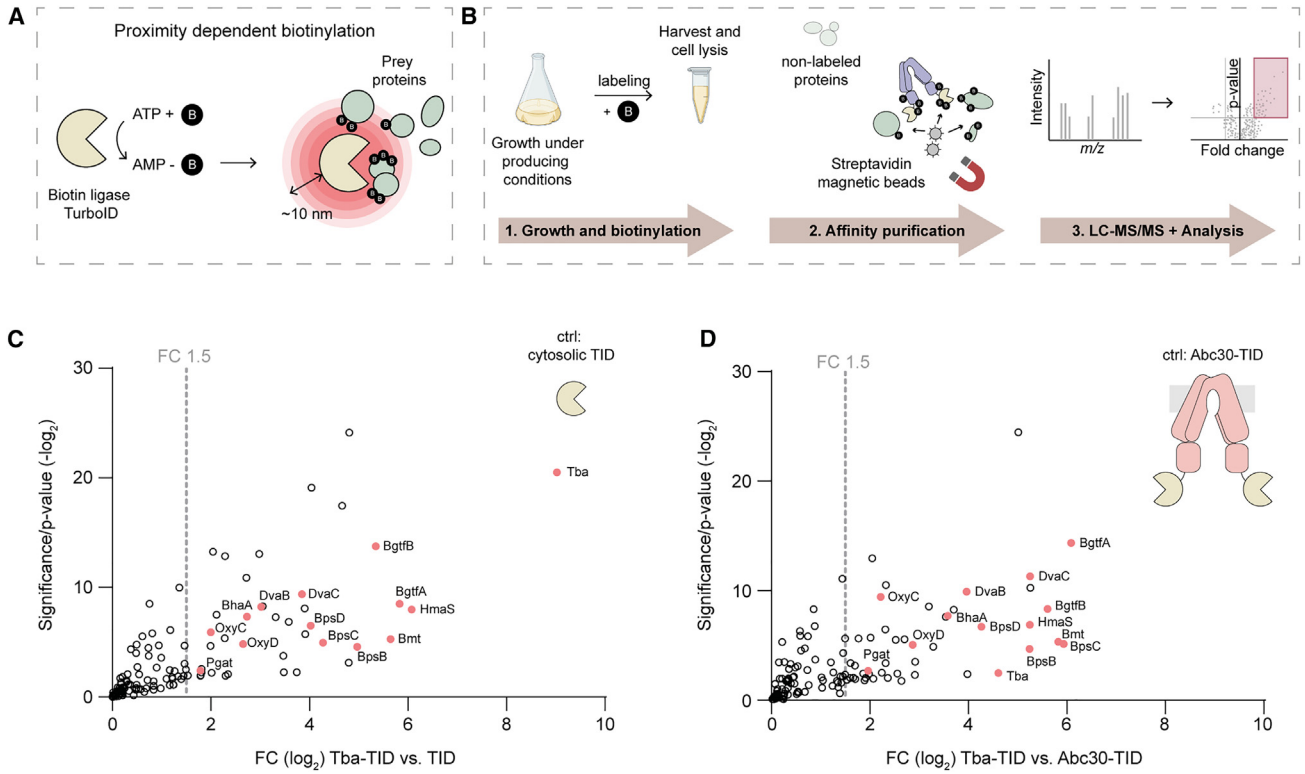

Figure 6. Identification of Tba's microenvironment by proximity dependent biotinylation

(A) Schematic overview of the concept of proximity dependent biotinylation by the promiscuous biotin ligase TurboID. B: Biotin.

(B) Schematic representation of the experimental procedure of proximity dependent biotinylation in *A. balhimycina*.

(C and D) Representation of all log2 fold change positive proteins detected by LC-MS/MS after proximity dependent biotinylation. Hits of Tba-TID compared to cytosolic TID (C) or membrane protein Abc30 (D). Proteins detected and encoded in the BGC of balhimycin are colored in salmon. NRPSs (BpsB and BpsC), modification enzymes (OxyC, BhaA, BgtfAB, and Bmt), and enzymes involved in precursor supply (Pgat, BpsD, OxyD, HmaS, DvaB, and DvaC).

This hypothesis was further supported by MD-simulation and *in vivo* export analysis. Only the ABC transporters Tba and Tva, which are encoded in BGCs of type I GPAs, were found to export comparable quantities of balhimycin. In contrast, the putative ristomycin (type III GPA) ABC transporter Tri exported significantly less balhimycin. Our results suggest that the selectivity of GPA-associated ABC transporters is due to the chemical composition of the peptide backbone, since in ristomycin it consists exclusively of aromatic aa, whereas balhimycin has two aliphatic aa at position AA1 and AA3. We showed that Tba exports a non-glycosylated derivative of balhimycin at significantly higher levels than the fully glycosylated form. This suggests that the bulky and flexible sugar moieties, although crucial for biological activity, impedes efficient transport. There are examples of transporters in ribosomally synthesized and post-translationally modified peptides (RiPPs) produced by a wide range of bacteria that have been experimentally characterized. NisT, a transporter associated with the lantibiotic peptide nisin, is an example of a transporter with a broad substrate specificity.[34] In contrast, the MjcD transporter exhibits high specificity for its cognate substrate, the lassopeptide Microcin J25.[35] In contrast to RiPPs, the specificity of GPA-associated ABC transporters has been less well characterized. Our study reveals that GPA ABC transporters exhibit specificity toward their cognate substrates based on backbone composition, whereas they show greater promiscuity with respect to modifications of it.

In a previous study,[10] we showed that *tba* deletion in *A. balhimycina* leads to accumulation of balhimycin, which stands in contrast to the findings of the current study. Here, we demonstrated that deletion or functional inactivation of the Tba transporter significantly reduces the amount of produced balhimycin. The discrepancy may be attributed to differences in the quantification method used; Menges et al. relied on inhibition zone diameters for quantification,[10] whereas we employed state-of-the-art HPLC-MS analysis. Importantly, impaired biosynthesis in the *A. balhimycina tba* mutants is not due to toxic effects of balhimycin, as resistance is facilitated constitutively through cell wall precursor remodeling.[11,36–38] Similar findings were reported previously, with deletion of transporter genes in particular BGCs leading to a reduction in the production levels of the respective compounds. Studies on the microcystin BGC in *Microcystis aeruginosa* showed that deletion of the transporter gene *mcyH* completely abolished the production of microcystin.[39] Comparable observations were made in *Streptomyces ghanaensis* ATCC14672, in which the deletion of two transporter genes *moeX5moeP5* and *moeD5moeJ5* led to a significant reduction in the production of moenomycin A.[14] Another example is provided by the NRPS derived compound cereulide

and its cognate ABC transporter CesCD. The deletion or inactivation of CesCD resulted in a greatly reduced biosynthesis of cereulide by the producer strain *Bacillus cereus*.[15] These studies point to an important role of the cognate transporters in regulating the biosynthetic machinery of natural products and strongly highlights active transport as a crucial factor for continuous biosynthesis.

To elucidate the mechanism behind transport-dependent balhimycin production, we investigated different levels of regulation and showed that transcription is not affected by the absence of Tba, as previously observed for microcystin biosynthesis in the absence of the cognate transporter.[39] Feedback regulatory mechanisms have been reported in balhimycin biosynthesis, involving enzymes and intermediates from the shikimate-pathway.[40,41] It was shown that the aromatic aa tyrosine and phenylalanine act as feedback enzymatic inhibitors of the shikimate pathway, thereby reducing the provision of balhimycin precursors. Our metabolomic analysis shows that none of the precursors accumulated in the *A. balhimycina* Δ*tba* deletion mutant, ruling out an inhibitory effect on biosynthetic enzymes. Furthermore, none of the intermediates of the NRPS assembly line appeared to be present at significantly higher concentrations. We conclude that feedback inhibition is not the reason for reduced biosynthesis of balhimycin in the absence of a functional transporter.

The results of our proximity dependent biotinylation experiment provide an alternative explanation: we showed that many of the enzymes responsible for assembly and modification of the balhimycin backbone as well as supply of precursors are in close proximity to Tba, possibly forming a microcompartment specialized in GPA production. Based on the general ABC transporter mechanisms,[18] we speculate that upon substrate binding, Tba undergoes a conformational change that is required for stimulation of balhimycin biosynthesis. However, it remains elusive whether the transporter directly interacts with the biosynthetic enzymes and how exactly this interaction impacts balhimycin biosynthesis. There is evidence that biosynthetic enzymes of secondary metabolites interact with the corresponding transporter and that compound biosynthesis might be membrane-associated, as exemplified by the cereulide and nisin biosynthesis. Both biosynthetic machineries were shown to build a complex and co-localize with the corresponding ABC transporter.[15,42,43]

Among the biotinylated proteins with significant fold changes in the Tba^{TID} mutant, we identified a paraslipin protein, suggesting its close proximity to Tba and consequently to other proteins of the balhimycin biosynthetic machinery. Paraslipins belong to the stomatin, prohibitin, flotillin, and HflK/C (SPFH) superfamily and are known to be associated with the formation of functional membrane microdomains (FMM).[44] Our finding suggests that Tba may be integrated into an FMM, serving as an anchor of biosynthetic enzymes. We speculate that the biosynthesis of balhimycin occurs within a specialized microcompartment and is likely regulated by the presence of catalytically active Tba, as suggested by our *in vivo trans* complementation assays. There is evidence that bacteria use microcompartments to optimize their metabolic processes. Carboxysomes are among the best studied and represent an example of how compartmentalization can increase the efficiency of metabolic reactions, in this specific case of carbon fixation by photoautotrophs and chemoautotrophs. Carboxysomes concentrate CO_2 owing to the activity of a carbonic anhydrase and the selective permeability of the protein shell, which in turn increases both the rates and specificity of the encapsulated carbon-fixing enzyme ribulose 1,5-bisphosphate carboxylase/oxygenase (RuBisCO).[45] Another example is the propanediol-utilizing microcompartment (Pdu MCP) of enteric bacteria like *Salmonella*. The Pdu MCP allows the degradation of 1,2-propanediol and enteric pathogenesis.[46] However, further studies are required to confirm that in *A. balhimycina* GPA biosynthesis occurs in compartments associated with the membrane, and to fully elucidate the scope of the transporter's potential roles in this process.

Limitations of the study

Despite detailed investigation of the substrate specificity using *insilico* models, *in vitro* studies are essential to fully characterize the binding pocket of the ABC transporter Tba for the GPA balhimycin. Structural elucidation of Tba-balhimycin complex would provide crucial insights into the binding mechanism.

Additionally, the hypothesis that Tba interacts with the biosynthetic machinery requires further validation. Investigating the regulatory function of Tba through direct protein-protein interaction studies would be key to understanding its precise impact on the balhimycin biosynthesis.

RESOURCE AVAILABILITY

Lead contact

Further information and requests for resources and reagents should be directed to and will be fulfilled by the lead contact, Evi Stegmann (evi.stegmann@uni-tuebingen.de)

Materials availability

This study did not generate new unique reagents.

Data and code availability

- All MD simulation trajectories, interaction data and MD quality control data, representative PDB files from the alphaFold models, phylogenetic trees and metabolomics raw data are available under the DOIs: https://doi.org/10.5281/zenodo.7547342, https://doi.org/10.5281/zenodo.7732071 and https://doi.org/10.5281/zenodo.7547403 and https://doi.org/10.5281/zenodo.14918266 are publicly available as of the date of publication.
- All RNA-seq Illumina read files as well as the raw counts have been deposited in NCBI's Gene Expression Omnibus and are accessible under accession number GSE274067.
- The mass spectrometry proteomics data have been deposited to the ProteomeXchange Consortium via the PRIDE[47] partner repository with the dataset identifier PXD054387.
- This study did not generate any unique code.
- Any additional information required to reanalyze the data reported in this paper is available from the lead contact upon request.

ACKNOWLEDGMENTS

The work in the laboratory of S.W., E.S., W.W., N.Z., B.M., and K.N. related to this study was funded by the Deutsche Forschungsgemeinschaft (DFG) as part of the transregional collaborative research center TRR 261 'Cellular Mechanisms of Antibiotic Action and Production' (Projects B01/B02/B05/Z03). It was supported by the de.NBI Cloud within the German Network for Bioinformatics Infrastructure (de.NBI) and ELIXIR-DE (Forschungszentrum Jülich

and W-de.NBI-001, W-de.NBI-004, W-de.NBI-008, W-de.NBI-010, W-de.NBI-013, W-de.NBI-014, W-de.NBI-016, W-de.NBI-022). NGS sequencing methods were performed with the support of the DFG-funded NGS Competence Center Tübingen (INST 37/1049-1). Data management and storage of raw data for this project were supported by the Quantitative Biology Center (QBiC), University of Tübingen, Germany. The authors would like to thank Libera Lo Presti for her support in writing, comments on the manuscript, and fruitful discussions. S.W., E.S., W.W., T.K., and N.Z. acknowledges the German Center for Infection Research (DZIF, TTU09.716). S.W., E.S., W.W., T.K., and N.Z. acknowledges funding by the Clusters of Excellence EXC2124 CMFI (project ID 390838134) and T.K. the TüCAD2 the Federal Ministry of Education and Research (BMBF) and the Baden-Württemberg Ministry of Science as part of the Excellence Strategy of the German Federal and State Governments – Germany, by the means of the program TüCAD$_2$, as well as the German Center for Infection Research (T.K.: DZIF, TTU06.716) (W.W. TTU09.826). The authors would like to thank the CSC—Finland for the generous provided resources, Ana Monica Daneliuc for contributing to refining HMM search for the creation of the BGC dataset and Anke Biedermann and Irina Droste-Borel from the Proteome Center Tübingen for technical support. Graphical abstract was created in BioRender. Stegmann, E. (2025) https://BioRender.com/x66x647. We acknowledge support from the Open Access Publication Fund of the University of Tübingen.

AUTHOR CONTRIBUTIONS

N.G. performed *in silico* analysis of transporter sequences and phylogenetic analysis. N.G. and D.B. performed *in vivo* experiments and analyzed all data. T.K. performed MD simulations. S.W., E.S., and W.W. designed the study. N.G., D.B., T.K., S.W., E.S., and W.W. drafted the paper and wrote the original manuscript. A.K. performed HPLC-MS measurements. M.F.-W. and B.M. performed proteomics. A.G. identified BGCs and putative transporters and did the correlation of BGCs and substrates. U.S. did statistical analysis of *in vivo* data. J.R. and H.L. performed metabolomics. T.H. and K.N. performed RNA sequencing and analyzed the data. I.G. provided bioinformatic support.

DECLARATION OF INTERESTS

The authors declare no competing interests.

STAR★METHODS

Detailed methods are provided in the online version of this paper and include the following:

- KEY RESOURCES TABLE
- EXPERIMENTAL MODEL AND STUDY PARTICIPANT DETAILS
- METHOD DETAILS
  - Identification of transporter sequences of biosynthetic gene clusters
  - Bioinformatic analysis of transporters
  - Phylogenetic analysis of GPA associated ABC transporter
  - Chemicals and reagents
  - Bacterial strains, plasmids, and growth conditions
  - Molecular cloning
  - Genetic manipulation of *A. balhimycina*
  - Generation of *A. balhimycina* deletion mutants
  - Crude membrane preparation
  - BN-PAGE, SDS-PAGE, and immunoblotting
  - Balhimycin production, export assay and bioactivity assay
  - HPLC-MS analysis and quantification of balhimycin
  - Molecular modeling and molecular dynamics simulation
  - Transcriptomic analysis
  - Measurement of amino acid levels by metabolomic analysis
  - Proximity dependent biotinylation and proteomic analysis
- QUANTIFICATION AND STATISTICAL ANALYSIS

SUPPLEMENTAL INFORMATION

Supplemental information can be found online at https://doi.org/10.1016/j.isci.2025.112135.

Received: November 19, 2024
Revised: January 16, 2025
Accepted: February 26, 2025
Published: March 3, 2025

REFERENCES

1. Zeng, D., Debabov, D., Hartsell, T.L., Cano, R.J., Adams, S., Schuyler, J.A., McMillan, R., and Pace, J.L. (2016). Approved glycopeptide antibacterial drugs: Mechanism of action and resistance. Cold Spring Harb. Perspect. Med. *6*, a026989.
2. Culp, E.J., Waglechner, N., Wang, W., Fiebig-Comyn, A.A., Hsu, Y.P., Koteva, K., Sychantha, D., Coombes, B.K., Van Nieuwenhze, M.S., Brun, Y.V., and Wright, G.D. (2020). Evolution-guided discovery of antibiotics that inhibit peptidoglycan remodelling. Nature *578*, 582–587.
3. Nicolaou, K.C., Boddy, C.N., Bräse, S., and Winssinger, N. (1999). Chemistry, biology, and medicine of the glycopeptide antibiotics. Angew Chem. Int. Ed. Engl. *38*, 2096–2152.
4. Gavriilidou, A., Adamek, M., Rodler, J.P., Kubach, N., Kramer, S., Huson, D.H., Cryle, M.J., Stegmann, E., and Ziemert, N. (2023). Phylogenetic distance and structural diversity directing a reclassification of glycopeptide antibiotics. Preprint at bioRxiv. https://doi.org/10.1101/2023.02.10.526856.
5. Recktenwald, J., Shawky, R., Puk, O., Pfennig, F., Keller, U., Wohlleben, W., and Pelzer, S. (2002). Nonribosomal biosynthesis of vancomycin-type antibiotics: a heptapeptide backbone and eight peptide synthetase modules. Microbiol. Read. Engl *148*, 1105–1118.
6. Bischoff, D., Pelzer, S., Höltzel, A., Nicholson, G.J., Stockert, S., Wohlleben, W., Jung, G., and Süssmuth, R.D. (2001). The Biosynthesis of vancomycin-type glycopeptide antibiotics –New insights into the cyclization steps. Angew. Chem. Int. Ed. *40*, 1693–1696.
7. Stegmann, E., Pelzer, S., Bischoff, D., Puk, O., Stockert, S., Butz, D., Zerbe, K., Robinson, J., Süssmuth, R.D., and Wohlleben, W. (2006). Genetic analysis of the balhimycin (vancomycin-type) oxygenase genes. J. Biotechnol. *124*, 640–653.
8. Haslinger, K., Peschke, M., Brieke, C., Maximowitsch, E., and Cryle, M.J. (2015). X-domain of peptide synthetases recruits oxygenases crucial for glycopeptide biosynthesis. Nature *521*, 105–109.
9. Yim, G., Thaker, M.N., Koteva, K., and Wright, G. (2014). Glycopeptide antibiotic biosynthesis. J. Antibiot. (Tokyo) *67*, 31–41.
10. Menges, R., Muth, G., Wohlleben, W., and Stegmann, E. (2007). The ABC transporter Tba of *Amycolatopsis balhimycina* is required for efficient export of the glycopeptide antibiotic balhimycin. Appl. Microbiol. Biotechnol. *77*, 125–134.
11. Schäberle, T.F., Vollmer, W., Frasch, H.J., Hüttel, S., Kulik, A., Röttgen, M., von Thaler, A.K., Wohlleben, W., and Stegmann, E. (2011). Self-resistance and cell wall composition in the glycopeptide producer *Amycolatopsis balhimycina*. Antimicrob. Agents Chemother. *55*, 4283–4289.
12. Biemans-Oldehinkel, E., Doeven, M.K., and Poolman, B. (2006). ABC transporter architecture and regulatory roles of accessory domains. FEBS Lett. *580*, 1023–1035.
13. Biemans-Oldehinkel, E., Mahmood, N.A.B.N., and Poolman, B. (2006). A sensor for intracellular ionic strength. Proc. Natl. Acad. Sci. USA *103*, 10624–10629.
14. Ostash, B., Doud, E., and Walker, S. (2012). ABC transporter genes from *Streptomyces ghanaensis* moenomycin biosynthetic gene cluster: roles in antibiotic production and export. Arch. Microbiol. *194*, 915–922.
15. Gacek-Matthews, A., Chromiková, Z., Sulyok, M., Lücking, G., Barák, I., and Ehling-Schulz, M. (2020). Beyond toxin transport: Novel role of ABC

Transporter for enzymatic machinery of cereulide NRPS assembly line. mBio *11*, e01577-20.

16. Neumüller, A.M., Konz, D., and Marahiel, M.A. (2001). The two-component regulatory system BacRS is associated with bacitracin 'self-resistance' of *Bacillus licheniformis* ATCC 10716. Eur. J. Biochem. *268*, 3180–3189.
17. Ohki, R., Giyanto, Tateno, K., Masuyama, W., Moriya, S., Kobayashi, K., and Ogasawara, N. (2003). The BceRS two-component regulatory system induces expression of the bacitracin transporter, BceAB, in *Bacillus subtilis*. Mol. Microbiol. *49*, 1135–1144.
18. Thomas, C., and Tampé, R. (2020). Structural and mechanistic principles of ABC transporters. Annu. Rev. Biochem. *89*, 605–636.
19. Hessa, T., Meindl-Beinker, N.M., Bernsel, A., Kim, H., Sato, Y., Lerch-Bader, M., Nilsson, I., White, S.H., and von Heijne, G. (2007). Molecular code for transmembrane-helix recognition by the Sec61 translocon. Nature *450*, 1026–1030.
20. Brigham, R.B., and Pittenger, R.C. (1956). *Streptomyces orientalis*, n. sp., the source of vancomycin. Antibiot. Chemother. *6*, 642–647.
21. Xu, L., Huang, H., Wei, W., Zhong, Y., Tang, B., Yuan, H., Zhu, L., Huang, W., Ge, M., Yang, S., et al. (2014). Complete genome sequence and comparative genomic analyses of the vancomycin-producing *Amycolatopsis orientalis*. BMC Genom. *15*, 363.
22. Tan, G.Y.A., Robinson, S., Lacey, E., Brown, R., Kim, W., and Goodfellow, M. (2007). *Amycolatopsis regifaucium* sp. nov., a novel actinomycete that produces kigamicins. Int. J. Syst. Evol. Microbiol. *57*, 2562–2567.
23. Hansen, M.H., Adamek, M., Iftime, D., Petras, D., Schuseil, F., Grond, S., Stegmann, E., Cryle, M.J., and Ziemert, N. (2023). Resurrecting ancestral antibiotics: unveiling the origins of modern lipid II targeting glycopeptides. Nat. Commun. *14*, 7842.
24. Bibb, M.J., Janssen, G.R., and Ward, J.M. (1985). Cloning and analysis of the promoter region of the erythromycin resistance gene (*ermE*) of *Streptomyces erythraeus*. Gene *38*, 215–226.
25. Dawson, R.J.P., and Locher, K.P. (2006). Structure of a bacterial multidrug ABC transporter. Nature *443*, 180–185.
26. Jumper, J., Evans, R., Pritzel, A., Green, T., Figurnov, M., Ronneberger, O., Tunyasuvunakool, K., Bates, R., Žídek, A., Potapenko, A., et al. (2021). Highly accurate protein structure prediction with AlphaFold. Nature *596*, 583–589.
27. Thomas, C., Aller, S.G., Beis, K., Carpenter, E.P., Chang, G., Chen, L., Dassa, E., Dean, M., Duong Van Hoa, F., Ekiert, D., et al. (2020). Structural and functional diversity calls for a new classification of ABC transporters. FEBS Lett. *594*, 3767–3775.
28. Puk, O., Huber, P., Bischoff, D., Recktenwald, J., Jung, G., Süssmuth, R.D., van Pée, K.H., Wohlleben, W., and Pelzer, S. (2002). Glycopeptide biosynthesis in *Amycolatopsis mediterranei* DSM5908: Function of a halogenase and a haloperoxidase/perhydrolase. Chem. Biol. *9*, 225–235.
29. Stegmann, E., Frasch, H.-J., and Wohlleben, W. (2010). Glycopeptide biosynthesis in the context of basic cellular functions. Curr. Opin. Microbiol. *13*, 595–602.
30. Shawky, R.M., Puk, O., Wietzorrek, A., Pelzer, S., Takano, E., Wohlleben, W., and Stegmann, E. (2007). The border sequence of the balhimycin biosynthesis gene cluster from *Amycolatopsis balhimycina* contains *bbr*, encoding a StrR-like pathway-specific regulator. Microb. Physiol. *13*, 76–88.
31. Branon, T.C., Bosch, J.A., Sanchez, A.D., Udeshi, N.D., Svinkina, T., Carr, S.A., Feldman, J.L., Perrimon, N., and Ting, A.Y. (2018). Efficient proximity labeling in living cells and organisms with TurboID. Nat. Biotechnol. *36*, 880–887.
32. Kim, D.I., Birendra, K.C., Zhu, W., Motamedchaboki, K., Doye, V., and Roux, K.J. (2014). Probing nuclear pore complex architecture with proximity-dependent biotinylation. Proc. Natl. Acad. Sci. USA *111*, E2453–E2461.
33. Waglechner, N., McArthur, A.G., and Wright, G.D. (2019). Phylogenetic reconciliation reveals the natural history of glycopeptide antibiotic biosynthesis and resistance. Nat. Microbiol. *4*, 1862–1871.
34. Kuipers, A., de Boef, E., Rink, R., Fekken, S., Kluskens, L.D., Driessen, A.J.M., Leenhouts, K., Kuipers, O.P., and Moll, G.N. (2004). NisT, the transporter of the lantibiotic nisin, can transport fully modified, dehydrated, and unmodified prenisin and fusions of the leader peptide with non-lantibiotic peptides. J. Biol. Chem. *279*, 22176–22182.
35. Romano, M., Fusco, G., Choudhury, H.G., Mehmood, S., Robinson, C.V., Zirah, S., Hegemann, J.D., Lescop, E., Marahiel, M.A., Rebuffat, S., et al. (2018). Structural basis for natural product selection and export by bacterial ABC transporters. ACS Chem. Biol. *13*, 1598–1609.
36. Frasch, H.-J., Kalan, L., Kilian, R., Martin, T., Wright, G.D., and Stegmann, E. (2015). Alternative pathway to a glycopeptide-resistant cell wall in the balhimycin producer *Amycolatopsis balhimycina*. ACS Infect. Dis. *1*, 243–252.
37. Kilian, R., Frasch, H.-J., Kulik, A., Wohlleben, W., and Stegmann, E. (2016). The VanRS homologous two-component system VnlRSAb of the glycopeptide producer *Amycolatopsis balhimycina* activates transcription of the $vanHAX_{Sc}$ genes in *Streptomyces coelicolor*, but not in *A. balhimycina*. Microb. Drug Resist. *22*, 499–509.
38. Unsleber, S., Wohlleben, W., and Stegmann, E. (2019). Diversity of peptidoglycan structure – Modifications and their physiological role in resistance in antibiotic producers. Int. J. Med. Microbiol. *309*, 151332.
39. Pearson, L.A., Hisbergues, M., Börner, T., Dittmann, E., and Neilan, B.A. (2004). Inactivation of an ABC transporter gene, *mcyH*, results in loss of microcystin production in the *Cyanobacterium microcystis aeruginosa* PCC 7806. Appl. Environ. Microbiol. *70*, 6370–6378.
40. Thykaer, J., Nielsen, J., Wohlleben, W., Weber, T., Gutknecht, M., Lantz, A.E., and Stegmann, E. (2010). Increased glycopeptide production after overexpression of shikimate pathway genes being part of the balhimycin biosynthetic gene cluster. Metab. Eng. *12*, 455–461.
41. Goldfinger, V., Spohn, M., Rodler, J.P., Sigle, M., Kulik, A., Cryle, M.J., Rapp, J., Link, H., Wohlleben, W., and Stegmann, E. (2023). Metabolic engineering of the shikimate pathway in *Amycolatopsis* strains for optimized glycopeptide antibiotic production. Metab. Eng. *78*, 84–92.
42. Chen, J., van Heel, A.J., and Kuipers, O.P. (2020). Subcellular localization and assembly process of the nisin biosynthesis machinery in *Lactococcus lactis*. mBio *11*, e02825-20.
43. Chen, J., van Heel, A.J., and Kuipers, O.P. (2021). Visualization and analysis of the dynamic assembly of a heterologous lantibiotic biosynbhesis complex in *Bacillus subtilis*. mBio *12*, e0121921.
44. Browman, D.T., Hoegg, M.B., and Robbins, S.M. (2007). The SPFH domain-containing proteins: more than lipid raft markers. Trends Cell Biol. *17*, 394–402.
45. Kerfeld, C.A., Aussignargues, C., Zarzycki, J., Cai, F., and Sutter, M. (2018). Bacterial microcompartments. Nat. Rev. Microbiol. *16*, 277–290.
46. Yang, M., Simpson, D.M., Wenner, N., Brownridge, P., Harman, V.M., Hinton, J.C.D., Beynon, R.J., and Liu, L.N. (2020). Decoding the stoichiometric composition and organisation of bacterial metabolosomes. Nat. Commun. *11*, 1976.
47. Perez-Riverol, Y., Bai, J., Bandla, C., García-Seisdedos, D., Hewapathirana, S., Kamatchinathan, S., Kundu, D.J., Prakash, A., Frericks-Zipper, A., Eisenacher, M., et al. (2022). The PRIDE database resources in 2022: a hub for mass spectrometry-based proteomics evidences. Nucleic Acids Res. *50*, D543–D552.
48. Bowers, K.J., Chow, E., Xu, H., Dror, R.O., Eastwood, M.P., Gregersen, B.A., Klepeis, J.L., Kolossvary, I., Moraes, M.A., Sacerdoti, F.D., et al. (2006). Scalable algorithms for molecular dynamics simulations on commodity clusters. In *Proceedings of the 2006 ACM/IEEE conference on Supercomputing* 84-es (Association for Computing Machinery). https://doi.org/10.1145/1188455.1188544.

49. Lu, C., Wu, C., Ghoreishi, D., Chen, W., Wang, L., Damm, W., Ross, G.A., Dahlgren, M.K., Russell, E., Von Bargen, C.D., et al. (2021). OPLS4: Improving force field accuracy on challenging regimes of chemical space. J. Chem. Theor. Comput. *17*, 4291–4300.
50. Friesner, R.A., Murphy, R.B., Repasky, M.P., Frye, L.L., Greenwood, J.R., Halgren, T.A., Sanschagrin, P.C., and Mainz, D.T. (2006). Extra precision glide: docking and scoring incorporating a model of hydrophobic enclosure for protein-ligand complexes. J. Med. Chem. *49*, 6177–6196.
51. Shelley, J.C., Cholleti, A., Frye, L.L., Greenwood, J.R., Timlin, M.R., and Uchimaya, M. (2007). Epik: a software program for pK(a) prediction and protonation state generation for drug-like molecules. J. Comput. Aided Mol. Des. *21*, 681–691.
52. Seemann, T. (2014). Prokka: rapid prokaryotic genome annotation. Bioinforma. Oxf. Engl. *30*, 2068–2069.
53. Emms, D.M., and Kelly, S. (2019). OrthoFinder: phylogenetic orthology inference for comparative genomics. Genome Biol. *20*, 238.
54. Virtanen, P., Gommers, R., Oliphant, T.E., Haberland, M., Reddy, T., Cournapeau, D., Burovski, E., Peterson, P., Weckesser, W., Bright, J., et al. (2020). SciPy 1.0: fundamental algorithms for scientific computing in Python. Nat. Methods *17*, 261–272.
55. Kumar, S., Stecher, G., Li, M., Knyaz, C., Tamura, K., and MEGA, X. (2018). Molecular evolutionary genetics analysis across computing platforms. Mol. Biol. Evol. *35*, 1547–1549.
56. Edgar, R.C. (2004). MUSCLE: multiple sequence alignment with high accuracy and high throughput. Nucleic Acids Res. *32*, 1792–1797.
57. Letunic, I., and Bork, P. (2021). Interactive Tree Of Life (iTOL) v5: an online tool for phylogenetic tree display and annotation. Nucleic Acids Res. *49*, W293–W296.
58. Capella-Gutiérrez, S., Silla-Martínez, J.M., and Gabaldón, T. (2009). trimAl: a tool for automated alignment trimming in large-scale phylogenetic analyses. Bioinformatics *25*, 1972–1973.
59. Le, S.Q., and Gascuel, O. (2008). An improved general amino acid replacement matrix. Mol. Biol. Evol. *25*, 1307–1320.
60. Kieser, T., Bibb, M.J., Buttner, M.J., Chater, K.F., and Hopwood, D.A. (2000). Practical Streptomyces Genetics (John Innes Foundation).
61. Pelzer, S., Reichert, W., Huppert, M., Heckmann, D., and Wohlleben, W. (1997). Cloning and analysis of a peptide synthetase gene of the balhimycin producer *Amycolatopsis mediterranei* DSM5908 and development of a gene disruption/replacement system. J. Biotechnol. *56*, 115–128.
62. Gibson, D.G., Young, L., Chuang, R.Y., Venter, J.C., Hutchison, C.A., 3rd, and Smith, H.O. (2009). Enzymatic assembly of DNA molecules up to several hundred kilobases. Nat. Methods *6*, 343–345.
63. Madoń, J., and Hütter, R. (1991). Transformation system for *Amycolatopsis* (*Nocardia) mediterranei*: direct transformation of mycelium with plasmid DNA. J. Bacteriol. *173*, 6325–6331.
64. Dietsche, T., Tesfazgi Mebrhatu, M., Brunner, M.J., Abrusci, P., Yan, J., Franz-Wachtel, M., Schärfe, C., Zilkenat, S., Grin, I., Galán, J.E., et al. (2016). Structural and functional characterization of the bacterial type III secretion export apparatus. PLoS Pathog *12*, e1006071. https://doi.org/10.1371/journal.ppat.1006071.
65. Zilkenat, S., Kim, E., Dietsche, T., Monjarás Feria, J.V., Torres-Vargas, C.E., Mebrhatu, M.T., and Wagner, S. (2024). Blue native PAGE analysis of bacterial secretion complexes in bacterial secretion systems. In Methods and Protocols, L. Journet and E. Cascales, eds. (Springer US), pp. 331–362. https://doi.org/10.1007/978-1-0716-3445-5_22.
66. Davis, B.D., and Mingioli, E.S. (1950). Mutants of *Escherichia coli* requiring methionine or vitamin B12. J. Bacteriol. *60*, 17–28.
67. St-Pierre, J.-F., Bunker, A., Róg, T., Karttunen, M., and Mousseau, N. (2012). Molecular Dynamics Simulations of the bacterial ABC transporter SAV1866 in the closed form. J. Phys. Chem. B *116*, 2934–2942.
68. (2004). Glide: a new approach for rapid, accurate docking and scoring. 1. Method and assessment of docking accuracy. J. Med. Chem. *47*, 1739–1749.
69. Vesga, L.C., Kronenberger, T., Tonduru, A.K., Kita, D.H., Zattoni, I.F., Bernal, C.C., Bohórquez, A.R.R., Mendez-Sánchez, S.C., Ambudkar, S.V., Valdameri, G., and Poso, A. (2021). Tetrahydroquinoline/4,5-dihydroisoxazole molecular hybrids as inhibitors of breast cancer resistance protein (BCRP/ABCG2). Chem. Med. Chem. *16*, 2686–2694.
70. Zattoni, I.F., Kronenberger, T., Kita, D.H., Guanaes, L.D., Guimarães, M.M., de Oliveira Prado, L., Ziasch, M., Vesga, L.C., Gomes de Moraes Rego, F., Picheth, G., et al. (2022). A new porphyrin as selective substrate-based inhibitor of breast cancer resistance protein (BCRP/ABCG2). Chem. Biol. Interact. *351*, 109718.
71. Jorgensen, W.L., Chandrasekhar, J., Madura, J.D., Impey, R.W., and Klein, M.L. (1983). Comparison of simple potential functions for simulating liquid water. J. Chem. Phys. *79*, 926–935.
72. Darden, T., York, D., and Pedersen, L. (1993). Particle mesh Ewald: An N·log(N) method for Ewald sums in large systems. J. Chem. Phys. *98*, 10089–10092.
73. Berendsen, H.J.C., Postma, J.P.M., van Gunsteren, W.F., DiNola, A., and Haak, J.R. (1984). Molecular dynamics with coupling to an external bath. J. Chem. Phys. *81*, 3684–3690.
74. Martyna, G.J., Klein, M.L., and Tuckerman, M. (1992). Nosé–Hoover chains: The canonical ensemble via continuous dynamics. J. Chem. Phys. *97*, 2635–2643.
75. Martyna, G.J., Tuckerman, M.E., Tobias, D.J., and Klein, M.L. (1996). Explicit reversible integrators for extended systems dynamics. Mol. Phys. *87*, 1117–1157.
76. Wingett, S.W., and Andrews, S. (2018). FastQ Screen: A tool for multi-genome mapping and quality control. F1000Res. *7*, 1338.
77. Schwengers, O., Jelonek, L., Dieckmann, M.A., Beyvers, S., Blom, J., and Goesmann, A. (2021). Bakta: rapid and standardized annotation of bacterial genomes via alignment-free sequence identification. Microb. Genom. *7*, 000685.
78. Kim, D., Langmead, B., and Salzberg, S.L. (2015). HISAT: a fast spliced aligner with low memory requirements. Nat. Methods *12*, 357–360.
79. Li, H., Handsaker, B., Wysoker, A., Fennell, T., Ruan, J., Homer, N., Marth, G., Abecasis, G., and Durbin, R.; 1000 Genome Project Data Processing Subgroup (2009). The Sequence Alignment/Map format and SAMtools. Bioinformatics *25*, 2078–2079.
80. Okonechnikov, K., Conesa, A., and García-Alcalde, F. (2016). Qualimap 2: advanced multi-sample quality control for high-throughput sequencing data. Bioinformatics *32*, 292–294.
81. Liao, Y., Smyth, G.K., and Shi, W. (2014). featureCounts: an efficient general purpose program for assigning sequence reads to genomic features. Bioinformatics *30*, 923–930.
82. Love, M.I., Huber, W., and Anders, S. (2014). Moderated estimation of fold change and dispersion for RNA-seq data with DESeq2. Genome Biol. *15*, 550.
83. Guder, J.C., Schramm, T., Sander, T., and Link, H. (2017). Time-optimized isotope ratio LC-MS/MS for high-throughput quantification of primary metabolites. Anal. Chem. *89*, 1624–1631.
84. Rappsilber, J., Mann, M., and Ishihama, Y. (2007). Protocol for micro-purification, enrichment, pre-fractionation and storage of peptides for proteomics using StageTips. Nat. Protoc. *2*, 1896–1906.
85. Semanjski, M., Germain, E., Bratl, K., Kiessling, A., Gerdes, K., and Macek, B. (2018). The kinases HipA and HipA7 phosphorylate different substrate pools in *Escherichia coli* to promote multidrug tolerance. Sci. Signal. *11*, eaat5750.
86. Cox, J., and Mann, M. (2008). MaxQuant enables high peptide identification rates, individualized p.p.b.-range mass accuracies and proteome-wide protein quantification. Nat. Biotechnol. *26*, 1367–1372.
87. Cox, J., Neuhauser, N., Michalski, A., Scheltema, R.A., Olsen, J.V., and Mann, M. (2011). Andromeda: A peptide search engine integrated into the MaxQuant environment. J. Proteome Res. *10*, 1794–1805.

88. Elias, J.E., and Gygi, S.P. (2007). Target-decoy search strategy for increased confidence in large-scale protein identifications by mass spectrometry. Nat. Methods *4*, 207–214.

89. Luber, C.A., Cox, J., Lauterbach, H., Fancke, B., Selbach, M., Tschopp, J., Akira, S., Wiegand, M., Hochrein, H., O'Keeffe, M., and Mann, M. (2010). Quantitative proteomics reveals subset-specific viral recognition in dendritic cells. Immunity *32*, 279–289.

90. Schwanhäusser, B., Busse, D., Li, N., Dittmar, G., Schuchhardt, J., Wolf, J., Chen, W., and Selbach, M. (2011). Global quantification of mammalian gene expression control. Nature *473*, 337–342.

91. Aguilan, J.T., Kulej, K., and Sidoli, S. (2020). Guide for protein fold change and *p* -value calculation for non-experts in proteomics. Mol. Omics *16*, 573–582.

92. R Core Team (2023). R: A Language and Environment for Statistical Computing (R Foundation for Statistical Computing).

93. Wickham, H., François, R., Henry, L., Müller, K., and Vaughan, D. (2023). dplyr: A Grammar of Data Manipulation. R package version 1.1.4. https://github.com/tidyverse/dplyr.

94. Wickham, H., and Bryan, J. (2025). readxl: Read Excel Files. R package version 1.4.5. https://github.com/tidyverse/readxl.

95. Wickham, H. (2016). ggplot2: Elegant Graphics for Data Analysis (New York: Springer-Verlag). https://doi.org/10.1007/978-3-319-24277-4_9.

96. Wickham, H. (2007). Reshaping Data with the reshape Package. J. Stat. Software *21*, 1–20.

STAR★METHODS

KEY RESOURCES TABLE

REAGENT or RESOURCE	SOURCE	IDENTIFIER
Antibodies		
anti-FLAG® M2	Sigma-Aldrich	RRID:AB_259529
Rabbit polyclonal anti-BirA IgG	Thermo-Fisher	RRID:AB_2787583
goat anti-Mouse IgG DyLight™ 800	Thermo-Fisher	RRID:AB_2556774
goat anti-Rabbit IgG DyLight™ 800	Thermo-Fisher	RRID:AB_2556775
Streptavidin DyLight™ 800	Thermo-Fisher	RRID:AB_11152196
Bacterial and virus strains		
See Table S5 in the SI	This work	
Chemicals, peptides, and recombinant proteins		
Q5® Hot Start High-Fidelity DNA Polymerase	NEB	M0491L
Phusion® High-Fidelity DNA Polymerase	Thermo-Fisher	F-530XL
Taq DNA Polymerase	Thermo-Fisher	EP0401
NdeI	Thermo-Fisher	ER0585
XbaI	Thermo-Fisher	ER0683
KpnI	Thermo-Fisher	ER0522
Apramycin	Genaxxon	M3450.0005
Ampicillin	Roth	K029.4
Erythromycin	Roth	4166.2
Deposited data		
MD simulation trajectories, interaction data and MD quality control data, representative PDB files from the alphaFold models and phylogenetic trees	This work	https://doi.org/10.5281/zenodo.7547342 https://doi.org/10.5281/zenodo.7732071 https://doi.org/10.5281/zenodo.7547403
RNA-Seq Illumina read files as well as the raw counts	This work	GSE274067
Mass spectrometry proteomics data	This work	PXD054387
Metabolomics raw data	This work	https://doi.org/10.5281/zenodo.14918266
Oligonucleotides		
See Table S4 for cloning primers	This work	
Recombinant DNA		
See Table S6 for plasmids	This work	
Software and algorithms		
AlphaFold (v2.2.2)~~/Alphafold3~~	Jumper et al.[26]	
Desmond	Bowers et al.[48]	
OPLS4 force-field	Lu et al.[49]	
Glide	Friesner et al.[50]	
LigPrep	Shelley et al.[51]	
Maestro (v2022.4)	www.schrodinger.com	
prokka (v1.14.16)	Seemann[52]	
OrthoFinder platform (v2.3.11)	Emms and Kelly[53]	
blastP	https://blast.ncbi.nlm.nih.gov/	
scipy (v1.9.3)	Virtanen et al.[54]	
ΔG prediction server (v1.0)	Hessa et al.[19]	
MEGAX (v10.2.4)	Kumar et al.[55]	
MUSCLE algorithm	Edgar[56]	

(*Continued on next page*)

Continued

REAGENT or RESOURCE	SOURCE	IDENTIFIER
iTOL (v6.6)	Letunic and Bork[57]	
Other		
Serva, NativePAGE™ 3 to 12% (Bis-Tris, 1.0 mm, Mini Protein Gels)	Thermo-Fisher	BN1001BOX
Immun-Blot® polyvinylidene difluoride (PVDF) membrane (0.2 μm)	Bio-Rad	#1620177

EXPERIMENTAL MODEL AND STUDY PARTICIPANT DETAILS

The bacterial strains and plasmids used in this study are described with the necessary information in Tables S5 and S6.

METHOD DETAILS

Identification of transporter sequences of biosynthetic gene clusters

The biosynthetic gene clusters (BGC) of glycopeptide antibiotics (GPAs) were identified either by literature search[2] or by a hidden Markov model (HMM) search in the NCBI database using the X-domain sequence of non-ribosomal peptide synthetases (NRPS) of known GPAs.[4] If necessary, genomes and clusters were re-annotated with prokka (v1.14.16) using default parameters with specified genus.[52] Subsequently, genes encoding putative ATP binding cassette (ABC) transporters were identified by using the OrthoFinder platform (v2.3.11).[53] This tool classifies all genes into groups whose members are orthologous with each other and therefore suitable for phylogenetic analyses. The correlation of BGC to GPA types was done manually. Every gene in the BGC was blasted and studied in order to classify the BGC in one of the five classical types of GPAs (I-V). The criteria used were the predicted amino acids at positions one and three of the backbone, the number of P450 monooxygenase genes and the presence of an acyltransferase-encoding gene.

Bioinformatic analysis of transporters

Amino acid sequence identities of the transporters were calculated by blastP pairwise comparison and displayed in a heatmap representation. The order of the transporters is based on a hierarchical clustering calculated with the python library scipy (v1.9.3) and using the function "scipy.cluster.hierarchy.linkage". The algorithm used was "Weighted Pair Group Method with Arithmetic Mean" (WPGMA), which builds a hierarchy of the clusters (of similar transporters) using an agglomerative approach.[54] The full protein scan option of the ΔG prediction server (v1.0)[19] was used to identify putative transmembrane (TM) helices (full protein scan; helix length 19–23; +length correction). Common sequence motifs of the NBDs of the ABC transporters[18] were manually identified after multiple sequence alignment (MSA) of all transporters using MEGAX (v10.2.4).[55]

Phylogenetic analysis of GPA associated ABC transporter

The evolutionary relationship between GPA associated ABC transporters was analyzed by phylogenetic tree construction. MSA, model testing, and calculation of the Maximum Likelihood phylogenetic tree were performed using the software MEGA-X (v10.2.4).[55] Trimming of the MSA was done with the trimAl tool (v1.4.rev15 build[2013-12-17]) using default parameters,[58] or manually. An unrelated ABC transporter (Abc30) of *A. balhimycina* was used as an outgroup. The phylogenetic tree was constructed as follows: all sequences were aligned using the MUSCLE algorithm[56] and then used to analyze the best amino acid substitution model. The model testing identified as the most suitable the model of Le & Gascuel (LG)[59] with frequencies (+F) and gamma distributed rates (number of discrete gamma categories = 5) (+G), and this was used by the ML algorithm with bootstrap test of 1000 repetitions to calculate phylogenetic trees. Visualization of phylogenetic trees was performed with iTOL (v6.6).[57]

Chemicals and reagents

Unless otherwise indicated, chemicals and enzymes were purchased from Sigma-Aldrich, Thermo-Fisher, and New England Biolabs. Primers listed in Table S4 were synthesized by Eurofins Scientific or IDT. Antibodies were purchased from Sigma-Aldrich (Mouse monoclonal anti-FLAG M2 (F3165)) and Thermo-Fisher (Rabbit polyclonal anti-BirA IgG (PA5-80251); goat anti-Mouse IgG DyLight 800 (SA5-35521); goat anti-Rabbit IgG DyLight 800 (SA5-35571); Streptavidin DyLight 800 (21851)). SERVAGel TG PRiME 8–16% precast gels were purchased from Serva, NativePAGE 3 to 12% (Bis-Tris, 1.0 mm, Mini Protein Gels) from Thermo-Fisher, and Immun-Blot polyvinylidene difluoride (PVDF) membrane (0.2 μm) from Bio-Rad.

Bacterial strains, plasmids, and growth conditions

All bacterial strains and plasmids used in this study are listed in Tables S5 and S6, respectively. *E. coli* was cultivated aerobically at 37°C in 10 mL tubes and shaken at 180 rpm in liquid LB medium (0.5% (w/v) yeast extract, 1% (w/v) tryptone, 85.56 mM NaCl) or on

solid LB agar (1.5% (w/v)) medium. If necessary, the medium was supplemented with 100 μg/mL apramycin or 100 μg/mL ampicillin for plasmid selection. Unless otherwise indicated, *A. balhimycina* was cultivated aerobically at 29°C in baffled flasks with a steel coil, and shaken at 120 rpm in R5 medium[60] or on the respective solid agar (1.5% (w/v)) medium. Fifty μg/ml apramycin or 50 μg/mL erythromycin was used for plasmid selection. All *A. balhimycina* strains in this study are derivatives of DSM 44591.

Molecular cloning

Different DNA modification techniques were used in this study. Polymerase chain reaction (PCR) with "Q5 Hot Start High-Fidelity DNA Polymerase" and "Phusion High-Fidelity DNA Polymerase" were used to amplify genes and DNA fragments, while "Taq DNA Polymerase" was used for colony PCR. pRM4[10] vector DNA was linearized using the restriction endonucleases *NdeI*/*XbaI*, pSP1[61] vector was linearized using the restriction endonuclease *KpnI*. Assembly of DNA fragments was performed using standard gibson assembly method.[62] All primers used in this study are listed in Table S4.

Genetic manipulation of *A. balhimycina*

Chromosomal integration of genes into the genome of *A. balhimycina* was achieved by direct transformation (D-Trafo), as first described for *Amycolatopsis mediterranei*[63] and later adapted for *A. balhimycina*.[61] Demethylated plasmid DNA was isolated from *E. coli* JM110 or ET12567 and used for the transformation of *A. balhimycina* after 48 h of growth. Correct integration was confirmed by PCR.

Generation of *A. balhimycina* deletion mutants

In-frame *A. balhimycina* deletion mutants were generated using the non-replicative plasmid pSP1,[61] which contains homologous flanking regions of ≈1.5 kB upstream and downstream of the target genes *tba* or *bgtfB*, resulting in the plasmids pSP1Δ*tba* and pSP1Δ*bgtfB*, respectively. *A. balhimycina* was transformed with the plasmids using D-Trafo. For single mutants, pSP1Δ*tba* and pSP1Δ*bgtfB* were introduced into *A. balhimycina* wildtype, whereas for the generation of the double mutant *A. balhimycina ΔbhaAΔbgtfB,* we introduced pSP1Δ*bgtfB* into the existing mutant *A. balhimycina ΔbhaA*.[28] Erythromycin resistant clones harboring either pSP1Δ*tba* or pSP1Δ*bgtfB* were confirmed by PCR using the primers P1-2 (Table S4), and subsequently used for the stress protocol to increase the frequency of double crossover events.[28] The resulting protoplasts were streaked onto R5 agar plates and R5 agar plates supplemented with 50 μg/mL erythromycin for selection. Erythromycin sensitive clones were screened for in-frame deletion by PCR using primers P9-10 and P15-16 (Table S4).

Crude membrane preparation

Crude membranes of *A. balhimycina* were prepared as reported previously by the group.[64] In brief, 300 mg of culture wet weight was used. The cells were washed with 1xPBS, resuspended in 750 μL buffer K (50 mM triethanolamine (TEA), pH 7.5, 250 mM sucrose, 1 mM EDTA, 1 mM $MgCl_2$, 10 μg/mL DNAse, 2 mg/mL lysozyme, 1:100 protease inhibitor cocktail (Sigma-Aldrich (P8849)) and incubated for 30 min at 4°C. Afterward, the cells were mixed with glass beads (Ø = 150–212 μm) and lysed through a bead mill (2 min, continuously). Cell debris was removed by centrifugation at 10,000 x *g* for 10 min. The crude membranes were precipitated by centrifugation at 55,000 x *g* at 4°C for 45 min and resuspended in 75 μL 1xPBS.

BN-PAGE, SDS-PAGE, and immunoblotting

Analysis of native transporter complexes was performed as described previously.[65] Crude membranes were solubilized for 1 h at 4°C using 1% Lauryl Maltose Neopentyl Glycol (LMNG). Non-solubilized materials were separated by centrifugation at 100,000 *x g* at 4°C for 30 min. Fifteen μg of solubilized membrane proteins were subjected to BN-PAGE (NativePAGE 3 to 12%) before transfer to a PVDF membrane. Similarly, for the analysis of denatured proteins, samples were subjected to SDS-PAGE (SERVAGel TG PRiME 8–16%). Membranes were probed with mouse anti-FLAG primary antibody (1:10,000), rabbit anti-BirA (1:5,000), anti-mouse secondary antibody (1:10,000), anti-rabbit secondary antibody (1:10,000), or Streptavidin DyLight 800 (1:10,000). Detection and analysis were performed using a Li-Cor Odyssey system and image Studio (Li-Cor) (v5.2).

Balhimycin production, export assay and bioactivity assay

All relevant strains were inoculated in 20 mL of R5 medium and incubated for 48 h as preculture. Five mL of the preculture was used for inoculation of 100 mL main culture in R5 medium. After 96 h of growth, 10 mL of every culture was sampled and separated by centrifugation into supernatant and mycelium. The supernatant was directly used for bioactivity assays as well as for High Performance Liquid Chromatography-Electrospray Ionisation-Mass Spectrometry (HPLC-ESI-MS) measurements. The mycelium was further processed in order to extract intracellular balhimycin. First, it was washed with 10 mL deionized water (diH_2O), 5 mL carbonate buffer (pH 9.7) and again with 10 mL diH_2O, to remove trace amounts of cell wall bound balhimycin. Then, the mycelium was lyophilized and weighed for dry cell weight (DCW) determination and used for normalization. Five mL of methanol was used to extract balhimycin from the mycelium (12–16 h). The methanol fraction was separated from the mycelium by centrifugation and collected. The mycelium was washed with 5 mL diH_2O and the supernatant was also collected. The methanol and water wash fractions were pooled and the extract was evaporated using a Genevac EZ-2 (Genevac Ltd, Suffolk, UK). Finally, the evaporated extracts were dissolved in 0.3 mL of H_2O and used for bioactivity assays as well as HPLC-ESI-MS measurements. For bioactivity assays we used MM1

medium[66] indicator plates containing *B. subtilis* DSM10 spores (5x10^6 spores/mL) and applied 30–40 μL culture supernatant of various *A. balhimycina* strains. The plates were incubated at 37°C overnight.

HPLC-MS analysis and quantification of balhimycin

For the detection of balhimycin 2.5 μL of the culture supernatants and mycelium extracts were analyzed by means of HPLC–ESI-MS using a Nucleosil 100-C18 column (3 μm, 100 by 2 mm) (precolumn, 10 by 2 mm) (Dr. Maisch GmbH, Ammerbuch-Entringen, Germany) coupled to an ESI mass spectrometer. LC-MS measurements were obtained from the liquid chromatograph/mass selective detector (LC/MSD) Ultra Trap system XCT 6330 (Agilent Technologies, Waldbronn, Germany). Analysis was carried out at a flow rate of 400 μL/min with gradient elution. Solvent A was 0.1% formic acid, and solvent B 0.06% formic acid in acetonitrile. Gradient elution was performed as follows: t0 = 0% B, t15 = t17 = 100% B, post time 5 min 0% B. The flow rate was 400 μL/min, and the temperature was 40°C. For MS analysis an electrospray ionization (alternating positive and negative ionization) in Ultra Scan mode with a capillary voltage of 3.5 kV and a drying gas temperature of 350°C was used. The detection of m/z values was performed with Agilent DataAnalysis for 6300 series Ion Trap LC/MS 6.1 software (v3.4) (Bruker-Daltonik GmbH).

Molecular modeling and molecular dynamics simulation

Protein structure prediction

The structural model of relevant transporter members was retrieved from the AlphaFold (v2.2.2) Protein Structure Database using the multimer preset.[26] All structure models can be found in the Zenodo repository or upon reasonable request. Previous Sav1866 unbiased simulations,[67] starting from the experimentally available outward open conformation (PDB 2HYD), revealed small conformational changes in the NBD. Alternatively, steered dynamics suggested that, despite the large opening-closing NBD movement, TMD conformational changes are independent. Based on that, we hypothesized that our current simulation length would be insufficient to observe the inward-open transition. This prompted us to generate an inward-open Sav1866 model (UniProt ID: Q99T13, similar to PDB 5MKK), in order to allow a direct comparison against the Tva, Tri and Tba inward-open models. Sav1866 model structure was generated based on the heterodimeric ABC transporter TmrAB (PDB ID: 5MKK), selected based on sequence similarity, using the Homology Model package from Maestro (v2022.4).

Binding site prediction and molecular docking

System preparation and docking calculations were performed using the Schrödinger Drug Discovery suite for molecular modeling (v2022.4). Protein−ligand complex was prepared with the Protein Preparation Wizard to fix protonation states of amino acids, add hydrogens, and fix missing side-chain atoms. All ligands for docking were drawn using Maestro and prepared using LigPrep[51] to generate the 3D conformation, adjust the protonation state to physiological pH (7.4), and calculate the partial atomic charges with the OPLS4 force field. Docking studies with the prepared ligands were performed using Glide (v7.7)[50,68] with the flexible modality of induced-fit docking with extra precision (XP), followed by a side-chain minimization step using Prime. Ligands were docked within a grid around 12 Å from the centroid of the predicted binding site pocket, determined using SiteMap.

Molecular dynamics simulation

MD simulations for similar ABC transporters were previously validated by the group.[69,70] MD simulations were carried out using Desmond,[48] with the OPLS4 force-field.[49] The simulated system encompassed the protein-ligand complexes, a predefined water model (TIP3P[71]) as a solvent and counterions. The system was treated in an orthorhombic box with periodic boundary conditions specifying the box's shape and size as 10 Å distance from the box edges to any atom of the protein. POPC membranes were assigned to the transmembrane helices using the System Setup, with standard options. In all simulations, we used a time step of 1 fs, the short-range coulombic interactions were treated using a cut-off value of 9.0 Å using the short-range method, while the Smooth Particle Mesh Ewald method (PME) handled long-range coulombic interactions.[72] Initially, the system's relaxation was performed using Steepest Descent and the limited-memory Broyden-Fletcher-Goldfarb-Shanno algorithms in a hybrid manner, according to the established protocol available in the Desmond standard settings. During the equilibration step, the simulation was performed under the NPT ensemble for 5 ns implementing the Berendsen thermostat and barostat methods.[73] A constant temperature of 310 K was kept throughout the simulation using the Nose-Hoover thermostat algorithm[74] and Martyna-Tobias-Klein Barostat[75] algorithm to maintain 1 atm of pressure, respectively. After minimization and relaxation of the system, we continued with the production step of at least 800 ns, with frames being recorded/saved every 1,000 ps. Five independent replicas were produced for each substrate, resulting in a total of 4 μs simulation/ligand. Trajectories and interaction data are available on the Zenodo repository (see data availability session). The representative structures were selected by inspecting changes in the Root-mean-square deviation (RMSD), meaning for figures a representative frame was selected at random at points of the trajectory where the RMSD for were not fluctuating, after equilibration. Variation of the RMSD values along with the simulation, for both template crystal structures and simulations with docking pose are provided in the repository. Additionally, the changes in the Root-mean-square fluctuation (RMSF), normalized by residue for the protein backbone, are also provided in the Zenodo repository.

Transcriptomic analysis

For the transcriptomic analysis, *A. balhimycina* wildtype, Δ*tba* and Δ*bbr* were cultivated in balhimycin production conditions for 48 h followed by RNA extraction using the "Zymo Quick RNA Fungal/Bacterial Kit" (Zymo Research, CN#R2014) according to the manufacturer's instructions. The RNA integrity was checked by agarose gel electrophoresis and residual DNA was removed by DNAseI

treatment using the "DNA-free DNA Removal Kit" (ThermoFischer, CN#AM1906). Successful digestion was initially checked by PCR. The total RNA was quantified with a "Qubit RNA BR Assay Kit" (Thermo Fisher) and RNA integrity was checked by an Agilent 2100 BioAnalyzer with the "RNA 6000 Pico kit" (Agilent). Library preparation and ligation were performed using "Illumina Stranded Total RNA Prep" and "Ribo-Zero Plus Microbiome", respectively, according to the manufacturer's instructions. In brief, 100 ng of total RNA per sample were subjected to rRNA depletion, followed by cDNA library construction, adapter ligation, and 15 cycles of barcoding PCR. The obtained libraries were quantified with the "Qubit 1x DNA HS Assay Kit" (Thermo Fisher) and the fragment distribution was checked with an Agilent 2100 BioAnalyzer using the "High Sensitivity DNA Kit" (Agilent). Libraries were subsequently pooled and sequenced on an Illumina NovaSeq 6000 device using "NovaSeq 6000 SP Reagent Kit" (v1.5) (100 cycles) with a run mode 75,10,10,0. The average number of reads obtained was 13-21x106. The sequencing was demultiplexed with the latest version of the nextflow pipeline: nf-core/demultiplex. For demultiplexing, "bcl2fastq" was used and the quality was checked with "fastp".

Sequencing statistics, including the quality per base and adapter content assessment, were conducted with FastQC (v0.11.8).[76] All reads mappings were performed against the assembled strain *A. balhimycina* DSM 44591. The strain was annotated using BAKTA (v1.9.1).[77] The annotation of the cluster genes (positions 6028489 to 6094273) was manually curated. The mappings of all samples were conducted with HISAT2 (v2.1.0),[78] using the following parameters: spliced alignment of reads was disabled and strand-specific information was set to reverse complemented (HISAT2 parameter –no-spliced-alignment and –rna-strandness "R"). The resulting mapping files in SAM format were converted to BAM format using SAMtools (v1.9).[79] Mapping statistics, including strand specificity estimation and percentage of mapped reads, were conducted with the RNA-Seq module of QualiMap2 (v2.2.2-a).[80] Gene counts for all samples were computed with featureCounts (v1.6.4),[81] where the selected feature type was set to transcript records (featureCounts parameter -t transcript). A quality check for ribosomal rRNA was performed with a self-written script based on the absolute counts of annotated rRNAs. To assess variability across the replicates of each time series, a principal component analysis (PCA) was conducted with the DESeq2 package (v1.28.1).[82]

For the computation of genes differentially expressed between the mutants, DESeq2 was applied to the absolute gene counts as computed with featureCounts. For differences between the two mutants and the wildtype strain, genes with an adjusted *p*-value (FDR) < 0.05 and absolute log2 fold change (FC) > 1 were reported as differentially expressed.

Measurement of amino acid levels by metabolomic analysis

For metabolomic measurements, *A. balhimycina* wildtype and Δ*tba* were cultivated under balhimycin production conditions and harvested after 48 h. Two hundred μl of liquid cultures were filtered (Merck, Durapore 0.45 μm PVDF) using a vacuum pump. The obtained biomass was extracted with 1 mL of an acetonitrile:methanol:water solution (40:40:20) for 1 h at −20°C. The mixture was transferred to a tube with glass beads (Ø = 0.1–0.11 mm) and homogenized using a Precellys (2 × 30 s, 6.5 m/s). The mixture was centrifuged at −9°C and 13,000 rpm for 15 min. The supernatant was subsequently used for the LC-MS/MS measurement. Amino acids were measured via targeted LC-MS/MS as described previously.[83] The obtained ratios were further processed by normalizing the values to the dry cell weight (DCW). These values were then used to calculate the differences between the Δ*tba* mutant and the wildtype. The differences were expressed as log2 fold changes in relation to a 13C internal standard.

Proximity dependent biotinylation and proteomic analysis

For the proximity dependent biotinylation studies, *A. balhimycina* was cultivated under balhimycin producing conditions, as described in previous sections. Fifty mL of culture was harvested after 48 h at 5,000 *x g*, 4°C for 10 min. The cell pellet was washed with 20 mL of 1xPBS buffer and centrifuged at 4,600 *x g*, 4°C for 10 min. Biotin labeling was carried out in 20 mL 1xPBS supplemented with 500 μM biotin for 1 h at 37 °C at 650 rpm. The reaction was stopped at 4°C and three subsequent wash steps with ice-cold 1xPBS. The cells were resuspended in 15 mL lysis buffer (0.1 M Tris-HCl (pH 8.0), 0.15 M NaCl, 1 mM EDTA, 10 μg/mL DNAse, 2 mg/mL lysozyme, 1:100 protease inhibitor cocktail (Sigma-Aldrich (P8849), 1 mM $MgCl_2$) and sequentially disrupted by sonication (Branson sonifier 250) (output control "4", 35% duty cycle 2 × 30 s/10 s pause), followed by homogenization by a Constant System CF-1 homogenizer (I&L Biosystems) (2x 40,000 psi). The cell lysate was cleared twice at 10,000 *x g*, 4°C for 3 and 10 min. The protein concentration was measured using Pierce BCA Protein Assay Kits (Thermo Fisher). Five mg of total protein (Input) was used for enrichment of biotinylated proteins using 150 μL of MagStrep Strep-Tactin beads (IBA). Binding of proteins to the streptavidin magnetic beads was performed by overhead rotation at 4°C overnight. Washing and elution were performed as described by the manufacturer. Input, flowthrough, and elution fractions were applied to an SDS-PAGE gel as a control and probed after western blotting with an anti-BirA antibody or streptavidin.

For subsequent mass spectrometry analysis, 20 μL of every eluate fraction was loaded on an SDS-PAGE gel and run until the loading front reached approx. 1 cm of the gel. The proteins were stained using a standard Coomassie staining solution. Until further processing, the gel was stored in 5% acetic acid. The bands were excised and cut further into small pieces. Proteins were then digested in the gel with trypsin, whereby all incubation steps were carried out under shaking conditions: for destaining, gel pieces were washed three times with 5 mM ammonium bicarbonate (ABC) in acetonitrile (ACN) (1:1, v/v) for 20 min. After a dehydration step with 100% ACN for 10 min, disulfide bonds were reduced by adding 10 mM dithiothreitol (DTT) in 20 mM ABC for 45 min at 56°C. Thiol groups were carbamidomethylated with 55 mM iodoacetamide (IAA) in 20 mM ABC for 45 min in the dark. Subsequently, gel pieces were washed two times with 5 mM ABC in ACN (1:1, v/v) for 20 min and dehydrated with 100% ACN for 15 min. Liquid was evaporated by vacuum centrifugation for 10 min and sequencing grade trypsin (Promega) was added in a concentration of 12.5 ng/μL in

20 mM ABC, pH 8.0. Gel pieces were soaked for 10 min at room temperature (RT), then covered with 20 mM ABC, and proteins were digested at 37°C overnight. Peptide extraction was performed in three consecutive steps with different extraction buffers for 30 min: first 3% (v/v) trifluoroacetic acid (TFA) in 30% (v/v) ACN was added, followed by 0.5% (v/v) formic acid (FA) in 80% (v/v) ACN, and completed by 100% ACN. Supernatants were pooled and ACN was evaporated by vacuum centrifugation. Peptides were further purified with C18 StageTips[84] and analyzed on an EASY-nLC 1200 UHPLC coupled to a Q Exactive HF mass spectrometer (both Thermo Scientific) as described previously[85] with slight modification: peptides were eluted from the analytical column using a 46 min segmented gradient of 10-33-50% of HPLC solvent B (80% acetonitrile in 0.1% formic acid) at a flow rate of 200 nL/min. In the mass spectrometer, MS and MS/MS spectra were acquired at resolution 60k. Full MS target value and maximum IT were set to $3x10^6$ and 25 ms, respectively. In each scan cycle, the 7 most intense precursor ions were picked up, whereby MS/MS target value was set to 10^5 charges with a maximum IT of 110 ms.

MS data were processed using default parameters of the MaxQuant software (v2.4.12.0).[86] Extracted peak lists were submitted to database search using the Andromeda search engine[87] to query a target-decoy[88] database of *A. balhimycina* (9,427 entries, downloaded on 30th of January 2024) and 286 commonly observed contaminants.

In database search, full tryptic specificity was required and up to two missed cleavages were allowed. Carbamidomethylation of cysteine was set as fixed modification, whereas protein N-terminal acetylation, and oxidation of methionine were set as variable modifications. For the main search, the peptide mass tolerance was set to 4.5 ppm, and 20 ppm at the fragment ion level. Peptide, protein, and modification site identifications were filtered at a false discovery rate (FDR) of 0.01. The iBAQ (Intensity Based Absolute Quantification) and LFQ (Label-Free Quantification) algorithms were enabled, as was the "match between runs" option.[89,90]

Downstream statistical analysis was performed using LFQ values and according to Aguilan et al.[91] with an additional filtering step to remove hits that were only detected in one replicate and condition.

QUANTIFICATION AND STATISTICAL ANALYSIS

The extra- and intracellular amounts of balhimycin were quantified using the HPLC-MS data. For this purpose, the peak intensities of each data point in the MS chromatogram corresponding to the masses of balhimycin were summed to a total intensity value. The concentration of balhimycin in the analyzed samples was calculated by using a standard curve, in which the total intensities of pure balhimycin were used. The concentration values were used to determine the total amount of balhimycin in the supernatant or mycelium extracts, respectively. The export and accumulation levels of balhimycin were normalized to the dry cell weight (DCW). Normalized values were used for statistical analysis using R (v4.3.1)[92] including the additional packages "dplyr" (v1.1.3),[93] "readxl" (v1.4.3),[94] "ggplot2" (v3.5.0),[95] and "reshape" (v.1.4.4).[96] We used the "Wilcoxon signed-rank test" and the "Benjamini-Hochberg Procedure" to calculate significance levels (*p*-values) for all data analyzed. *p*-values <0.05 were considered as statistically significant. The results of this analysis are found in Figures 2 and 4 and the respective figure legend. Every datapoint represent one independent experiment and quantification (n). At least three independent experiments were performed per strain. Figure 2: *A. balhimycina* wildtype ($n = 11$), Δ*tba* ($n = 12$), Δ*tba* + *tba* ($n = 12$), Δ*tba* + tba^{3xFLAG} ($n = 11$), Δ*tba* + tri^{3xFLAG} ($n = 11$), Δ*tba* + tva^{3xFLAG} ($n = 8$), Δ*tba* + $tbaE545Q^{3xFLAG}$ ($n = 6$), Δ*tba* + $sav1866^{3xFLAG}$ ($n = 8$). Figure 4: *A. balhimycina* wildtype ($n = 3$), Δ*tba* ($n = 3$), Δ*tba* + tba^{3xFLAG} ($n = 3$), Δ*tba* + $tbaQ309G^{3xFLAG}$ ($n = 6$), Δ*tba* + $tbaR310A^{3xFLAG}$ ($n = 6$), Δ*tba* + $tbaT316A^{3xFLAG}$ ($n = 6$).

4.2.1 **Supplementary information of publication 1**

Gericke, N., Beqaj, D., Kronenberger, T., Kulik, A., Gavriilidou, A., Franz-Wachtel, M., Schoppmeier, U., Harbig, T., Rapp, J., Grin, I., Ziemert, N., Link, H., Nieselt, K., Macek, B., Wohlleben, W., Stegmann, E., Wagner, S., Unveiling the substrate specificity of the ABC transporter Tba and its role in glycopeptide biosynthesis, ISCIENCE (2025)

DOI: *https://doi.org/10.1016/j.isci.2025.112135*.

Tables S1 and S2 are not included in this document, but can be downloaded from DOI: https://doi.org/10.1016/j.isci.2025.112135.

iScience, Volume *28*

Supplemental information

Unveiling the substrate specificity of the ABC transporter Tba and its role in glycopeptide biosynthesis

Nicola Gericke, Dardan Beqaj, Thales Kronenberger, Andreas Kulik, Athina Gavriilidou, Mirita Franz-Wachtel, Ulrich Schoppmeier, Theresa Harbig, Johanna Rapp, Iwan Grin, Nadine Ziemert, Hannes Link, Kay Nieselt, Boris Macek, Wolfgang Wohlleben, Evi Stegmann, and Samuel Wagner

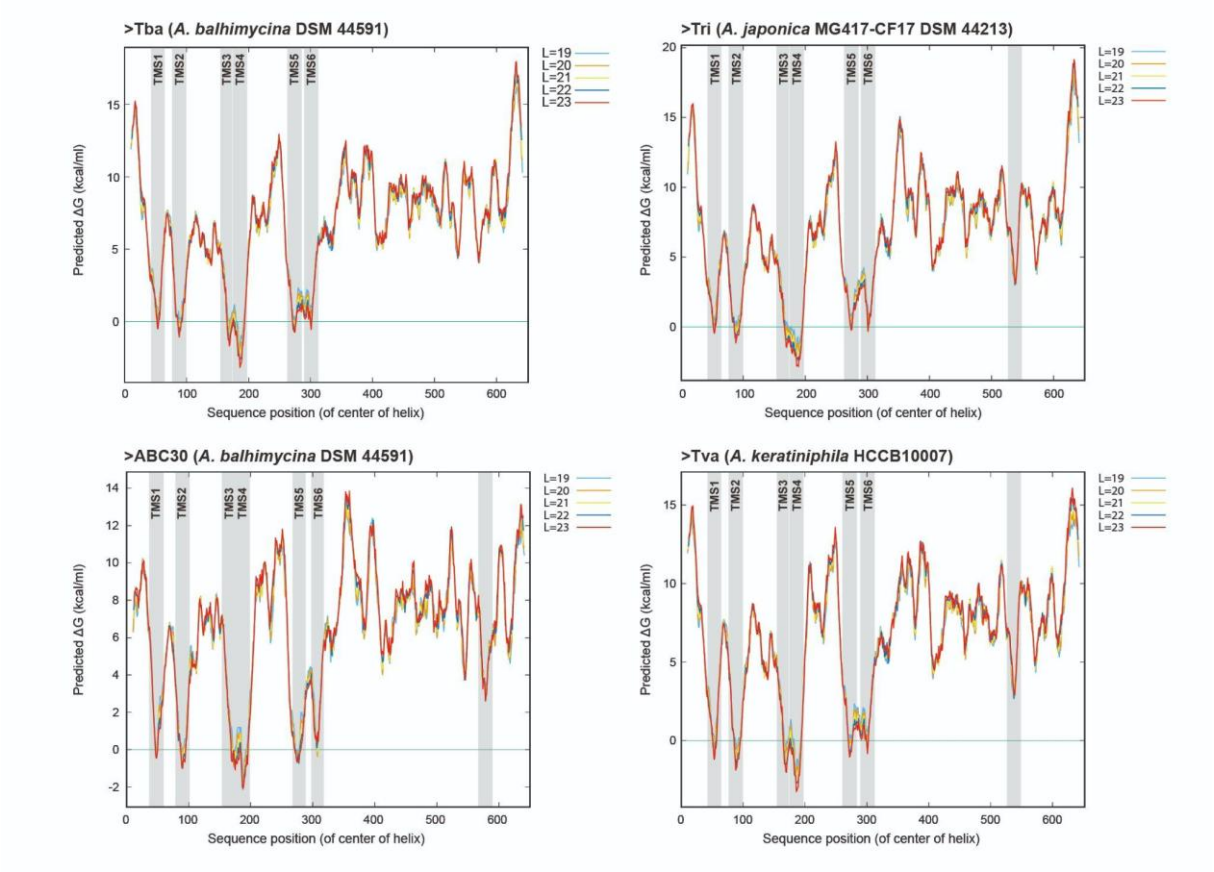

Figure S1. Prediction of transmembrane topology of different GPA ABC transporters. Prediction of transmembrane topology of ABC transporters encoded in the GPA BGC of *A. balhimycina* (Balhimycin producer), *A. japonica* (Ristomycin producer), *A. keratiniphila* (Vancomycin producer), and the non GPA transporter Abc30 of *A. balhimycina*. Topology was predicted based on the membrane integration propensity of segments (19-23 AA)[1]. Putative transmembrane segments (TMS) are marked in gray.

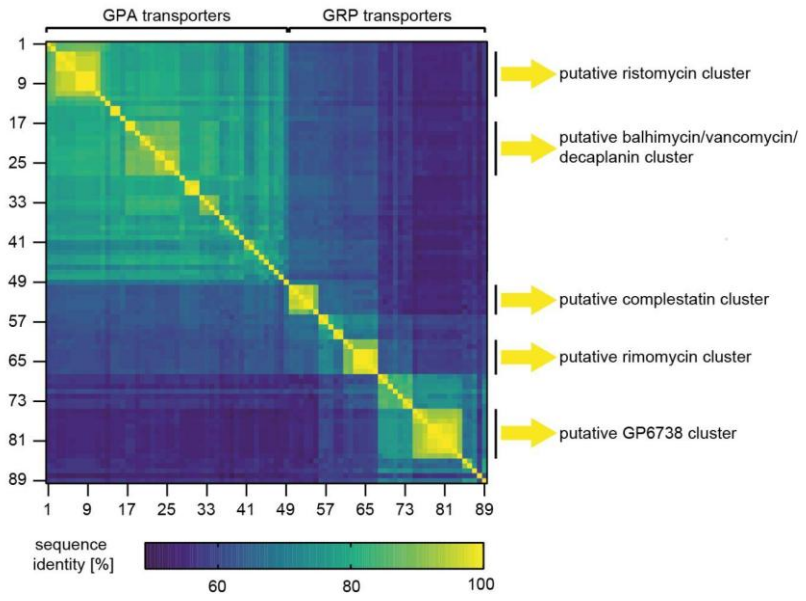

Figure S2. Similarity matrix of amino acid sequence identities of transporters. Heatmap representation of amino acid sequence identities of all 89 GPA and GRP associated ABC transporters. Identities were determined by a BlastP pairwise comparison analysis and are displayed in percent (%) of identity. Each number represents one transporter. The corresponding strains from which the sequences originate and numberings used in the heatmap are listed in supplementary table 1.

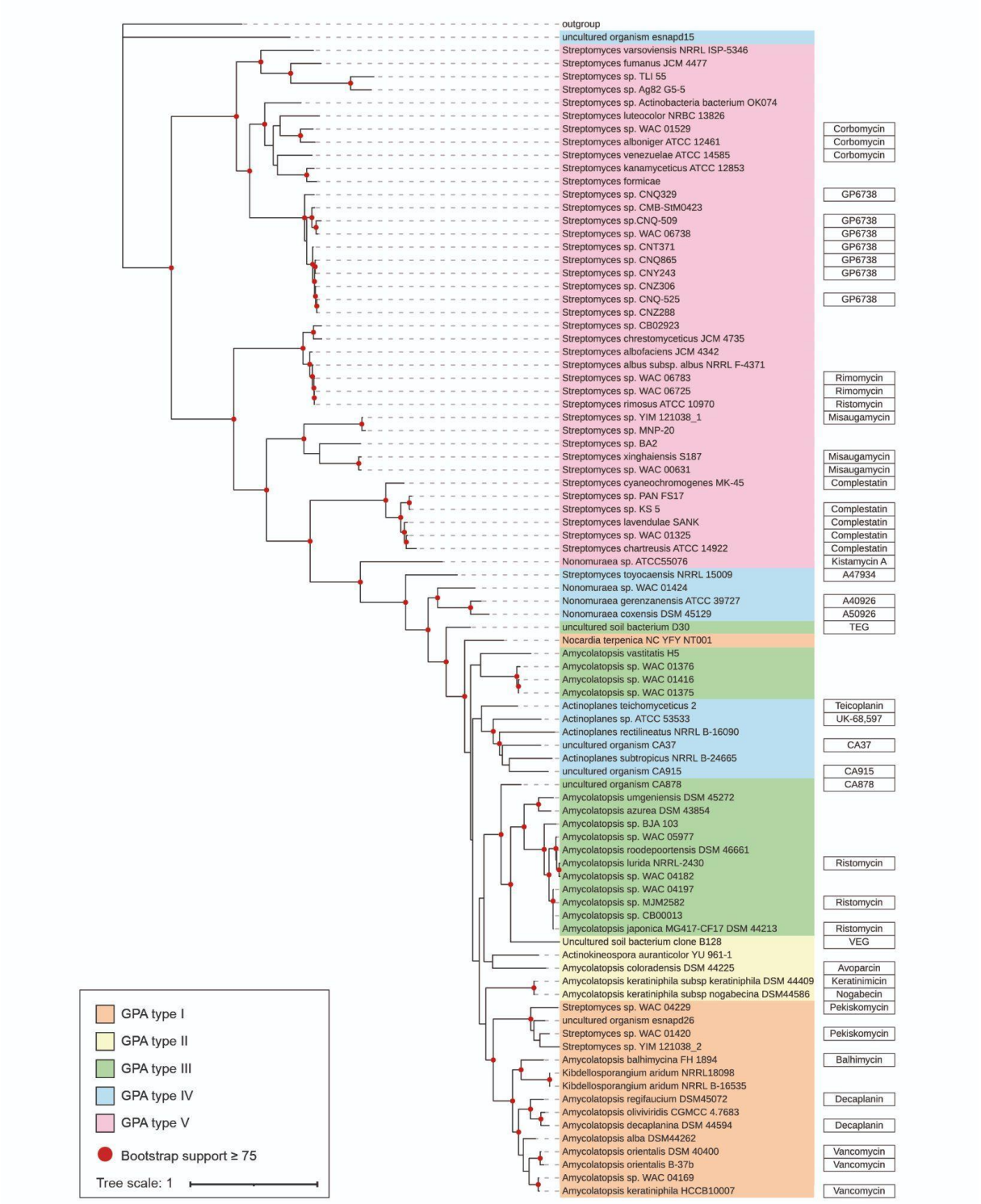

Figure S3. Evolutionary relationship within the group of GPA and GRP associated ABC exporters. Phylogenetic tree of ABC transporters encoded in BGC of GPAs and GRPs. The tree was calculated using the Maximum Likelihood (LG+F+G) algorithm with 1000 bootstrap repetitions. Nodes with bootstrap support ≥ 75 are marked by red dots. The tree was rooted using a putative ABC transporter encoded in an unknown BGC in *A. balhimycina* (Abc30). The strain from which the cluster and thus the associated ABC transporter originate is indicated in the tree. (Predicted) GPA types are labeled accordingly: type I (orange), type II (yellow), type III (green), type IV (blue), type V (pink). Known and predicted GPAs are mentioned behind the branches.

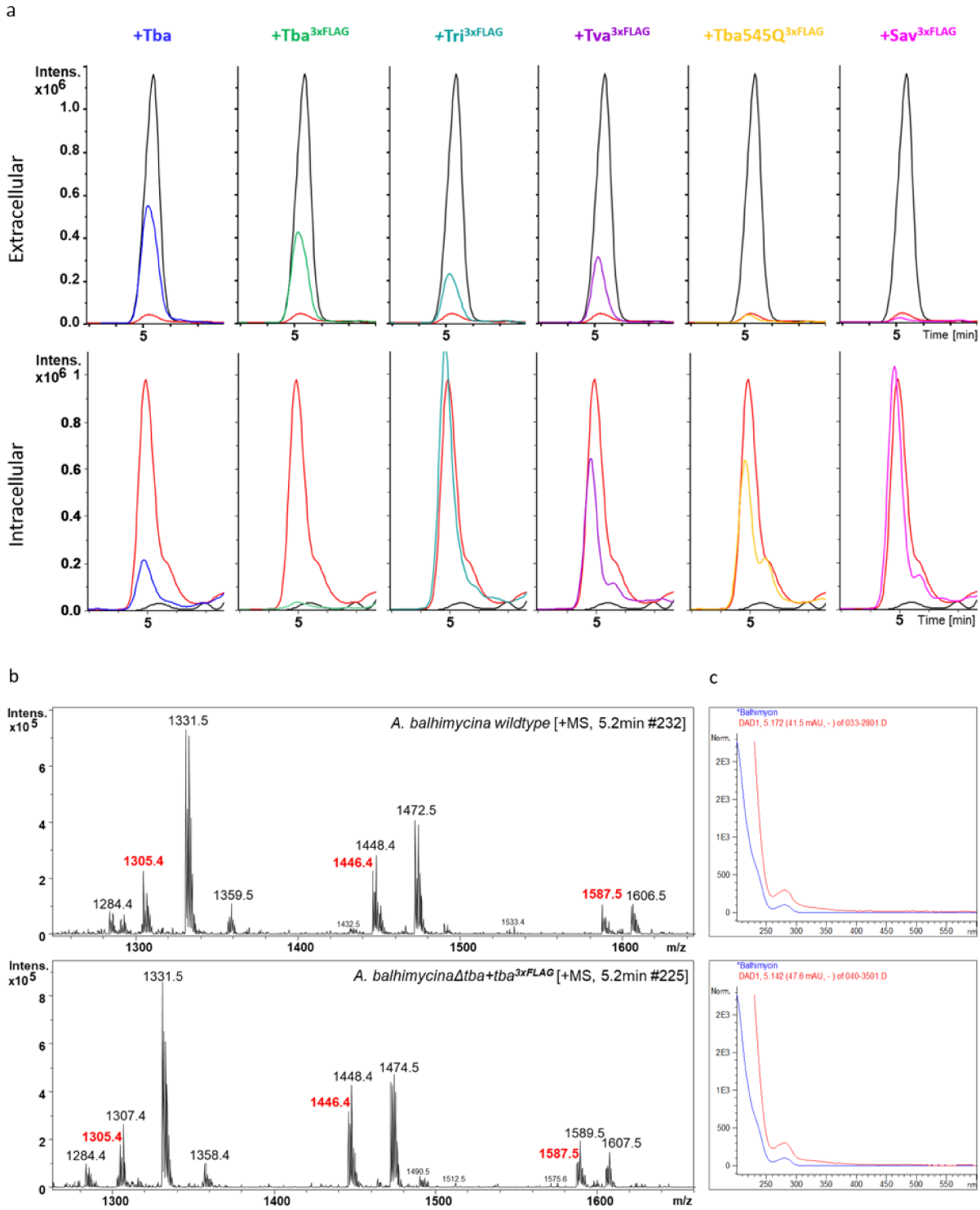

Figure S4. Export assay of balhimycin by diverse ABC transporters. a: HPLC-MS chromatograms of the culture supernatants (Extracellular) as well as mycelium extracts (Intracellular). The peaks (retention time 5-5.5 min) represent the extracted ion chromatogram (EIC) of the protonated balhimycin mass *m/z* 1446.41 $[M+H]^+$ (positive mode, smoothed 10.63-10.76 GA). In each chromatogram view, the EIC of *A. balhimycina* wildtype (black) and Δ*tba* (red) are overlaid with the respective EIC of the Δ*tba* mutant complemented with different transporters. **b:** Depicted mass spectra of *A. balhimycina* wildtype (top) and *A. balhimycina Δtba+tba*^{3xFLAG}(bottom) showing detected masses of the balhimycin molecules as $[M+H]^+$(red). **c:** UV-spectra of balhimycin derived from HPLC-DAD analysis of supernatants of *A.*

balhimycina wildtype (top) and *A. balhimycinaΔtba+tba*^{3xFLAG} (bottom) compared to in-house UV database of balhimycin standard.

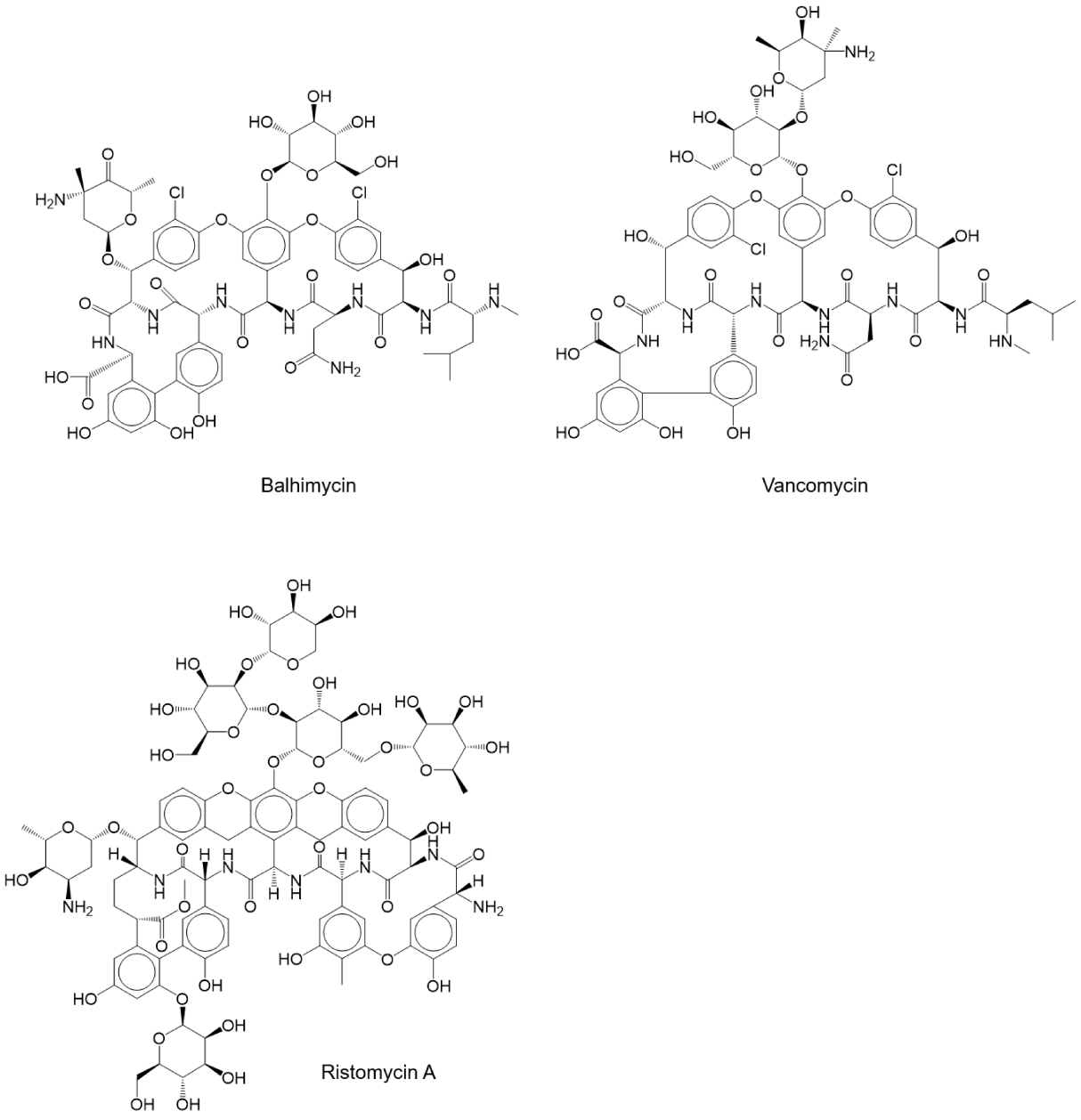

Figure S5. Chemical structure of the glycopeptides molecules.
Balhimycin (ChemSpider ID10249894), vancomycin (ChemSpider ID14253) and ristomycin A (ChemSpider ID16736169)

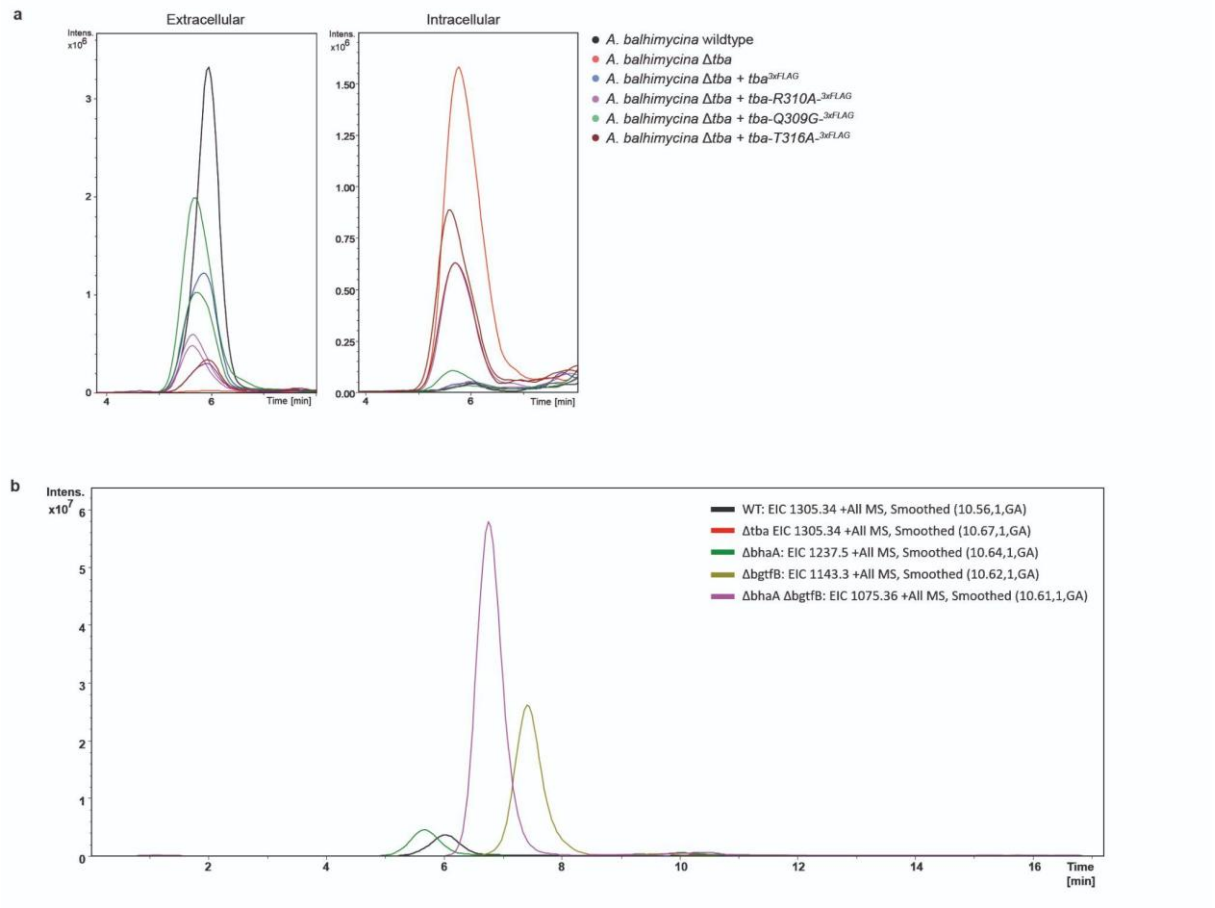

Figure S6. HPLC-MS chromatograms of mutants carrying point mutations in the TMD and mutants lacking the genes for chlorination and glycosylation. a: HPLC-MS chromatograms of the culture supernatants (Extracellular) as well as mycelium extracts (intracellular) of the mutants expressing *tba-Q309G-*^{3xFLAG}, *tba-R310A-*^{3xFLAG} and *tba-T316A-*^{3xFLAG}. The peaks (retention time 5-5,5 min) represent the extracted ion chromatogram (EIC) of the protonated balhimycin mass 1446.41 m/z [M+H] (positive mode, smoothed 10.63-10.76 GA). The EICs of each mutant are overlaid and compared to the wildtype (black) and Δ*tba* (orange) as well as *tba*^{3xFLAG}. **b:** HPLC-MS analyzed culture supernatants of mutants, missing the *bhaA* and *bgtfB* genes. Each chromatogram represents EICs of the corresponding derivative produced by the mutant. As controls, the EICs of wildtype (black) and Δ*tba* (red) are overlaid.

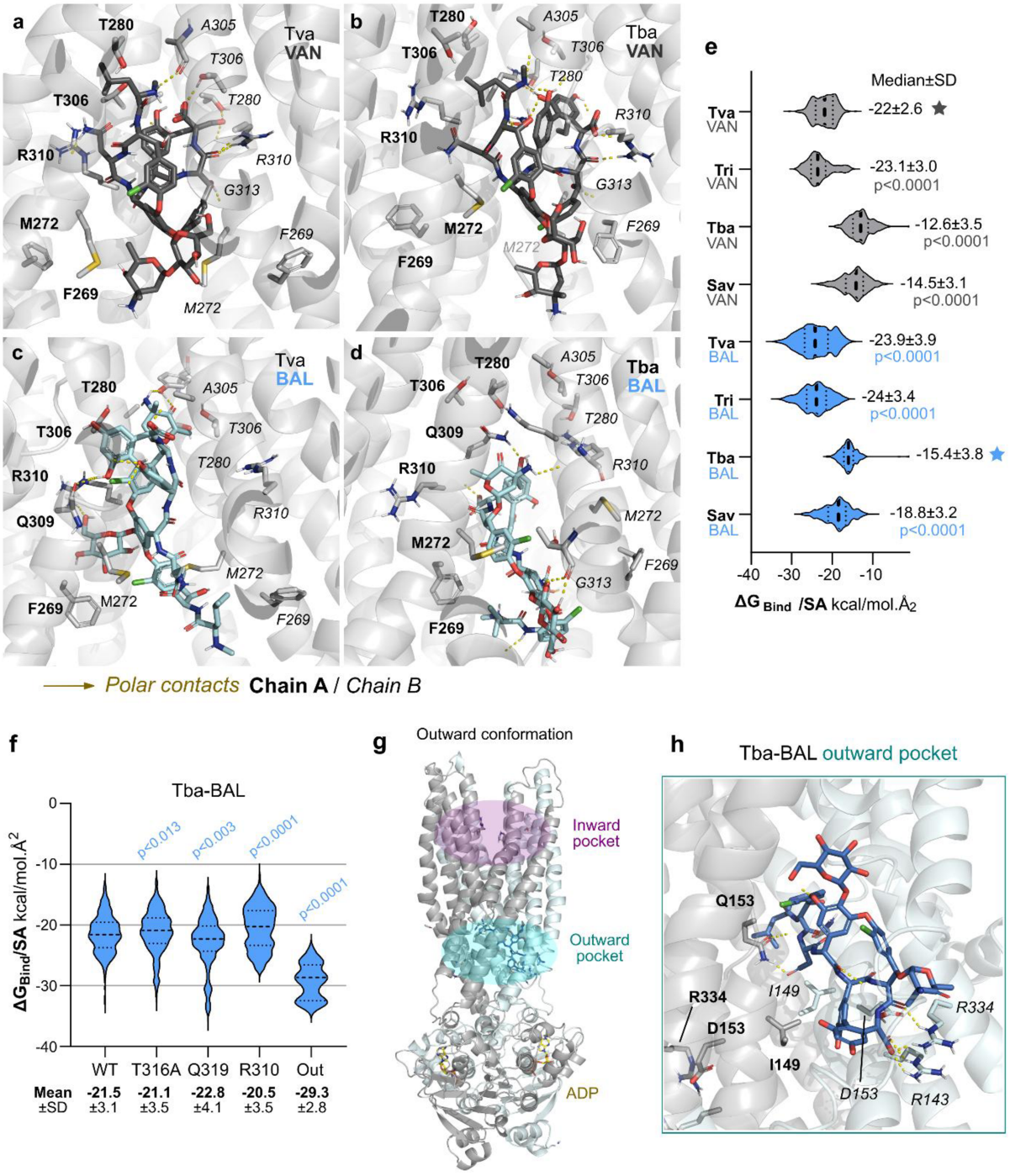

Figure S7. GPA potential binding mode and their respective predicted binding energies. Representative conformation from the MD simulation for the vancomycin (**VAN**) binding transporters Tva (**a**) and Tba (**b**), as well as their balhimycin (**BAL**) counterparts in (**c, d**). Conformations highlight that GPAs proposed binding mode points the R1-sugar moieties towards the cytoplasmic cavity beyond the substrate binding pocket (in the TMD). Predicted binding energy (**e, f**). Violin plot depicting the variation of free binding energy calculated along the trajectory normalized by the ligand's surface for: (**E**) WT-GPA transporters with VAN (gray) or BAL (blue) and (**f**) for different point mutations of Tba bound to BAL. Median energy values are depicted above each ligand. Mann-Whitney tests were performed to compare all groups against the control group's cumulative distribution, highlighted with a star from the respective group; exact p-values are depicted when available. Comparisons between the same transporter with different binding GPA yielded no significant results and therefore are not

displayed. **g**: 3D representation of a type IV GPA transporter Tba based on the SAV1866 (PDB 2HYD) followed by short MD simulations (5x200 ns). **h:** Proposed binding mode for relevant GPAs, generated from representative conformations from the MD simulation for the transporter Tba bound to balhimycin.

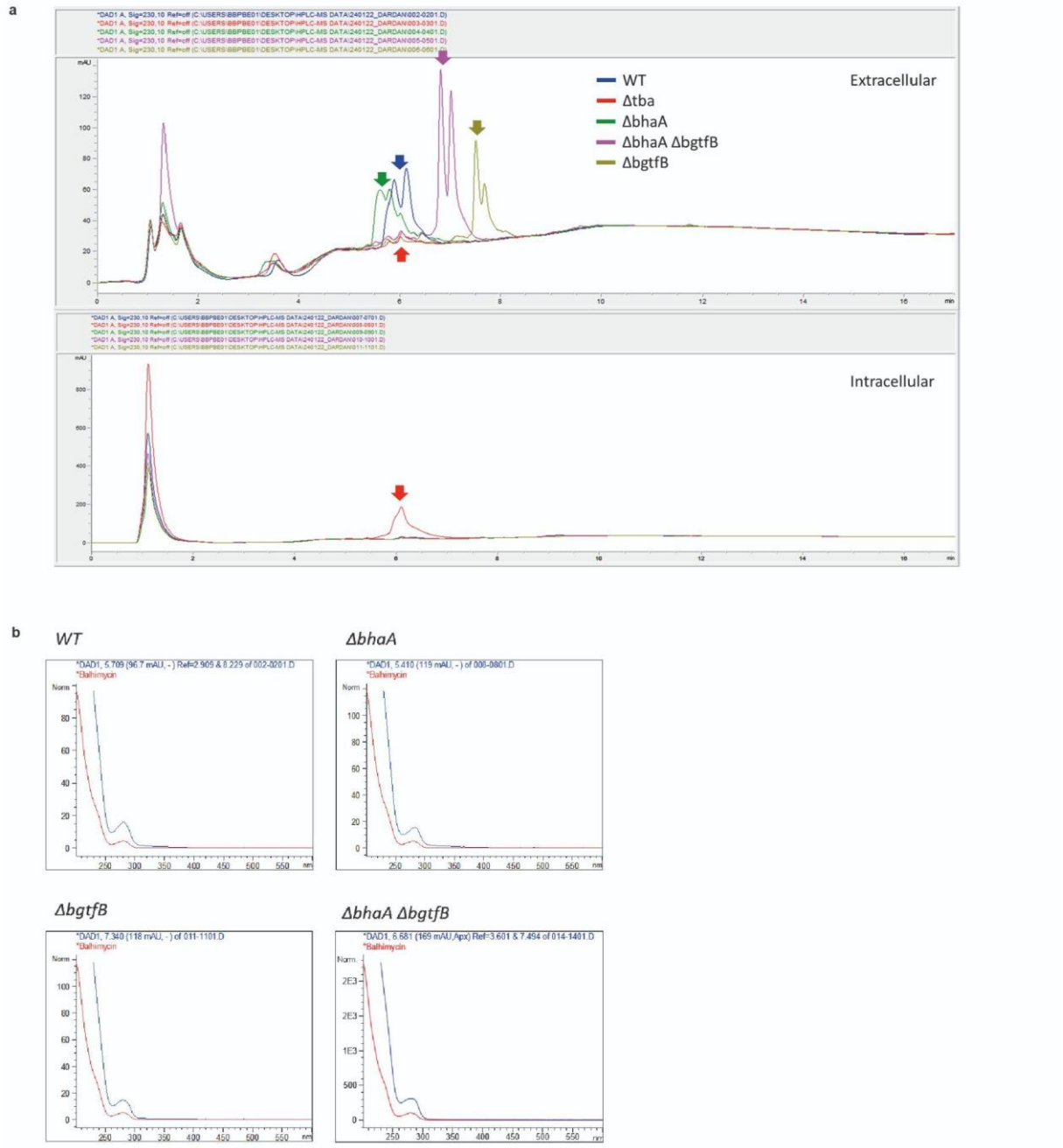

Figure S8. UV spectra of the analyzed deletion mutants Δ*bhaA*, Δ*bgtfB* and Δ*bhaA*Δ*bgtfB*. a: The UV spectrum at 230 nm after HPLC-DAD of each analyzed supernatant are overlaid and marked with arrows indicating the peak corresponding to the balhimycin derivatives produced by the respective mutant. **b:** UV-spectra of balhimycin and its derivatives derived from HPLC-DAD analysis of supernatants of each *A. balhimycina* mutant (blue) compared to in-house UV database of balhimycin standard (red).

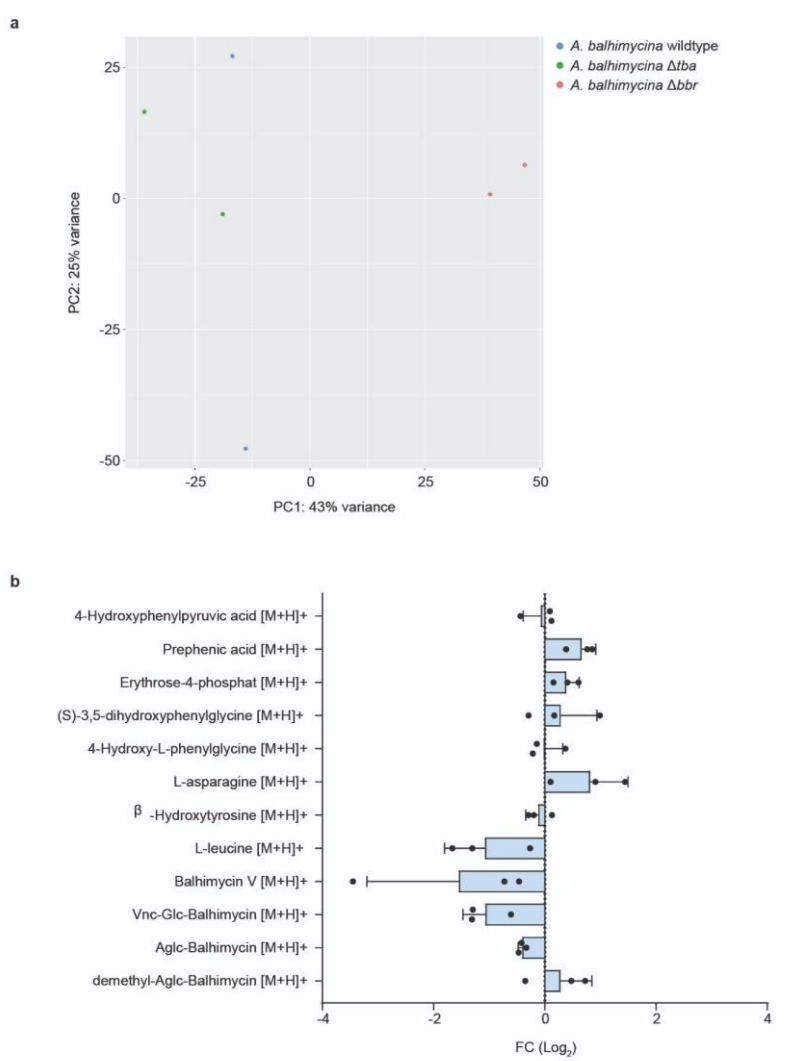

Figure S9. Transcriptome and metabolome analysis of *A. balhimycina Δtba*. a: Comparison of two individual replicates of *A. balhimycina* wildtype (blue), Δ*tba* (green), and Δ*bbr* (salmon) using principal component analysis (PCA). **b:** Levels of balhimycin intermediates after 48 h measured by flow-injection mass spectrometry. Values display *A. balhimycina* Δ*tba* in comparison to *A. balhimycina* wildtype**.**

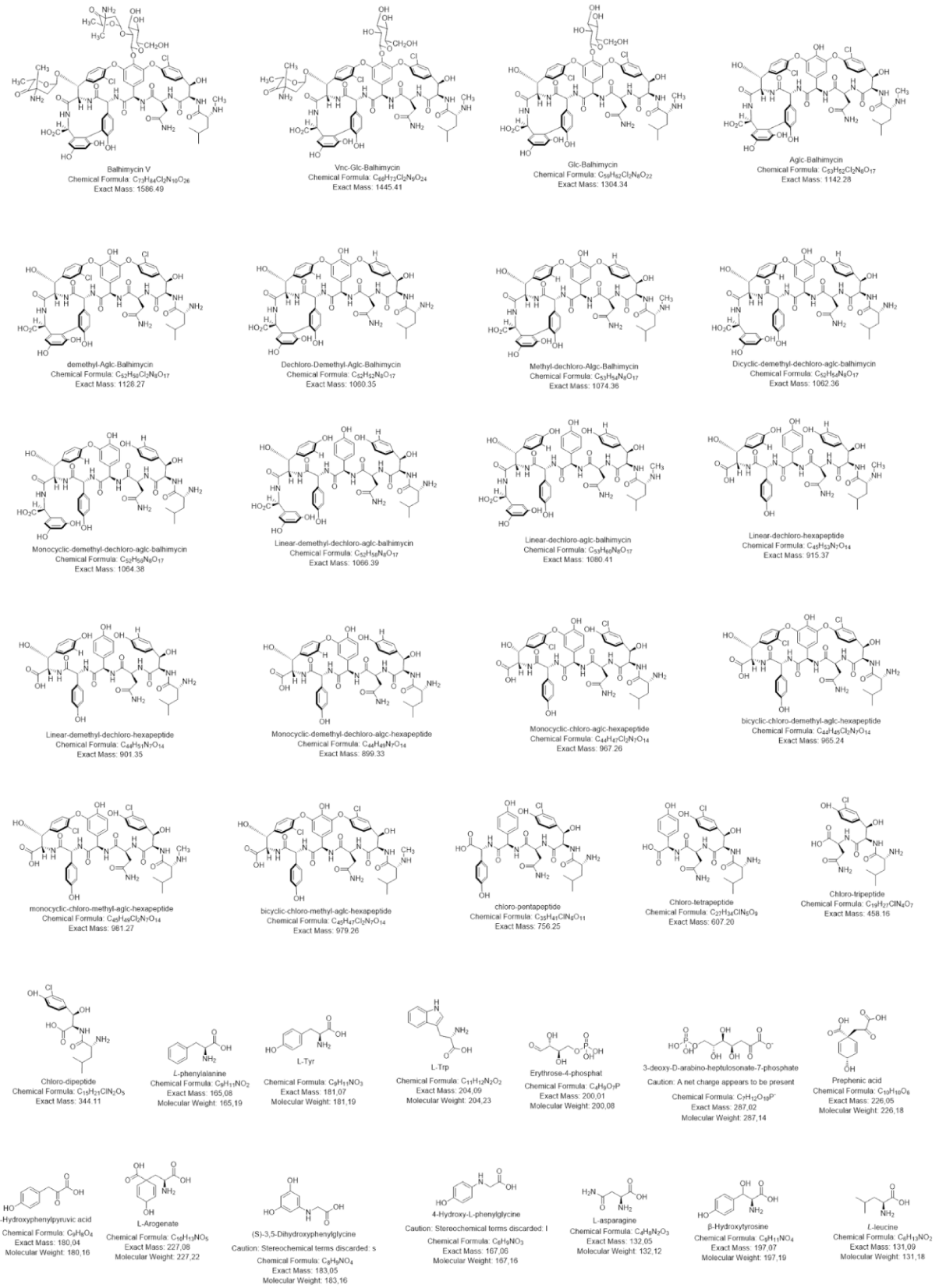

Figure S10. List of balhimycin intermediates. Structure, chemical formula, exact mass and molecular weight of balhimycin, putative intermediates, and precursors.

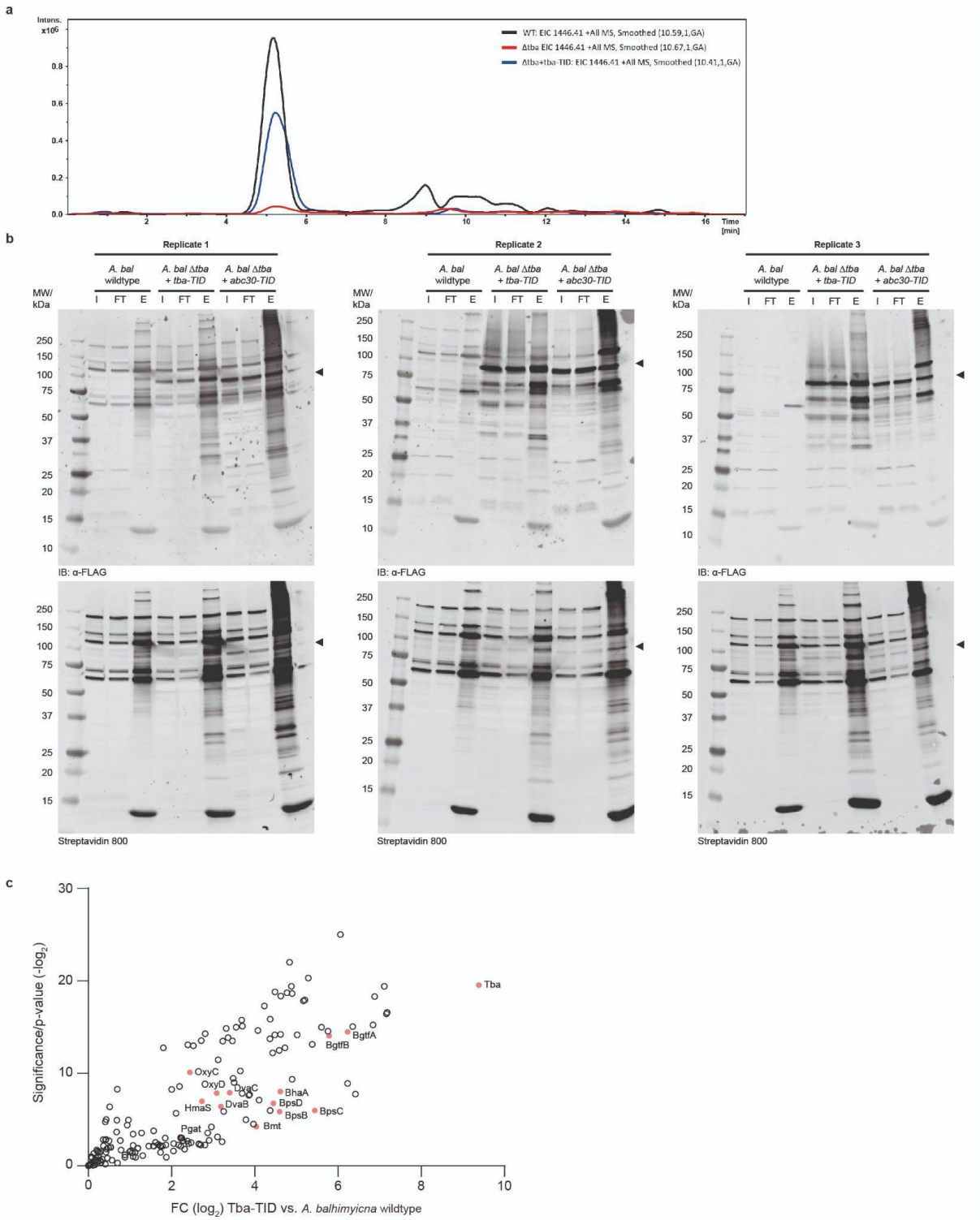

Figure S11. Proximity dependent biotinylation. a: HPLC-MS chromatograms of the culture supernatants of *A. balhimycina* Δ*tba* complemented with *tba-TID*. The peaks (retention time 5-5.5 min) represent the extracted ion chromatogram (EIC) of the protonated balhimycin mass *m/z* 1446.41 $[M+H]^+$ (positive mode, smoothed 10.41-10.67 GA). **b:** Immunoblotting (top) and fluorescence labeling with Streptavidin 800 (bottom) after SDS-PAGE of input (I) biotinylated proteins after enrichment (E) and flowthrough after enrichment (FT) from the recombinant strains expressing TID fusion proteins. **c:** Representation of all log2 fold change positive proteins detected by LC-MS/MS after biotinylation. Hits of Tba-TID compared to the wildtype strain *A. balhimycin*a without TID.

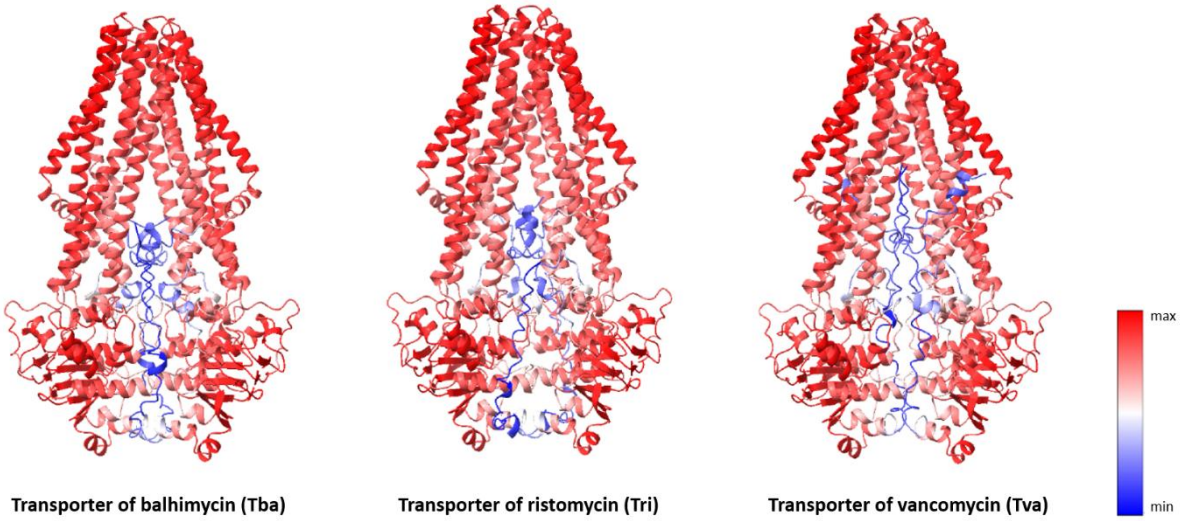

Figure S12. AlphaFold2 models of Tba, Tri and Tva and coloration based on B-factor coloured by model per-residue confidential score. The coloration is displayed in red as maximum and in blue as lowest value of the per-residue score. TMD regions were modelled with high confidence while the N-terminal could not, therefore it was removed from the calculations, to generate a truncated protein model.

Table S3. Mass list of balhimycin intermediates and precursors

Nr	Name	Molecular formula	Exact Mass
1	Chloro-dipeptide	C15H21ClN2O5	344.113901
2	Chloro-tripeptide	C19H27ClN4O7	458.156829
3	Chloro-tetrapeptide	C27H34ClN5O9	607.204508
4	chloro-pentapeptide	C35H41ClN6O11	756.252187
5	bicyclic-chloro-methyl-aglc-hexapeptide	C45H47Cl2N7O14	979.255809
6	monocyclic-chloro-methyl-aglc-hexapeptide	C45H49Cl2N7O14	981.271459
7	bicyclic-chloro-demethyl-aglc-hexapeptide	C44H45Cl2N7O14	965.240159
8	Monocyclic-chloro-aglc-hexapeptide	C44H47Cl2N7O14	967.255809
9	Monocyclic-demethyl-dechloro-algc-hexapeptide	C44H49N7O14	899.333753
10	Linear-demethyl-dechloro-hexapeptide	C44H51N7O14	901.349402
11	Linear-dechloro-hexapeptide	C45H53N7O14	915.365053
12	Linear-dechloro-aglc-balhimycin	C53H60N8O17	1080.407647
13	Linear-demethyl-dechloro-aglc-balhimycin	C52H58N8O17	1066.391997
14	Monocyclic-demethyl-dechloro-aglc-balhimycin	C52H56N8O17	1064.376347
15	Dicyclic-demethyl-dechloro-aglc-balhimycin	C52H54N8O17	1062.360697
16	Methyl-dechloro-Algc-Balhimycin	C53H54N8O17	1074.360697
17	Dechloro-Demethyl-Aglc-Balhimycin	C52H52N8O17	1060.345047
18	demethyl-Aglc-Balhimycin	C52H50Cl2N8O17	1128.267103

19	Aglc-Balhimycin	C53H52Cl2N8O17	1142.282753
20	Glc-Balhimycin	C59H62Cl2N8O22	1304.335578
21	Vnc-Glc-Balhimycin	C66H73Cl2N9O24	1445.414557
22	Balhimycin V	C73H84Cl2N10O26	1586.493536
Precursors			
NR	Name	Molecular formula	Exact mass
1	L-leucine	C6H13NO2	131.094629
2	β-Hydroxytyrosine	C9H11NO4	197.068809
3	L-asparagine	C4H8N2O3	132.053493
4	4-Hydroxy-L-phenylglycine	C8H9NO3	167.058244
5	(S)-3,5-dihydroxyphenylglycine	C8H9NO4	183.053159
6	Erythrose-4-phosphat	C4H9O7P	200.008593
7	3-deoxy-D-arabino-heptulosonate-7-phosphate	C7H12O10P	287.016812
8	Prephenic acid	C10H10O6	226.04774
9	4-Hydroxyphenylpyruvic acid	C9H8O4	180.04226

Table S4 | Primers used in this study

ID	Primer	Sequence (5'□3')
P1	seq_ermE_prom_f	TTG TGG GCA CAA TCG TGC CGG
P2	seq_lacZa_r	GCA CTG GCC GTC GTT TTA CAA CGT
P3	tba_UP_f	TAA AGG GAG AGA CGA ATT CGA GCT CGG TAC GCC AAG CCG CAC CCG C
P4	tba_UP_r	GCT GCG GAA TTC ATC CAT CCG GTC ACC TCT CT
P5	tba_Down_f	AGA GGT GAC CGG ATG GAT GAA TTC CGC AGC GCG GAC CA
P6	tba_Down_r	GCA GGT CGA CTC TAG AGG ATC CCC GGG TAC GCT CGG TGC CCG CCC
P7	tba_pRM4_f	CTG CAG GAA TTC GAT ATC AAG CTT TCA TCC TCC GTA GCC CAT GTG
P8	tba_pRM4_r	CCA GGG GAG GAC CCA TAT GAT GGA CAT GGT GTT GCG TTT
P9	KO_tba_f	ACG CCC CGC ACG TGG TGG CGT
P10	KO_tba_r	TCG GAC GCG CCC TCC TCG GCG GCG
P11	bgtfB_down_f	GCG ATA TCC GCG AAA CTG CTG CTC G
P12	bgtfB_down_r	GGA TCG TCT AGA TGG CCA CCT TCG C
P13	bgtfB_UP_f	GTG GAA TTC GGC AGC TCG TCC GGA C
P14	bgtfB_UP_r	TTG ATA TCC GGT TGT TCC GCT CCC
P15	KO_bgtfB_f	AAC CTA CGG AAC AGA GGG TGC
P16	KO_bgtfB_r	GTC TCC TCT TTG CTT TGT CTT CGA AGA
P11	gib_uni_pRM4_f	TCT AGA GTC GAC CTG CAG CCC GAG
P12	gib_uni_tba_r	TCC TCC GTA GCC CAT GTG TTG GAT C
P13	gib_pRM4_3xFLAG_f	GAT CCA ACA CAT GGG CTA CGG AGG ATC TAG AGA CTA CAA AGA CCA TGA C

P14	gib_pRM4_3xFLAG_r	CTC GGG CTG CAG GTC GAC TCT AGA TCA TTT GTC ATC GTC ATC CTT GTA ATC
P15	gib_pRM4_Tri2_f	ATA AGC TAG CCA GGG GAG GAC CCA TAT GGA AGT AAT GTT GCG CTT CGG
P16	gib_pRM4_Tri_r	GCT CGG GCT GCA GGT CGA CTC TAG ATC ATC CTC CGT AGA CCA CGG T
P17	gib_tri_3xFLAG_f	GGA CAC CGT GGT CTA CGG AGG ATC TAG AGA CTA CAA AGA CCA TGA C
P18	gib_pRM4_Sav1866_f	ATA AGC TAG CCA GGG GAG GAC CCA TAT GAT TAA ACG ATA TTT GCA ATT TGT TAA GCC
P19	gib_pRM4_Sav1866_r	CTC GGG CTG CAG GTC GAC TCT AGA TTA TAA GTT TTG AAT GCT ATA TAA ATG CTC GTA AG
P20	gib_Sav1866_FLAG_f	AGG TGC TTA CGA GCA TTT ATA TAG CAT TCA AAA CTT ATC TAG AGA CTA CAA AGA CCA TGA C
P21	gib_FLAG_Sav1866_r	CAC CGT CAT GGT CTT TGT AGT CTC TAG ATA AGT TTT GAA TGC TAT ATA AAT GCT CGT AAG
P22	gib_pRM4_Tva_f	ATA AGC TAG CCA GGG GAG GAC CCA TAT GGA AGT GGT GTT GCG CTT C
P23	gib_pRM4_Tva_r	CTC GGG CTG CAG GTC GAC TCT AGA TCA TCC TCC GAA GCC AAT GG
P24	gib_FLAG_Tva_r	CAC CGT CAT GGT CTT TGT AGT CTC TAG ATC CTC CGA AGC CAA TGG GTT G
P25	gib_Tva_FLAG_f	GAT CCA ACC CAT TGG CTT CGG AGG ATC TAG AGA CTA CAA AGA CCA TGA C
P26	gib2_pRM4_Tba_f	ATA AGC TAG CCA GGG GAG GAC CCA TAT GGA CAT GGT GTT GCG TTT CGA G
P27	gib_TbaE545Q_r	GGG CGG TGG CTT GGT CGA GGA CGA CGA TC
P28	gib_Tba545Q_f	GAT CGT CGT CCT CGA CCA AGC CAC CGC CC
P29	gib_pRM4_3XFLAG_r	CTC GGG CTG CAG GTC GAC TCT AGA TCA TTT GTC ATC GTC ATC CTT GTA ATC
P30	gib_TbaR310A_r	CGG CCC GAA CAG CGC CTG GAG CAG GGT G
P31	gib_TbaR310A_f	CAC CCT GCT CCA GGC GCT GTT CGG GCC G
P32	gib_TbaQ309G_r	CGA ACA GCC GCC CGA GCA GGG TGG CGA TG
P33	gib_TbaQ309G_f	CAT CGC CAC CCT GCT CGG GCG GCT GTT CG
P34	gib_TbaT316A_r	CCC GGA CAG CTG GGC GAT CGG CCC GAA CA
P35	gib_TbaT316A_f	TGT TCG GGC CGA TCG CCC AGC TGT CCG GG
P36	gib_GSTurboID_Tba_r	GAG CGA TCA GCT TCA GAG GCA CAG TAT TGT CTT TGC TCC CTC CTC CGT AGC CCA TGT GTT GG
P37	gib_Tba_GSTurboID_f	CGG TGA TCC AAC ACA TGG GCT ACG GAG GAG GGA GCA AAG ACA ATA CTG TGC CTC TGA AGC
P38	gib_pRM4_His6_r	CAA GCT CGG GCT GCA GGT CGA CTC TAG ATC AGT GGT GGT GGT GGT GGT GCT C
P39	gib_pRM4_ABC30_f	ATA AGC TAG CCA GGG GAG GAC CCA TAT GAC CAT TGG AGA CGA CCC GAG C
P40	gib_GSTurboID_ABC30_r	GAG CGA TCA GCT TCA GAG GCA CAG TAT TGT CTT TGC TCC CGC CCA AAG CAC GGT TCC CGC
P41	gib_pRM4_TurboID_f	CCA AGA GCG GGA ACC GTG CTT TGG GCG GGA GCA AAG ACA ATA CTG TGC CTC TGA AGC

Table S5 | Strains used in this study

Strain	Relevant features	Reference
E. coli NEB5α	Cloning host for plasmid generation	New England Biolabs
E. coli NovaBlue	Cloning host for plasmid generation	Novagen®
E. coli JM110	*lacY dam dcm* [F' *lacI*^{q} Z Δ *M15*] (Methylation deficient strain)	[97]

E. coli ET12567	F^- *dam*-13::Tn9 *dcm*-6 *hsdM hsdR* (Methylation deficient)	[98]
A. balhimycina DSM 44591	Balhimycin producing wild type	[99,100]
A. balhimycina Δ*tba*	*tba* deletion mutant	This study
A. balhimycina Δ*tba* [+*tba*]	Apr^R, *tba* deletion mutant, ΦC31attB(pRM4-*tba*)	This study
A. balhimycina Δ*tba* [+*tba-3xFLAG*]	Apr^R, *tba* deletion mutant, ΦC31attB(pRM4-*tba-3xFLAG*)	This study
A. balhimycina Δ*tba* [+*tri-3xFLAG*]	Apr^R, *tba* deletion mutant, ΦC31attB(pRM4-*tri-3xFLAG*)	This study
A. balhimycina Δ*tba* [+*tva*-3*xFLAG*]	Apr^R, *tba* deletion mutant, ΦC31attB(pRM4-*amoh-3xFLAG*)	This study
A. balhimycina Δ*tba* [+*sav1866*-3*xFLAG*]	Apr^R, *tba* deletion mutant, ΦC31attB(pRM4-*sav1866-3xFLAG*)	This study
A. balhimycina Δ*tba* [+*tbaE545Q*-3*xFLAG*]	Apr^R, *tba* deletion mutant, ΦC31attB(pRM4-*tbaE545Q-3xFLAG*)	This study
A. balhimycina Δ*tba* [+*tbaR310A*-3*xFLAG*]	Apr^R, *tba* deletion mutant, ΦC31attB(pRM4-*tbaR310A-3xFLAG*)	This study
A. balhimycina Δ*tba* [+*tbaQ309G*-3*xFLAG*]	Apr^R, *tba* deletion mutant, ΦC31attB(pRM4-*tbaQ309G-3xFLAG*)	This study
A. balhimycina Δ*tba* [+*tbaT316A*-3*xFLAG*]	Apr^R, *tba* deletion mutant, ΦC31attB(pRM4-*tbaT316A-3xFLAG*)	This study
A. balhimycina Δ*bhaA*	*bhaA* deletion mutant	[28]
A. balhimycina Δ*bgtfB*	*bgtfB* deletion mutant	This study
A. balhimycina Δ*bgtfB*Δ*bhaA*	*bhaA and bgtfB* double-deletion mutant	This study
A. balhimycina Δ*tba* [+*tba-TID*]	Apr^R, *tba* deletion mutant, ΦC31attB(pRM4-tba-*TID*)	This study
A. balhimycina [+*TID*]	ΦC31attB(pRM4-*TID*)	This study
B. subtilis DSM10	Indicator strain for bioactivity assay	[101]

*Apr^R (Apramycin resistance)

Table S6 | Plasmids used in this study

Plasmid	Annotation	Resistance	Reference
pRM4	pSET152*ermEp** derived Φ31 integration vector with artificial ribosomal binding site	Apr^R	[10]
pSP1	pT7/T3-α19 derived gene disruption vector, with *ermE* gene in *Sap*I site	Ery^R/ Amp^R	[57]
pSP1Δ*tba*	pSP1 derived deletion vector for *tba* gene	Ery^R/ Amp^R	This study
pSP1Δ*bgtfB*	pSP1 derived deletion vector for *bgtfB* gene	Ery^R/ Amp^R	This study
pRM4-tba	pRM4 derived integrative *tba* expression vector	Apr^R	This study
pRM4-tba-3xFLAG	pRM4 derived integrative *tba-3xFLAG* expression vector	Apr^R	This study
pRM4-tri-3xFLAG	pRM4 derived integrative *tri-3xFLAG* expression vector	Apr^R	This study
pRM4-tva-3xFLAG	pRM4 derived integrative *tva-3xFLAG* expression vector	Apr^R	This study
pRM4-sav1866-3xFLAG	pRM4 derived integrative *sav1866-3xFLAG* (multidrug exporter of *S. aureus*) expression vector	Apr^R	This study
pRM4-tbaE545Q-3xFLAG	pRM4 derived integrative *tbaE545Q-3xFLAG* expression vector	Apr^R	This study
pRM4-tbaR310A-3xFLAG	pRM4 derived integrative *tbaR310A-3xFLAG* expression vector	Apr^R	This study
pRM4-tbaQ309G-3xFLAG	pRM4 derived integrative *tbaQ309G-3xFLAG* expression vector	Apr^R	This study
pRM4-tbaT316A-3xFLAG	pRM4 derived integrative *tbaT316A-3xFLAG* expression vector	Apr^R	This study
pET21a-TurboID-His6 (Addgene #107177)	TurboID expression vector; under control of P_{T7}	Amp^R	[31]
pRM4-tba-TID	pRM4 derived integrative *tba-TID* expression vector	Apr^R	This study
pRM4-TID	pRM4 derived integrative *TID* expression vector	Apr^R	This study
pRM4-abc30-TID	pRM4 derived integrative *abc30-TID* expression vector	Apr^R	This study

*Apr^R (Apramycin resistance), *Ery^R (Erythromycin resistance),*Amp^R (Ampicillin resistance)

References supplementary information

1. Hessa, T. *et al.* Molecular code for transmembrane-helix recognition by the Sec61 translocon. *Nature* **450**, 1026–1030 (2007).

4.3 Exploring potential interaction partners of Tba in its native environment

The investigation of the microenvironment of Tba in its native environment, i.e., in *A. balhimycina,* by proximity biotinylation (Fig. 6 - Publication 1) and affinity purification (Fig. 18) suggested that Tba and the enzymes involved in balhimycin biosynthesis are in close proximity to each other and potentially interact. To further explore this hypothesis, co-immunoprecipitation was performed using *A. balhimycina* Δ*tba* chromosomally complemented with Tba-3xFLAG, Tba^{E545Q}-3xFLAG, or Tba at the *ϕC31* attachment site under the control of a strong constitutive promoter (*ermE*p)*. Immunoprecipitation was carried out using anti-FLAG antibodies covalently bound to an agarose gel matrix. Tba without a 3xFLAG tag was used as a negative control to identify non-specifically bound proteins. Tba-3xFLAG was used to identify the interactome of the wild-type transporter. The mutant transporter Tba^{E545Q}-3xFLAG carries a point mutation in the nucleotide binding domain (NBD), resulting in a complete loss of ATP hydrolysis function and consequently loss of transport function (Fig. 2C - Publication 1). This mutant was used to investigate whether an active transport cycle influences potential interactions. The bacteria were cultivated under balhimycin-producing conditions for three days in R5 medium. Lysis, clearance from cell debris, and preparation of the crude membrane were performed as described previously (Chapter 4.1.5). Equal amounts of crude membranes from each strain were used for solubilization with 1% (w/v) LMNG, and the soluble fraction after ultracentrifugation was used for co-immunoprecipitation. Proteins eluted from the 3xFLAG affinity gel after immunoprecipitation were identified by HPLC-MS/MS (Fig. 19).

The proteins co-precipitated with Tba-3xFLAG (Table S1) or Tba^{E545Q}-3xFLAG (Table S2) were compared with those eluted with the Tba control, and their log2-fold change and its statistical significance (p-value) were calculated after different normalization steps. This allowed proteins that were not specifically enriched to be distinguished from proteins that are true interaction candidates of the bait proteins Tba-3xFLAG and Tba^{E545Q}-3xFLAG. In both cases, the bait protein was identified as the one with the highest log2 fold change and significance, thereby serving as a positive control for the experiment (Fig. 19). Both led to an enrichment of enzymes involved in different steps of balhimycin biosynthesis with a log2 fold change of at least 2 in comparison to the control Tba (Fig. 19). These were NRPS enzymes (BpsB, BpsC), responsible for the biosynthesis of the peptide backbone, modification enzymes (BhaA, BgtfA, Bmt), and enzymes involved in the biosynthesis of precursor molecules (HmaS, DvaB, DvaC, DvaD, Pgat). The co-immunoprecipitation of these proteins strongly indicates an interaction of Tba-3xFLAG and Tba^{E545Q}-3xFLAG with the above-mentioned enzymes involved in the biosynthesis of balhimycin. Interestingly, three proteins involved in the biosynthesis of balhimycin were only co-precipitated, with a log2 fold-change of at least 2, using Tba-3xFLAG or Tba^{E545Q}-3xFLAG. The P450 monooxygenases OxyC and OxyD were only co-precipitated by Tba-3xFLAG (Fig. 19A), while the NRPS enzyme BpsD, involved in the biosynthesis of the precursor βHt, was only detected in proteins co-precipitated by the mutant transporter Tba^{E545Q}-3xFLAG (Figure 19B). Additionally, both Tba-3xFLAG and Tba^{E545Q}-3xFLAG led to the co-precipitation of two members of the SPFH protein family: Paraslipin and a Flotillin-like protein.

A total of 43 proteins were identified as having significantly different intensity levels (log2 fold change ≥ |2|) when comparing the proteins that co-precipitated using Tba-3xFLAG and Tba^{E545Q}-3xFLAG (Table S3). The protein function of these was predicted by the UniProtKB database. Among the proteins that were more abundant when Tba-3xFLAG was used as bait were: OxyC, YidC, eight transport proteins, three subunits of complex I of the aerobic respiratory chain, two other uncharacterized membrane proteins, three proteins of the central carbon metabolism, two ribosomal subunits, a protease, an integration host factor, and eight other proteins whose specific role in a pathway in *A. balhimycina* could not be clearly predicted. The proteins that were more abundant when Tba^{E545Q}-3xFLAG was used as bait protein were three transporters, two regulators, one ribosomal subunit, and eight proteins that were not further characterized for their specific function in *A. balhimycina*.

262 proteins were identified in Tba-3xFLAG samples with a log2 fold change ≥ |2|, in addition to the biosynthetic enzymes (Table S1). 92 of the 262 proteins were membrane proteins or membrane associated proteins. The majority of membrane proteins were classified as ABC transporters that transport sugars, amino acids, or were not further characterized. Furthermore, subunits of all four aerobic respiratory chain complexes and of ATP synthase were found, as well as the insertase YidC, involved in membrane protein insertion and folding, and subunits of the Sec translocation complex (SecY, SecF, SecA). Other proteins identified included RNA polymerase subunits, ribosomal subunits, proteins involved in the central carbon metabolism, chaperones (DnaK, GroEL, HtpG), different peptidases and proteases, elongation factors (EF-G, EF-Tu, EF-Ts), as well as transcriptional regulators, an unrelated NRPS, scaffold proteins of the type VII secretion system (EccC, EccE), and proteins that could not be directly linked to a specific pathway or function in *A. balhimycina*.

In conclusion, these results showed that the transporters Tba-3xFLAG and Tba^{E545Q}-3xFLAG led to a specific co-immunoprecipitation of numerous enzymes involved in the balhimycin biosynthesis. These were the NRPS enzymes (BpsB, BpsC), modification enzymes (BhaA, BgtfA, Bmt), and precursor synthesizing enzymes (HmaS, DvaB, DvaC, DvaD, Pgat). This finding reveals that the proteins are not only present in the vicinity of the transporter, as previously investigated (Fig. 6 - Publication 1), but presumably also interact directly or indirectly with it. However, since these proteins were co-immunoprecipitated with both Tba-3xFLAG and Tba^{E545Q}-3xFLAG, the results show that an inactive transporter, which exists in only one conformation, can interact with the biosynthetic proteins. The only protein that shows a significant high log2 fold-change (5.69) between the two is OxyC. In addition, a number of other proteins were identified as potential interaction candidates of Tba-3xFLAG and Tba^{E545Q}-3xFLAG, some of which are very abundant (membrane) proteins, as well as two SPFH family proteins. This experiment provides a starting point for the investigation of direct protein-protein interactions of Tba and for the differentiation of proteins that were only co-precipitated through indirect effects.

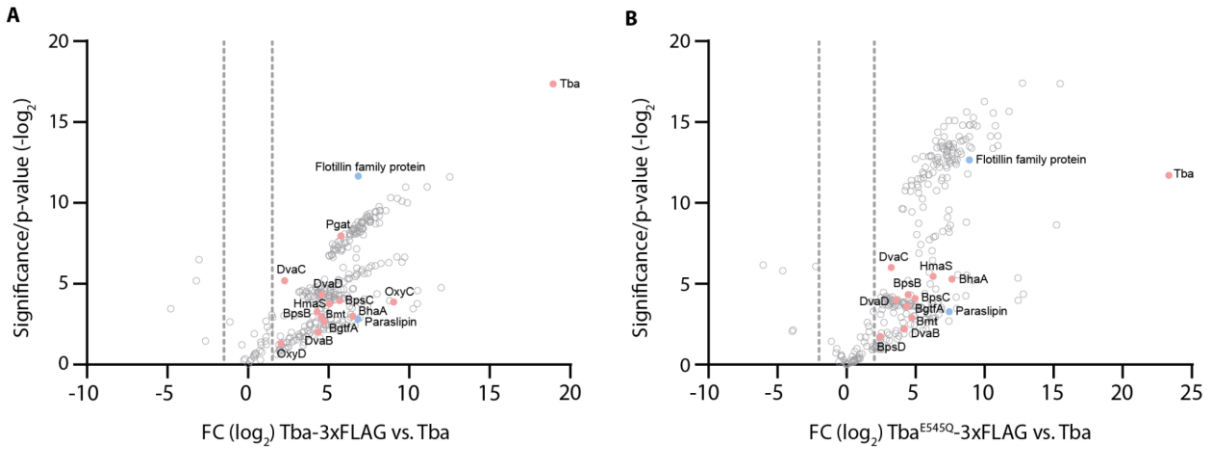

Figure 19 | Identification of possible interaction partners of Tba-3xFLAG and TbaE545Q-3xFLAG in *A. balhimycina* by co-immunoprecipitation.
Representation of all proteins detected by LC-MS/MS after enrichment by co-immunoprecipitation using Tba-3xFLAG, Tba^{E545Q}-3xFLAG, and Tba (control) as bait. LFQ intensities were used to calculate log2 fold change (FC) and significance level. Proteins involved in the biosynthesis of balhimycin and members of the SPFH protein family are shown in salmon and blue, respectively. FC of |2| is marked by dotted lines. (**A**) Hits of Tba-3xFLAG compared to Tba and (**B**) Tba^{E545Q}-3xFLAG compared to Tba. Proteins detected and encoded in the BGC of balhimycin: NRPSs (BpsB, BpsC), modification enzymes (OxyC, BhaA, BgtfA, Bmt), and enzymes involved in precursor supply (Pgat, BpsD, OxyD, HmaS, DvaB, DvaC). **Repetitions:** Three individual experiments were performed using the parameters described. **Abbreviations:** LFQ: Label-free quantification.

5 Discussion*[1]

Parts of the results discussed below were obtained collaboratively and compiled in publication 1 'Unveiling the substrate specificity of the ABC transporter Tba and its role in glycopeptide biosynthesis' (*iScience*). The individual contributions are listed in the Chapters 3 and 4.2.8. However, all results are included in this discussion.

Glycopeptide antibiotics (GPAs) - e.g. vancomycin - are potent natural products that have been used for many years as a last resort in the treatment of bacterial infections by inhibiting cell wall biosynthesis [140]. They are produced by various species of Actinomycetota as part of their secondary metabolism via non-ribosomal peptide synthetases (NRPS) and modified by a variety of tailoring enzymes [204]. The majority of the enzymes required for the biosynthesis of the modified heptapeptides are encoded in biosynthetic gene clusters (BGCs). Although many aspects of the biosynthesis of GPAs have been extensively studied, the mechanisms underlying their export remain poorly understood. The export is crucial for the GPAs to reach their molecular target on the cell envelope of other bacteria. To date, the only GPA transporter that has been investigated experimentally is Tba, which is essential for the export of the type I GPA balhimycin in *A. balhimycina* [168]. However, little is known about its specificity, transport kinetics, and functional integration within the cellular and biosynthetic environment.

In this thesis I focused on the functional dissection of the transport process during GPA production, with a primary emphasis on Tba. Additionally, homologous transporters involved in the export of other GPAs were analyzed to explore their evolutionary relationship and functional redundancy. Bioinformatic analysis revealed that all GPA BGCs analyzed in this study encode one ABC transporter with a high degree of similarity between them in terms of sequence and predicted structure. Despite the high similarity, phylogenetic analysis indicated a specificity towards the peptide backbone of their respective GPA substrate. This was confirmed by *in vivo* export assays, which also suggested a regulatory mechanism that stops biosynthesis in the absence of Tba. However, the exact mechanism is not yet understood. I optimized the purification conditions of Tba and the homologous ristomycin transporter from *A. japonicum* (Tri) and showed that expression and purification using the native or a near-native host resulted in a very pure protein. This provides a starting point for future purifications with higher protein yields for functional *in vitro* analysis. Finally, it was shown for the first time that Tba is closely associated with a number of biosynthetic enzymes and may interact with them, possibly forming a microcompartment. However, based on this work, I can only speculate about specific interactions and their relevance for the regulation of biosynthesis.

*[1] Parts of this chapter were previously published in publication 1 'Unveiling the substrate specificity of the ABC transporter Tba and its role in glycopeptide biosynthesis', by Gericke and Beqaj et al. (2025) [97].

5.1 Elucidation of substrate specificity of GPA ABC transporters*[2]

Initially, to elucidate the specificity of GPA ABC transporters, 89 BGCs encoding enzymes involved in the biosynthesis of various type I-V GPAs were bioinformatically analyzed for the presence of transporter-related genes. This revealed one gene in each BGC encoding a homodimeric ABC transporter similar to Tba of the balhimycin BGC in *A. balhimycina* (Fig. S2; Table S1 - Publication 1). The majority of natural product BGCs encode transport proteins, often belonging to the group of ABC transporters or the major facilitator superfamily (MFS) of transporters [167]. Based on sequence motifs commonly found in the nucleotide binding domain (NBD), membrane topology, and structural features (Figs. 3, S1 - Publication 1), they were classified as type IV according to the new ABC transporter nomenclature [91] and as B-family ABC exporters according to the old nomenclature [79]. Tba and all other identified GPA ABC transporters form homodimers, since only one gene was identified within the respective BGC, each encoding a half-transporter. However, other type IV ABC transporters are heterodimeric, e.g., the bacterial multidrug-resistance (MDR) transporter TmrAB [108] or monomeric, e.g., the mammalian MDR transporter P-gp (formerly ABCB1) [205]. All representatives of type IV ABC transporters share a 6+6 organization of the transmembrane helices (TMH), which was confirmed for the GPA ABC transporters by predicting the propensity of each region of the sequence to integrate into the cytoplasmic membrane (Fig. S1 - Publication 1) [206]. The characteristic domain swap of TMH4 and TMH5 to the opposite half-transporter and the short N-terminal elbow helix (EH) were identified in all structures after modeling with AlphaFold2 (Fig. 3 - Publication 1) [207]. The models represent an inward-facing (IF) conformation of the transporters and were considered reliable based on high confidence scores in the NBDs and transmembrane domains (TMD). In contrast, the N-terminal stretches in front of the EH were only predicted with a low level of confidence (Fig. S7.2 - Publication 1). These are not commonly found in existing ABC transporter structures and were shown as unstructured regions of the protein because AlphaFold2 predictions are based on known structures. Despite the high confidence scores in most domains of the transporter, this structural prediction represents at most one physiologically relevant conformation. However, it was shown that ABC transporters have a complex transport cycle with different structures that vary greatly [108].

The following phylogenetic analysis revealed differences between the transporters, as these clustered according to their predicted GPA types (Figs. 1, S3 - Publication 1). The arrangement suggests that type I-IV GPA transporters evolved from type V, with type I being the least ancestral. This resembles the evolutionary trajectory of their predicted substrates, as proposed by Waglechner et al. [208] and Hansen et al. [209]. Furthermore, the specific clustering of transporters that are predicted to export the same GPA type suggests that they have a similar functional activity and may be specific for that particular GPA type. The phylogenetic tree of ABC transporters constructed here has a high bootstrap value of over 75 in many clades. However, some of the clades, such as the two formed by putative type IV GPA transporters and the smaller of the two clades formed by putative type III transporters, do not reach this

*[2] Parts of this chapter were previously published in publication 1 'Unveiling the substrate specificity of the ABC transporter Tba and its role in glycopeptide biosynthesis', by Gericke and Beqaj et al. (2025) [97].

high value, thus calling into question the reliability of the tree. Therefore, in order to draw more precise conclusions from the phylogenetic tree, further quality tests, such as testing the probability of obtaining a particular subtree, would need to be performed to increase the overall robustness of the analysis [210].

The suggested specificity towards GPA types was confirmed by an *in vivo* export assay in which *A. balhimycina* Δ*tba* was complemented with different GPA ABC transporters. Balhimycin was shown to be exported equally well by another putative type I GPA transporter, namely Tva from *A. keratiniphila*, which is thought to export vancomycin (Fig. 2 - Publication 1). In contrast, the putative ristomycin transporter from *A. japonicum*, Tri, exported significantly less balhimycin. The type I GPAs, balhimycin and vancomycin, are composed of five aromatic and two aliphatic amino acids at positions AA1 and AA3, while the type III GPAs, like ristomycin, consist exclusively of aromatic amino acids. Therefore, these results strongly supported the hypothesis that GPA-associated ABC transporters exhibit substrate selectivity based on the peptide backbone of their respective GPA substrates.
There is no general mechanism for substrate discrimination in ABC transporters. Some ABC transporters, mostly MDR transporters, are polyspecific for different substrates, while others are highly selective for one substrate. For example, it has been shown that polyspecificity of the MDR transporter P-gp is partially achieved by multiple binding pockets [114]. Additionally, it can take up a variety of hydrophobic substrates from the inner leaflet of the cytoplasmic membrane [112,113]. Other transporters are thought to adopt different substrate-binding site conformations due to the high flexibility of their TMH in the IF conformation during the nucleotide- and substrate-free state, like the functional homolog of P-gp in *Lactococcus lactis* (*L. lactis*), LmrA [211]. Some others select the substrates according to their charge, such as the amino acid transporter Art$(QN)_2$ from *Thermoanaerobacter tengcongensis* [110], which imports exclusively positively charged amino acids because of negatively charged residues facing the substrate tunnel. ABC transporters involved in the export of non-ribosomally synthesized peptides have not been investigated for their substrate specificity. However, analysis of some ABC transporters of ribosomally synthesized and post-translationally modified peptides (RiPPs), which, like GPAs, are natural products, has shown that there is no general mechanism either. For example, NisT, the transporter of the lantibiotic peptide nisin of *L. lactis*, has a relaxed substrate specificity for precursor peptides and fusion peptides containing the nisin leader peptide [212]. By contrast, MjcD of *E. coli* is highly specific for the lasso peptide microcin J25 [111]. These examples highlight the wide variability in substrate binding mechanisms and selectivity within the group of ABC transporters.

But what exactly determines the substrate specificity of GPA ABC transporters? Since GPAs are usually not highly charged and are rather hydrophilic molecules, it is likely that these substrates bind to the corresponding ABC transporters via polar interactions. Notably, docking and MD simulation of different GPAs and GPA ABC transporters revealed polar contacts of the putative substrate binding pocket and the peptide backbone of the GPAs (Fig. 3 - Publication 1). The influence of three of these residues potentially involved in binding during the transport of balhimycin was then investigated by site-directed mutagenesis in Tba and *in vivo* export assays. Only the T316A mutation significantly reduced the export of balhimycin

(Fig. 4 - Publication 1). T316 is located on the cytosolic side of the putative substrate binding pocket on TMH6. For the ABC transporter TmrAB, TMH6 has been shown to act as a gatekeeper, switching between two different IF conformations of the transporter and thereby controlling substrate uptake [108]. In the ABC transporter LmrA, the same helix is involved in conformational changes upon ATP binding [211]. It is possible that TMH6 of Tba is equally important for substrate recognition or conformational dynamics in the transport process of balhimycin, which was partially disrupted by mutagenesis. However, this is a hypothesis that requires further investigation. The discrepancy between the *in silico* modeling data and the *in vivo* validation of the other two mutations tested, Q309G and R310A (Figs. 3, 4 - Publication 1), may be explained by the fact that the MD simulations were based on the structural snapshot predicted by AlphaFold2 and only analyzed binding. However, substrate transport involves multiple conformational changes and is unlikely to depend solely on individual amino acid residues. This complexity might not be fully reflected in the simulation.
Additionally, the simulation data suggested that the R1 sugar moiety of different GPAs points to the cytoplasmic site, indicating that these may not be primarily involved in binding (Fig. 3 - Publication 1). This is in line with the hypothesis that substrate binding depends on specific interactions with the peptide backbone and was confirmed by *in vivo* export assays using mutants that are not able to synthesize fully modified balhimycin (Fig. 4 - Publication 1). It was shown that the absence of both sugar moieties R1 and R2 increases the export of balhimycin, indicating that the bulky molecules impede efficient export. The cell seems to compromise by accepting a lower export rate in favor of biological activity, which is significantly improved by the modifications (Fig. 4 - Publication 1).

In conclusion, GPA ABC transporters exhibit specificity for their cognate substrate type based on backbone composition, whereas they show greater promiscuity with respect to additional modifications. Further investigations should address the exact binding mode of the GPAs within the putative substrate binding pocket, possibly by additional mutagenesis studies. This has been hampered by the low genetic amenability of *A. balhimycina*. To overcome this limitation, the export of GPAs could be studied in *A. japonicum*, as the methods for transferring foreign DNA and genetic modification are more diverse in this species. To resolve the complete transport cycle, structural analysis of different conformational states of the transporter should be performed.

5.1.1 Evaluation of the overexpression and purification of GPA ABC transporter in *E. coli* and in the native environment

To further characterize the specificity of the GPA ABC transporters *in vitro*, I focused on developing a purification protocol to obtain functional proteins for binding and transport kinetics analysis. Previous efforts have succeeded in purifying Tba with an N-terminal 6xHis tag from *E. coli* BL21(DE3). However, only basal ATPase activity (26 nmol min^{-1} mg^{-1}) without balhimycin induction was measured using a malachite green assay [168]. Therefore, it appears that under these conditions, no fully functional Tba was purified.

In this work, initial expression and purification experiments were carried out in *E. coli* Lemo21(DE3) (Lemo21) and Mutant56(DE3) (Mt56) optimized for heterologous membrane protein expression, before switching the host to *S. lividans* T7 and *A. balhimycina*. In addition, different affinity tags and expression conditions were tested. While the conditions tested in *E. coli* resulted in the successful expression of various Tri fusion proteins, the expression of Tba fusion proteins was generally weaker or sometimes absent (Figs. 4, 9, 13, 15). For this reason, the optimization effort using an *E. coli* expression host was focused mainly on Tri. However, this approach only led to a low specific protein yield and was associated with many unspecific impurities (Figs. 12, 14, 16). The expression of Tba fusion proteins in *S. lividans* T7 and *A. balhimycina* was successful, resulting in highly pure protein (Figs. 17, 18). Nevertheless, a significant protein yield of either Tba or Tri was not achieved under any of the conditions tested and therefore represents the focus for further optimization.

Membrane protein biogenesis is a complex process that requires a well-orchestrated balance between different steps, including transcription, (co-)translation, membrane targeting, insertion, and folding. The T7RNAP used in this study usually allows high transcription rates, resulting in high yields of recombinant proteins [64]. However, it has been shown that high levels of membrane protein overexpression can add to the metabolic burden of the host cell that occurs during overexpression and cause saturation of the Sec translocon [70]. Therefore, slowing down the biogenesis of membrane proteins is generally considered beneficial for the production of recombinant membrane proteins. This was addressed by using Lemo21, which allows the expression of the T7RNAP to be controlled by varying rhamnose concentration [72], and Mt56, which promotes slower expression due to a mutation in the T7RNAP [74]. The main challenges that complicated the purification of Tri and Tba from *E. coli* in this work were: (i) achieving high expression levels, (ii) incorrect membrane insertion, (iii) proteolysis of the fusion tag and the ABC transporters themselves, and (iv) lack of efficient detergent extraction, and will be addressed below.

(i) Expression of *tri* and *tba* in Lemo21 and Mt56 was screened using three different translational fusion tags. Firstly, a C-terminal GFP protein tag was used as a folding indicator, fluorescing only when the N-terminal protein is correctly folded [190]. This strategy also facilitates monitoring protein production during the purification process. Since large protein tags such as GFP can interfere with membrane insertion, a C-terminal 6xHis tag was also used in an independent approach. Due to its small size, this tag usually does not interfere with expression

or membrane insertion. Thirdly, an N-terminal SUMO tag was used. SUMO is described as a solubility enhancing tag and can protect the fusion partner from N-terminal degradation, resulting in higher expression levels [213]. In fact, the highest expression levels of *tri* and *tba* were achieved with an N-terminal SUMO tag in Lemo21 without the addition of rhamnose at 18°C and 30°C, respectively (Fig. 15A, B). The expression of *tri* was also possible with a GFP and a 6xHis tag (Figs. 4, 13). However, their purification resulted in high levels of non-specifically purified proteins containing multiple histidine residues and thus also exhibiting a high affinity for the Ni^{2+}-containing chromatography resin (Figs. 12, 14). This effect is particularly noticeable when the specific protein concentration of the protein to be purified is low.
In addition, different growth conditions were investigated. It was generally observed that long induction times of at least 15 hours, a low temperature of 18°C, and growth in TB medium resulted in high cell densities and thus high expression of *tri*. Since low growth temperatures of 15-20°C slow down protein biosynthesis and reduce hydrophobic interactions that can cause aggregation [214–216], it is plausible that this also promotes slow membrane protein biogenesis and thus counteracts Sec saturation. Additional means of fine-tuning the expression of *tri* and *tba* were not investigated here. One possibility to increase the expression could be to codon optimize the sequence of *tri* and *tba* for *E. coli*. Another potential approach involves increasing expression through a transcriptional fusion. For instance, transcriptional fusions with *mstX*, which encodes Mistic, an integral membrane protein capable of unassisted folding into the cytoplasmic membrane, have been demonstrated to enhance the expression of multiple membrane proteins [217,218].

(ii) The second major challenge was to identify the conditions under which Tri and Tba were correctly inserted into the cytoplasmic membrane. Incorrect membrane insertion became apparent when Tri-GFP and Tba-GFP were expressed in Lemo21 under all conditions tested (Figs. 6, 7, 8). Neither of the two transporter fusions co-localized exclusively with the inner membrane (IM) fractions of Lemo21 upon membrane fractionation but rather with the outer membrane (OM) fractions (Fig. 6). It is known that protein aggregates, as well as OM, equilibrate at high sucrose concentrations or sometimes co-sediment with the OM [196], suggesting that the transporters were not properly integrated into the inner membrane but were present in an aggregated form. Since large amounts of cytoplasmic aggregates were excluded (Fig. 7), these may be intramembranous aggregates. In addition, epifluorescence microscopy confirmed that both transporter GFP fusions were not co-localized with the membrane (Fig. 8). In contrast, when *tri-gfp* was expressed in Mt56 at 18°C, both epifluorescence microscopy and membrane fractionation confirmed that the protein was localized in the IM and was not aggregated (Figs. 9, 10). These results highlight that a low growth temperature of 18°C promotes not only expression but also membrane insertion.

(iii) The third major challenge was proteolytic cleavage of the fusion protein GFP and digestion of the ABC transporters themselves. Although GFP fusion proteins often serve as a folding indicator for overexpressed membrane proteins [190], the relative fluorescence signal obtained for Tri-GFP and Tba-GFP in Lemo21 did not clearly correlate with the amount of full-length protein detected by immunodetection (Fig. 4). This indicates that free but functional GFP was

present in the cells, which was supported by the detection of a band corresponding to the size of GFP in all immunoblots of whole cells (Lemo21) expressing either *tri-GFP* or *tba-GFP*. Furthermore, when crude membranes were prepared from Lemo21 or Mt56 expressing *tri-GFP*, the majority of the fluorescence signal was still measurable in the cytosolic fraction (Figs. 5, 12). It is therefore likely that the GFP tag is cleaved by cellular endopeptidases and fluoresces in the cytoplasm. Compared to other fusion tags used in protein purification, GFP, with a molecular weight of ≈26 kDa, is relatively large and may interfere with proper membrane insertion and folding and was consequently cleaved.
In addition, N-terminal degradation of both transporters, Tri and Tba, was visible after expression with a C-terminal GFP or a 6xHis tag (Figs. 4, 12, 14). Many other bands were detected by immunodetection with specific antibodies. When *tri* was expressed with an N-terminal SUMO tag, these bands were significantly weaker, confirming that the SUMO tag can partially protect the transporter from N-terminal degradation (Fig. 16).

(iv) A further problem was the inefficient extraction of the membrane transporters with various detergents. Extraction of Tri-GFP from the cytoplasmic membrane of Lemo21 grown at 25°C was not possible with the commonly used detergents DDM, DM, LMNG, or DMNG (Fig. 5), whereas LMNG and DDM were both able to extract Tri-GFP from Mt56 membranes after growth at 18°C (Fig. 11). Since Tri-GFP was not correctly inserted into the membrane of Lemo21 (Figs. 5, 6, 7, 8), this is a possible explanation for why the detergents were unable to extract the protein. In contrast, Tri-GFP extraction was possible when the fusion protein was correctly inserted into the cytoplasmic membranes of Mt56 (Figs. 9, 10, 11). The extraction of Tri-6xHis, expressed in Mt56, was partially possible with DDM and LMNG (Fig. 13B). Extraction of SUMO-Tri with DDM resulted only in large aggregates detected by BN-PAGE, whereas the harsh detergent FC-12 extracted a complex (Fig. 16C). However, it was not possible to evaluate from the BN-PAGE gel whether this was the correct oligomeric conformation of SUMO-Tri, as the size of the detergent micelles could not unambiguously be determined. For this purpose, it is useful to perform size exclusion chromatography with multi-angle light scattering (SEC-MALS), which allows the determination of the absolute molar mass of a protein within a detergent micelle [219]. FC-12 is also known to extract aggregated proteins from the membrane and stabilize non-native conformations [202], questioning the quality of the extraction. However, further analysis was not possible for another reason: after solubilization, none of the FC-12-solubilized proteins bound to the Ni^{2+}-containing resin during immobilized metal affinity chromatography (IMAC) (Fig. 16). This may be due to possible masking effects of the detergent, which hinders the binding of the N-terminal 6xHis tag to the chromatography resin.
As the detergents were unable to effectively extract and stabilize large amounts of Tri or Tba, detergent-free extraction using, for example, SMA (polystyrene-co-maleic acid) copolymers could be used to overcome this problem [76]. These are able to penetrate the membrane and extract small membrane discs containing both proteins and adjacent lipids. SMA lipid particles (SMALP) can have a stabilizing effect on the protein due to preserved protein-lipid interactions and have been successfully applied to several ABC transporters in the past [220].

All attempts to optimize the purification of Tri or Tba from Lemo21 or Mt56 resulted in very low specific protein concentrations, regardless of the tag, growth condition, or detergent used. This was most likely due to a cumulative effect of the major challenges described above and was therefore not pursued further. Instead, an alternative approach was chosen, focusing on the expression of GPA ABC transporters in a more native environment. This was only investigated for Tba. The phylum of Actinomycetota, to which *A. balhimycina* belongs, is phylogenetically distinct and distant from *E. coli* and the class of *Gammaproteobacteria* [221]. Although all bacteria share common mechanisms, including protein biogenesis, there may be additional strain- or species-specific factors that influence membrane protein biogenesis that are not present in *E. coli*. These potentially include membrane organization, lipid composition, specialized chaperones, or necessary interactions of the transporter with other proteins. Therefore, it was investigated whether the expression and purification of Tba-3xFLAG in a more native environment is superior to *E. coli*.

Recombinant expression of Tba-3xFLAG was possible in *S. lividans* T7 and in the native organism *A. balhimycina*. In *S. lividans* T7, the expression of a codon-optimized T7RNAP can be induced by the addition of thiostrepton. Membrane insertion was not specifically investigated because extraction of a complex using mild detergents (LMNG or DMNG) was possible without any optimization of the conditions. The transporter could then be purified by affinity chromatography in both cases. It was particularly striking that this purification resulted in a high-purity elution and low non-specific contamination, in contrast to purifications using a GFP or 6xHis tag in *E. coli*. In comparison to a His tag, the 3xFLAG tag is known for its high specificity in affinity purification, resulting in less contamination [222]. Degradation of Tba-3xFLAG at the N-terminus was observed in both strains, but slightly less in *S. lividans* T7 than in *A. balhimycina*. Streptomyces strains, such as *S. lividans*, are known for their low endogenous proteolytic activity and are therefore well suited for heterologous protein expression [223].

Interestingly, the purification of Tba-3xFLAG in *A. balhimycina* also led to the co-purification of two members of the SPFH protein family (Stomatin, Prohibitin, Flotillin, and HflK/C): Paraslipin and a Flotillin-like protein. In other bacteria, such as *Bacillus subtilis*, Flotillins have been shown to be involved in membrane organization by acting as scaffolding proteins and forming functional membrane microdomains (FMMs) that can modulate membrane composition and fluidity [33,224]. FMMs have already been shown to be essential for the functionality of some membrane proteins [225]. Therefore, expression and purification of Tba from *A. balhimycina* appears to be a good option, as the transporter may depend on a functional environment. However, I would like to highlight that this is a hypothesis that still awaits validation. The possible dependency of Tba on Paraslipin or the Flotillin-like protein needs to be further investigated, e.g. by deletion mutants of the two SPFH family proteins and their influence on balhimycin production.

In conclusion, the purification of Tba-3xFLAG using *S. lividans* T7 or *A. balhimycina* resulted in highly pure protein without many contaminants and represents a prominent starting point for further optimization. These should focus on increasing the overall yield of Tba in order to obtain

sufficient protein for *in vitro* transport assays or structural analysis. Possible optimization approaches include increasing the expression strength, e.g., as described above using transcriptional fusions and increasing the culture volume, e.g., in a large fermenter, or optimizing the extraction efficiency by detergent screening, or using SMA copolymers.

In principle, both organisms are suitable for the expression of Tba. However, the methods for genetic modification of *S. lividans* T7 are more diverse than for *A. balhimycina*. For example, plasmid-based expression is possible, which would allow large-scale screening of different GPA ABC transporters. However, if the naive environment in *A. balhimycina* is crucial for its function, this would be a better expression strain.

5.2 Investigation of potential regulatory constraints and interaction partners of Tba in *A. balhimycina*[*3]

Alongside the investigation of the specificity of GPA ABC transporters, a major focus of this work was to characterize the functional environment of Tba in its native environment, including the identification of possible interaction partners. This revealed a previously uncharacterized regulatory mechanism in *A. balhimycina* that stops the biosynthesis of balhimycin when the export is impaired, either by deletion of the native transporter Tba or by functional inactivation by mutagenesis of the NBD. It was discovered by *in vivo* export analysis and determination of intracellular balhimycin concentration (Fig. 2 - Publication 1). The observation differs from a previous study describing balhimycin accumulation after deletion of the transporter. The discrepancy may be a result of differences in methodology: Menges et al. determined the intracellular balhimycin concentration by inhibition zone diameters after a bioactivity assay [168]. In the present work, however, the intracellular balhimycin concentration was quantified by state-of-the-art HPLC-MS measurements.

RNA sequencing revealed that the described transport-dependent regulation of balhimycin biosynthesis does not occur at the transcriptional level, as originally hypothesized. In fact, transcripts of the balhimycin BGC genes were still detected in the wild-type and after deletion of Tba but not when the pathway-specific regulator Bbr was absent (Figs. 5A, S9A - Publication 1). Similar observations have been made in *Microcystis aeruginosa*, where the biosynthesis of microcystin was impaired in the absence of the cognate transporter McyH, but transcripts of other *mcy* genes were not affected [226]. In contrast, there are examples of transcriptional down-regulation when export is impaired, such as daunorubicin production in *Streptomyces peucetius* (*S. peucetius*). Here, the disruption of the putative ABC transporter DrrAB leads to transcriptional repression of genes essential for daunorubicin production, presumably through intracellular sensing of daunorubicin accumulation [227]. This mechanism is essential for *S. peucetius* because DrrAB also functions as a self-resistance mechanism, and high levels of daunorubicin are toxic to the cells. However, Tba is not part of the intrinsic resistance mechanism in *A. balhimycina*, which is achieved by cell wall remodeling [171,188,228]. Therefore, high intracellular concentrations are not necessarily toxic, and the regulatory mechanism may be in place to avoid energy dissipation.

It is also conceivable that the arrest of balhimycin biosynthesis is triggered by the accumulation of individual intermediates or precursors and is mediated by feedback inhibition. A similar mechanism has already been identified in *A. balhimycina* at the interplay between primary and secondary metabolism, where tyrosine acts as a feedback enzyme inhibitor in the shikimate pathway, thus regulating the production of balhimycin precursors [149,151]. However, metabolomic analyses showed no significant accumulation of individual amino acids or balhimycin intermediates in the absence of the transporter compared to the wild-type (Figs. 5B, S9B - Publication 1). It was therefore concluded that the transport-dependent down-regulation of

[*3] Parts of this chapter were previously published in publication 1 'Unveiling the substrate specificity of the ABC transporter Tba and its role in glycopeptide biosynthesis', by Gericke and Beqaj et al. (2025) [97].

balhimycin biosynthesis was not affected by feedback inhibition of a specific enzyme involved in balhimycin biosynthesis.

Rather, the results of this work point towards a different regulatory level. Analysis of the microenvironment of Tba-TID in *A. balhimycina* by *in vivo* proximity biotinylation and co-immunoprecipitation of Tba-3xFLAG suggests interactions between the transporter and close-by biosynthetic enzymes, which are perhaps important in the regulatory process. However, the exact direct protein-protein interactions and the mechanism by which biosynthesis may be halted still need to be investigated in detail.

Using proximity biotinylation, two NRPS enzymes (BpsB, BpsC), five modifying enzymes (OxyC, BhaA, BgtfA, BgtfB, Bmt), and enzymes involved in the synthesis of amino acid and sugar precursors (Pgat, BpsD, OxyD, HmaS, DvaB, DvaC) could be identified in the close proximity of the transporter (Fig. 6 - Publication 1). This suggests the presence of a microcompartment comprising enzymes involved in balhimycin biosynthesis in the vicinity of Tba. Bacteria are known to use proteinaceous microcompartments to optimize metabolic processes, such as the propanediol-using microcompartment (Pdu MCP) of *Salmonella enterica* serovar Typhimurium LT2 [229]. Another example are carboxysomes formed by cyanobacteria to increase the efficiency of carbon fixation by encapsulating the ribulose 1,5-bisphosphate carboxylase/oxygenase (RuBisCO) in a semipermeable protein shell that prevents CO_2 leakage [230,231]. Whether GPA biosynthesis in *A. balhimycina* is organized within a bacterial microcompartment could be investigated by thin-section transmission electron microscopy, as shown for Pdu MCP and carboxysomes [229,231,232]. In addition, fluorescence microscopy could be used to determine which biosynthetic enzymes are co-localized with the transporter Tba at the cell membrane. For example, co-localization microscopy showed that the cereulide ABC transporter CesCD in *Bacillus cereus* can localize the NRPS enzyme CesA to the membrane and thus plays an important role in the biosynthetic process [233]. The same study also points to specific interactions by a bacterial two-hybrid assay. There is also evidence that other biosynthesis enzymes of secondary metabolites interact with the respective transporters, for example, the nisin transporter NisT in *L. lactis* [234,235].

By co-immunoprecipitation using Tba-3xFLAG as a bait protein, almost all biosynthesis enzymes identified by *in vivo* proximity biotinylation were identified as potential interaction partners of Tba, with the exception of BgtfB and BpsD. In addition, DvaD was identified. However, it is not possible at this stage to speculate which of the enzymes interact directly with the transporter and which co-purified through indirect effects, e.g., because they possibly also interact with each other. Since ABC transporters undergo a major conformational change in their transport cycle [e.g.,108,236,237] , it is possible that an interaction that takes place in one conformation is disrupted in another conformation. This hypothesis was supported by the fact that inactivation of Tba (Tba^{E545Q}) also led to a halt in biosynthesis (Fig. 2 - Publication 1). It was therefore suspected that an active transporter, and, possibly, interactions that can only take place in one conformation that are not represented by Tba^{E545Q}, play a role in the regulation of balhimycin biosynthesis. Interestingly, co-immunoprecipitation using Tba^{E545Q}-3xFLAG as a bait protein identified the majority of biosynthesis enzymes that were also found

when wild-type Tba was used as a bait protein. The only enzyme that co-precipitated with the wild-type transporter with a significant log2 fold-change compared to the inactive transporter was OxyC, one of the three P450 monooxygenases, responsible for oxidative cross-linking of the peptide backbone of balhimycin. OxyC forms the final cross-link between AA5 and AA7, and in an *oxyC* deletion mutant, balhimycin intermediates are still exported [160]. However, to my knowledge, no quantitative analysis has ever been performed to determine whether or not transport efficiency is affected. Based on these results, it is possible that a specific interaction between Tba and OxyC is important for efficient biosynthesis and transport. This could be investigated *in vitro* with purified OxyC and Tba using bioanalytical methods such as nano differential scanning fluorimetry (nDSF) or surface plasmon resonance (SPR) spectroscopy. However, since balhimycin intermediates are still exported and thus produced in the absence of OxyC, it is not plausible that this interaction is the only regulatory factor.

In addition to the proteins involved in the biosynthesis of balhimycin, other proteins were co-precipitated and identified as potential interaction partners of Tba-3xFLAG and Tba^{E545Q}-3xFLAG (Fig. 19). These included some highly abundant membrane proteins, such as proteins of the bacterial respiratory chain, as well as proteins of the Sec translocon and YidC, which are essential for the integration and folding of membrane proteins. In addition, two members of the SPFH protein family were found: Paraslipin and a Flotillin-like protein. Paraslipin was also identified to be in close proximity to Tba by *in vivo* proximity biotinylation. As previously described, SPFH family proteins play a vital role in the spatiotemporal organization of membranes. This is achieved through the formation of FMMs and their function as scaffolding proteins. They are structurally and functionally conserved and were shown to directly regulate key reactions at the cytoplasmic membrane, like peptidoglycan synthesis, transport processes, protein secretion, or signaling cascades in bacteria [33,225,238]. The co-precipitation of Paraslipin and the Flotillin-like protein therefore suggests that they may play a role in the functionality of Tba and thus for the entire biosynthesis of balhimycin. This hypothesis could be further investigated, as mentioned before (5.1.1), by gene knockouts of the two scaffold proteins and subsequent investigation of the quantitative influence on the biosynthesis of balhimycin. Furthermore, it was shown that treatment of the cytoplasmic membrane with mild detergents leads to two different membrane fractions, with the Flotillin-like proteins and their interaction partners being found together in the detergent-resistant fraction [33]. It could strengthen the evidence for possible interactions if Tba and Flotillin-like proteins would be found in the same fraction.

In conclusion, neither transcriptional regulation of the balhimycin BGC nor a regulatory feedback loop based on substrate inhibition of enzymes involved in biosynthesis are responsible for the transport-dependent regulation of balhimycin. However, it has been demonstrated that enzymes involved in balhimycin biosynthesis, modification, and precursor supply accumulate in the close proximity of Tba at the cytoplasmic membrane and possibly interact with the transporter. Based on these findings, it was suspected that the interactions between Tba and the biosynthetic enzymes are crucial for biosynthesis and cannot be formed if the transporter is absent or inactive. However, most of the biosynthetic enzymes co-precipitated with Tba-3xFLAG were also identified as potential interaction partners of the

inactive transporter Tba^{E545Q}-3xFLAG. I therefore speculate that the interactions are important for effective biosynthesis and transport, but that there is another regulatory component that unfortunately has not yet been elucidated in this work.

One hypothesis is the formation of a microcompartment, which could possibly give the biosynthetic enzymes a competitive advantage over the primary metabolite regarding the shared precursor molecules. Furthermore, the balhimycin intermediates would then be protected from possible proteolytic degradation. It is also conceivable that the transporter Tba is organized within a FMM, whose scaffold proteins could possibly also serve as an interaction hub for biosynthesis proteins. From an energetic point of view, the spatial accumulation of related metabolic processes is efficient and can positively influence biosynthesis and export rates through high local substrate concentrations and short diffusion trajectories. *A. balhimycina* is commonly found in soil environments. This habitat is characterized by a high population density of different microorganisms that are in constant competition for essential nutrients. Therefore, it is crucial that processes that provide a competitive advantage, such as the production and export of antibiotics, are subject to tight regulation in order to facilitate rapid adaptation to changing conditions, optimize energy balance, and avoid unnecessary expenditure of resources.

6 Outlook

The objective of this work was to functionally dissect the transport process during GPA production. To that end, the focus was directed towards two main aspects: the specificity of GPA transporters and their possible interaction with the biosynthetic machinery. The biosynthesis of the GPA balhimycin in *A. balhimycina* was used as a model for *in vitro* and *in vivo* studies.

It was observed that all analyzed GPA BGCs harbor a transport-related gene encoding an ABC transporter. The substrate selectivity of this transporter depends on the peptide composition of the respective GPA substrate and not on its modifications. Furthermore, it was shown that functional integration of the export process into the biosynthetic process is critical for efficient biosynthesis and that balhimycin production is halted when the export is impaired. There are indications that the regulation of balhimycin biosynthesis partly depends on specific interactions with the transporter, but rather on global and higher-order mechanisms, such as FMM or specialized microcompartments. However, this is speculation and the precise mechanism by which *A. balhimycina* modulates biosynthetic activity in the absence of export remains to be elucidated. Moreover, the foundation for prospective *in vitro* analyses was laid by optimizing a purification protocol for Tri, the transporter of ristomycin from *A. japonicum*, and Tba, the transporter of balhimycin from *A. balhimycina*.

Further studies should mainly focus on two aspects. Firstly, the elucidation of the regulation of the biosynthesis and the analysis of specific interactions between Tba, the biosynthetic enzymes, and other cellular compartments in *A. balhimycina*. Secondly, a detailed investigation of the substrate specificity, including the analysis of the exact binding mode and substrate binding site of Tba. In general, it would be interesting to test if the results of this and future work are transferable to other GPA producers. If so, this would contribute greatly to expanding knowledge of GPA biosynthesis, ABC transporter mechanisms, and the functional significance of export of natural products in the producer cell. This could, for example, be used to improve the biotechnological production routes of GPAs and thus contribute to the fight against the challenging AMR crisis.

7 Materials and Methods

Methods that exclusively describe experiments included in publication 1 ‘Unveiling the substrate specificity of the ABC transporter Tba and its role in glycopeptide biosynthesis' are listed in Chapter 4.1 and not additionally in this chapter.

7.1 Chemicals, materials, and consumables

Unless otherwise stated, all chemicals and consumables used in this study were purchased from Anatrace Products LLC, AppliChem GmbH, Avantor, Becton Dickinson, Biorad, Biozym Scientific, Carl Roth GmbH + Co. KG, Dianova, IBA Lifesciences, Macherey-Nagel GmbH & Co. KG (MN), Merck Group, Novagen, SERVA Electrophoresis GmbH, Thermo Fisher Scientific Inc., or QIAGEN GmbH. Enzymes were purchased from New England Biolabs (NEB). Chromatography columns were purchased from Cytiva. Oligonucleotides were synthesized by Eurofins Genomics or Integrated DNA Technologies (IDT).

7.1.1 **Media, buffers, and antibiotics**

The growth media and buffers used in this study are listed in Table 1. Unless otherwise indicated, media and buffers were prepared with dH_2O. For solid media, 1.5% (w/v) agar was used unless otherwise noted. Media and supplemental buffers were autoclaved or sterile filtered prior to use. The antibiotics and final concentrations used for plasmid selection in the media are listed in Table 2.

7.1.2 **Detergents and antibodies**

The detergents and their relevant properties are listed in Table 3. The antibodies used in this study are listed in Table 4. All antibodies were dissolved according to the manufacturer's protocol and further diluted in TBS-T before use.

7.2 Bacterial strains and growth conditions

The bacterial strains and plasmids used in this study are listed in Table 5 and Table 6, respectively. Unless otherwise noted, *E. coli* was grown aerobically at 37°C in liquid medium in growth flasks or in 10 ml test tubes shaken at 180 rpm, or on solid agar plates. Growth in liquid medium was monitored by measuring the absorbance at a wavelength of 600 nm (OD_{600}). *A. balhimycina* and *S. lividans* were usually grown aerobically at 29°C in liquid medium in baffled flasks with a steel coil, shaken at 120 rpm, or on solid agar plates. Liquid cultures were inoculated with approximately 1 cm^2 of mycelium from a solid agar plate or from a liquid preculture. Balhimycin production by *A. balhimycina* is only achieved in R5 medium. Long-term storage of *A. balhimycina* is carried out in R5 medium at -20°C, that of *E. coli* in stock medium at -80°C, and that of *S. lividans* in spore stocks at -20°C. *S. lividans* spores were collected from a sporulating plate by filtration with ddH_2O through a sterile cotton pad and stored at -20°C.

7.3 Molecular cloning and plasmid construction

Different molecular cloning techniques were used to modify and construct plasmids. Vector and insert DNA fragments were amplified by polymerase chain reaction (PCR) using “Q5® Hot Start High-Fidelity DNA Polymerase” or “Phusion® High-Fidelity DNA Polymerase”, followed by a DpnI digestion step (4 µl, 37°C, 2-16 h) to remove methylated template DNA. The oligonucleotides used for PCR are listed in Table 7. Amplified DNA fragments were analyzed on 1% (w/v) agarose gel in TAE buffer and purified using the “QIAquick PCR Purification Kit” (Qiagen). The standard Gibson assembly method was used to assemble plasmids in a one-step reaction [239]. The vector DNA of pRM4 (*NdeI*/*XbaI*) and pGM202T7 (*NdeI*/*HindIII*) was not amplified by PCR but was instead digested using restriction endonucleases and purified from a 1.5% (w/v) agarose gel using the “QIAquick Gel Extraction Kit” (Qiagen). Vector and insert DNA were then assembled using the aforementioned Gibson assembly method (50 ng of vector DNA, 1:3 molar ratio to insert). Assembled plasmids were transformed into chemically competent *E. coli* NEB5a cells using a standard heat shock transformation protocol [240]. The resulting colonies were screened by colony PCR using “One*Taq*® DNA Polymerase”. Positive clones were inoculated, and the plasmids were extracted from an overnight culture using the “QIAprep Spin Miniprep Kit” (Qiagen). All constructed plasmids were sequenced by Eurofins Genomics using Sanger sequencing. Fifty to 100 ng/µl of plasmid DNA was mixed with the respective sequencing primer at a concentration of 10 µM. All kits and reactions were performed according to the manufacturer’s instructions.

7.4 Genetic methods for Actinomycetes

7.4.1 Isolation of DNA from Actinomycetes

Total DNA from the different Actinomycetes strains used in this study was required for PCR amplification of genes and to verify correct genomic integration. This was performed using the “NucleoSpin Microbial DNA Mini Kit for DNA from microorganisms” (MN) with 40 mg wet weight of culture and 200 µl of elution buffer, otherwise following the manufacturer’s instructions. For plasmid extraction from *S. lividans*, 1.5 ml of a liquid culture was used. The cells were resuspended in P1 buffer of the “QIAprep Spin Miniprep Kit” (Qiagen) supplemented with 5 mg/ml lysozyme and incubated for 45 minutes at 37°C while shaking. Further extraction was performed according to the manufacturer's instructions.

7.4.2 Genomic modification of *A. balhimycina* (Direct transformation)

Chromosomal integration of DNA into the genome of *A. balhimycina* is based on an integration vector carrying the Φ31 bacteriophage integrase system in addition to the gene of interest. In this study, the pRM4 vector [168], a derivative of pRSET152 [241], mediated the site-specific recombination at the corresponding pseudo *attP* site in the *A. balhimycina* genome. The strains were transformed with demethylated vector DNA using the direct transformation method (D-Trafo) first introduced in 1991 [242] and later adapted to *A. balhimycina* by Pelzer et al. [243].

Demethylated plasmid DNA was extracted from *E. coli* JM110 or ET12567. In this study, the highest transformation efficiency was achieved with a culture grown for 48 hours.

7.4.3 **Genomic modification of *A. japonicum* and *S. lividans* (Conjugation)**

Conjugation was used to transfer integrative or stable plasmids into *A. japonicum* and *S. lividans*, respectively. The mobilizing strain *E. coli* S17-1 was transformed with the plasmid to be transferred to the recipient strain. A 50 ml overnight culture of the donor strain in LB medium with the respective antibiotic was harvested (5,000 x *g*, 10 min, 4°C) and washed twice with LB medium without antibiotics. After the washing steps, the pellet was resuspended in 1 ml of LB medium. Approximately 1 cm^2 of *A. japonicum* mycelium or ≈10^8 pre-activated (10 min at 50°C in YT medium) *S. lividans* spores were mixed with the donor strain, and various volumes were plated on MS agar plates (containing 2 mM $MgCl_2$) and incubated at 29°C for 16-20 hours. After incubation, the plates were overlaid with 25 µg/ml nalidixic acid to kill all *E. coli* donor cells and the appropriate antibiotic for plasmid selection in the recipient strain. The plates were further incubated at 29°C for 3-7 days until exconjugants were visible. The genomic or plasmid DNA was isolated from the clones and tested by PCR for correct insertion or uptake of DNA.

7.5 Standard protein biochemical and immunological methods

7.5.1 **SDS-PAGE, Western blotting, and immunodetection of proteins**

Protein samples were denatured in SB buffer for 10 min at 50°C, unless otherwise noted, and then applied to “SERVAGel™ TG PRiME™ 8–16%” precast gels for sodium dodecyl sulfate (SDS) polyacrylamide gel electrophoresis (PAGE). In addition, the “Precision Plus Protein™ All Blue Prestained Protein Standard” (Biorad) was used as a protein standard. A two-step electrophoresis in 1x SDS running buffer was performed at 100 V for 15 min followed by 210 V for 1.5 h. The gel was either stained using a standard Coomassie staining method [244] or transferred to an “Immun-Blot® polyvinylidene difluoride” (PVDF) membrane (0.2 µm) (Biorad) using a standard Western blotting procedure. Transfer was performed at 35 V for 3.5 h at 4°C in 1x transfer buffer. To reduce non-specific antibody-binding, the membrane was blocked with “BlueBlock PF” in TBS for 1 h. The membrane was then treated for 1 h with the respective primary and secondary antibodies diluted in TBS-T. Between each step, the membrane was washed three times for 10 minutes with TBS-T. Finally, the fluorescence signal of the conjugated secondary antibodies was detected using a Li-Cor Odyssey system and analyzed using Image Studio (Li-Cor) software (v5.2).

7.5.2 **Blue Native PAGE**

Protein samples under near native conditions were mixed with BN loading buffer and applied to a “NativePAGE™ 3 to 12% (Bis-Tris, 1.0 mm, Mini Protein Gels)” (Thermo Fisher) for blue native (BN) PAGE. For size approximation, 8 µl of “NativeMark™ Unstained Protein Standard”

(Thermo Fisher) was used as protein standard. Electrophoresis was first performed in anode buffer and cathode buffer I at 130 V and 200 mA until the Coomassie front reached approximately ⅓ of the gel and then switched to cathode buffer II and 300 V until the Coomassie front ran out of the gel. After electrophoresis, the gel was equilibrated in 1x SDS running buffer for 30 min and then either stained with a Coomassie staining solution or transferred to a PVDF membrane as described previously (5.5.1). After Western blotting, the membrane was washed with 100% (v/v) methanol to remove the blue Coomassie staining, followed by immunodetection of the proteins.

7.5.3 **Crude membrane preparation**

The crude membrane preparation was described previously [245] and slightly adapted here for *A. balhimycina*. Briefly, 150-300 mg wet weight of culture was washed with 1x PBS and resuspended in lysis buffer (buffer K supplemented with 1 mM EDTA, 1 mM $MgCl_2$, 10 µg/ml DNAse, 2 mg/ml lysozyme, and 1:100 protease inhibitor cocktail (Sigma-Aldrich (P8849)). Cells were incubated at 4°C for 30 min, mixed with glass beads (Ø=150-212 µm), and lysed using a bead mill (2 min, continuous mode). Cell debris was removed by centrifugation (10,000 x *g*, 10 min, 4°C). Finally, the membranes were precipitated by centrifugation (55,000 x *g*, 45 min, 4°C) and resuspended in 75 µl of 1x PBS. The protein concentration was determined using the colorimetric "Pierce™ BCA Protein Assay Kits" (Thermo Fisher Scientific) according to the manufacturer's protocol. For analysis by SDS or BN-PAGE, 15-20 µg of crude membranes were applied.

7.5.4 **Membrane solubilization**

Membranes were solubilized using detergents to extract membrane proteins. The detergents were used to stabilize the proteins in aqueous solution while the native lipids were removed. All detergents used for solubilization in this study are listed in Table 3. A 10% (w/v) stock solution was prepared, and the extraction of membrane proteins was performed at a final concentration of 1% (w/v). The stock solution was prepared in the buffer of choice in which the crude membrane extract was resuspended. Solubilization was performed for 1 hour at 4°C under shaking conditions. Non-solubilized material was removed by centrifugation (100,000 x *g*, 30 min, 4°C).

7.6 GFP fluorescence measurement in whole cells

GFP fluorescence intensity was measured in cells expressing GFP or GFP fusion proteins. After growth, 1 ml of the culture was harvested (14,000 rpm, 3 min). The pellet was resuspended in 100 µl of 1x PBS (4°C) and incubated at 4°C for 1 h. The cell suspension was then transferred to a black 96-well plate, and the fluorescence intensity of whole cells was determined at an excitation wavelength of 485 nm and an emission wavelength of 535 nm using a Tecan plate reader. The same samples were used for OD_{600} measurements to normalize the signal to the number of cells per sample. (Device: Tecan Spark)

7.7 Epifluorescence microscopy

For microscopic analysis of GFP in *E. coli*, the cells were cultivated and used for microscopy in the exponential growth phase. 2 µl of the culture was applied to a freshly prepared agarose pad and covered with a coverslip. The agarose pads were prepared as follows: three stripes of tapestry were stuck on top of each other on two slides. To cast a fresh agarose pad, one slide was placed between the two slides with the tapestry, and another slide was placed across it. This created a square cavity between slides 1 and 4, which was slowly filled with 0.5-1 ml of liquid 1% (w/v) agarose in H_2O using a pipette. After about 5 minutes, the upper slide was carefully removed, and the agarose pad was divided into four equal parts with a scalpel and used for microscopy. (Microscope: Leica DRME; Light source: Leica EL6000)

7.8 Membrane fractionation

Membrane fractionation was performed to separate the outer (OM) and inner (IM) membranes of *E. coli* cells. To this end, 1,000 ODU units of a previously incubated culture were harvested (8,000 x *g*, 4°C, 15 min) and washed in 30 ml of 4°C cold 1x PBS (6,000 x *g*, 4°C, 15 min). For the crude membrane preparation, the cell pellet was resuspended in 4°C cold lysis buffer (buffer K supplemented with 1 mM EDTA, 1 mM $MgCl_2$, 10 µg/ml DNAse, 2 mg/ml lysozyme, and 1:100 protease inhibitor cocktail (Sigma-Aldrich (P8849)) lysed using a french press (3x 18,000 psi). Cell debris and unbroken cells were removed by two centrifugation steps (2,000 x *g*, 4°C, 15 min; 24,000 x *g*, 4°C, 20 min). The membrane fraction was separated from the cytosolic fraction by ultracentrifugation (45,000 rpm, 4°C, 45 min). Then the membrane fraction was resuspended in 1.5 ml of 1x buffer M, and 750 µl were loaded on top of a 30-53% (w/w) sucrose gradient in SW41 centrifugation tubes. Sucrose density centrifugation was carried out in a Beckmann SW41 rotor using slow acceleration and deceleration (41,000 rpm, 4°C, 14 h). The gradient was then fractionated into 12 equal fractions by piston fractionation of a gradient station and stored at 4°C until SDS-PAGE analysis. (Gradient station: BioComp-Gradient/Fractionation Combo)

7.9 Aggregation protocol

To purify cytoplasmic protein aggregates, a 20 ml *E. coli* Lemo21(DE3) culture in TB medium expressing either *tri-gfp* (+250 µM Rha, 15 h), *tba-gfp* (+100 µM Rha, 12 h), *yedZ-gfp* (+50 µM Rha, 12 h) or *gfp* (+0 µM Rha, 12 h) was used. After incubation, the cells were harvested (7,500 x g, 4°C, 15 min), resuspended in 200 µl lysis buffer (buffer A2 supplemented with 10 µg/ml DNase, 1 mg/ml lysozyme, and 1:100 protease inhibitor cocktail (Sigma-Aldrich (P8849))) and incubated for 25 min at 4°C. Then 1 mM $MgCl_2$ was added, and the cells were incubated for 10 min at 4°C. Next, 1 ml buffer 2 was added, and the cells were lysed using a bead mill (2 min, continuous mode). The glass beads were removed by centrifugation (1,000 x *g*, 4°C, 2 min). Cell debris and unbroken cells were removed by centrifugation (2,000 x *g*, 4°C, 15 min). The supernatant was then centrifuged again (20,8000 x *g*, 4°C, 20 min) to

precipitate the outer membrane and aggregates. The resulting pellet was resuspended in 1 ml buffer B2 and sonicated (Branson Sonifier 250) for 5 s (output control "4", constant duty cycle, level 2.5). The suspension was then centrifuged (20,8000 x *g*, 4°C, 20 min), the pellet resuspended in 0.8 ml buffer B2 and sonicated again under the same conditions as before. 200 µl of 10% (v/v) NP-40 was added and centrifuged (20,8000 x *g*, 4°C, 20 min). This washing step was repeated twice. The resulting pellet was then washed again in 1 ml buffer B2 (20,8000 x *g*, 4°C, 20 min) and sonicated. The pellet then contained purified aggregates, which were analyzed by SDS-PAGE and immunodetection. 7 ODUs were loaded per condition.

7.10 Protein purification

7.10.1 **Recombinant protein production**

Recombinant protein production was performed in *E. coli* Lemo21(DE3), *E. coli* Mutant56(DE3), *S. lividans* T7, or *A. balhimycina*. Overexpression in *E. coli* strains was performed using a pET28a base vector, in *S. lividans* T7 a pGM202T7 base vector, and chromosomal integration in *A. balhimycina* was done using a pRM4 base vector. The standard growth conditions are described in Chapter 7.2. If different conditions were used, this is indicated in the context of the respective experiment. Small-scale expression tests in *E. coli* Lemo21(DE3) and *E. coli* Mutant56(DE3) were carried out in 12 ml culture volumes in 50 ml Falcon tubes. Large-scale expression was carried out in 1 L culture volume in 2.5 L plastic baffled flasks. For all expression and purification approaches, freshly transformed *E. coli* cells, not older than one week, were used. An overnight culture in LB medium was used to inoculate the expression culture to a starting OD_{600} of 0.05 in TB or LB medium with the respective antibiotics or additives. Induction with 0.4 mM IPTG was carried out at the beginning of the exponential phase at approximately OD_{600}=0.4. Prior to induction, cultures were incubated at 4°C for at least 30 min. After induction, the cultures were incubated at the respective expression temperature (18°C, 25°C, 30°C) and time. These details are specified in the results together with every experiment. *S. lividans T7* and *A. balhimycina* expression cultures were cultivated as described in Chapter 7.2. 5 ml of a preculture was used to inoculate 100 ml of expression culture. Induction with thiostrepton (6.25, 12.5, or 25 mM) in *S. lividans* T7 was performed at the time of inoculation.

7.10.2 **Protein purification**

After expression, the cells were harvested (8,000 x *g*, 4°C, 15 min), resuspended in 4°C cold 1x PBS buffer, washed (8,000 x *g*, 4°C, 15 min), and the crude membranes were prepared as described in Chapter 7.5.3 with minimal adjustments as described below. The cells were resuspended in lysis buffer (1x PBS supplemented with 1 mM EDTA, 10 µg/ml DNAse, 2 mg/ml lysozyme, and 1:100 protease inhibitor cocktail (Sigma-Aldrich (P8849))) and incubated for 30 min at 4°C. Then the cells were lysed by a french press (3x 18,000 psi) or a cell homogenizer (I&L Biosystems) (2x 40,000 psi). After lysis, 1 mM $MgCl_2$ was added. The lysate was centrifuged twice (2x 20,000-24,000 x *g*, 4°C, 15 min) to remove cell debris and unbroken cells.

The supernatant was then used for ultracentrifugation (45,000 rpm, 4°C, 45 min) to separate the crude membrane fraction from the cytosolic fraction. The crude membrane fraction was resuspended in buffer A, and the membranes were solubilized using detergents as described in Chapter 7.5.4. The soluble fraction was used for further purification.
The purification of proteins with a C-terminal GFP-6xHis tag, 6xHis tag, or N-terminal 6xHis-SUMO tag was performed using an ÄKTA UPC-900 chromatography system (Cytiva) or ÄKTA pure 25 chromatography system (v.2.1.0.1) (Cytiva). Programming and analysis were performed using the corresponding Unicorn software (v5.31 and v7.6). Affinity purification was performed using HisTrap™ HP 1 ml or HisTrap™ HP 5 ml (Cytiva) columns, according to the manufacturer's protocol. Purification of proteins with a C-terminal 3xFLAG tag was carried out in batch mode using Anti-FLAG M2-Affinity gel, according to the manufacturer's protocol. Size exclusion chromatography (SEC) was performed using either a Superdex 200 Increase 10/300 GL or Superose 6 Increase 3.2/300 column, according to the manufacturer's protocol. Concentration of proteins was performed using Amicon Ultra Centrifugal filters.

7.11 Co-Immunoprecipitation of Tba-3xFLAG

Co-Immunoprecipitation was carried out in *A. balhimycina* Δ*tba*, using Tba-3xFLAG, Tba^{E545Q}-3xFLAG, or Tba as bait proteins. The precultures were incubated for 2 days in 20 ml TSB medium supplemented with 50 µg/ml apramycin. The main culture was incubated for 3 days under balhimycin producing conditions in R5 medium supplemented with 50 µg/ml apramycin. The experiment was performed in triplicates. Five main cultures with 100 ml culture volume were inoculated from one preculture for each condition and replicate. The cells were harvested by centrifugation (5,000 rpm, 4°C, 10 min), and the pellets of the same conditions and replicates were pooled and stored at -20°C for one week. The cell pellets were then thoroughly thawed at 4°C and washed using 4°C cold 1x PBS (4,600 x *g*, 4°C, 10 min) and resuspended in lysis buffer (buffer K supplemented with 1 mM EDTA, 10 µg/ml DNAse, 2 mg/ml lysozyme, and 1:100 protease inhibitor cocktail (Sigma-Aldrich (P8849))). The cells were disrupted using a two-step lysis. First, the cells were lysed by sonication (Branson Sonifier 250) (output control "4", 35% duty cycle 2x 30 sec/10 sec pause), followed by lysis using a cell homogenizer (I&L Biosystems) (2x 40,000 psi). After lysis, 1 mM $MgCl_2$ was added. Thereafter, the cells were cleared from the cell debris and unbroken cells by two centrifugation steps (1: 10,000 x *g*, 4°C, 3 min; 2: 10,000 x *g*, 4°C, 10 min).
Thereafter, the crude membrane fraction was separated from the cytosolic fraction by ultracentrifugation (45,000 rpm, 4°C, 45 min). The membrane pellet was resuspended in buffer A, and the protein concentration was determined using the colorimetric "Pierce™ BCA Protein Assay Kits" (Thermo Fisher Scientific) according to the manufacturer's protocol. After that the protein concentration of every sample was adjusted to 4.6 mg/ml and used for solubilization with 1% (w/v) LMNG as described in Chapter 7.5.4. The solubilized membrane was then used for co-immunoprecipitation using Anti-FLAG M2-Affinity gel. The affinity gel was equilibrated with buffer A supplemented with 0.1% (w/v) LMNG, and 3.3 µl of the packed affinity gel was used per 1 mg of membranes. Binding was performed for 3 h at 4°C and overhead rotation. Thereafter, the matrix was washed three times with buffer A supplemented with 0.1% (w/v)

LMNG for 15 min. Afterwards, the bound proteins were eluted from the affinity gel by two elution steps with 150 ng/µl 3xFLAG peptide in the 1x packed bead volume for 45 min and overnight by overhead rotation. Between the washing and elution steps, the affinity gel was centrifuged at 300 x *g* and 4°C for 2 min to remove the supernatant. Both elution fractions were pooled and concentrated using an Amicon Ultra Centrifugal Filter Unit with a cutoff of 10 kDa until a volume of 150 µl was reached. Thereafter, the elution fraction was mixed with 4x SDS loading buffer, and 30 µl were loaded to an SDS-PAGE gel and run until the loading front reached approximately 1 cm of the gel. The proteins were stained using a Coomassie staining solution. The bands were then cut out of the gel and stored in 5% (v/v) acetic acid until further use. The detection of proteins using mass spectrometry and data processing was performed as described in Chapter 4.2 (Publication 1).

7.12 Tables

Table 1 | Growth media and buffers used in this study.

Name	Composition
Media used for *E. coli*	
Lysogeny broth (LB) modified from 246	0.5% (w/v) NaCl, 1% (w/v) tryptone, 0.5% (w/v) yeast extract;
Terrific broth (TB) [192]	1.2% (w/v) tryptone, 2.4% (w/v) yeast extract, 0.5% (w/v) glycerol, (pH 7.2); add after autoclaving: 17 mM KH_2PO_4, 72 mM K_2HPO_4
Super optimal broth (SOB) modified from 247	2% (w/v) tryptone, 0.5% (w/v) yeast extract, 8.56 mM NaCl, 2.5 mM KCl, (pH 6.8-7); add after autoclaving: 10 mM $MgCl_2$, 10 mM $MgSO_4$ (pH 6.8-7.0)
SOB with catabolic repressor (SOC) modified from 247	SOB + 20 mM glucose, (pH 6.8-7.0)
Stock medium	2% (w/v) peptone, 10% (w/v) glycerol
Media used for *A. balhimycina*, *A. japonicum*, or *S. lividans*	
Tryptic soy broth (TSB)	30 g/L TSB powder
R5 medium [248]	103 g/L sucrose, 10 g/L glucose, 0.25 g/L K_2SO_4, 10.12 g/L $MgCl_2{\cdot}6H_2O$, 0.1 g/L casamino acids, 5 g/L yeast extract, 5.73 g/L TES, 2 ml trace elements solution (R5), (pH 7.2); add after autoclaving: 0.0772% (w/v) $CaCl_2$, 0.0054% KH_2PO_4, 0.3% L-Proline
Trace elements solution (for R5 medium) [248]	0.2 g/L $FeCl_3{\cdot}6H_2O$, 0.01 g/L $Na_2B_4O_7{\cdot}10H_2O$, 0.01 g/L $(NH_4)_6MoO_{24}{\cdot}4H_2O$, 0.01 g/L $CuCl_2{\cdot}2H_2O$, 0.01 g/L $MnCl_2{\cdot}4H_2O$, 0.04 g $ZnCl_2$
S27M medium [242]	5 g/L peptone, 3 g/L yeast extract, 73 g/L mannitol
TSB-D	20 g/L peptone, 5 g/L NaCl, 3.3 g/L $K_2HPO_4{\cdot}3H_2O$, 2.5 g/L glucose
Nutrient broth (NB) (soft agar)	16 g/L nutrient broth powder, 0.5% (w/v) agar; storage at 60°C
R2L soft agar medium [249]	0.1 g/L casamino acids, 10 g/L glucose, 5 g/L yeast extract, 0.25 g/L K_2SO_4, 73.2 g/L mannitol, 18 g/L $MgCl_2{\cdot}6H_2O$, 7 g/L agarose; storage at 60°C; add after autoclaving: 25 mM TES (pH 7.2), 0.3% $CaCl_2{\cdot}2H_2O$
2xYT medium	16 g/L tryptone, 10g/L yeast extract, 5 g/L NaCl
Mannitol soya flour (MS) medium (Cullum) [250]	10 g/L soy flour (low fat), 10 g/L soy flour (full fat), 20 g/L mannitol, 16 g/L agar, (+2 g/L $MgCl_2$ for conjugation)
MM1 medium [251]	7g/L K_2HPO_4, KH_2PO_4 3g/L, 0.5 g/L Na_3-citrate$\cdot 3H_2O$, 0.1 g/L $MgSO_4{\cdot}3H_2O$, 0.1 g/L $(NH_4)_2SO_4$, 2 g/L glucose; (pH 7.0)
Buffers	
TE10.1 buffer	10 mM Tris/HCl (pH 8.0), 1 mM EDTA
TES buffer	0.25 M TES (pH 7.2)
6x DNA loading buffer	30% (v/v) glycerol, 0.05% (w/v) bromophenol blue; (pH 8.8)
4x solubilization buffer (SB)	250 mM Tris/HCl, 20% (v/v) glycerol, 8% (w/v) SDS, 0.05% (w/v) bromophenol blue; add prior to use: 20% (v/v) β-mercaptoethanol; (pH 6.8)
10x PBS	1.37 M NaCl, 26.8 mM KCl, 80.9 mM $Na_2HPO_4{\cdot}2x\ H_2O$, 17.6 mM KH_2PO_4, (pH 6.8, will be pH 7.4 in 1x PBS)
10x SDS running buffer modified from 252	30 g/L tris base, 144.13 g/L glycine, 10 g/L SDS,
10x transfer buffer	30 g/L tris base, 144.13 g/L glycine, 2.5 g/L SDS, add to 1x dilution: 10% (v/v) ethanol
10x TBS	84 g/L NaCl, 30 g/L tris base (pH 8.0)
TBS-T	1x TBS + 0.05% (v/v) Tween20
50x TAE buffer	2 M tris base, 1 M ml glacial acetic acid, 100 mM EDTA

Buffer K	50 mM TEA, 250 mM sucrose, 1 mM EDTA, (pH 7.5)
2x Buffer M	100 mM TEA, 2 mM EDTA
Buffer A	20 mM Hepes-NaOH (pH 7.4), 150 mM NaCl; if required add freshly: 0.01% (w/v) of respective detergent
Buffer A2	10 mM potassium phosphate buffer (pH 6.5), 1 mM EDTA, 20% (w/v) sucrose
Buffer B2	10 mM potassium phosphate buffer (pH 6.5), 1 mM EDTA,
10x Buffer W	1 M Tris/HCl, 1.5 mM NaCl, 10 mM EDTA, (pH 8.0)
5x ISO mix	500 mM Tris/HCl (pH 7.5), 50 mM $MgCl_2$, 1 mM dNTP mix, 50 mM DTT, 25% (w/v) PEG 8000, 5 mM NAD; stored at -20°C
Gibson master mix	1.33x IOS mix, 5.34 U/ml T5 exonuclease, 33.34 U/ml Phusion DNA polymerase, 5340 U/ml Taq DNA ligase
10x Anode buffer [253]	500 mM Bis-Tris/HCl, (pH 7.0); storage at 4°C
10x Cathode buffer I [253]	500 mM tricine, 150 mM Bis-Tris, 0.2% (w/v) Serva Blue G; storage at 4°C
10x Cathode buffer II [253]	500 mM tricine, 150 mM Bis-Tris; storage at 4°C
10x BlueNative (BN) loading buffer [253]	250 mM aminocaproic acid, 25% glycerol, 5% (w/v) Serva Blue G
Coomassie staining solution	0.02% (w/v) CBB G250 (Serva Blue G), 5% (w/v) $Al_2(SO_4)_3 \cdot 16H_2O$, 10% (v/v) ethanol, 2% (v/v) orthophosphoric acid
Coomassie destaining solution	10% (v/v) ethanol, 2% (v/v) orthophosphoric acid

Table 2 | Antibiotics and media supplements with corresponding solvent and final concentration used in this study.

Antibiotic	Final concentration	Solvent
Kanamycin (Kan)	50 µg/ml	H_2O
Chloramphenicol (Cm)	50 µg/ml	70% (v/v) Ethanol
Apramycin (Apr)	100 µg/ml (*E. coli*); 50 µg/ml (*A. balhimycina*)	H_2O
Thiostrepton (Tsr)	50 µg/ml	DMSO
Erythromycin (Ery)	50 µg/ml	75% (v/v) Ethanol
Carbenicillin (Cb)	100 µg/ml	H_2O
Nalidixic acid (Nal)	25 µg/ml	200 mM NaOH
Isopropyl β-d-1-thio-galactopyranoside (IPTG)	0.4 mM	H_2O
L-Rhamnose	50 µM - 1000 µM	H_2O

Table 3 | Detergents used for membrane solubilization in this study.

Abbreviation	Name	Class	CMC (H_2O)
DDM	n-Dodecyl-β-D-Maltopyranoside	Non-ionic	0.17 mM (0.0087%)
LMNG	Lauryl Maltose Neopentyl Glycol	Non-ionic	0.01 mM (0.001%)
DM	n-Decyl-β-D-Maltopyranoside	Non-ionic	1.8 mM (0.087%)
DMNG	Decyl Maltose Neopentyl Glycol	Non-ionic	0.036 mM (0.0034%)
CYMAL-4	4-Cyclohexyl-1-Butyl-β-D-Maltoside	Non-ionic	7.6 mM (0.37%)
CYMAL-6	6-Cyclohexyl-1-Hexyl-β-D-Maltoside	Non-ionic	0.56 mM (0.028%)
GDN	glyco-diosgenin	Non-ionic	18 µM (0.0021%)
UDM	n-Undecyl-β-D-Maltoside	Non-ionic	0.59 mM (0.029%)
OG	n-Octyl-β-D-Glucopyranoside	Non-ionic	18-20 mM (0.53%)
CHAPS	3-[(3-Cholamidopropyl)dimethylammonio]-1-propanesulfonate	Zwitterionic	8 mM (0.49%)
FC-12	n-Dodecylphosphocholine	Zwitterionic	1.5 mM (0.047%)
LDAO	n-Dodecyl-N,N-Dimethylamine-N-Oxide	Zwitterionic	1-2 mM (0.023%)

Table 4 | Antibodies used in this study.

Antibody	Origin	Clonality	Dilution	Order
anti-His	mouse	monoclonal	1:1,000	primary
anti-FLAG M2	mouse	monoclonal	1:10,000	primary
anti-GFP	rabbit	polyclonal	1:1,000	primary
anti-BirA (TID)	rabbit	polyclonal	1:10.000	primary
anti-mouse DyLight 800	goat	polyclonal	1:10,000	secondary
anti-mouse DyLight 680	goat	polyclonal	1:10,000	secondary
anti-rabbit DyLight 800	goat	polyclonal	1:10,000	secondary
anti-rabbit DyLight 680	goat	polyclonal	1:10,000	secondary

Table 5 | Bacterial strains used and constructed in this study.
Abbreviations: *D.B.: in collaboration with Dardan Beqaj.

Name	Description/Genotype	Reference
E. coli NEB5α	Strain for plasmid construction: *fhuA2Δ(argF-lacZ)U169 phoA glnV44 Φ80Δ(lacZ)M15 gyrA96 recA1 relA1 endA1 thi-1 hsdR17*	New England Biolabs (NEB)
E. coli BL21(DE3)	Strain for T7 based expression: *fhuA2 [lon] ompT gal (λ DE3) [dcm] ΔhsdSλ DE3 = λ sBamHIo ΔEcoRI-B int::(lacI::PlacUV5::T7 gene1) i21 Δnin5*	Lab stock
E. coli Lemo21(DE3)	Strain for tunable T7 based expression: *fhuA2 [lon] ompT gal (λ DE3) [dcm] ΔhsdS/* pLemo (Cam^R) *λ DE3 = λ sBamHIo ΔEcoRI-B int::(lacI::PlacUV5::T7 gene1) i21 Δnin5* pLemo = pACYC184-*PrhaBAD-lysY*	[72]
E. coli Mutant56(DE3)	Strain for T7 based expression: *E. coli* BL21(DE3) *t7rnap$_{mt56}$ fryA'*	[74]
E. coli JM110	Methylation deficient strain: *F'[traD36 proA+ proB+ lacIq Δ(lacZ)M15] dam dcm supE44*	[254]

	hsdR17 thi leu thr rpsL lacY galK galT ara tonA tsx Δ(lac-proAB) lambda-	
E. coli ET12567	Methylation deficient strain: *F- dam-13:Tn9 dcm-6 hsdM hsdR zjj-202::Tn10 recF143 galK2 galT22 ara-14 lacY1 xyl-5 leuB6 thi-1 tonA31 rpsL136 hisG4 tsx-78 mtl-1 gln*	[255]
E. coli S17-1	Mobilizing strain for conjugation: Tri^{R}, *recA pro hsdR RP4-2-Tc:Mu-Km::*Tn7 integrated into the chromosome	[256]
A. balhimycina DSM 44591	Balhimycin producing wild-type; All strains constructed in this study are derived from this strain.	[136,137]
A. balhimycina Δ*tba*	*tba* deletion mutant	Dardan Beqaj
A. balhimycina Δ*tba* [+*tba*]	Apr^{R}, *tba* deletion mutant, ΦC31attB(pRM4-*tba*)	This study*[D.B.]
A. balhimycina Δ*tba* [+*tba-3xFLAG*]	Apr^{R}, *tba* deletion mutant, ΦC31attB(pRM4-*tba-3xFLAG*)	This study*[D.B.]
A. balhimycina Δ*tba* [+*tri*]	Apr^{R}, *tba* deletion mutant, ΦC31attB(pRM4-*tri*)	This study*[D.B.]
A. balhimycina Δ*tba* [+*tri-3xFLAG*]	Apr^{R}, *tba* deletion mutant, ΦC31attB(pRM4-*tri-3xFLAG*)	This study*[D.B.]
A. balhimycina Δ*tba* [+*tva*]	Apr^{R}, *tba* deletion mutant, ΦC31attB(pRM4-*tva*)	This study*[D.B.]
A. balhimycina Δ*tba* [+*tva*-3x*FLAG*]	Apr^{R}, *tba* deletion mutant, ΦC31attB(pRM4-*tva*-3x*FLAG*)	This study*[D.B.]
A. balhimycina Δ*tba* [+*sav1866*]	Apr^{R}, *tba* deletion mutant, ΦC31attB(pRM4-*sav1866*)	This study*[D.B.]
A. balhimycina Δ*tba* [+*sav1866*-3x*FLAG*]	Apr^{R}, *tba* deletion mutant, ΦC31attB(pRM4-*sav1866*-3x*FLAG*)	This study*[D.B.]
A. balhimycina Δ*tba* [+*tba*^{E545Q}-3x*FLAG*]	Apr^{R}, *tba* deletion mutant, ΦC31attB(pRM4-*tbaE545Q*-3x*FLAG*)	This study*[D.B.]
A. balhimycina Δ*tba* [+*tba*^{R310A}-3x*FLAG*]	Apr^{R}, *tba* deletion mutant, ΦC31attB(pRM4-*tbaR310A*-3x*FLAG*)	This study*[D.B.]
A. balhimycina Δ*tba* [+*tba*^{Q309G}-3x*FLAG*]	Apr^{R}, *tba* deletion mutant, ΦC31attB(pRM4-*tbaQ309G*-3x*FLAG*)	This study*[D.B.]
A. balhimycina Δ*tba* [+*tba*^{T316A}-3x*FLAG*]	Apr^{R}, *tba* deletion mutant, ΦC31attB(pRM4-*tbaT316A*-3x*FLAG*)	This study*[D.B.]
A. balhimycina Δ*tba* [+*tba-TID*]	Apr^{R}, *tba* deletion mutant, ΦC31attB(pRM4-*tba-TID*)	This study*[D.B.]
A. balhimycina [+*TID*]	Apr^{R}, *tba* deletion mutant, ΦC31attB(pRM4-*TID*)	This study*[D.B.]
A. balhimycina Δ*bhaA*	*bhaA* deletion mutant	[165]
A. balhimycina Δ*bgtfB*	*bgtfB* deletion mutant	Dardan Beqaj
A. balhimycina Δ*bgtfB*Δ*bhaA*	*bhaA* and *bgtfB* deletion mutant	Dardan Beqaj
B. subtilis DSM10	Indicator strain for bioactivity assay	[257]
S. lividans 10T7	Apr^{R}, Tsr^{R}, ΦC31attB(pFX583-tipAT7*)	[203]

Table 6 | Plasmids used and constructed in this study.
Abbreviations: B: Backbone; I1: Insert 1; I2: Insert 2; Kan^R: Kanamycin resistance; Amp^R: Ampicillin resistance; Apr^R: Apramycin resistance; Tsr^R: Thiostrepton resistance.

Plasmid	Cloning	Description	Resistance	Reference
pGFPe		Bacterial expression vector; IPTG inducible *T7* promoter (P_{T7}); C-terminal TEV-GFP-ag	Kan^R	Lab stock
pET28a		Bacterial expression vector; IPTG inducible *T7* promoter (P_{T7})	Kan^R	Lab stock
pSUMO		Bacterial expression vector; IPTG inducible *T7* promoter (P_{T7}); N-terminal 6xHis-SUMO-tag	Kan^R	Provided by Marcus Hartman
pRM4		ΦC31 integration vector; constitutive *ermE** promoter (P_{ermE*})	Apr^R	[168]
pGM202T7 (Addgene #69993)		Bacterial expression vector; IPTG inducible *T7* promoter (P_{T7}); N/C-terminal 6xHis-tag	Kan^R/Tsr^R	[258]
pGM1190 (Addgene #69994)		Bacterial expression vector; Thiostrepton inducible *TipA* promoter (P_{tipA})	Apr^R/Tsr^R	[258]
pET21a-TurboID-His6 (Addgene #107177)		Bacterial expression vector; IPTG inducible *T7* promoter (P_{T7}); TurboID-6xHis	Amp^R	[259]
pMIB7121	B: P91/P108 I1: P35/P109	pGFPe-tva-GFP (Encoding the ABC transporter encoded in vancomycin BGC of *A. keratiniphila HCCB10007)*	Kan^R	This study
pMIB7122		pGFPe-tri-GFP (Encoding the ABC transporter encoded in ristomycin BGC of *A. japonicum)*	Kan^R	Lab stock (Mirjam Forberger)
pMIB7123		pGFPe-tba-GFP (Encoding the ABC transporter encoded in balhimycin BGC of *A. balhimycina)*	Kan^R	Lab stock (Mirjam Forberger)
pMIB7124		pGFPe-amL-GFP (Encoding the ABC transporter encoded in ristomycin BGC of *A. lurida)*	Kan^R	Lab stock (Mirjam Forberger)
pMIB7125	B: P91/P108 I1: P33/P110	pGFPe-amAz-GFP (Encoding the ABC transporter encoded in type III BGC of *A. azuera)*	Kan^R	This study
pMIB7126		pGFPe-amD-GFP (Encoding the ABC transporter encoded in decaplanin BGC of *A. decaplanina)*	Kan^R	Lab stock (Mirjam Forberger)
pMIB7737	B: P89/P91 I1: P34/P106	pET28a-tba-TEV-8xHis	Kan^R	This study
pMIB7734	B: P88/P96 I1: P64/P30	pET28a-tba-TEV-2xStrepII	Kan^R	This study
pMIB7739	B: P102/P97 I1: P80/P31	pET28a-tba-TEV-3xFLAG	Kan^R	This study
pMIB7736	B: P89/P32 I1: P82/P79	pET28a-tri-TEV-8xHis	Kan^R	This study
pMIB7731	B: P88/P98 I1: P81/P30	pET28a-tri-TEV-2xStrepII	Kan^R	This study
pMIB7738	B: P88/P97 I1: P80/P31	pET28a-tri-TEV-3xFLAG	Kan^R	This study
pMIB7745	B: P94/P95 I1: P58/P59	pSUMO-tba	Kan^R	This study
pMIB7746	B: P94/P95 I1: P60/P61	pSUMO-tri	Kan^R	This study
pMIB8111	B: P101/P105 I1: P56/P57	pSUMO-2xStrepII-SUMO-tri	Kan^R	This study

pMIB8113	B: P94/P93 I1: P52/P53	pSpot1-tba	Kan^R	This study
pMIB8112	B: P94/P93 I1: P54/P55	pSpot1-tri	Kan^R	This study
pMIB8466	B: XhoI/HindIII I1: P50/P51	pRSETb-6xHis-tba	Amp^R	This study
pRM4-tba		pRM4-tba	Apr^R	Dardan Beqaj
pMIB7732	B: P92/P96 I1: P38/P39	pRM4-tba-3xFLAG	Apr^R	This study
pMIB7749	B: NdeI/XbaI I1: P47/P46	pRM4-tri	Apr^R	This study
pMIB7750	B: NdeI/XbaI I1: P47/P3	pRM4-tri-3xFLAG	Apr^R	This study
pMIB8116	B: NdeI/XbaI I1: P40/P41	pRM4-tva	Apr^R	This study
pMIB8117	B: NdeI/XbaI I1: P40/P25 I2: P107/P39	pRM4-tva-3xFLAG	Apr^R	This study
pMIB8114	B: NdeI/XbaI I1: P43/P44	pRM4-sav1866	Apr^R	This study
pMIB8115	B: NdeI/XbaI I1: P43/P44 I2: P62/P39	pRM4-sav1866-3xFLAG	Apr^R	This study
pMIB8128	B: NdeI/XbaI I1: P104/P69 I2: P68/P39	pRM4-tba-E545Q-3xFLAG	Apr^R	This study
pMIB8462	B: NdeI/XbaI I1: P104/P75 I2: P74/P39	pRM4-tba-Q309G-3xFLAG	Apr^R	This study
pMIB8463	B: NdeI/XbaI I1: P104/P73 I2: P72/P39	pRM4-tba-R310A-3xFLAG	Apr^R	This study
pMIB8464	B: NdeI/XbaI I1: P104/P77 I2: P76/P39	pRM4-tba-T316A-3xFLAG	Apr^R	This study
pMIB8129	B: NdeI/XbaI I1: P104/P28 I2: P70/P42	pRM4-tba-TurboID	Apr^R	This study
pMIB8130	B: NdeI/XbaI I1: P103/P27 I2: P29/P42	pRM4-abc30-TurboID	Apr^R	This study
pMIB8461	B: NdeI/XbaI I1: P49/P42	pRM4-TurboID	Apr^R	This study
pMIB7740	B: P99/P100 I1: P37/P36	pGM202T7-tri-8xHis	Kan^R/Tsr^R	This study
pMIB7743	B: P99/P100 I1: P37/P22	pGM202T7-tri-2xStrepII	Kan^R/Tsr^R	This study
pMIB7742	B: P99/P100 I1: P37/P21	pGM202T7-tri-3xFLAG	Kan^R/Tsr^R	This study
pMIB8465	B: NdeI/BamHI I1: P63/P23	pGM202T7-tba-3xFLAG	Kan^R/Tsr^R	This study
pMIB8120	B: NdeI/XbaI I1: P45/P86 I2: P78/P39	pRM4-TMD-tba-NBD-tri-3xFLAG	Apr^R	This study
pMIB8123	B: NdeI/XbaI I1: P48/P71 I2: P87/P39	pRM4-TMD-tri-NBD-tba-3xFLAG	Apr^R	This study
pMIB8121	B: NdeI/XbaI I1: P45/P26 I2: P67/P39	pRM4-tba-Cex-3xFLAG	Apr^R	This study
pMIB8124	B: NdeI/XbaI I1: P48/P24 I2: P85/P39	pRM4-tri-Cex-3xFLAG	Apr^R	This study

pMIB8119	B: NdeI/XbaI I1: P45/P84 I2: P65/P39	pRM4-tba-Cex+triCex-3xFLAG	Apr^R	This study
pMIB8122	B: NdeI/XbaI I1: P48/P66 I2: P83/P39	pRM4-tri-Cex+tbaCex-3xFLAG	Apr^R	This study

Table 7 | DNA oligonucleotides used in this study.

ID	Name	Sequence (5' → 3')
DNA oligonucleotides for sequencing and colony PCR		
P1	pGFPs_seq_r	AAT CCG GAT ATA GTT CCT CC
P2	seq_ermE_prom_f	TT GTG GGC ACA ATC GTG CCG G
P3	seq_lacZa_r	ACG TTG TAA AAC GAC GGC CAG TGC
P4	seq_NysABC_intern_f	GGA ACC GGA CGA CGG TAT CG
P5	seq_pGM_r	CAC TCC GCT GAA ACT GTT GAA AG
P6	seq_pRM4_f	GAT GCT AGT CGC GGT TGA TCG
P7	seq_pRM4_int1_f	GTG ATC GAA GCG CGC TTC TCG ATG
P8	seq_pRM4_int2_f	CAG CGG TAA GAG TCC TTG ATC GAT TC
P9	seq_pRM4_int3_f	CGG ATT ACG TCG GGC TCG AAC TC
P10	seq_pRM4_int4_f	GCG CTC GAC TTC GCG CTG AAG
P11	seq_pRM4_r	CTG CGC AAC TGT TGG GAA GG
P12	seq_pRM4_RP4ori_f	CGC ACG ATA TAC AGG ATT TTG CCA AAG G
P13	seq_pSpot1_r	CCA AGG GGT TAT GCT AGT TAT TGC
P14	seq_tba_intern2_f	GAA GTG ACG CCG GAT GTC CTG C
P15	seq_tba_intern3_f	CGC TGG TCG CCA TCG CCA C
P16	seq_tri_intern1_f	CTG CTG ATG GCG GCC ACC AG
P17	seq_tri_intern2_f	GCA CCA TGA CGC ATC TGG TGT CG
P18	T7p	TAA TAC GAC TCA CTA TAG GGG AAT TG
P19	T7p-pGM	TTA ATA CGA CTC ACT ATA GGG AGA C
P20	tipAP	GAT CGG GGA TCT GGG CTG
DNA oligonucleotides used for molecular cloning		
P21	gib_ pGM1190_3XFLAG_r	CGA CAA AAC TTT AGA TCT GGG GAA TTC TCA TTT GTC ATC GTC ATC CTT GTA ATC GAT G
P22	gib_ pGM1190_StrepII_r	CGA CAA AAC TTT AGA TCT GGG GAA TTC TCA TTT TTC GAA CTG CGG GTG GCT C
P23	gib_3xFLAG_pGM202_r	GAT GAT GAT GGG ATC TCG AGC TCG GAT CCT CAT TTG TCA TCG TCA TCC TTG TA
P24	gib_3xFLAG_tri-C_r	CAC CGT CAT GGT CTT TGT AGT CTC TAG ATC CCG CGT TGT TCT CCG G
P25	gib_FLAG_AmOH_r	CAC CGT CAT GGT CTT TGT AGT CTC TAG ATC CTC CGA AGC CAA TGG GTT G
P26	gib_FLAG_tba-C_r	CAC CGT CAT GGT CTT TGT AGT CTC TAG ATC CGT CGT TGG CGG CCG GGT TG
P27	gib_GSTurboID_NysABC_r	GAG CGA TCA GCT TCA GAG GCA CAG TAT TGT CTT TGC TCC CGC CCA AAG CAC GGT TCC CGC

P28	gib_GSTurboID_Tba_r	GAG CGA TCA GCT TCA GAG GCA CAG TAT TGT CTT TGC TCC CTC CTC CGT AGC CCA TGT GTT GG
P29	gib_NysABC_GSTurboID_f	CCA AGA GCG GGA ACC GTG CTT TGG GCG GGA GCA AAG ACA ATA CTG TGC CTC TGA AGC
P30	gib_pET28_StrepII_r	TTC GGG CTT TGT TAG CAG CCG GAT CTC ATT TTT CGA ACT GCG GGT GGC TCC ACG ATC C
P31	gib_pET28a_3XFLAG_r	TTC GGG CTT TGT TAG CAG CCG GAT CTCA TTT GTC ATC GTC ATC CTT GTA ATC
P32	gib_pET28a-tri_r	TCT TGA GGA TGC CGC CGT CGA TGA G
P33	gib_pGFPe_AazABC_f	GTT TAA CTT TAA GAA GGA GAC TCG AGA TGG ACG TGG TGT TGA ACT TC
P34	gib_pGFPe_AbaABC_f	GTT TAA CTT TAA GAA GGA GAC TCG AGA TGG ACA TGG TGT TGC GTT TC
P35	gib_pGFPe_Ao1ABC_f	GTT TAA CTT TAA GAA GGA GAC TCG AGA TGG ACG TGG TTC TGC GCT TC
P36	gib_pGM1190_His_r	GAC AAA ACT TTA GAT CTG GGG AAT TCT CAG TGG TGG TGG TGG TGA TGA TG
P37	gib_pGM202T7_tri_f	GTT TAA CTT TAA GAA GGA GAT ATA CAT ATG GAA GTA ATG TTG CGC TTC GG
P38	gib_pRM4_3XFLAG_f	GAT CCA ACA CAT GGG CTA CGG AGG ATCT AGA GAC TAC AAA GAC CAT GAC
P39	gib_pRM4_3XFLAG_r	CTC GGG CTG CAG GTC GAC TCT AGA TCA TTT GTC ATC GTC ATC CTT GTA ATC
P40	gib_pRM4_AmOH_f	ATA AGC TAG CCA GGG GAG GAC CCA TAT GGA AGT GGT GTT GCG CTT C
P41	gib_pRM4_AmOH_r	CTC GGG CTG CAG GTC GAC TCT AGA TCA TCC TCC GAA GCC AAT GG
P42	gib_pRM4_His6_r	CAA GCT CGG GCT GCA GGT CGA CTC TAG ATC AGT GGT GGT GGT GGT GGT GCT C
P43	gib_pRM4_Sav1866_f	ATA AGC TAG CCA GGG GAG GAC CCA TAT GAT TAA ACG ATA TTT GCA ATT TGT TAA GCC
P44	gib_pRM4_Sav1866_r	CTC GGG CTG CAG GTC GAC TCT AGA TTA TAA GTT TTG AAT GCT ATA TAA ATG CTC GTA AG
P45	gib_pRM4_tba_f	GAT AAG CTA GCC AGG GGA GGA CCC ATA TGA TGG ACA TGG TGT TGC GTT TCG AGG GGG TG
P46	gib_pRM4_Tri_r	GCT CGG GCT GCA GGT CGA CTC TAG ATC ATC CTC CGT AGA CCA CGG T
P47	gib_pRM4_Tri2_f	ATA AGC TAG CCA GGG GAG GAC CCA TAT GGA AGT AAT GTT GCG CTT CGG
P48	gib_pRM4_tri2_f	ATA AGC TAG CCA GGG GAG GAC CCA TAT GGA AGT AAT GTT GCG CTT CGG
P49	gib_pRM4_TurboID_f	ATA AGC TAG CCA GGG GAG GAC CCA TAT GAA AGA CAA TAC TGT GCC TCT GAA G
P50	gib_pRSETb_Tba_f	GTA CGA CGA TGA CGA TAA GGA TCC GAG CGA CAT GGT GTT GCG TTT CGA GGG
P51	gib_pRSETb_Tba_r	CTT TCG GGC TTT GTT AGC AGC CGG ATC ATC CTC CGT AGC CCA TGT GTT GG
P52	gib_pSpot_tba_f	GCA GTC TCT CAC TGG AGC AGC GGA TCC GAC ATG GTG TTG CGT TTC GAG GG

P53	gib_pSpot_tba_r	CAT TAC TTA CTC GAG TGC GGC CGC AAG CTT TTA TCC TCC GTA GCC CAT GTG TTG G
P54	gib_pSpot_tri_f	GCA GTC TCT CAC TGG AGC AGC GGA TCC GAA GTA ATG TTG CGC TTC GGG GC
P55	gib_pSpot_tri_r	CAT TAC TTA CTC GAG TGC GGC CGC AAG CTT TTA TCC TCC GTA GAC CAC GGT GTC
P56	gib_pSUMO_StrepII_f	TTA AGA AGG AGA TAT ACA TAT GGG TTG GAG CCA CCC GCA GTT CGA GAA AGG TGG AGG T
P57	gib_pSUMO_StrepII_r	CTT GAT TGA CTT CTG AGT CCG AAC CTT TTT CGA ACT GCG GGT GGC TCC ACG ATC CAC CTC C
P58	gib_pSUMO_tba_f	ATT GAG GCT CAC AGA GAA CAG ATT GGT GGT GAC ATG GTG TTG CGT TTC GAG GGG
P59	gib_pSUMO_tba_r	GGT GCT CGA GTG CGG CCG CAA GCT TTT ATC CTC CGT AGC CCA TGT GTT GGA TC
P60	gib_pSUMO_tri_f	ATT GAG GCT CAC AGA GAA CAG ATT GGT GGT GAA GTA ATG TTG CGC TTC GGG GCG
P61	gib_pSUMO_tri_r	GGT GCT CGA GTG CGG CCG CAA GCT TTT ATC CTC CGT AGA CCA CGG TGT CC
P62	gib_Sav1866_FLAG_f	AGG TGC TTA CGA GCA TTT ATA TAG CAT TCA AAA CTT ATC TAG AGA CTA CAA AGA CCA TGA C
P63	gib_Tba_pGM202_f	TTT TGT TTA ACT TTA AGA AGG AGA TAT ACA TAT GGA CAT GGT GTT GCG TTT CGA G
P64	gib_Tba_TEV_f	GAT CCA ACA CAT GGG CTA CGG AGG AGT ACC TGG ATC CGA AAA CCT GTA CTT CCA G
P65	gib_tba626_tri627_f	CAG TTC GCC AAC CCG GCC GCC AAC GAC GCC AAA CCG GAG CCC GA
P66	gib_tba626_tri-C_r	GAG CTC GTC CTC GAT CTC CGG CTT GGG CGC GTT GTT CTC CGG CCT GGC G
P67	gib_tba-c_3xFLAG_f	GTT CGC CAA CCC GGC CGC CAA CGA CGG ATC TAG AGA CTA CAA AGA CCA TGA C
P68	gib_TbaE545Q_f	GAT CGT CGT CCT CGA CCA AGC CAC CGC CC
P69	gib_TbaE545Q_r	GGG CGG TGG CTT GGT CGA GGA CGA CGA TC
P70	gib_TbaGSTurboID_f	CGG TGA TCC AAC ACA TGG GCT ACG GAG GAG GGA GCA AAG ACA ATA CTG TGC CTC TGA AGC
P71	gib_TbaNBD_TriTMD_r	CGA TCG CGT CGG GGC GTT CCT GGA TCA GCG GCT TCA GGT CGA GCA G
P72	gib_TbaQ309G_f	CAT CGC CAC CCT GCT CGG GCG GCT GTT CG
P73	gib_TbaQ309G_r	CGA ACA GCC GCC CGA GCA GGG TGG CGA TG
P74	gib_TbaR310A_f	CAC CCT GCT CCA GGC GCT GTT CGG GCC G
P75	gib_TbaR310A_r	CGG CCC GAA CAG CGC CTG GAG CAG GGT G
P76	gib_TbaT316A_f	TGT TCG GGC CGA TCG CCC AGC TGT CCG GG
P77	gib_TbaT316A_r	CCC GGA CAG CTG GGC GAT CGG CCC GAA CA
P78	gib_TbaTMD_TriNBD_f	GGT CTT CGA GCT GCT CGA CCT CAA GCC ACT GAT CCA GGA ACG CCC G
P79	gib_Tev_His_r	TGG TGG TGA TGA TGA TGG GCC GCG CTG AAT TGA CCC TGG AAG TAC AGG TTT T
P80	gib_TEVGS_3XFLAG_f	GTA CTT CCA GGG TCA ATT CGG GAG CTCT AGA GAC TAC AAA GAC CAT GAC

P81	gib_Tri_TEV_f	GCT GGA CAC CGT GGT CTA CGG AGG A GTA CCT GGA TCC GAA AAC CTG TAC TTC CA
P82	gib_tri2_tri1_f	CTC ATC GAC GGC GGC ATC CTC AAG A ACG ACT TCG GTG TCG TGA TCC TGA TG
P83	gib_tri626_tba627_f	GCA GTT CGC CAG GCC GGA GAA CAA CGC GCC CAA GCC GGA GAT CGA G
P84	gib_tri626_tba-C_r	CGT CTT CCT CGG GCT CCG GTT TGG CGT CGT TGG CGG CCG GGT TGG C
P85	gib_tri-c_3xFLAG_f	GTT CGC CAG GCC GGA GAA CAA CGC GGG ATC TAG AGA CTA CAA AGA CCA TGA C
P86	gib_TriNBD_TbaTMD_r	CCT TCG CGT CCG GGC GTT CCT GGA TCA GTG GCT TGA GGT CGA GCA GCT CGA AGA C
P87	gib_TriTMD_TbaNBD_f	GAT CTT CGA GCT GCT CGA CCT GAA GCC GCT GAT CCA GGA ACG CCC C
P88	gib_uni_pET28_f	GAT CCG GCT GCT AAC AAA GCC
P89	gib_uni_pET28a-His_NG_f	GCG GCC CAT CAT CAT CAC CAC CAC
P90	gib_uni_pGFPe_NG_f	GTA CCT GGA TCC GAA AAC CTG
P91	gib_uni_pGFPe_r	CTC GAG TCT CCT TCT TAA AGT TAA AC
P92	gib_uni_pRM4_f	TCT AGA GTC GAC CTG CAG CCC GAG
P93	gib_uni_pSpot1_r	GGA TCC GCT GCT CCA GTG AGA G
P94	gib_uni_pSUMO_f	AAG CTT GCG GCC GCA CTC GAG
P95	gib_uni_pSUMO_r	ACC ACC AAT CTG TTC TCT GTG AGC C
P96	gib_uni_tba_r	TCC TCC GTA GCC CAT GTG TTG GAT C
P97	gib_uni_TEV_r	GAA TTG ACC CTG GAA GTA CAG GTT TTC
P98	gib_uni_tri_r	TCC TCC GTA GAC CAC GGT GTC C
P99	gib_uni2_pGM1190_f	GAA TTC CCC AGA TCT AAA GTT TTG TCG TCT TTC CAG ACG
P100	gib_uni2_pGM202T7_r	ATG TAT ATC TCC TTC TTA AAG TTA AAC AAA ATT ATC TAG AGG GAA ACC GTT GTG
P101	gib_uni2_pSUMO_f	GGT TCG GAC TCA GAA GTC AAT CAA G
P102	gib_unipET28_f	GAT CCG GCT GCT AAC AAA GCC
P103	gib_pRM4_NysABC_f	ATA AGC TAG CCA GGG GAG GAC CCA TAT GAC CAT TGG AGA CGA CCC GAG C
P104	gib2_pRM4_Tba_f	ATAAGCTAGCCAGGGGAGGACCCAT ATG GAC ATG GTG TTG CGT TTC GAG
P105	gib_uni2_pSUMO_r	ACC CAT ATG TAT ATC TCC TTC TTA AAG TTA AAC
P106	gib_pGFPe_AbaABC_r	GTA CAG GTT TTC GGA TCC AGG TAC TCC TCC GTA GCC CAT GTG TTG
P107	gib_AmOH_FLAG_f	GAT CCA ACC CAT TGG CTT CGG AGG ATC TAG AGA CTA CAA AGA CCA TGA C
P108	gib_uni_pGFPe_NG_f	GTA CCT GGA TCC GAA AAC CTG
P109	gib_pGFPe_Ao1ABC_r	GTA CAG GTT TTC GGA TCC AGG TAC TCC TCC GAA GCC GAT GGG
P110	gib_pGFPe_AazABC_r	GTA CAG GTT TTC GGA TCC AGG TAC CCC TCC ATG GCC CAT AAA G

List of Figures

Figures included in introduction, result Chapter 4.1, and result Chapter 4.3:

Figures included in result Chapter 4.2 (Publication 1):

List of Tables

Supplementary data

Table S1 | List of proteins obtained by co-immunoprecipitation of Tba-3xFLAG vs. Tba.
Proteins with a log2 fold change of ≥ |2| are listed.

Majority protein ID	Protein names	Gene Names	Log2 FC	p-value
Q799B1	Putative ABC transporter ATP-binding protein	tba	18.94	17.35
O87675	p450 monooxygenase	oxyC	9.05	3.88
O87676	Halogenase	bhaA	6.51	3.00
Q939Y4	Phenylglycine amino transferase	pgat	5.77	7.95
Q939Y9	Peptide synthetase	bpsC	5.70	3.95
Q939Y0	Putative hydroxyphenyl pyruvate dioxygenase	hmaS	5.06	3.76
O87677	Glycosyltransferase	bgtfA (+bgtfC)	4.74	2.65
Q939X4	Putative 3,5 epimerase	dvaD	4.59	4.33
Q939Y5	Putative N-methyl transferase	bmt	4.55	2.93
Q939X5	Putative C-3 amino transferase	dvaB	4.36	2.02
Q939Z0	Peptide synthetase	bpsB (+bpsA)	4.30	3.27
Q939Y7	Putative C-3 methyl transferase	dvaC	2.28	5.19
Q939Y1	Putative P450 monooxygenase	oxyD	2.04	1.32
A0A428WXV8	Flotillin family protein	Flotillin family protein	6.84	11.66
A0A428WTH7	Paraslipin	Paraslipin	6.82	2.81
A0A428VZF5	Phosphoenolpyruvate-protein phosphotransferase (EC 2.7.3.9) (Phosphotransferase system, enzyme I)	ptsP DMA12_41360	12.52	11.61
A0A428WJU7	Phosphate-specific transport system accessory protein PhoU	phoU DMA12_19055	11.99	4.75
A0A428W9N5	Succinate dehydrogenase, cytochrome b556 subunit	sdhC DMA12_28515	11.12	11.00
A0A428WQD5	NAD(P)/FAD-dependent oxidoreductase	DMA12_14720	10.53	4.57
A0A428W9K8	Succinate dehydrogenase iron-sulfur subunit (EC 1.3.5.1)	DMA12_28500	10.51	3.78
A0A428WA21	Succinate dehydrogenase	DMA12_28510	10.25	3.46
A0A428X4C1	Large ribosomal subunit protein bL12	rplL DMA12_02555	9.88	10.01
A0A428WC65	Transport permease protein	DMA12_26010	9.78	10.98
A0A428WND1	Phytoene desaturase	DMA12_15560	9.73	6.65
A0A428WXB4	carbonic anhydrase (EC 4.2.1.1)	DMA12_08485	9.56	6.34
A0A428X2E0	ATP synthase subunit a (ATP synthase F0 sector subunit a) (F-ATPase subunit 6)	atpB DMA12_03505	9.56	10.11
A0A428X4E3	Small ribosomal subunit protein uS4	rpsD DMA12_02845	9.27	10.28
A0A428WGN6	PH domain-containing protein	DMA12_21950	9.23	6.66
A0A428W997	Phage holin family protein	DMA12_29015	8.85	10.32
A0A428VYT0	K(+)-insensitive pyrophosphate-energized proton pump (EC 7.1.3.1) (Membrane-bound proton-translocating pyrophosphatase) (Pyrophosphate-energized inorganic pyrophosphatase) (H(+)-PPase)	hppA DMA12_42005	8.80	3.96
A0A428VUQ3	Cell division ATP-binding protein FtsE	ftsE DMA12_47870	8.74	6.30
A0A428VUP2	Cell division protein FtsX	DMA12_47865	8.56	9.52
A0A428X2U6	Protein translocase subunit SecA (EC 7.4.2.8)	secA DMA12_04315	8.25	6.26
A0A428W9C0	UDP-N-acetylglucosamine 2-epimerase	DMA12_29410	8.19	9.55
A0A428WDA0	Branched-chain amino acid ABC transporter permease	DMA12_25035	8.18	9.51
A0A428X2W2	ABC transporter permease	DMA12_04510	8.15	8.75
A0A428X4M6	Protein translocase subunit SecY	secY DMA12_02805	8.15	9.22
A0A428W0L9	Xylose transport system permease protein XylH	DMA12_39775	8.14	9.78
A0A428WAC2	Glycerol-3-phosphate dehydrogenase (EC 1.1.5.3)	DMA12_28885	8.02	4.37
A0A428WR66	Amino acid ABC transporter ATP-binding protein	DMA12_13735	7.95	9.42
A0A428X2Z9	ABC transporter permease	DMA12_04515	7.92	8.72
A0A428W6I7	ABC transporter permease	DMA12_32080	7.90	9.48
A0A428WIU6	DUF2771 domain-containing protein	DMA12_20375	7.90	6.11

A0A428VYB3	Cytochrome bc1 complex cytochrome b subunit (EC 7.1.1.8) (Cytochrome bc1 reductase complex subunit QcrB)	DMA12_42825	7.88	9.11
A0A428WD83	ABC transporter ATP-binding protein	DMA12_25045	7.66	6.11
A0A428X414	Demethylmenaquinone methyltransferase (EC 2.1.1.163)	menG DMA12_02115	7.62	8.88
A0A428W9B4	Uncharacterized protein	DMA12_29095	7.61	8.95
A0A428WTI9	Polyprenol monophosphomannose synthase	DMA12_11505	7.59	8.82
A0A428W307	Phosphatase PAP2 family protein	DMA12_36465	7.56	9.17
A0A428WXQ4	Amino acid ABC transporter permease	DMA12_07765	7.54	8.80
A0A428VVT3	Glycosyltransferase family 2 protein	DMA12_46390	7.54	9.34
A0A428VVF9	FHA domain-containing protein	DMA12_47015	7.53	6.00
A0A428W994	ABC transporter permease	DMA12_29360	7.46	8.92
A0A428WMA4	Nickel import system ATP-binding protein NikD (EC 7.2.2.11)	DMA12_16620	7.45	9.11
A0A428WMA1	ABC transporter ATP-binding protein	DMA12_16625	7.45	5.66
A0A428X4C5	Small ribosomal subunit protein uS3	rpsC DMA12_02730	7.42	3.61
A0A428W136	PspA/IM30 family protein	DMA12_39390	7.38	9.25
A0A428X5K6	Aldo/keto reductase	DMA12_00090	7.36	9.12
A0A428WXT3	GNAT family N-acetyltransferase	DMA12_07880	7.30	9.03
A0A428WD72	Branched-chain amino acid ABC transporter permease	DMA12_25040	7.22	4.06
A0A428W1H2	Cytochrome c oxidase subunit 1 (EC 7.1.1.9)	ctaD DMA12_38800	7.21	5.63
A0A428W873	Phosphoglycerate kinase (EC 2.7.2.3)	pgk DMA12_30020	7.17	8.03
A0A428W2F0	Glycerophosphoryl diester phosphodiesterase membrane domain-containing protein	DMA12_37510	7.16	8.42
A0A428W984	ABC transporter permease	DMA12_29365	7.11	8.39
A0A428WNC5	Rieske (2Fe-2S) protein	DMA12_15575	7.10	8.88
A0A428W6M3	Glycine/betaine ABC transporter substrate-binding protein	DMA12_32065	7.08	8.74
A0A428WXV9	Amino acid ABC transporter permease	DMA12_07770	7.08	5.87
A0A428X451	NADH-quinone oxidoreductase subunit C (EC 7.1.1.-) (NADH dehydrogenase I subunit C) (NDH-1 subunit C)	nuoC DMA12_02135	7.06	8.41
A0A428WR68	Secreted protein	DMA12_14000	7.06	8.77
A0A428W5G2	Ribonuclease E/G	DMA12_33530	7.04	5.77
A0A428W7M9	Protein-export membrane protein SecF	secF DMA12_31020	7.03	8.81
A0A428WMY6	ABC transporter ATP-binding protein	DMA12_16570	6.97	8.59
A0A428WAW9	Alpha-hydroxy-acid oxidizing protein	DMA12_27635	6.97	8.21
A0A428WCU5	D-3-phosphoglycerate dehydrogenase (EC 1.1.1.95)	DMA12_25680	6.95	3.82
A0A428WEC7	P-II family nitrogen regulator	DMA12_24085	6.94	2.90
A0A428W6W3	DUF4328 domain-containing protein	DMA12_31870	6.94	8.22
A0A428WBY2	Methyltransferase domain-containing protein	DMA12_26875	6.94	8.45
A0A428VU60	Membrane protein	DMA12_48585	6.87	8.53
A0A428X2P1	Transcription termination factor Rho (EC 3.6.4.-) (ATP-dependent helicase Rho)	rho DMA12_03575	6.82	8.83
A0A428VVS3	ABC transporter ATP-binding protein	DMA12_46385	6.78	8.27
A0A428W0L8	Sugar ABC transporter ATP-binding protein	DMA12_39770	6.77	5.98
A0A428X4F8	Uncharacterized protein	DMA12_02865	6.75	8.16
A0A428WNN0	NAD(P)/FAD-dependent oxidoreductase	DMA12_15540	6.75	8.09
A0A428X4F7	Type VII secretion protein EccC	DMA12_02905	6.74	5.62
A0A428X300	ABC transporter ATP-binding protein	DMA12_04500	6.74	7.16
A0A428WQD1	Short chain dehydrogenase	DMA12_14475	6.73	5.52
A0A428VYG5	Cytochrome bc1 complex Rieske iron-sulfur subunit (Cytochrome bc1 reductase complex subunit QcrA) (Rieske iron-sulfur protein)	DMA12_42820	6.71	6.61
A0A428W389	ATPase	DMA12_36170	6.66	8.24
A0A428VXI1	Acyl-CoA synthetase	DMA12_44015	6.66	5.43
A0A428WJV0	Phosphate transport system permease protein	pstC DMA12_19040	6.66	8.62
A0A428X2E2	Na+/galactose cotransporter	DMA12_03365	6.63	2.43
A0A428X2N8	ABC transporter ATP-binding protein	DMA12_04115	6.61	8.43
A0A428VSY5	TIGR04222 domain-containing membrane protein	DMA12_48935	6.58	8.08
A0A428W2S7	RNase adapter RapZ	DMA12_37300	6.57	8.34

A0A428X4S5	Type VII secretion protein EccE	eccE DMA12_02870	6.57	8.09
A0A428W6Z4	ABC transporter	DMA12_32075	6.54	4.70
A0A428VVP6	Decaprenyl-phosphate phosphoribosyltransferase	DMA12_46450	6.54	8.41
A0A428WR01	ABC transporter ATP-binding protein	DMA12_13435	6.53	3.88
A0A428WCF3	DUF4162 domain-containing protein	DMA12_26015	6.53	8.42
A0A428WMM5	ABC transporter permease	DMA12_16615	6.50	8.33
A0A428W9L1	Succinate dehydrogenase flavoprotein subunit (EC 1.3.5.1)	DMA12_28505	6.50	4.67
A0A428W7Q7	Adenosylhomocysteinase (EC 3.13.2.1) (S-adenosyl-L-homocysteine hydrolase) (AdoHcyase)	ahcY DMA12_31180	6.46	3.49
A0A428WIW9	histidine kinase (EC 2.7.13.3)	DMA12_20575	6.42	8.26
A0A428X4A8	Elongation factor G (EF-G)	fusA DMA12_02685	6.38	2.94
A0A428WM54	beta-mannosidase (EC 3.2.1.25)	DMA12_16630	6.37	3.10
A0A428VXG1	Amino acid ABC transporter permease	DMA12_44215	6.34	8.05
A0A428VZY9	ABC transporter permease	DMA12_40420	6.30	3.59
A0A428VW51	Extracellular solute-binding protein	DMA12_45915	6.30	7.95
A0A428W341	Proteasome subunit alpha (20S proteasome alpha subunit) (Proteasome core protein PrcA)	prcA DMA12_36455	6.29	7.67
A0A428WIN4	Citrate synthase	DMA12_20090	6.29	8.12
A0A428W9B7	ABC transporter ATP-binding protein	DMA12_29355	6.28	5.34
A0A428W003	Fructose-bisphosphate aldolase (FBP aldolase) (EC 4.1.2.13)	DMA12_40530	6.28	5.32
A0A428W9B3	Glycosyltransferase family 2 protein	DMA12_29390	6.26	5.60
A0A428X424	NADH-quinone oxidoreductase subunit B (EC 7.1.1.-) (NADH dehydrogenase I subunit B) (NDH-1 subunit B)	nuoB DMA12_02130	6.25	4.11
A0A428WND3	Catalase-peroxidase (CP) (EC 1.11.1.21) (Peroxidase/catalase)	katG DMA12_15640	6.24	2.78
A0A428VYD0	Membrane protein insertase YidC (Foldase YidC) (Membrane integrase YidC) (Membrane protein YidC)	DMA12_42925	6.22	7.27
A0A428VVF7	protein-serine/threonine phosphatase (EC 3.1.3.16)	DMA12_47010	6.17	5.32
A0A428VX74	Amino acid ABC transporter substrate-binding protein	DMA12_44220	6.16	4.27
A0A428WED3	Large ribosomal subunit protein bL19	rplS DMA12_24185	6.08	2.46
A0A428X441	NADH-quinone oxidoreductase subunit D (EC 7.1.1.-) (NADH dehydrogenase I subunit D) (NDH-1 subunit D)	nuoD DMA12_02140	6.07	7.54
A0A428X437	NADH-quinone oxidoreductase subunit L	DMA12_02180	5.99	7.55
A0A428X4C9	Small ribosomal subunit protein uS8	rpsH DMA12_02770	5.99	2.26
A0A428W2W9	Carbohydrate ABC transporter permease	DMA12_36945	5.98	8.08
A0A428W171	Non-ribosomal peptide synthetase	DMA12_39080	5.96	5.11
A0A428W5M7	ABC transporter ATP-binding protein	DMA12_33510	5.94	4.66
A0A428W0Z3	Amino acid permease	DMA12_39325	5.94	4.13
A0A428VVP1	Glycosyltransferase family 2 protein	DMA12_46420	5.91	6.02
A0A428WSM4	PTS mannose transporter subunit IIAB	DMA12_12420	5.86	7.17
A0A428W0W5	Small ribosomal subunit protein uS15	rpsO DMA12_39180	5.85	4.07
A0A428X4B2	Elongation factor Tu (EF-Tu)	tuf DMA12_02690	5.85	2.64
A0A428WQU6	ABC transporter	DMA12_13425	5.82	7.10
A0A428W2R9	Adenylyltransferase/sulfurtransferase MoeZ	DMA12_36755	5.81	7.46
A0A428VXE6	Amino acid ABC transporter ATP-binding protein	DMA12_44210	5.80	7.03
A0A428WEZ5	ATP-dependent zinc metalloprotease FtsH (EC 3.4.24.-)	ftsH DMA12_23910	5.77	4.64
A0A428WTG0	ABC transporter permease	DMA12_11200	5.72	7.67
A0A428X0L8	ATP-grasp domain-containing protein	DMA12_05540	5.71	4.01
A0A428VT18	Small ribosomal subunit protein bS6	rpsF DMA12_48750	5.69	4.29
A0A428VUV7	PadR family transcriptional regulator	DMA12_47880	5.66	2.52
A0A428VZA5	Protein translocase subunit SecA (EC 7.4.2.8)	secA DMA12_41520	5.64	5.18
A0A428WB17	ABC transporter permease	DMA12_27650	5.63	4.24
A0A428W526	Sugar ABC transporter substrate-binding protein	DMA12_33715	5.60	2.41
A0A428VRW7	Polyphosphate kinase (EC 2.7.4.1) (ATP-polyphosphate phosphotransferase) (Polyphosphoric acid kinase)	ppk DMA12_48985	5.60	5.27

A0A428W9B9	Glycosyl transferase	DMA12_29405	5.60	7.61
A0A428X4J7	DNA-directed RNA polymerase subunit beta (RNAP subunit beta) (EC 2.7.7.6) (RNA polymerase subunit beta) (Transcriptase subunit beta)	rpoB DMA12_02645	5.60	4.94
A0A428VT59	Sensor-like histidine kinase SenX3 (EC 2.7.13.3)	DMA12_48715	5.59	7.23
A0A428WR96	Chaperone protein DnaK (HSP70) (Heat shock 70 kDa protein) (Heat shock protein 70)	dnaK DMA12_13940	5.52	2.75
A0A428X2U1	Adenosylhomocysteinase (EC 3.13.2.1) (S-adenosyl-L-homocysteine hydrolase) (AdoHcyase)	ahcY DMA12_04400	5.48	7.07
A0A428W194	ABC transporter ATP-binding protein	DMA12_39100	5.43	4.29
A0A428VV83	DUF4191 domain-containing protein	DMA12_47260	5.43	4.04
A0A428VWD2	Cell division protein CrgA	crgA DMA12_45785	5.41	7.08
A0A428X450	NADH-quinone oxidoreductase subunit N (EC 7.1.1.-) (NADH dehydrogenase I subunit N) (NDH-1 subunit N)	nuoN DMA12_02190	5.41	4.33
A0A428X2Y3	YdbS-like PH domain-containing protein	DMA12_03695	5.39	7.36
A0A428W611	DUF5130 domain-containing protein	DMA12_32945	5.38	2.20
A0A428WVB7	ABC transporter substrate-binding protein	DMA12_09770	5.38	4.01
A0A428W6L5	ABC transporter permease	DMA12_32070	5.36	4.18
A0A428W7Y4	PH domain-containing protein	DMA12_31080	5.33	7.18
A0A428W296	CTP synthase (EC 6.3.4.2) (Cytidine 5'-triphosphate synthase) (Cytidine triphosphate synthetase) (CTP synthetase) (CTPS) (UTP--ammonia ligase)	pyrG DMA12_37730	5.33	4.46
A0A428WX22	PPOX class F420-dependent oxidoreductase	DMA12_08185	5.33	7.11
A0A428W2J7	MoxR family ATPase	DMA12_37495	5.29	4.18
A0A428WA50	Acyl-CoA synthetase	DMA12_28145	5.28	4.81
A0A428WAT2	Vitamin B12-dependent ribonucleotide reductase (EC 1.17.4.1)	DMA12_28420	5.28	6.64
A0A428WMB5	Sugar ABC transporter substrate-binding protein	DMA12_16675	5.26	2.35
A0A428WUE1	UvrABC system protein B (Protein UvrB) (Excinuclease ABC subunit B)	uvrB DMA12_10570	5.25	7.45
A0A428W6H1	DUF1707 domain-containing protein	DMA12_31970	5.24	2.49
A0A428W801	non-specific serine/threonine protein kinase (EC 2.7.11.1)	DMA12_30465	5.22	4.89
A0A428W2Q7	Integration host factor	DMA12_37190	5.21	6.78
A0A428WAQ2	Peroxiredoxin	DMA12_27620	5.19	2.43
A0A428W876	Transketolase (EC 2.2.1.1)	DMA12_30080	5.18	6.82
A0A428W0P2	Cation acetate symporter	DMA12_39440	5.18	4.19
A0A428W013	Nucleoside/nucleotide kinase family protein	DMA12_40435	5.17	4.42
A0A428VZY6	Sugar ABC transporter ATP-binding protein	DMA12_40425	5.15	2.81
A0A428W185	ABC transporter substrate-binding protein	DMA12_39150	5.13	3.89
A0A428WA25	Uncharacterized protein	DMA12_28010	5.10	4.79
A0A428WG47	Large ribosomal subunit protein bL25 (General stress protein CTC)	rplY ctc DMA12_22585	5.09	4.14
A0A428VYD7	asparagine synthase (glutamine-hydrolyzing) (EC 6.3.5.4)	asnB DMA12_42775	5.08	4.64
A0A428X4E9	DNA-directed RNA polymerase subunit alpha (RNAP subunit alpha) (EC 2.7.7.6) (RNA polymerase subunit alpha) (Transcriptase subunit alpha)	rpoA DMA12_02850	5.06	4.28
A0A428X4B4	Mce-associated membrane protein	DMA12_02610	5.05	6.71
A0A428W8A3	Glucose-6-phosphate 1-dehydrogenase (G6PD) (EC 1.1.1.49)	zwf DMA12_30065	5.05	3.92
A0A428X4W9	Geranylgeranyl reductase family protein	DMA12_02120	5.03	6.76
A0A428X4B5	Small ribosomal subunit protein uS7	rpsG DMA12_02680	5.03	2.45
A0A428W148	ABC transporter substrate-binding protein	DMA12_39090	5.03	2.18
A0A428VYP6	RDD family protein	DMA12_42345	5.01	4.29
A0A428WXN5	Amino acid ABC transporter ATP-binding protein	DMA12_07755	5.01	4.26
A0A428WXT6	Phosphatidylglycerol--prolipoprotein diacylglyceryl transferase (EC 2.5.1.145)	lgt DMA12_08035	4.98	4.14
A0A428X4G1	Small ribosomal subunit protein uS9	rpsI DMA12_02945	4.92	3.09
A0A428W3D7	AAA ATPase forming ring-shaped complexes (ARC)	arc DMA12_36395	4.85	2.43
A0A428W2J9	PTS N-acetylglucosamine transporter subunit IIBC	DMA12_37050	4.82	3.45
A0A428X426	NADH-quinone oxidoreductase (EC 7.1.1.-)	DMA12_02155	4.81	3.29

A0A428W7D8	Peptidylprolyl isomerase	DMA12_31070	4.79	2.71
A0A428X4D1	Polyprenyl synthetase family protein	DMA12_02240	4.79	4.73
A0A428VV58	Ricin B lectin domain-containing protein	DMA12_47325	4.76	4.53
A0A428WEE4	Small ribosomal subunit protein uS2	rpsB DMA12_24235	4.76	5.27
A0A428X4B8	DNA-directed RNA polymerase subunit beta' (RNAP subunit beta') (EC 2.7.7.6) (RNA polymerase subunit beta') (Transcriptase subunit beta')	rpoC DMA12_02650	4.75	4.38
A0A428WF14	ATP-dependent Clp protease ATP-binding subunit	DMA12_23810	4.72	2.66
A0A428WFL0	Nitrate ABC transporter substrate-binding protein	DMA12_23000	4.71	2.49
A0A428WJT6	Sulfurtransferase	DMA12_19005	4.69	2.25
A0A428W945	Crp/Fnr family transcriptional regulator	DMA12_29060	4.69	2.16
A0A428WM50	AGE family epimerase/isomerase	DMA12_16600	4.65	4.24
A0A428WLJ3	Sodium:solute symporter	DMA12_17265	4.62	2.79
A0A428VUD9	histidine kinase (EC 2.7.13.3)	DMA12_48270	4.59	4.46
A0A428WH98	histidine kinase (EC 2.7.13.3)	DMA12_21305	4.58	4.47
A0A428WVC0	ABC transporter substrate-binding protein	DMA12_09780	4.56	2.97
A0A428X443	Aminopeptidase N (EC 3.4.11.2)	DMA12_02075	4.56	3.49
A0A428WZV3	Chaperone protein HtpG (Heat shock protein HtpG) (High temperature protein G)	htpG DMA12_05610	4.53	4.34
A0A428VZF8	Succinate--CoA ligase [ADP-forming] subunit alpha (EC 6.2.1.5) (Succinyl-CoA synthetase subunit alpha) (SCS-alpha)	sucD DMA12_41105	4.52	2.25
A0A428VV69	Two-component sensor histidine kinase	DMA12_47050	4.51	4.69
A0A428VWA9	Peptidyl-prolyl cis-trans isomerase (PPIase) (EC 5.2.1.8)	DMA12_45770	4.50	4.29
A0A428X4G5	Small ribosomal subunit protein uS13	rpsM DMA12_02830	4.48	1.64
A0A428WYK2	M50 family peptidase	DMA12_06600	4.47	4.36
A0A428WU64	Ribonucleoside-diphosphate reductase (EC 1.17.4.1)	DMA12_10275	4.46	3.81
A0A428W7V5	DUF445 domain-containing protein	DMA12_30770	4.45	4.07
A0A428WD97	ABC transporter ATP-binding protein	DMA12_25050	4.43	4.88
A0A428W0J8	AcrB/AcrD/AcrF family protein	DMA12_39750	4.42	4.42
A0A428VWU6	DUF948 domain-containing protein	DMA12_44845	4.38	4.48
A0A428W028	Amino acid permease	DMA12_40605	4.36	4.27
A0A428WM61	alpha-galactosidase (EC 3.2.1.22)	DMA12_16660	4.35	2.12
A0A428W8C6	Peptidyl-prolyl cis-trans isomerase (EC 5.2.1.8)	DMA12_30100	4.34	4.51
A0A428WGV1	Glycosyltransferase family 2 protein	DMA12_22135	4.31	4.48
A0A428VX34	Gfo/Idh/MocA family oxidoreductase	DMA12_44365	4.29	4.37
A0A428X2I8	ATP synthase gamma chain (ATP synthase F1 sector gamma subunit) (F-ATPase gamma subunit)	atpG DMA12_03480	4.21	2.55
A0A428X316	ABC transporter permease	DMA12_04160	4.20	4.79
A0A428W7P7	Secreted protein	DMA12_30455	4.19	3.93
A0A428W0W2	Polyribonucleotide nucleotidyltransferase (EC 2.7.7.8) (Polynucleotide phosphorylase) (PNPase)	pnp DMA12_39185	4.19	2.65
A0A428W311	Proteasome subunit beta (EC 3.4.25.1) (20S proteasome beta subunit) (Proteasome core protein PrcB)	prcB DMA12_36450	4.18	2.27
A0A428WJW2	Phosphate ABC transporter ATP-binding protein	DMA12_19050	4.05	3.85
A0A428W543	LacI family transcriptional regulator	DMA12_33755	4.02	2.95
A0A428X4F1	Large ribosomal subunit protein uL23	rplW DMA12_02710	4.00	1.78
A0A428W2V0	NarK/NasA family nitrate transporter	DMA12_36735	3.96	4.58
A0A428WXP6	Fumarate reductase/succinate dehydrogenase flavoprotein subunit	DMA12_07810	3.89	2.44
A0A428WB97	YjbQ family protein	DMA12_27770	3.88	1.97
A0A428VQQ5	Serine/threonine protein kinase	DMA12_49235	3.84	4.26
A0A428WFR4	DUF11 domain-containing protein	DMA12_23425	3.84	4.75
A0A428W6D3	Mechanosensitive ion channel protein MscS	DMA12_32965	3.83	2.54
A0A428WG35	Peptidase M75 family protein	DMA12_22400	3.82	2.46
A0A428VVN6	DUF3558 domain-containing protein	DMA12_46400	3.80	1.89
A0A428W622	NAD-glutamate dehydrogenase	DMA12_32995	3.79	4.37
A0A428X484	Transcription termination/antitermination protein NusG	nusG DMA12_02525	3.73	4.16
A0A428VVC4	L,D-transpeptidase	DMA12_46825	3.71	2.11

A0A428WTD0	Malate dehydrogenase (EC 1.1.1.37)	mdh DMA12_11035	3.71	4.21
A0A428W8G9	Alpha-1,6-mannosyltransferase	DMA12_30150	3.63	4.52
A0A428WAT1	Pyruvate dehydrogenase E1 component (EC 1.2.4.1)	aceE DMA12_27630	3.60	1.75
A0A428VWV3	NAD(P)(+) transhydrogenase (Si-specific) (EC 1.6.1.1) (NAD(P)(+) transhydrogenase [B-specific])	DMA12_44775	3.58	4.43
A0A428VXI3	Amino acid ABC transporter substrate-binding protein	DMA12_44230	3.53	2.35
A0A428VYA0	Probable cytosol aminopeptidase (EC 3.4.11.1) (Leucine aminopeptidase) (LAP) (EC 3.4.11.10) (Leucyl aminopeptidase)	pepA DMA12_42700	3.50	1.61
A0A428X416	NADH-quinone oxidoreductase subunit I (EC 7.1.1.-) (NADH dehydrogenase I subunit I) (NDH-1 subunit I)	nuoI DMA12_02165	3.48	2.06
A0A428VT29	Large ribosomal subunit protein bL9	rplI DMA12_48765	3.47	1.37
A0A428W000	Sugar ABC transporter substrate-binding protein	DMA12_40415	3.43	1.18
A0A428W6Z2	KR domain-containing protein	DMA12_32040	3.41	4.30
A0A428X2P3	Multifunctional oxoglutarate decarboxylase/oxoglutarate dehydrogenase thiamine pyrophosphate-binding subunit/dihydrolipoyllysine-residue succinyltransferase subunit (EC 4.1.1.71)	kgd DMA12_04140	3.38	4.59
A0A428VV97	non-specific serine/threonine protein kinase (EC 2.7.11.1)	pknB DMA12_46990	3.35	1.98
A0A428X5W1	Sugar-binding protein	DMA12_00750	3.26	1.76
A0A428VY77	DNA gyrase subunit A (EC 5.6.2.2)	gyrA DMA12_42975	3.24	4.53
A0A428W2Z0	ABC transporter substrate-binding protein	DMA12_36955	3.19	1.73
A0A428WEY5	Pantothenate synthetase (PS) (EC 6.3.2.1) (Pantoate--beta-alanine ligase) (Pantoate-activating enzyme)	panC DMA12_23860	3.16	4.50
A0A428WXS9	LLM class F420-dependent oxidoreductase	DMA12_07950	3.14	1.88
A0A428WLN8	Carbon monoxide dehydrogenase	DMA12_17415	3.14	1.74
A0A428WG26	Enolase (EC 4.2.1.11) (2-phospho-D-glycerate hydro-lyase) (2-phosphoglycerate dehydratase)	eno DMA12_22375	3.02	1.53
A0A428X2C5	ATP synthase subunit alpha (EC 7.1.2.2) (ATP synthase F1 sector subunit alpha) (F-ATPase subunit alpha)	atpA DMA12_03485	2.90	3.03
A0A428WEF6	Elongation factor Ts (EF-Ts)	tsf DMA12_24240	2.84	1.50
A0A428X4J2	Chaperonin GroEL (EC 5.6.1.7) (60 kDa chaperonin) (Chaperonin-60) (Cpn60)	groL groEL DMA12_03150	2.73	1.40
A0A428WQH5	ABC transporter substrate-binding protein	DMA12_14765	2.69	1.99
A0A428W866	Triosephosphate isomerase (TIM) (TPI) (EC 5.3.1.1) (Triose-phosphate isomerase)	tpiA DMA12_30025	2.61	1.69
A0A428X183	Peptidase M14	DMA12_05015	2.55	1.59
A0A428W8F5	Glucose-6-phosphate dehydrogenase assembly protein OpcA	opcA DMA12_30060	2.51	1.10
A0A428X4K7	Large ribosomal subunit protein uL3	rplC DMA12_02700	2.49	1.08
A0A428WTH0	NfeD family protein	DMA12_11250	2.43	1.38
A0A428WK33	Aliphatic sulfonate ABC transporter substrate-binding protein	DMA12_19490	2.37	1.02
A0A428WEA1	Small ribosomal subunit protein bS16	rpsP DMA12_24165	2.28	1.02
A0A428X2G9	ATP synthase subunit beta (EC 7.1.2.2) (ATP synthase F1 sector subunit beta) (F-ATPase subunit beta)	atpD DMA12_03475	2.23	3.02
A0A428VWI4	L-glutamate gamma-semialdehyde dehydrogenase (EC 1.2.1.88) (L-glutamate gamma-semialdehyde dehydrogenase)	pruA DMA12_45200	2.20	1.37
A0A428W2L3	Transcriptional regulator	DMA12_37145	2.10	1.19
A0A428W9N4	Primosomal protein	DMA12_28575	2.01	0.87
A0A428X4C7	Small ribosomal subunit protein uS17	rpsQ DMA12_02745	2.01	1.75
A0A428X479	Large ribosomal subunit protein uL1	rplA DMA12_02535	-2.64	1.47
A0A428WBT7	S9 family peptidase	DMA12_26890	-3.05	6.49
A0A428WKJ4	DUF3068 domain-containing protein	DMA12_18650	-3.21	5.20
A0A428W147	Ribonuclease J (RNase J) (EC 3.1.-.-)	rnj DMA12_39315	-4.80	3.46

Table S2 | List of proteins obtained by co-immunoprecipitation of Tba-^{E545Q}-3xFLAG vs. Tba.
Proteins with a log2 fold change of ≥ |2| are listed

Majority protein ID	Protein names	Gene Names	Log2 FC	p-value
Q799B1	Putative ABC transporter ATP-binding protein	tba	23.35	11.71
O87676	Halogenase	bhaA	7.63	5.29
Q939Y0	Putative hydroxyphenyl pyruvate dioxygenase	hmaS	6.27	5.46
Q939Y9	Peptide synthetase	bpsC	4.96	4.09
Q939Y5	Putative N-methyl transferase	bmt	4.72	2.89
Q939Z0	Peptide synthetase	bpsB (+bpsA)	4.45	4.32
O87677	Glycosyltransferase	bgtfA (+bgtfC)	4.37	3.60
Q939X5	Putative C-3 amino transferase	dvaB	4.18	2.21
Q939Y4	Phenylglycine amino transferase	pgat	4.11	3.88
Q939X4	Putative 3,5 epimerase	dvaD	3.58	4.02
Q939Y7	Putative C-3 methyl transferase	dvaC	3.23	6.01
Q939Y2	Peptide synthetase	bpsD	2.43	1.75
A0A428WXV8	Flotillin family protein	Flotillin family protein	8.89	12.66
A0A428WTH7	Paraslipin	Paraslipin	7.44	3.27
A0A428VZF5	Phosphoenolpyruvate-protein phosphotransferase (EC 2.7.3.9) (Phosphotransferase system, enzyme I)	ptsP DMA12_41360	15.47	17.37
A0A428WJU7	Phosphate-specific transport system accessory protein PhoU	phoU DMA12_19055	15.22	8.64
A0A428W9K8	Succinate dehydrogenase iron-sulfur subunit (EC 1.3.5.1)	DMA12_28500	12.79	4.36
A0A428W9N5	Succinate dehydrogenase, cytochrome b556 subunit	sdhC DMA12_28515	12.75	17.41
A0A428WA21	Succinate dehydrogenase	DMA12_28510	12.44	3.98
A0A428WQD5	NAD(P)/FAD-dependent oxidoreductase	DMA12_14720	12.41	5.36
A0A428X4C1	Large ribosomal subunit protein bL12	rplL DMA12_02555	11.76	15.65
A0A428WND1	Phytoene desaturase	DMA12_15560	10.96	14.15
A0A428WC65	Transport permease protein	DMA12_26010	10.95	13.54
A0A428X2E0	ATP synthase subunit a (ATP synthase F0 sector subunit a) (F-ATPase subunit 6)	atpB DMA12_03505	10.77	14.78
A0A428WGN6	PH domain-containing protein	DMA12_21950	10.63	15.56
A0A428WXB4	carbonic anhydrase (EC 4.2.1.1)	DMA12_08485	10.60	13.38
A0A428VUQ3	Cell division ATP-binding protein FtsE	ftsE DMA12_47870	10.43	14.13
A0A428X4E3	Small ribosomal subunit protein uS4	rpsD DMA12_02845	9.98	16.28
A0A428WR66	Amino acid ABC transporter ATP-binding protein	DMA12_13735	9.45	14.76
A0A428WTI9	Polyprenol monophosphomannose synthase	DMA12_11505	9.20	14.84
A0A428X2U6	Protein translocase subunit SecA (EC 7.4.2.8)	secA DMA12_04315	9.17	15.27
A0A428WAC2	Glycerol-3-phosphate dehydrogenase (EC 1.1.5.3)	DMA12_28885	9.12	5.21
A0A428W997	Phage holin family protein	DMA12_29015	9.04	13.40
A0A428X414	Demethylmenaquinone methyltransferase (EC 2.1.1.163)	menG DMA12_02115	8.94	14.81
A0A428WMA1	ABC transporter ATP-binding protein	DMA12_16625	8.91	13.49
A0A428W9C0	UDP-N-acetylglucosamine 2-epimerase	DMA12_29410	8.90	14.83
A0A428VVT2	Decaprenylphospho-beta-D-erythro-pentofuranosid-2-ulose 2-reductase	DMA12_46435	8.89	14.09
A0A428WMA4	Nickel import system ATP-binding protein NikD (EC 7.2.2.11)	DMA12_16620	8.78	11.78
A0A428VVT3	Glycosyltransferase family 2 protein	DMA12_46390	8.70	15.63
A0A428W9L1	Succinate dehydrogenase flavoprotein subunit (EC 1.3.5.1)	DMA12_28505	8.70	5.52
A0A428WIU6	DUF2771 domain-containing protein	DMA12_20375	8.68	8.81
A0A428W136	PspA/IM30 family protein	DMA12_39390	8.64	13.94
A0A428VYT0	K(+)-insensitive pyrophosphate-energized proton pump (EC 7.1.3.1) (Membrane-bound proton-translocating pyrophosphatase) (Pyrophosphate-energized inorganic pyrophosphatase) (H(+)-PPase)	hppA DMA12_42005	8.63	4.26
A0A428X4J6	sn-glycerol-3-phosphate ABC transporter ATP-binding protein UgpC	DMA12_03010	8.43	13.88
A0A428W0Z3	Amino acid permease	DMA12_39325	8.41	14.80

A0A428VUP2	Cell division protein FtsX	DMA12_47865	8.30	13.02
A0A428X4L7	Large ribosomal subunit protein uL14	rplN DMA12_02750	8.28	13.83
A0A428WCF3	DUF4162 domain-containing protein	DMA12_26015	8.23	13.19
A0A428W873	Phosphoglycerate kinase (EC 2.7.2.3)	pgk DMA12_30020	8.15	14.12
A0A428VZY6	Sugar ABC transporter ATP-binding protein	DMA12_40425	8.06	5.57
A0A428W9B4	Uncharacterized protein	DMA12_29095	8.03	13.08
A0A428X2W2	ABC transporter permease	DMA12_04510	7.99	12.67
A0A428WCU5	D-3-phosphoglycerate dehydrogenase (EC 1.1.1.95)	DMA12_25680	7.98	3.48
A0A428X4C5	Small ribosomal subunit protein uS3	rpsC DMA12_02730	7.95	4.17
A0A428X300	ABC transporter ATP-binding protein	DMA12_04500	7.95	12.40
A0A428W6I7	ABC transporter permease	DMA12_32080	7.88	12.53
A0A428X4M6	Protein translocase subunit SecY	secY DMA12_02805	7.81	12.70
A0A428WNC5	Rieske (2Fe-2S) protein	DMA12_15575	7.81	15.09
A0A428W984	ABC transporter permease	DMA12_29365	7.75	13.43
A0A428W0L9	Xylose transport system permease protein XylH	DMA12_39775	7.75	13.66
A0A428WMY6	ABC transporter ATP-binding protein	DMA12_16570	7.71	13.15
A0A428X2Z9	ABC transporter permease	DMA12_04515	7.67	12.63
A0A428W5G2	Ribonuclease E/G	DMA12_33530	7.66	13.28
A0A428VVS3	ABC transporter ATP-binding protein	DMA12_46385	7.54	13.47
A0A428WBY2	Methyltransferase domain-containing protein	DMA12_26875	7.51	8.62
A0A428WXT3	GNAT family N-acetyltransferase	DMA12_07880	7.47	12.58
A0A428WXQ4	Amino acid ABC transporter permease	DMA12_07765	7.47	12.45
A0A428W994	ABC transporter permease	DMA12_29360	7.44	13.54
A0A428W7M9	Protein-export membrane protein SecF	secF DMA12_31020	7.43	13.65
A0A428W0L8	Sugar ABC transporter ATP-binding protein	DMA12_39770	7.43	8.19
A0A428W013	Nucleoside/nucleotide kinase family protein	DMA12_40435	7.42	15.09
A0A428X5K6	Aldo/keto reductase	DMA12_00090	7.41	9.55
A0A428VT42	Uncharacterized protein	DMA12_48795	7.41	2.70
A0A428WD83	ABC transporter ATP-binding protein	DMA12_25045	7.39	13.62
A0A428X4F8	Uncharacterized protein	DMA12_02865	7.37	12.85
A0A428WEZ5	ATP-dependent zinc metalloprotease FtsH (EC 3.4.24.-)	ftsH DMA12_23910	7.35	8.42
A0A428X4S5	Type VII secretion protein EccE	eccE DMA12_02870	7.33	13.45
A0A428W0W5	Small ribosomal subunit protein uS15	rpsO DMA12_39180	7.31	9.12
A0A428VVF9	FHA domain-containing protein	DMA12_47015	7.30	12.74
A0A428W2J7	MoxR family ATPase	DMA12_37495	7.29	13.22
A0A428W6W3	DUF4328 domain-containing protein	DMA12_31870	7.29	11.56
A0A428W2F0	Glycerophosphoryl diester phosphodiesterase membrane domain-containing protein	DMA12_37510	7.27	12.98
A0A428VV83	DUF4191 domain-containing protein	DMA12_47260	7.27	12.18
A0A428VYB3	Cytochrome bc1 complex cytochrome b subunit (EC 7.1.1.8) (Cytochrome bc1 reductase complex subunit QcrB)	DMA12_42825	7.25	13.18
A0A428W389	ATPase	DMA12_36170	7.22	12.31
A0A428WR68	Secreted protein	DMA12_14000	7.21	12.94
A0A428WLR0	Sugar ABC transporter ATP-binding protein	DMA12_17345	7.11	11.06
A0A428WAW9	Alpha-hydroxy-acid oxidizing protein	DMA12_27635	7.07	13.32
A0A428W2S7	RNase adapter RapZ	DMA12_37300	7.06	14.09
A0A428VXI1	Acyl-CoA synthetase	DMA12_44015	7.05	14.73
A0A428X4F7	Type VII secretion protein EccC	DMA12_02905	6.97	13.36
A0A428W6M3	Glycine/betaine ABC transporter substrate-binding protein	DMA12_32065	6.96	8.24
A0A428W2R9	Adenylyltransferase/sulfurtransferase MoeZ	DMA12_36755	6.93	13.52
A0A428WMM5	ABC transporter permease	DMA12_16615	6.93	11.54
A0A428WNN0	NAD(P)/FAD-dependent oxidoreductase	DMA12_15540	6.88	11.40
A0A428WM54	beta-mannosidase (EC 3.2.1.25)	DMA12_16630	6.87	3.53

A0A428X4E9	DNA-directed RNA polymerase subunit alpha (RNAP subunit alpha) (EC 2.7.7.6) (RNA polymerase subunit alpha) (Transcriptase subunit alpha)	rpoA DMA12_02850	6.86	13.76
A0A428X4A8	Elongation factor G (EF-G)	fusA DMA12_02685	6.85	3.41
A0A428VU60	Membrane protein	DMA12_48585	6.78	13.48
A0A428WIW9	histidine kinase (EC 2.7.13.3)	DMA12_20575	6.71	12.53
A0A428WXN5	Amino acid ABC transporter ATP-binding protein	DMA12_07755	6.71	12.21
A0A428X4B2	Elongation factor Tu (EF-Tu)	tuf DMA12_02690	6.67	3.10
A0A428W6Z4	ABC transporter	DMA12_32075	6.66	3.91
A0A428W9B7	ABC transporter ATP-binding protein	DMA12_29355	6.61	12.83
A0A428X4B8	DNA-directed RNA polymerase subunit beta' (RNAP subunit beta') (EC 2.7.7.6) (RNA polymerase subunit beta') (Transcriptase subunit beta')	rpoC DMA12_02650	6.60	12.70
A0A428VT13	Serine/threonine protein kinase	DMA12_48950	6.59	14.37
A0A428VXE6	Amino acid ABC transporter ATP-binding protein	DMA12_44210	6.56	12.40
A0A428VYD7	asparagine synthase (glutamine-hydrolyzing) (EC 6.3.5.4)	asnB DMA12_42775	6.54	13.41
A0A428W0P2	Cation acetate symporter	DMA12_39440	6.53	10.76
A0A428X2P1	Transcription termination factor Rho (EC 3.6.4.-) (ATP-dependent helicase Rho)	rho DMA12_03575	6.48	12.59
A0A428WZV3	Chaperone protein HtpG (Heat shock protein HtpG) (High temperature protein G)	htpG DMA12_05610	6.46	13.85
A0A428VVP1	Glycosyltransferase family 2 protein	DMA12_46420	6.45	4.68
A0A428X2N8	ABC transporter ATP-binding protein	DMA12_04115	6.44	7.94
A0A428W7Q7	Adenosylhomocysteinase (EC 3.13.2.1) (S-adenosyl-L-homocysteine hydrolase) (AdoHcyase)	ahcY DMA12_31180	6.42	2.91
A0A428VYG5	Cytochrome bc1 complex Rieske iron-sulfur subunit (Cytochrome bc1 reductase complex subunit QcrA) (Rieske iron-sulfur protein)	DMA12_42820	6.31	7.89
A0A428WED3	Large ribosomal subunit protein bL19	rplS DMA12_24185	6.30	2.66
A0A428WFY4	Iron transporter	DMA12_22395	6.30	12.36
A0A428WEC7	P-II family nitrogen regulator	DMA12_24085	6.29	2.84
A0A428W2W9	Carbohydrate ABC transporter permease	DMA12_36945	6.24	11.88
A0A428WR01	ABC transporter ATP-binding protein	DMA12_13435	6.23	6.45
A0A428X0L8	ATP-grasp domain-containing protein	DMA12_05540	6.19	7.05
A0A428W307	Phosphatase PAP2 family protein	DMA12_36465	6.18	3.56
A0A428VZY9	ABC transporter permease	DMA12_40420	6.14	3.79
A0A428WQD1	Short chain dehydrogenase	DMA12_14475	6.13	12.85
A0A428W9B9	Glycosyl transferase	DMA12_29405	6.10	12.95
A0A428VX74	Amino acid ABC transporter substrate-binding protein	DMA12_44220	6.05	5.00
A0A428W5M7	ABC transporter ATP-binding protein	DMA12_33510	6.00	5.71
A0A428VUD9	histidine kinase (EC 2.7.13.3)	DMA12_48270	5.99	7.73
A0A428W9B3	Glycosyltransferase family 2 protein	DMA12_29390	5.98	12.88
A0A428VVP6	Decaprenyl-phosphate phosphoribosyltransferase	DMA12_46450	5.96	11.72
A0A428W7Y4	PH domain-containing protein	DMA12_31080	5.96	11.76
A0A428W3D7	AAA ATPase forming ring-shaped complexes (ARC)	arc DMA12_36395	5.90	3.13
A0A428X441	NADH-quinone oxidoreductase subunit D (EC 7.1.1.-) (NADH dehydrogenase I subunit D) (NDH-1 subunit D)	nuoD DMA12_02140	5.90	11.16
A0A428WR96	Chaperone protein DnaK (HSP70) (Heat shock 70 kDa protein) (Heat shock protein 70)	dnaK DMA12_13940	5.90	3.20
A0A428X2E2	Na+/galactose cotransporter	DMA12_03365	5.76	2.19
A0A428WND3	Catalase-peroxidase (CP) (EC 1.11.1.21) (Peroxidase/catalase)	katG DMA12_15640	5.75	2.82
A0A428VW51	Extracellular solute-binding protein	DMA12_45915	5.71	12.20
A0A428WAQ2	Peroxiredoxin	DMA12_27620	5.71	2.81
A0A428WEE4	Small ribosomal subunit protein uS2	rpsB DMA12_24235	5.66	4.39
A0A428VZA5	Protein translocase subunit SecA (EC 7.4.2.8)	secA DMA12_41520	5.58	11.77
A0A428X2U1	Adenosylhomocysteinase (EC 3.13.2.1) (S-adenosyl-L-homocysteine hydrolase) (AdoHcyase)	ahcY DMA12_04400	5.57	11.56
A0A428VT59	Sensor-like histidine kinase SenX3 (EC 2.7.13.3)	DMA12_48715	5.55	9.74

A0A428VUV7	PadR family transcriptional regulator	DMA12_47880	5.53	2.12
A0A428VRW7	Polyphosphate kinase (EC 2.7.4.1) (ATP-polyphosphate phosphotransferase) (Polyphosphoric acid kinase)	ppk DMA12_48985	5.52	12.87
A0A428WTG0	ABC transporter permease	DMA12_11200	5.52	11.89
A0A428VYC6	DUF3043 domain-containing protein	DMA12_42760	5.51	3.50
A0A428VV69	Two-component sensor histidine kinase	DMA12_47050	5.49	10.27
A0A428X451	NADH-quinone oxidoreductase subunit C (EC 7.1.1.-) (NADH dehydrogenase I subunit C) (NDH-1 subunit C)	nuoC DMA12_02135	5.43	3.50
A0A428WUE1	UvrABC system protein B (Protein UvrB) (Excinuclease ABC subunit B)	uvrB DMA12_10570	5.38	7.42
A0A428WDA0	Branched-chain amino acid ABC transporter permease	DMA12_25035	5.38	3.57
A0A428WR74	DNA-binding response regulator	DMA12_13795	5.36	11.48
A0A428W171	Non-ribosomal peptide synthetase	DMA12_39080	5.24	6.89
A0A428WM62	Carbohydrate ABC transporter permease	DMA12_16670	5.22	8.74
A0A428W7V5	DUF445 domain-containing protein	DMA12_30770	5.22	10.62
A0A428W7H9	Protein translocase subunit SecD	secD DMA12_31015	5.20	3.53
A0A428VWU6	DUF948 domain-containing protein	DMA12_44845	5.18	10.98
A0A428WA50	Acyl-CoA synthetase	DMA12_28145	5.17	11.49
A0A428X3Y4	HAD-IB family hydrolase	DMA12_01895	5.11	11.12
A0A428W194	ABC transporter ATP-binding protein	DMA12_39100	5.08	8.04
A0A428W0X9	Divalent metal cation transporter MntH	mntH DMA12_39300	5.05	3.57
A0A428W801	non-specific serine/threonine protein kinase (EC 2.7.11.1)	DMA12_30465	4.99	12.72
A0A428W296	CTP synthase (EC 6.3.4.2) (Cytidine 5'-triphosphate synthase) (Cytidine triphosphate synthetase) (CTP synthetase) (CTPS) (UTP--ammonia ligase)	pyrG DMA12_37730	4.99	3.69
A0A428WMB5	Sugar ABC transporter substrate-binding protein	DMA12_16675	4.95	3.00
A0A428W945	Crp/Fnr family transcriptional regulator	DMA12_29060	4.90	2.47
A0A428WF14	ATP-dependent Clp protease ATP-binding subunit	DMA12_23810	4.85	3.01
A0A428VWI9	Polyphosphate--nucleotide phosphotransferase	DMA12_45310	4.81	3.63
A0A428WXV9	Amino acid ABC transporter permease	DMA12_07770	4.81	3.63
A0A428X4C9	Small ribosomal subunit protein uS8	rpsH DMA12_02770	4.77	1.87
A0A428WQU6	ABC transporter	DMA12_13425	4.74	9.44
A0A428WA61	Esterase	DMA12_28095	4.71	11.10
A0A428VWD2	Cell division protein CrgA	crgA DMA12_45785	4.69	11.39
A0A428W1H2	Cytochrome c oxidase subunit 1 (EC 7.1.1.9)	ctaD DMA12_38800	4.66	3.80
A0A428WJV0	Phosphate transport system permease protein	pstC DMA12_19040	4.65	3.72
A0A428X4B5	Small ribosomal subunit protein uS7	rpsG DMA12_02680	4.64	2.51
A0A428VZ91	Lysine--tRNA ligase (EC 6.1.1.6) (Lysyl-tRNA synthetase) (LysRS)	lysS DMA12_41490	4.63	10.72
A0A428WVB7	ABC transporter substrate-binding protein	DMA12_09770	4.62	4.31
A0A428WKH2	Choline dehydrogenase (EC 1.1.99.1)	betA DMA12_18485	4.61	3.79
A0A428W2L8	S-adenosylmethionine synthase (AdoMet synthase) (EC 2.5.1.6) (MAT) (Methionine adenosyltransferase)	metK DMA12_37210	4.57	3.63
A0A428W0B6	DUF3710 domain-containing protein	DMA12_39900	4.55	3.64
A0A428WXW4	Protein RecA (Recombinase A)	recA DMA12_07850	4.50	3.62
A0A428W8A3	Glucose-6-phosphate 1-dehydrogenase (G6PD) (EC 1.1.1.49)	zwf DMA12_30065	4.44	5.22
A0A428W622	NAD-glutamate dehydrogenase	DMA12_32995	4.32	11.02
A0A428W0W2	Polyribonucleotide nucleotidyltransferase (EC 2.7.7.8) (Polynucleotide phosphorylase) (PNPase)	pnp DMA12_39185	4.32	3.15
A0A428X426	NADH-quinone oxidoreductase (EC 7.1.1.-)	DMA12_02155	4.30	3.59
A0A428W9B0	Dipeptide/oligopeptide/nickel ABC transporter ATP-binding protein	DMA12_29350	4.27	3.54
A0A428W707	Histidine kinase	DMA12_31550	4.24	10.77
A0A428WJW2	Phosphate ABC transporter ATP-binding protein	DMA12_19050	4.23	3.70
A0A428VYY9	FAD-dependent monooxygenase	DMA12_41850	4.22	3.88

A0A428W148	ABC transporter substrate-binding protein	DMA12_39090	4.15	1.91
A0A428WGY6	2,3,4,5-tetrahydropyridine-2,6-dicarboxylate N-succinyltransferase (EC 2.3.1.117) (Tetrahydrodipicolinate N-succinyltransferase) (THDP succinyltransferase) (THP succinyltransferase) (Tetrahydropicolinate succinylase)	dapD DMA12_22215	4.14	3.79
A0A428X4J2	Chaperonin GroEL (EC 5.6.1.7) (60 kDa chaperonin) (Chaperonin-60) (Cpn60)	groL groEL DMA12_03150	4.12	2.22
A0A428X2D7	Glycosyltransferase	DMA12_03545	4.11	9.62
A0A428WZ16	LacI family transcriptional regulator	DMA12_07375	4.10	3.78
A0A428WJT6	Sulfurtransferase	DMA12_19005	4.09	2.61
A0A428W110	Serine/threonine protein kinase	DMA12_39305	4.03	3.85
A0A428VQQ5	Serine/threonine protein kinase	DMA12_49235	4.01	9.65
A0A428WVC0	ABC transporter substrate-binding protein	DMA12_09780	3.96	2.93
A0A428X4F1	Large ribosomal subunit protein uL23	rplW DMA12_02710	3.79	1.77
A0A428VVA8	Pentapeptide repeat-containing protein	DMA12_47210	3.73	3.65
A0A428X4K5	GuaB3 family IMP dehydrogenase-related protein	DMA12_03210	3.68	4.03
A0A428W611	DUF5130 domain-containing protein	DMA12_32945	3.67	1.60
A0A428X4W9	Geranylgeranyl reductase family protein	DMA12_02120	3.65	3.95
A0A428X2I8	ATP synthase gamma chain (ATP synthase F1 sector gamma subunit) (F-ATPase gamma subunit)	atpG DMA12_03480	3.58	2.09
A0A428VZF8	Succinate--CoA ligase [ADP-forming] subunit alpha (EC 6.2.1.5) (Succinyl-CoA synthetase subunit alpha) (SCS-alpha)	sucD DMA12_41105	3.55	1.92
A0A428X2U4	Cation diffusion facilitator family transporter	DMA12_04420	3.53	3.68
A0A428X2U3	Proline/glycine betaine ABC transporter ATP-binding protein	DMA12_04170	3.51	3.70
A0A428X2C5	ATP synthase subunit alpha (EC 7.1.2.2) (ATP synthase F1 sector subunit alpha) (F-ATPase subunit alpha)	atpA DMA12_03485	3.42	3.22
A0A428W7P7	Secreted protein	DMA12_30455	3.41	3.56
A0A428WHY7	DUF3592 domain-containing protein	DMA12_20950	3.40	3.81
A0A428WYP6	Ricin B lectin domain-containing protein	DMA12_06810	3.38	3.94
A0A428W9N6	peptidoglycan glycosyltransferase (EC 2.4.99.28)	DMA12_29130	3.30	4.19
A0A428WND5	Phytoene/squalene synthase family protein	DMA12_15555	3.28	4.00
A0A428WTG2	ABC transporter ATP-binding protein	DMA12_11205	3.26	3.88
A0A428WA47	Pyruvate kinase (EC 2.7.1.40)	pyk DMA12_28045	3.25	3.99
A0A428WIW2	ATP-binding protein	DMA12_20560	3.24	3.91
A0A428WYK2	M50 family peptidase	DMA12_06600	3.20	3.77
A0A428W8C6	Peptidyl-prolyl cis-trans isomerase (EC 5.2.1.8)	DMA12_30100	3.13	4.12
A0A428X443	Aminopeptidase N (EC 3.4.11.2)	DMA12_02075	3.13	3.80
A0A428WB97	YjbQ family protein	DMA12_27770	3.10	1.49
A0A428WR38	Pyruvate dehydrogenase (Acetyl-transferring) E1 component subunit alpha	pdhA DMA12_13685	3.09	4.02
A0A428VXI3	Amino acid ABC transporter substrate-binding protein	DMA12_44230	3.08	1.85
A0A428WK30	Threonine--tRNA ligase (EC 6.1.1.3)	thrS DMA12_19265	3.07	3.64
A0A428W5A4	Pentapeptide repeat-containing protein	DMA12_33975	2.99	3.71
A0A428X5W1	Sugar-binding protein	DMA12_00750	2.94	1.99
A0A428WA25	Uncharacterized protein	DMA12_28010	2.92	4.06
A0A428W8G9	Alpha-1,6-mannosyltransferase	DMA12_30150	2.89	4.12
A0A428X2P3	Multifunctional oxoglutarate decarboxylase/oxoglutarate dehydrogenase thiamine pyrophosphate-binding subunit/dihydrolipoyllysine-residue succinyltransferase subunit (EC 4.1.1.71)	kgd DMA12_04140	2.87	4.22
A0A428VVN6	DUF3558 domain-containing protein	DMA12_46400	2.86	1.57
A0A428VZH5	Succinate--CoA ligase [ADP-forming] subunit beta (EC 6.2.1.5) (Succinyl-CoA synthetase subunit beta) (SCS-beta)	sucC DMA12_41100	2.83	1.10
A0A428WXP6	Fumarate reductase/succinate dehydrogenase flavoprotein subunit	DMA12_07810	2.70	2.60
A0A428W0N3	DUF485 domain-containing protein	DMA12_39445	2.67	4.45
A0A428W000	Sugar ABC transporter substrate-binding protein	DMA12_40415	2.66	0.95
A0A428WDS4	Alpha/beta hydrolase	DMA12_24810	2.62	3.68
A0A428WUE3	TerC family protein	DMA12_10615	2.59	3.94
A0A428WAT2	Vitamin B12-dependent ribonucleotide reductase (EC 1.17.4.1)	DMA12_28420	2.57	3.41
A0A428W0R2	Co-chaperone YbbN	DMA12_39530	2.53	1.95

A0A428WEY5	Pantothenate synthetase (PS) (EC 6.3.2.1) (Pantoate--beta-alanine ligase) (Pantoate-activating enzyme)	panC DMA12_23860	2.50	4.15
A0A428WG35	Peptidase M75 family protein	DMA12_22400	2.48	1.59
A0A428X2E7	ATP synthase epsilon chain (ATP synthase F1 sector epsilon subunit) (F-ATPase epsilon subunit)	atpC DMA12_03470	2.48	0.93
A0A428X2G9	ATP synthase subunit beta (EC 7.1.2.2) (ATP synthase F1 sector subunit beta) (F-ATPase subunit beta)	atpD DMA12_03475	2.47	3.11
A0A428WXS9	LLM class F420-dependent oxidoreductase	DMA12_07950	2.40	1.69
A0A428VV97	non-specific serine/threonine protein kinase (EC 2.7.11.1)	pknB DMA12_46990	2.34	1.36
A0A428VYA0	Probable cytosol aminopeptidase (EC 3.4.11.1) (Leucine aminopeptidase) (LAP) (EC 3.4.11.10) (Leucyl aminopeptidase)	pepA DMA12_42700	2.32	1.13
A0A428WK33	Aliphatic sulfonate ABC transporter substrate-binding protein	DMA12_19490	2.31	0.96
A0A428W8F5	Glucose-6-phosphate dehydrogenase assembly protein OpcA	opcA DMA12_30060	2.20	1.13
A0A428W311	Proteasome subunit beta (EC 3.4.25.1) (20S proteasome beta subunit) (Proteasome core protein PrcB)	prcB DMA12_36450	2.17	1.17
A0A428WFL0	Nitrate ABC transporter substrate-binding protein	DMA12_23000	2.11	1.14
A0A428WD72	Branched-chain amino acid ABC transporter permease	DMA12_25040	2.07	1.04
A0A428X4G1	Small ribosomal subunit protein uS9	rpsI DMA12_02945	2.00	1.04
A0A428WBT7	S9 family peptidase	DMA12_26890	-2.23	6.07
A0A428VW10	Isoleucine--tRNA ligase (EC 6.1.1.5) (Isoleucyl-tRNA synthetase) (IleRS)	ileS DMA12_45830	-3.87	2.15
A0A428X479	Large ribosomal subunit protein uL1	rplA DMA12_02535	-3.94	2.06
A0A428W147	Ribonuclease J (RNase J) (EC 3.1.-.-)	rnj DMA12_39315	-4.63	5.80
A0A428WKJ4	DUF3068 domain-containing protein	DMA12_18650	-6.05	6.16

Table S3 | List of proteins obtained by co-immunoprecipitation of Tba-3xFLAG vs. Tba-^{E545Q}-3xFLAG. Proteins with a log2 fold change of ≥ |2| are listed

Majority protein ID	Protein names	Gene Names	Log2 FC	p-value
O87675	p450 monooxygenase	oxyC	5.69	2.48
A0A428W6H1	DUF1707 domain-containing protein	DMA12_31970	3.95	12.03
A0A428X424	NADH-quinone oxidoreductase subunit B (EC 7.1.1.-) (NADH dehydrogenase I subunit B) (NDH-1 subunit B)	nuoB DMA12_02130	3.55	5.33
A0A428W7D8	Peptidylprolyl isomerase	DMA12_31070	3.49	6.46
A0A428W003	Fructose-bisphosphate aldolase (FBP aldolase) (EC 4.1.2.13)	DMA12_40530	3.40	17.37
A0A428WD72	Branched-chain amino acid ABC transporter permease	DMA12_25040	3.38	2.83
A0A428VYD0	Membrane protein insertase YidC (Foldase YidC) (Membrane integrase YidC) (Membrane protein YidC)	DMA12_42925	3.30	5.50
A0A428VVF7	protein-serine/threonine phosphatase (EC 3.1.3.16)	DMA12_47010	3.21	17.78
A0A428WM61	alpha-galactosidase (EC 3.2.1.22)	DMA12_16660	3.18	13.96
A0A428X437	NADH-quinone oxidoreductase subunit L	DMA12_02180	3.11	8.15
A0A428W526	Sugar ABC transporter substrate-binding protein	DMA12_33715	2.97	2.67
A0A428X4G5	Small ribosomal subunit protein uS13	rpsM DMA12_02830	2.95	4.37
A0A428WLJ3	Sodium:solute symporter	DMA12_17265	2.91	12.36
A0A428W6L5	ABC transporter permease	DMA12_32070	2.56	2.22
A0A428W2Q7	Integration host factor	DMA12_37190	2.54	10.30
A0A428X450	NADH-quinone oxidoreductase subunit N (EC 7.1.1.-) (NADH dehydrogenase I subunit N) (NDH-1 subunit N)	nuoN DMA12_02190	2.51	2.31
A0A428VXG1	Amino acid ABC transporter permease	DMA12_44215	2.44	3.40
A0A428WAT1	Pyruvate dehydrogenase E1 component (EC 1.2.4.1)	aceE DMA12_27630	2.42	12.56
A0A428WG47	Large ribosomal subunit protein bL25 (General stress protein CTC)	rplY ctc DMA12_22585	2.42	2.33
A0A428W341	Proteasome subunit alpha (20S proteasome alpha subunit) (Proteasome core protein PrcA)	prcA DMA12_36455	2.37	4.01
A0A428W876	Transketolase (EC 2.2.1.1)	DMA12_30080	2.37	9.36
A0A428WXT6	Phosphatidylglycerol--prolipoprotein diacylglyceryl transferase (EC 2.5.1.145)	lgt DMA12_08035	2.35	2.31
A0A428X4B4	Mce-associated membrane protein	DMA12_02610	2.35	7.90
A0A428VSY5	TIGR04222 domain-containing membrane protein	DMA12_48935	2.29	3.05

A0A428W2J9	PTS N-acetylglucosamine transporter subunit IIBC	DMA12_37050	2.27	3.81
A0A428WIN4	Citrate synthase	DMA12_20090	2.25	2.49
A0A428VV58	Ricin B lectin domain-containing protein	DMA12_47325	2.15	2.52
A0A428WSM4	PTS mannose transporter subunit IIAB	DMA12_12420	2.14	3.41
A0A428WDA0	Branched-chain amino acid ABC transporter permease	DMA12_25035	2.05	2.02
A0A428VWA9	Peptidyl-prolyl cis-trans isomerase (PPIase) (EC 5.2.1.8)	DMA12_45770	2.01	2.37
A0A428WZ16	LacI family transcriptional regulator	DMA12_07375	-2.04	2.41
A0A428W110	Serine/threonine protein kinase	DMA12_39305	-2.05	2.50
A0A428VYY9	FAD-dependent monooxygenase	DMA12_41850	-2.10	2.46
A0A428X2D7	Glycosyltransferase	DMA12_03545	-2.12	6.52
A0A428W2L8	S-adenosylmethionine synthase (AdoMet synthase) (EC 2.5.1.6) (MAT) (Methionine adenosyltransferase)	metK DMA12_37210	-2.38	2.47
A0A428X3Y4	HAD-IB family hydrolase	DMA12_01895	-2.81	15.38
A0A428WLR0	Sugar ABC transporter ATP-binding protein	DMA12_17345	-3.03	4.65
A0A428VYC6	DUF3043 domain-containing protein	DMA12_42760	-3.05	2.56
A0A428X4J6	sn-glycerol-3-phosphate ABC transporter ATP-binding protein UgpC	DMA12_03010	-3.11	2.33
A0A428X4L7	Large ribosomal subunit protein uL14	rplN DMA12_02750	-3.48	3.05
A0A428WFY4	Iron transporter	DMA12_22395	-3.49	9.70
A0A428VT13	Serine/threonine protein kinase	DMA12_48950	-3.73	20.34
A0A428VVT2	Decaprenylphospho-beta-D-erythro-pentofuranosid-2-ulose 2-reductase	DMA12_46435	-3.73	2.91
A0A428VT42	Uncharacterized protein	DMA12_48795	-4.16	2.50

Acknowledgement

I would like to take this opportunity to express my gratitude to all scientific and non-scientific colleagues and people whose contributions have played a significant role in the success of my work.

First, I would like to thank my doctoral supervisor, **Samuel Wagner**, for giving me the opportunity to work on an exciting and, as it turned out, challenging project in his laboratory. I am grateful for your constant positivity, even in difficult times; for giving me great scientific advice; and for always finding slots in a tight schedule.

Many thanks to all members of **AG Wagner** for the pleasant and enjoyable working atmosphere, with apparently very funny (...) lunch breaks. Since it would be too much to name everyone I met during my time in the lab, I would like to highlight some special people here. Thank you, **Andrea**, for being the best technician a lab could wish for! You always had a helping hand and an open ear for me. Thank you for your support! Thank you, **Sara**, for being an amazing postdoc, a role model for me as a female scientist, and for giving me feedback on this thesis. You always gave me scientific advice when I needed it and encouraged me when I was struggling. Thank you, **Eunjin, Sarah, and Sophie** (the order is randomly chosen), for being the best fellow PhD students I could have ever wished for. Thank you for always being there for me, and for becoming such good friends and for your support inside (and outside) the lab.

Many thanks to **Evi Stegmann**, my second supervisor, who warmly welcomed me to my 'second lab' and always offered help and an open ear. Thank you for being very interested and detail-focused. I would also like to extend my thanks to the entire **AG Stegmann**, especially to **Dardan, Jens, and Alena**. You welcomed me kindly, always helped me when I couldn't find something, and often took on little things for me in the lab so that I didn't always have to 'come up' for them. Thank you very much for the great atmosphere! At this point, a very big thank you to **Dardan**: for the insightful discussions, for being a great lab partner, and I won't forget our MANY (!) D-Trafos anytime soon.

A very special thank you goes to **Libera**! Thank you for your corrections of our Manuscript, proofreading of this thesis, and the cakes on our cycling trips. I deeply appreciate not only your linguistic support but also your ability to quickly familiarize yourself with my topic and ask the right, critical questions to provide scientific advice. You are an incredible asset to everyone in the institute!

I would like to express my sincere gratitude to **all the collaborators** I've had the privilege to work with over the past years, who have introduced me to a wide range of fascinating topics. Special thanks to **Athina** for guiding me into the exciting world of phylogeny and bioinformatics. To **Thales** for the complex modeling projects I asked for and for patiently answering all my questions. And to **Uli** for your unwavering enthusiasm in helping us navigate the world of statistics.

Many thanks to **Gisela** and the entire **IGIM** team for an excellent graduate program, engaging summer schools, and for the swift handling of employment contracts ;-)!

Thanks to my **TAC committee**, consisting of Samuel, Evi, and Christian Löw, for holding TAC meetings and giving me insightful feedback for my work.

Thanks to all of my other friends who accompanied me on the way to completing this thesis. Thanks, **Urte,** for staying such a good friend ever since we met and a great pacemaker during my writing process; **Lena and Lukas**, for being amazing flatmates and friends throughout my time in Tübingen; and **Sophie and Lu** for offering me your sofa so often in the last few months.

Thank you, **Tobi**, for being by my side during my time in Tübingen. Thank you for everything outside the "lab universe", for the distraction and encouragement when I needed it. Thank you for always being there for me.

Finally, I would like to thank my dear **parents** who have always supported me on my journey. Thank you for giving me the opportunity to study my favorite subject and for your unconditional support. It has allowed me to make all my decisions the way I see fit and to become the person I am today. Thank you!

References

1. Fleming, A. On the Antibacterial Action of Cultures of a Penicillium, with Special Reference to their Use in the Isolation of B. influenzæ. *Br. J. Exp. Pathol.* **10**, 226 (1929).
2. Murray, C. J. L. *et al.* Global burden of bacterial antimicrobial resistance in 2019: a systematic analysis. *The Lancet* **399**, 629–655 (2022).
3. United Nations Environment Programme. Bracing for Superbugs: Strengthening environmental action in the One Health response to antimicrobial resistance. (2023).
4. Kohanski, M. A., Dwyer, D. J. & Collins, J. J. How antibiotics kill bacteria: from targets to networks. *Nat. Rev. Microbiol.* **8**, 423–435 (2010).
5. Schneider, T. & Sahl, H.-G. An oldie but a goodie – cell wall biosynthesis as antibiotic target pathway. *Int. J. Med. Microbiol.* **300**, 161–169 (2010).
6. Schleifer, K. H. & Kandler, O. Peptidoglycan types of bacterial cell walls and their taxonomic implications. *Bacteriol. Rev.* **36**, 407–477 (1972).
7. Rohde, M. The Gram-Positive Bacterial Cell Wall. *Microbiol. Spectr.* **7**, 10.1128/microbiolspec.gpp3-0044–2018 (2019).
8. Demchick, P. & Koch, A. L. The permeability of the wall fabric of Escherichia coli and Bacillus subtilis. *J. Bacteriol.* **178**, 768–773 (1996).
9. Armstrong, J. J. *et al.* Teichoic Acids from Bacterial Walls: Composition of Teichoic Acids from a Number of Bacterial Walls. *Nature* **184**, 247–248 (1959).
10. Peschel, A., Vuong, C., Otto, M. & Götz, F. The d-Alanine Residues ofStaphylococcus aureus Teichoic Acids Alter the Susceptibility to Vancomycin and the Activity of Autolytic Enzymes. *Antimicrob. Agents Chemother.* **44**, 2845–2847 (2000).
11. Oku, Y. *et al.* Pleiotropic Roles of Polyglycerolphosphate Synthase of Lipoteichoic Acid in Growth of Staphylococcus aureus Cells. *J. Bacteriol.* **191**, 141–151 (2009).
12. Fedtke, I. *et al.* A Staphylococcus aureus ypfP mutant with strongly reduced lipoteichoic acid (LTA) content: LTA governs bacterial surface properties and autolysin activity. *Mol. Microbiol.* **65**, 1078–1091 (2007).
13. Gross, M., Cramton, S. E., Götz, F. & Peschel, A. Key Role of Teichoic Acid Net Charge inStaphylococcus aureus Colonization of Artificial Surfaces. *Infect. Immun.* **69**, 3423–3426 (2001).
14. Weidenmaier, C. *et al.* Lack of Wall Teichoic Acids in Staphylococcus aureus Leads to Reduced Interactions with Endothelial Cells and to Attenuated Virulence in a Rabbit Model of Endocarditis. *J. Infect. Dis.* **191**, 1771–1777 (2005).
15. Barreteau, H. *et al.* Cytoplasmic steps of peptidoglycan biosynthesis. *FEMS Microbiol. Rev.* **32**, 168–207 (2008).
16. Sauvage, E., Kerff, F., Terrak, M., Ayala, J. A. & Charlier, P. The penicillin-binding proteins: structure and role in peptidoglycan biosynthesis. *FEMS Microbiol. Rev.* **32**, 234–258 (2008).
17. Reynolds, P. E. Structure, biochemistry and mechanism of action of glycopeptide antibiotics. *Eur. J. Clin. Microbiol. Infect. Dis.* **8**, 943–950 (1989).
18. Economou, N. J., Cocklin, S. & Loll, P. J. High-resolution crystal structure reveals molecular details of target recognition by bacitracin. *Proc. Natl. Acad. Sci.* **110**, 14207–14212 (2013).
19. Kahan, F. M., Kahan, J. S., Cassidy, P. J. & Kropp, H. The mechansim of action of Fosfomycin (Phosphonomycin). *Ann. N. Y. Acad. Sci.* **235**, 364–386 (1974).
20. Gorter, E. & Grendel, F. On biomolecular layers od lipoids on the chromocytes of the blood. *J. Exp. Med.* **41**, 439 (1925).
21. Wiener, M. C. & White, S. H. Structure of a fluid dioleoylphosphatidylcholine bilayer determined by joint refinement of x-ray and neutron diffraction data. III. Complete structure. *Biophys. J.* **61**, 434–447 (1992).
22. Walter, A. & Gutknecht, J. Permeability of small nonelectrolytes through lipid bilayer membranes. *J. Membr. Biol.* **90**, 207–217 (1986).
23. Edidin, M. Lipids on the frontier: a century of cell-membrane bilayers. *Nat. Rev. Mol. Cell Biol.* **4**, 414–418 (2003).
24. Harayama, T. & Riezman, H. Understanding the diversity of membrane lipid composition. *Nat. Rev. Mol. Cell Biol.* **19**, 281–296 (2018).
25. Coskun, Ü. & Simons, K. Cell Membranes: The Lipid Perspective. *Structure* **19**, 1543–1548 (2011).
26. Strahl, H. & Errington, J. Bacterial Membranes: Structure, Domains, and Function. *Annu. Rev. Microbiol.* **71**, 519–538 (2017).
27. van Meer, G., Voelker, D. R. & Feigenson, G. W. Membrane lipids: where they are and how they behave. *Nat. Rev. Mol. Cell Biol.* **9**, 112–124 (2008).
28. Singer, S. J. & Nicolson, G. L. The Fluid Mosaic Model of the Structure of Cell Membranes. *Science* **175**, 720–731 (1972).
29. Simons, K. & Ikonen, E. Functional rafts in cell membranes. *Nature* **387**, 569–572 (1997).
30. Bickel, P. E. *et al.* Flotillin and Epidermal Surface Antigen Define a New Family of Caveolae-associated Integral Membrane Proteins *. *J. Biol. Chem.* **272**, 13793–13802 (1997).
31. Tavernarakis, N., Driscoll, M. & Kyrpides, N. C. The SPFH domain: implicated in regulating targeted protein turnover in stomatins and other membrane-associated proteins. *Trends Biochem. Sci.* **24**, 425–427 (1999).
32. Zhao, F., Zhang, J., Liu, Y.-S., Li, L. & He, Y.-L. Research advances on flotillins. *Virol. J.* **8**, 479 (2011).
33. Bramkamp, M. & Lopez, D. Exploring the Existence of Lipid Rafts in Bacteria. *Microbiol. Mol. Biol. Rev.* **79**, 81–100 (2015).
34. Hedin, L. E., Illergård, K. & Elofsson, A. An Introduction to Membrane Proteins. *J. Proteome Res.* **10**, 3324–3331 (2011).
35. Maloney, P. C., Kashket, E. R. & Wilson, T. H. A Protonmotive Force Drives ATP Synthesis in Bacteria. *Proc. Natl. Acad. Sci.* **71**, 3896–3900 (1974).
36. von Heijne, G. Principles of membrane protein assembly and structure. *Prog. Biophys. Mol. Biol.* **66**, 113–139 (1996).
37. Papaloukas, C., Granseth, E., Viklund, H. & Elofsson, A. Estimating the length of transmembrane helices using Z-coordinate predictions. *Protein Sci.* **17**, 271–278 (2008).
38. Wimley, W. C. The versatile β-barrel membrane protein. *Curr. Opin. Struct. Biol.* **13**, 404–411 (2003).
39. Krogh, A., Larsson, B., von Heijne, G. & Sonnhammer, E. L. L. Predicting transmembrane protein topology with a hidden markov model: application to complete genomes1. *J. Mol. Biol.* **305**, 567–580 (2001).
40. Schibich, D. *et al.* Global profiling of SRP interaction with nascent polypeptides. *Nature* **536**, 219–223 (2016).
41. Luirink, J. *et al.* An alternative protein targeting pathway in Escherichia coli: studies on the role of FtsY. *EMBO J.* **13**, 2289–2296 (1994).
42. Hegde, R. S. & Keenan, R. J. The mechanisms of integral membrane protein biogenesis. *Nat. Rev. Mol. Cell Biol.* **23**, 107–124 (2022).
43. Berg, B. van den *et al.* X-ray structure of a protein-conducting channel. *Nature* **427**, 36–44 (2004).

44. Brundage, L., Hendrick, J. P., Schiebel, E., Driessen, A. J. M. & Wickner, W. The purified E. coli integral membrane protein SecY E is sufficient for reconstitution of SecA-dependent precursor protein translocation. *Cell* **62**, 649–657 (1990).
45. Akimaru, J., Matsuyama, S., Tokuda, H. & Mizushima, S. Reconstitution of a protein translocation system containing purified SecY, SecE, and SecA from Escherichia coli. *Proc. Natl. Acad. Sci.* **88**, 6545–6549 (1991).
46. Nishiyama, K., Hanada, M. & Tokuda, H. Disruption of the gene encoding p12 (SecG) reveals the direct involvement and important function of SecG in the protein translocation of Escherichia coli at low temperature. *EMBO J.* **13**, 3272–3277 (1994).
47. Rapoport, T. A., Li, L. & Park, E. Structural and Mechanistic Insights into Protein Translocation. *Annu. Rev. Cell Dev. Biol.* **33**, 369–390 (2017).
48. Hennon, S. W., Soman, R., Zhu, L. & Dalbey, R. E. YidC/Alb3/Oxa1 Family of Insertases *. *J. Biol. Chem.* **290**, 14866–14874 (2015).
49. Samuelson, J. C. *et al.* YidC mediates membrane protein insertion in bacteria. *Nature* **406**, 637–641 (2000).
50. Nagamori, S., Smirnova, I. N. & Kaback, H. R. Role of YidC in folding of polytopic membrane proteins. *J. Cell Biol.* **165**, 53–62 (2004).
51. Zhu, L., Kaback, H. R. & Dalbey, R. E. YidC Protein, a Molecular Chaperone for LacY Protein Folding via the SecYEG Protein Machinery *. *J. Biol. Chem.* **288**, 28180–28194 (2013).
52. Aschtgen, M.-S., Zoued, A., Lloubès, R., Journet, L. & Cascales, E. The C-tail anchored TssL subunit, an essential protein of the enteroaggregative Escherichia coli Sci-1 Type VI secretion system, is inserted by YidC. *MicrobiologyOpen* **1**, 71–82 (2012).
53. Peschke, M. *et al.* SRP, FtsY, DnaK and YidC Are Required for the Biogenesis of the *E. coli* Tail-Anchored Membrane Proteins DjlC and Flk. *J. Mol. Biol.* **430**, 389–403 (2018).
54. Lins, L. & Brasseur, R. The hydrophobic effect in protein folding. *FASEB J.* **9**, 535–540 (1995).
55. Wagner, S., Bader, M. L., Drew, D. & Gier, J.-W. de. Rationalizing membrane protein overexpression. *Trends Biotechnol.* **24**, 364–371 (2006).
56. Schlegel, S., Hjelm, A., Baumgarten, T., Vikström, D. & de Gier, J.-W. Bacterial-based membrane protein production. *Biochim. Biophys. Acta BBA - Mol. Cell Res.* **1843**, 1739–1749 (2014).
57. Joubert, O., Nehmé, R., Bidet, M. & Mus-Veteau, I. Heterologous Expression of Human Membrane Receptors in the Yeast Saccharomyces cerevisiae. in *Heterologous Expression of Membrane Proteins: Methods and Protocols* (ed. Mus-Veteau, I.) 87–103 (Humana Press, Totowa, NJ, 2010). doi:10.1007/978-1-60761-344-2_6.
58. Hitchman, R. B., Possee, R. D. & King, L. A. Baculovirus Expression Systems for Recombinant Protein Production in Insect Cells. *Recent Pat. Biotechnol.* **3**, 46–54 (2009).
59. Schwarz, D., Dötsch, V. & Bernhard, F. Production of membrane proteins using cell-free expression systems. *PROTEOMICS* **8**, 3933–3946 (2008).
60. Sezonov, G., Joseleau-Petit, D. & D'Ari, R. *Escherichia coli* Physiology in Luria-Bertani Broth. *J. Bacteriol.* **189**, 8746–8749 (2007).
61. Shiloach, J. & Fass, R. Growing *E. coli* to high cell density—A historical perspective on method development. *Biotechnol. Adv.* **23**, 345–357 (2005).
62. Sørensen, H. P. & Mortensen, K. K. Advanced genetic strategies for recombinant protein expression in *Escherichia coli*. *J. Biotechnol.* **115**, 113–128 (2005).
63. Pandey, A., Shin, K., Patterson, R. E., Liu, X.-Q. & Rainey, J. K. Current strategies for protein production and purification enabling membrane protein structural biology. *Biochem. Cell Biol.* **94**, 507–527 (2016).
64. Studier, F. W. & Moffatt, B. A. Use of bacteriophage T7 RNA polymerase to direct selective high-level expression of cloned genes. *J. Mol. Biol.* **189**, 113–130 (1986).
65. Snoeck, S., Guidi, C. & De Mey, M. "Metabolic burden" explained: stress symptoms and its related responses induced by (over)expression of (heterologous) proteins in Escherichia coli. *Microb. Cell Factories* **23**, 96 (2024).
66. Bonomo, J. & Gill, R. T. Amino acid content of recombinant proteins influences the metabolic burden response. *Biotechnol. Bioeng.* **90**, 116–126 (2005).
67. Haseltine, W. A. & Block, R. Synthesis of Guanosine Tetra- and Pentaphosphate Requires the Presence of a Codon-Specific, Uncharged Transfer Ribonucleic Acid in the Acceptor Site of Ribosomes. *Proc. Natl. Acad. Sci.* **70**, 1564–1568 (1973).
68. Hoffmann, F. & Rinas, U. Stress Induced by Recombinant Protein Production in Escherichia coli. in *Physiological Stress Responses in Bioprocesses: -/-* 73–92 (Springer, Berlin, Heidelberg, 2004). doi:10.1007/b93994.
69. Parsell, D. A. & Sauer, R. T. Induction of a heat shock-like response by unfolded protein in Escherichia coli: dependence on protein level not protein degradation. *Genes Dev.* **3**, 1226–1232 (1989).
70. Wagner, S. *et al.* Consequences of membrane protein overexpression in Escherichia coli. *Mol. Cell. Proteomics MCP* **6**, 1527–1550 (2007).
71. Zorman, S., Botte, M., Jiang, Q., Collinson, I. & Schaffitzel, C. Advances and challenges of membrane–protein complex production. *Curr. Opin. Struct. Biol.* **32**, 123–130 (2015).
72. Wagner, S. *et al.* Tuning *Escherichia coli* for membrane protein overexpression. *Proc. Natl. Acad. Sci.* **105**, 14371–14376 (2008).
73. Miroux, B. & Walker, J. E. Over-production of Proteins inEscherichia coli: Mutant Hosts that Allow Synthesis of some Membrane Proteins and Globular Proteins at High Levels. *J. Mol. Biol.* **260**, 289–298 (1996).
74. Baumgarten, T. *et al.* Isolation and characterization of the E. coli membrane protein production strain Mutant56(DE3). *Sci. Rep.* **7**, 45089 (2017).
75. Kotov, V. *et al.* High-throughput stability screening for detergent-solubilized membrane proteins. *Sci. Rep.* **9**, 10379 (2019).
76. Knowles, T. J. *et al.* Membrane Proteins Solubilized Intact in Lipid Containing Nanoparticles Bounded by Styrene Maleic Acid Copolymer. *J. Am. Chem. Soc.* **131**, 7484–7485 (2009).
77. Higgins, C. F. ABC Transporters: From Microorganisms to Man. *Annu. Rev. Cell Biol.* **8**, 67–113 (1992).
78. Rees, D. C., Johnson, E. & Lewinson, O. ABC transporters: The power to change. *Nat. Rev. Mol. Cell Biol.* **10**, 218–227 (2009).
79. Locher, K. P. Mechanistic diversity in ATP-binding cassette (ABC) transporters. *Nat. Struct. Mol. Biol.* **23**, 487–493 (2016).
80. Thomas, C. & Tampé, R. Structural and Mechanistic Principles of ABC Transporters. *Annu. Rev. Biochem.* **89**, 605–636 (2020).
81. Riordan, J. R. *et al.* Identification of the cystic fibrosis gene: cloning and characterization of complementary DNA. *Science* **245**, 1066–1073 (1989).
82. Allikmets, R. *et al.* A photoreceptor cell-specific ATP-binding transporter gene (ABCR) is mutated in recessive Starqardt macular dystrophy. *Nat. Genet.* **15**, 236–246 (1997).
83. Dawson, R. J. P. & Locher, K. P. Structure of a bacterial multidrug ABC transporter. *Nature* **443**, 180–185 (2006).
84. Orelle, C., Mathieu, K. & Jault, J.-M. Multidrug ABC transporters in bacteria. *Res. Microbiol.* **170**, 381–391 (2019).
85. Goldstein, L. J. *et al.* Expression of Multidrug Resistance Gene in Human Cancers. *JNCI J. Natl. Cancer Inst.* **81**, 116–124 (1989).

86. Gottesman, M. M., Fojo, T. & Bates, S. E. Multidrug resistance in cancer: role of ATP–dependent transporters. *Nat. Rev. Cancer* **2**, 48–58 (2002).
87. Robey, R. W. *et al.* Revisiting the role of ABC transporters in multidrug-resistant cancer. *Nat. Rev. Cancer* **18**, 452–464 (2018).
88. Walker, J. E., Saraste, M., Runswick, M. J. & Gay, N. J. Distantly related sequences in the alpha- and beta-subunits of ATP synthase, myosin, kinases and other ATP-requiring enzymes and a common nucleotide binding fold. *EMBO J.* **1**, 945–951 (1982).
89. Hung, L.-W. *et al.* Crystal structure of the ATP-binding subunit of an ABC transporter. *Nature* **396**, 703–707 (1998).
90. Locher, K. P. Structure and mechanism of ATP-binding cassette transporters. *Philos. Trans. R. Soc. B Biol. Sci.* **364**, 239–245 (2009).
91. Thomas, C. *et al.* Structural and functional diversity calls for a new classification of ABC transporters. *FEBS Lett.* **594**, 3767–3775 (2020).
92. Oancea, G. *et al.* Structural arrangement of the transmission interface in the antigen ABC transport complex TAP. *Proc. Natl. Acad. Sci. U. S. A.* **106**, 5551–5556 (2009).
93. Korkhov, V. M., Mireku, S. A. & Locher, K. P. Structure of AMP-PNP-bound vitamin B12 transporter BtuCD–F. *Nature* **490**, 367–372 (2012).
94. Koch, J., Guntrum, R., Heintke, S., Kyritsis, C. & Tampé, R. Functional Dissection of the Transmembrane Domains of the Transporter Associated with Antigen Processing (TAP) *. *J. Biol. Chem.* **279**, 10142–10147 (2004).
95. Demirel, Ö. *et al.* The lysosomal polypeptide transporter TAPL is stabilized by interaction with LAMP-1 and LAMP-2. *J. Cell Sci.* **125**, 4230–4240 (2012).
96. Aguilar-Bryan, L. *et al.* Cloning of the β Cell High-Affinity Sulfonylurea Receptor: a Regulator of Insulin Secretion. *Science* **268**, 423–426 (1995).
97. Gericke, N. *et al.* Unveiling the substrate specificity of the ABC transporter Tba and its role in glycopeptide biosynthesis. *iScience* 112135 (2025) doi:10.1016/j.isci.2025.112135.
98. Kim, I.-W. *et al.* The conserved tyrosine residues 401 and 1044 in ATP sites of human P-glycoprotein are critical for ATP binding and hydrolysis: evidence for a conserved subdomain, the A-loop in the ATP-binding cassette. *Biochemistry* **45**, 7605–7616 (2006).
99. Smith, P. C. *et al.* ATP Binding to the Motor Domain from an ABC Transporter Drives Formation of a Nucleotide Sandwich Dimer. *Mol. Cell* **10**, 139–149 (2002).
100. Moody, J. E., Millen, L., Binns, D., Hunt, J. F. & Thomas, P. J. Cooperative, ATP-dependent Association of the Nucleotide Binding Cassettes during the Catalytic Cycle of ATP-binding Cassette Transporters. *J. Biol. Chem.* **277**, 21111 (2002).
101. Zaitseva, J., Jenewein, S., Jumpertz, T., Holland, I. B. & Schmitt, L. H662 is the linchpin of ATP hydrolysis in the nucleotide-binding domain of the ABC transporter HlyB. *EMBO J.* **24**, 1901–1910 (2005).
102. Dalmas, O. *et al.* The Q-loop Disengages from the First Intracellular Loop during the Catalytic Cycle of the Multidrug ABC Transporter BmrA *. *J. Biol. Chem.* **280**, 36857–36864 (2005).
103. Procko, E., Ferrin-O'Connell, I., Ng, S.-L. & Gaudet, R. Distinct Structural and Functional Properties of the ATPase Sites in an Asymmetric ABC Transporter. *Mol. Cell* **24**, 51–62 (2006).
104. Grossmann, N. *et al.* Mechanistic determinants of the directionality and energetics of active export by a heterodimeric ABC transporter. *Nat. Commun.* **5**, 5419 (2014).
105. Stefan, E., Hofmann, S. & Tampé, R. A single power stroke by ATP binding drives substrate translocation in a heterodimeric ABC transporter. *eLife* **9**, e55943 (2020).
106. Jardetzky, O. Simple Allosteric Model for Membrane Pumps. *Nature* **211**, 969–970 (1966).
107. Ward, A., Reyes, C. L., Yu, J., Roth, C. B. & Chang, G. Flexibility in the ABC transporter MsbA: Alternating access with a twist. *Proc. Natl. Acad. Sci.* **104**, 19005–19010 (2007).
108. Hofmann, S. *et al.* Conformation space of a heterodimeric ABC exporter under turnover conditions. *Nature* **571**, 580–583 (2019).
109. Perez, C. *et al.* Structure and mechanism of an active lipid-linked oligosaccharide flippase. *Nature* **524**, 433–438 (2015).
110. Yu, J., Ge, J., Heuveling, J., Schneider, E. & Yang, M. Structural basis for substrate specificity of an amino acid ABC transporter. *Proc. Natl. Acad. Sci.* **112**, 5243–5248 (2015).
111. Romano, M. *et al.* Structural Basis for Natural Product Selection and Export by Bacterial ABC Transporters. *ACS Chem. Biol.* **13**, 1598–1609 (2018).
112. Aller, S. G. *et al.* Structure of P-glycoprotein reveals a molecular basis for poly-specific drug binding. *Science* **323**, 1718–1722 (2009).
113. Gatlik-Landwojtowicz, E., Aänismaa, P. & Seelig, A. Quantification and characterization of P-glycoprotein-substrate interactions. *Biochemistry* **45**, 3020–3032 (2006).
114. Shapiro, A. B. & Ling, V. Positively Cooperative Sites for Drug Transport by P-Glycoprotein with Distinct Drug Specificities. *Eur. J. Biochem.* **250**, 130–137 (1997).
115. Goodfellow, M. Phylum XXVI. Actinobacteria phyl. nov. in *Bergey's Manual® of Systematic Bacteriology* (eds. Goodfellow, M. et al.) 33–2028 (Springer New York, New York, NY, 2012). doi:10.1007/978-0-387-68233-4_3.
116. Lewin, G. R. *et al.* Evolution and Ecology of Actinobacteria and Their Bioenergy Applications. *Annu. Rev. Microbiol.* **70**, 235 (2016).
117. Goodfellow, M. & Williams, S. T. Ecology of actinomycetes. *Annu. Rev. Microbiol.* **37**, 189–216 (1983).
118. Gagneux, S. Ecology and evolution of Mycobacterium tuberculosis. *Nat. Rev. Microbiol.* **16**, 202–213 (2018).
119. Sangal, V. & Hoskisson, P. A. Evolution, epidemiology and diversity of *Corynebacterium diphtheriae*: New perspectives on an old foe. *Infect. Genet. Evol.* **43**, 364–370 (2016).
120. Lerat, S., Simao-Beaunoir, A.-M. & Beaulieu, C. Genetic and physiological determinants of Streptomyces scabies pathogenicity. *Mol. Plant Pathol.* **10**, 579–585 (2009).
121. Barka, E. A. *et al.* Taxonomy, Physiology, and Natural Products of Actinobacteria. *Microbiol. Mol. Biol. Rev. MMBR* **80**, 1 (2015).
122. Demain, A. L. & Fang, A. The natural functions of secondary metabolites. *Adv. Biochem. Eng. Biotechnol.* **69**, 1–39 (2000).
123. Doroghazi, J. R. & Metcalf, W. W. Comparative genomics of actinomycetes with a focus on natural product biosynthetic genes. *BMC Genomics* **14**, 611 (2013).
124. Adamek, M. *et al.* Comparative genomics reveals phylogenetic distribution patterns of secondary metabolites in Amycolatopsis species. *BMC Genomics* **19**, 426 (2018).
125. Albarano, L., Esposito, R., Ruocco, N. & Costantini, M. Genome Mining as New Challenge in Natural Products Discovery. *Mar. Drugs* **18**, 199 (2020).
126. Lechevalier, M. P., Prauser, H., Labeda, D. P. & Ruan, J.-S. Two New Genera of Nocardioform Actinomycetes: Amycolata gen. nov. and Amycolatopsis gen. nov. *Int. J. Syst. Evol. Microbiol.* **36**, 29–37 (1986).

127. Kisil, O. V., Efimenko, T. A. & Efremenkova, O. V. Looking Back to Amycolatopsis: History of the Antibiotic Discovery and Future Prospects. *Antibiotics* **10**, 1254 (2021).
128. Nishikiori, T. *et al.* Production by actinomycetes of (S,S)-N,N'-ethylenediamine-disuccinic acid, an inhibitor of phospholipase C. *J. Antibiot. (Tokyo)* **37**, 426–427 (1984).
129. Zwicker, N., Theobald, U., Zähner, H. & Fiedler, H.-P. Optimization of fermentation conditions for the production of ethylene-diamine-disuccinic acid by Amycolatopsis orientalis. *J. Ind. Microbiol. Biotechnol.* **19**, 280–285 (1997).
130. Edenhart, S. *et al.* Metabolic engineering of *Amycolatopsis japonicum* for optimized production of [*S,S*]-EDDS, a biodegradable chelator. *Metab. Eng.* **60**, 148–156 (2020).
131. Kshirsagar, S. D., Saratale, G. D., Saratale, R. G., Govindwar, S. P. & Oh, M. K. An isolated Amycolatopsis sp. GDS for cellulase and xylanase production using agricultural waste biomass. *J. Appl. Microbiol.* **120**, 112–125 (2016).
132. Maggi, N., Pasqualucci, C. R., Ballotta, R. & Sensi, P. Rifampicin: A New Orally Active Rifamycin. *Chemotherapia* **11**, 285–292 (1966).
133. Brigham, R. B. & Pittenger, R. C. Streptomyces orientalis, n. sp., the source of vancomycin. *Antibiot. Chemother. Northfield Ill* **6**, 642–647 (1956).
134. Zeng, D. *et al.* Approved Glycopeptide Antibacterial Drugs: Mechanism of Action and Resistance. *Cold Spring Harb. Perspect. Med.* **6**, a026989 (2016).
135. Mccormick, M. H. & Mcguire, J. M. Vancomycin, a new antibiotic. I. Chemical and biologic properties. https://pubmed.ncbi.nlm.nih.gov/13355336/ (1955).
136. Nadkarni, S. R. *et al.* Balhimycin, anew glycopeptide antibiotic produced by Amycolatopsis sp. Y-86, 21022. *J. Antibiot. (Tokyo)* **47**, (1994).
137. Wink, J. M. *et al.* Three New Antibiotic Producing Species of the Genus Amycolatopsis, Amycolatopsis balhimycina sp. nov., A. tolypomycina sp. nov., A. vancoresmycina sp. nov., and Description of Amycolatopsis keratiniphila subsp. keratiniphila subsp. nov. and A. keratiniphila subsp. nogabecina subsp. nov. *Syst. Appl. Microbiol.* **26**, 38–46 (2003).
138. Vongsangnak, W. *et al.* Genome-scale metabolic representation of Amycolatopsis balhimycina. *Biotechnol. Bioeng.* **109**, 1798–1807 (2012).
139. Towhid, S. T. *et al.* Stimulation of platelet apoptosis by balhimycin. *Biochem. Biophys. Res. Commun.* **435**, 323–326 (2013).
140. Yim, G., Thaker, M. N., Koteva, K. & Wright, G. Glycopeptide antibiotic biosynthesis. *J. Antibiot. (Tokyo)* **67**, 31–41 (2014).
141. Bischoff, D. *et al.* The Biosynthesis of Vancomycin-Type Glycopeptide Antibiotics—New Insights into the Cyclization Steps. *Angew. Chem. Int. Ed.* **40**, 1693–1696 (2001).
142. Stegmann, E. *et al.* Precursor-directed biosynthesis for the generation of novel glycopetides. *Ernst Scher. Res. Found. Workshop* 215–232 (2005) doi:10.1007/3-540-27055-8_10.
143. Nicolaou, K. C., Boddy, C. N., Bräse, S. & Winssinger, N. Chemistry, Biology, and Medicine of the Glycopeptide Antibiotics. *Angew. Chem. Int. Ed Engl.* **38**, 2096–2152 (1999).
144. Culp, E. J. *et al.* Evolution-guided discovery of antibiotics that inhibit peptidoglycan remodelling. *Nature* **578**, 582–587 (2020).
145. Gavriilidou, A. *et al.* Phylogenetic distance and structural diversity directing a reclassification of glycopeptide antibiotics. Preprint at https://doi.org/10.1101/2023.02.10.526856 (2023).
146. Stegmann, E., Frasch, H.-J. & Wohlleben, W. Glycopeptide biosynthesis in the context of basic cellular functions. *Curr. Opin. Microbiol.* **13**, 595–602 (2010).
147. Pelzer, S. *et al.* Identification and Analysis of the Balhimycin Biosynthetic Gene Cluster and Its Use for Manipulating Glycopeptide Biosynthesis in Amycolatopsis mediterranei DSM5908. *Antimicrob. Agents Chemother.* **43**, 1565–1573 (1999).
148. Donadio, S., Sosio, M., Stegmann, E., Weber, T. & Wohlleben, W. Comparative analysis and insights into the evolution of gene clusters for glycopeptide antibiotic biosynthesis. *Mol. Genet. Genomics* **274**, 40–50 (2005).
149. Thykaer, J. *et al.* Increased glycopeptide production after overexpression of shikimate pathway genes being part of the balhimycin biosynthetic gene cluster. *Metab. Eng.* **12**, 455–461 (2010).
150. Herrmann, K. M. & Weaver, L. M. The Shikimate Pathway. *Annu. Rev. Plant Physiol. Plant Mol. Biol.* **50**, 473–503 (1999).
151. Goldfinger, V. *et al.* Metabolic engineering of the shikimate pathway in Amycolatopsis strains for optimized glycopeptide antibiotic production. *Metab. Eng.* **78**, 84–92 (2023).
152. Puk, O. *et al.* Biosynthesis of chloro-beta-hydroxytyrosine, a nonproteinogenic amino acid of the peptidic backbone of glycopeptide antibiotics. *J. Bacteriol.* **186**, 6093–6100 (2004).
153. Cryle, M. J., Meinhart, A. & Schlichting, I. Structural Characterization of OxyD, a Cytochrome P450 Involved in β-Hydroxytyrosine Formation in Vancomycin Biosynthesis. *J. Biol. Chem.* **285**, 24562–24574 (2010).
154. Mulyani, S. *et al.* The Thioesterase Bhp is Involved in the Formation of β-Hydroxytyrosine during Balhimycin Biosynthesis in Amycolatopsis balhimycina. *ChemBioChem* **11**, 266–271 (2010).
155. Pfeifer, V. *et al.* A Polyketide Synthase in Glycopeptide Biosynthesis. *J. Biol. Chem.* **276**, 38370–38377 (2001).
156. Chen, H., Tseng, C. C., Hubbard, B. K. & Walsh, C. T. Glycopeptide antibiotic biosynthesis: Enzymatic assembly of the dedicated amino acid monomer (S)-3,5-dihydroxyphenylglycine. *Proc. Natl. Acad. Sci.* **98**, 14901–14906 (2001).
157. Recktenwald, J. *et al.* Nonribosomal biosynthesis of vancomycin-type antibiotics: a heptapeptide backbone and eight peptide synthetase modules. *Microbiol. Read. Engl.* **148**, 1105–1118 (2002).
158. Marahiel, M. A. & Essen, L. -O. Chapter 13 Nonribosomal Peptide Synthetases: Mechanistic and Structural Aspects of Essential Domains. in *Methods in Enzymology* vol. 458 337–351 (Elsevier, 2009).
159. Haslinger, K., Peschke, M., Brieke, C., Maximowitsch, E. & Cryle, M. J. X-domain of peptide synthetases recruits oxygenases crucial for glycopeptide biosynthesis. *Nature* **521**, 105–109 (2015).
160. Bischoff, D. *et al.* The Biosynthesis of Vancomycin-Type Glycopeptide Antibiotics—The Order of the Cyclization Steps. *Angew. Chem. Int. Ed.* **40**, 4688–4691 (2001).
161. Stegmann, E. *et al.* Genetic analysis of the balhimycin (vancomycin-type) oxygenase genes. *J. Biotechnol.* **124**, 640–653 (2006).
162. Gerhard, U., Mackay, J. P., Maplestone, R. A. & Williams, D. H. The role of the sugar and chlorine substituents in the dimerization of vancomycin antibiotics. *J. Am. Chem. Soc.* **115**, 232–237 (1993).
163. Schäfer, M., Sheldrick, G. M., Schneider, T. R. & Vértesy, L. Structure of Balhimycin and its Complex with Solvent Molecules. *Acta Crystallogr. D Biol. Crystallogr.* **54**, 175–183 (1998).
164. Chen, H. *et al.* Deoxysugars in glycopeptide antibiotics: Enzymatic synthesis of TDP-l-epivancosamine in chloroeremomycin biosynthesis. *Proc. Natl. Acad. Sci.* **97**, 11942–11947 (2000).
165. Puk, O. *et al.* Glycopeptide Biosynthesis in Amycolatopsis mediterranei DSM5908: Function of a Halogenase and a Haloperoxidase/Perhydrolase. *Chem. Biol.* **9**, 225–235 (2002).

166. O'Brien, D. P. *et al.* Expression and assay of an N-methyltransferase involved in the biosynthesis of a vancomycin group antibiotic. *Chem. Commun.* 103–104 (2000) doi:10.1039/A907953J.
167. Severi, E. & Thomas, G. H. Antibiotic export: transporters involved in the final step of natural product production. *Microbiol. Read. Engl.* **165**, 805–818 (2019).
168. Menges, R., Muth, G., Wohlleben, W. & Stegmann, E. The ABC transporter Tba of Amycolatopsis balhimycina is required for efficient export of the glycopeptide antibiotic balhimycin. *Appl. Microbiol. Biotechnol.* **77**, 125–134 (2007).
169. Cundliffe, E. & Demain, A. L. Avoidance of suicide in antibiotic-producing microbes. *J. Ind. Microbiol. Biotechnol.* **37**, 643–672 (2010).
170. Shawky, R. M. *et al.* The Border Sequence of the Balhimycin Biosynthesis Gene Cluster from *Amycolatopsis balhimycina* Contains *bbr*, Encoding a StrR-Like Pathway-Specific Regulator. *Microb. Physiol.* **13**, 76–88 (2007).
171. Frasch, H.-J. *et al.* Alternative Pathway to a Glycopeptide-Resistant Cell Wall in the Balhimycin Producer *Amycolatopsis balhimycina*. *ACS Infect. Dis.* **1**, 243–252 (2015).
172. Sosio, M., Stinchi, S., Beltrametti, F., Lazzarini, A. & Donadio, S. The Gene Cluster for the Biosynthesis of the Glycopeptide Antibiotic A40926 by Nonomuraea Species. *Chem. Biol.* **10**, 541–549 (2003).
173. Sosio, M. *et al.* Organization of the teicoplanin gene cluster in Actinoplanes teichomyceticus. *Microbiology* **150**, 95–102 (2004).
174. van der Heul, H. U., Bilyk, B. L., McDowall, K. J., Seipke, R. F. & van Wezel, G. P. Regulation of antibiotic production in Actinobacteria: new perspectives from the post-genomic era. *Nat. Prod. Rep.* **35**, 575–604 (2018).
175. Horbal, L., Zaburannyy, N., Ostash, B., Shulga, S. & Fedorenko, V. Manipulating the regulatory genes for teicoplanin production in Actinoplanes teichomyceticus. *World J. Microbiol. Biotechnol.* **28**, 2095–2100 (2012).
176. Grasso, L. L. *et al.* Two Master Switch Regulators Trigger A40926 Biosynthesis in Nonomuraea sp. Strain ATCC 39727. *J. Bacteriol.* (2015) doi:10.1128/jb.00262-15.
177. Horbal, L. *et al.* The pathway-specific regulatory genes, tei15* and tei16*, are the master switches of teicoplanin production in Actinoplanes teichomyceticus. *Appl. Microbiol. Biotechnol.* **98**, 9295–9309 (2014).
178. Alduina, R. *et al.* Phosphate-Controlled Regulator for the Biosynthesis of the Dalbavancin Precursor A40926. *J. Bacteriol.* **189**, 8120–8129 (2007).
179. Takano, E. *et al.* A bacterial hormone (the SCB1) directly controls the expression of a pathway-specific regulatory gene in the cryptic type I polyketide biosynthetic gene cluster of Streptomyces coelicolor. *Mol. Microbiol.* **56**, 465–479 (2005).
180. Allenby, N. E. E., Laing, E., Bucca, G., Kierzek, A. M. & Smith, C. P. Diverse control of metabolism and other cellular processes in Streptomyces coelicolor by the PhoP transcription factor: genome-wide identification of in vivo targets. *Nucleic Acids Res.* **40**, 9543–9556 (2012).
181. Santos-Beneit, F., Rodríguez-García, A., Sola-Landa, A. & Martín, J. F. Cross-talk between two global regulators in Streptomyces: PhoP and AfsR interact in the control of afsS, pstS and phoRP transcription. *Mol. Microbiol.* **72**, 53–68 (2009).
182. Tiffert, Y. *et al.* Proteomic analysis of the GlnR-mediated response to nitrogen limitation in Streptomyces coelicolor M145. *Appl. Microbiol. Biotechnol.* **89**, 1149–1159 (2011).
183. He, J.-M. *et al.* Direct Involvement of the Master Nitrogen Metabolism Regulator GlnR in Antibiotic Biosynthesis in Streptomyces*. *J. Biol. Chem.* **291**, 26443–26454 (2016).
184. Tahlan, K. *et al.* Initiation of actinorhodin export in Streptomyces coelicolor. *Mol. Microbiol.* **63**, 951–961 (2007).
185. Kim, E.-S., Hong, H.-J., Choi, C.-Y. & Cohen, S. N. Modulation of Actinorhodin Biosynthesis in Streptomyces lividans by Glucose Repression of afsR2 Gene Transcription. *J. Bacteriol.* **183**, 2198–2203 (2001).
186. Bhatnagar, R. K., Doull, J. L. & Vining, L. C. Role of the carbon source in regulating chloramphenicol production by Streptomyces venezuelae: studies in batch and continuous cultures. *Can. J. Microbiol.* **34**, 1217–1223 (1988).
187. Escalante, L., Lopez, H., Del Carmen Mateo, R., Larac, F. & Sanchez, S. Transient Repression of Erythromycin Formation in Streptomyces erythraeus. *Microbiology* **128**, 2011–2015 (1982).
188. Schäberle, T. F. *et al.* Self-Resistance and Cell Wall Composition in the Glycopeptide Producer Amycolatopsis balhimycina. *Antimicrob. Agents Chemother.* **55**, 4283–4289 (2011).
189. Bugg, T. D. H. *et al.* Molecular basis for vancomycin resistance in Enterococcus faecium BM4147: biosynthesis of a depsipeptide peptidoglycan precursor by vancomycin resistance proteins VanH and VanA. *Biochemistry* **30**, 10408–10415 (1991).
190. Drew, D. E., Heijne, G. von, Nordlund, P. & Gier, J.-W. L. de. Green fluorescent protein as an indicator to monitor membrane protein overexpression in Escherichia coli. *FEBS Lett.* **507**, 220–224 (2001).
191. Drew, D. *et al.* A scalable, GFP-based pipeline for membrane protein overexpression screening and purification. *Protein Sci.* **14**, 2011–2017 (2005).
192. Tartof, K. & Hobbs, C. Improved media for growing plasmid and cosmid clones. *Bethesda Res Lab Focus* **9**, 12 (1987).
193. Rath, A., Glibowicka, M., Nadeau, V. G., Chen, G. & Deber, C. M. Detergent binding explains anomalous SDS-PAGE migration of membrane proteins. *Proc. Natl. Acad. Sci.* **106**, 1760–1765 (2009).
194. Cytiva. Superose 6 Increase 3.2/300 Instructions for Use.
195. Houben, E. N. G. *et al.* Nascent Lep inserts into the Escherichia coli inner membrane in the vicinity of YidC, SecY and SecA. *FEBS Lett.* **476**, 229–233 (2000).
196. Laskowska, E. *et al.* Aggregation of heat-shock-denatured, endogenous proteins and distribution of the IbpA/B and Fda marker-proteins in Escherichia coli WT and grpE280 cells. *Microbiol. Read. Engl.* **150**, 247–259 (2004).
197. Chae, P. S. *et al.* Maltose–neopentyl glycol (MNG) amphiphiles for solubilization, stabilization and crystallization of membrane proteins. *Nat. Methods* **7**, 1003–1008 (2010).
198. Cytiva. Superdex 200 Increase 5/150 GLSuperdex 200 Increase 10/300 GL.
199. Malakhov, M. P. *et al.* SUMO fusions and SUMO-specific protease for efficient expression and purification of proteins. *J. Struct. Funct. Genomics* **5**, 75–86 (2004).
200. Zuo, X. *et al.* Enhanced Expression and Purification of Membrane Proteins by SUMO Fusion in Escherichia coli. *J. Struct. Funct. Genomics* **6**, 103–111 (2005).
201. Oxenoid, K. & Chou, J. J. The structure of phospholamban pentamer reveals a channel-like architecture in membranes. *Proc. Natl. Acad. Sci.* **102**, 10870–10875 (2005).
202. Löw, C. *et al.* High-throughput analytical gel filtration screening of integral membrane proteins for structural studies. *Biochim. Biophys. Acta BBA - Gen. Subj.* **1830**, 3497–3508 (2013).
203. Lussier, F.-X., Denis, F. & Shareck, F. Adaptation of the Highly Productive T7 Expression System to *Streptomyces lividans*. *Appl. Environ. Microbiol.* **76**, 967–970 (2010).
204. Gavriilidou, A. *et al.* Animating insights into the biosynthesis of glycopeptide antibiotics. *Curr. Opin. Microbiol.* **82**, 102561 (2024).
205. Li, J., Jaimes, K. F. & Aller, S. G. Refined structures of mouse P-glycoprotein. *Protein Sci.* **23**, 34–46 (2014).

206. Hessa, T. *et al.* Molecular code for transmembrane-helix recognition by the Sec61 translocon. *Nature* **450**, 1026–1030 (2007).
207. Jumper, J. *et al.* Highly accurate protein structure prediction with AlphaFold. *Nature* **596**, 583–589 (2021).
208. Waglechner, N., McArthur, A. G. & Wright, G. D. Phylogenetic reconciliation reveals the natural history of glycopeptide antibiotic biosynthesis and resistance. *Nat. Microbiol.* **4**, 1862–1871 (2019).
209. Hansen, M. H. *et al.* Resurrecting ancestral antibiotics: unveiling the origins of modern lipid II targeting glycopeptides. *Nat. Commun.* **14**, 7842 (2023).
210. Katsura, Y., Stanley, C. E., Kumar, S. & Nei, M. The Reliability and Stability of an Inferred Phylogenetic Tree from Empirical Data. *Mol. Biol. Evol.* **34**, 718–723 (2017).
211. Hellmich, U. A. *et al.* Probing the ATP Hydrolysis Cycle of the ABC Multidrug Transporter LmrA by Pulsed EPR Spectroscopy. *J. Am. Chem. Soc.* **134**, 5857–5862 (2012).
212. Kuipers, A. *et al.* NisT, the Transporter of the Lantibiotic Nisin, Can Transport Fully Modified, Dehydrated, and Unmodified Prenisin and Fusions of the Leader Peptide with Non-lantibiotic Peptides*. *J. Biol. Chem.* **279**, 22176–22182 (2004).
213. Butt, T. R., Edavettal, S. C., Hall, J. P. & Mattern, M. R. SUMO fusion technology for difficult-to-express proteins. *Protein Expr. Purif.* **43**, 1–9 (2005).
214. Wang, D.-N. *et al.* Practical aspects of overexpressing bacterial secondary membrane transporters for structural studies. *Biochim. Biophys. Acta BBA - Biomembr.* **1610**, 23–36 (2003).
215. Baneyx, F. & Mujacic, M. Recombinant protein folding and misfolding in Escherichia coli. *Nat. Biotechnol.* **22**, 1399–1408 (2004).
216. Vera, A., González-Montalbán, N., Arís, A. & Villaverde, A. The conformational quality of insoluble recombinant proteins is enhanced at low growth temperatures. *Biotechnol. Bioeng.* **96**, 1101–1106 (2007).
217. Roosild, T. P. *et al.* NMR Structure of Mistic, a Membrane-Integrating Protein for Membrane Protein Expression. *Science* **307**, 1317–1321 (2005).
218. Marino, J., Hohl, M., Seeger, M. A., Zerbe, O. & Geertsma, E. R. Bicistronic mRNAs to Enhance Membrane Protein Overexpression. *J. Mol. Biol.* **427**, 943–954 (2015).
219. Thomsen, M. Determination of the Molecular Mass of Membrane Proteins Using Size-Exclusion Chromatography with Multiangle Laser Light Scattering (SEC-MALLS). *Methods Mol. Biol. Clifton NJ* **2168**, 263–269 (2020).
220. Gulati, S. *et al.* Detergent-free purification of ABC (ATP-binding-cassette) transporters. *Biochem. J.* **461**, 269–278 (2014).
221. Hug, L. A. *et al.* A new view of the tree of life. *Nat. Microbiol.* **1**, 1–6 (2016).
222. Lichty, J. J., Malecki, J. L., Agnew, H. D., Michelson-Horowitz, D. J. & Tan, S. Comparison of affinity tags for protein purification. *Protein Expr. Purif.* **41**, 98–105 (2005).
223. Berini, F., Marinelli, F. & Binda, E. Streptomycetes: Attractive Hosts for Recombinant Protein Production. *Front. Microbiol.* **11**, 1958 (2020).
224. Álvarez-Mena, A. *et al.* Bacterial flotillins as destabilizers of phospholipid membranes. *Biochim. Biophys. Acta BBA - Biomembr.* **1867**, 184399 (2025).
225. Bach, J. N. & Bramkamp, M. Flotillins functionally organize the bacterial membrane. *Mol. Microbiol.* **88**, 1205–1217 (2013).
226. Pearson, L. A., Hisbergues, M., Börner, T., Dittmann, E. & Neilan, B. A. Inactivation of an ABC transporter gene, mcyH, results in loss of microcystin production in the cyanobacterium Microcystis aeruginosa PCC 7806. *Appl. Environ. Microbiol.* **70**, 6370–6378 (2004).
227. Srinivasan, P., Palani, S. N. & Prasad, R. Daunorubicin efflux in Streptomyces peucetius modulates biosynthesis by feedback regulation. *FEMS Microbiol. Lett.* **305**, 18–27 (2010).
228. Kilian, R., Frasch, H.-J., Kulik, A., Wohlleben, W. & Stegmann, E. The VanRS Homologous Two-Component System VnlRSAb of the Glycopeptide Producer Amycolatopsis balhimycina Activates Transcription of the vanHAXSc Genes in Streptomyces coelicolor, but not in A. balhimycina. *Microb. Drug Resist.* **22**, 499–509 (2016).
229. Yang, M. *et al.* Decoding the stoichiometric composition and organisation of bacterial metabolosomes. *Nat. Commun.* **11**, 1976 (2020).
230. Dou, Z. *et al.* CO2 Fixation Kinetics of Halothiobacillus neapolitanus Mutant Carboxysomes Lacking Carbonic Anhydrase Suggest the Shell Acts as a Diffusional Barrier for CO2*. *J. Biol. Chem.* **283**, 10377–10384 (2008).
231. Faulkner, M. *et al.* Direct characterization of the native structure and mechanics of cyanobacterial carboxysomes. *Nanoscale* **9**, 10662–10673 (2017).
232. Sun, Y. *et al.* Light Modulates the Biosynthesis and Organization of Cyanobacterial Carbon Fixation Machinery through Photosynthetic Electron Flow. *Plant Physiol.* **171**, 530–541 (2016).
233. Gacek-Matthews, A. *et al.* Beyond Toxin Transport: Novel Role of ABC Transporter for Enzymatic Machinery of Cereulide NRPS Assembly Line. *mBio* **11**, e01577-20 (2020).
234. Chen, J., van Heel, A. J. & Kuipers, O. P. Subcellular Localization and Assembly Process of the Nisin Biosynthesis Machinery in Lactococcus lactis. *mBio* **11**, e02825-20 (2020).
235. Chen, J., van Heel, A. J. & Kuipers, O. P. Visualization and Analysis of the Dynamic Assembly of a Heterologous Lantibiotic Biosynthesis Complex in Bacillus subtilis. *mBio* **12**, e0121921 (2021).
236. Husada, F. *et al.* Conformational dynamics of the ABC transporter McjD seen by single-molecule FRET. *EMBO J.* **37**, e100056 (2018).
237. Kopcho, N., Chang, G. & Komives, E. A. Dynamics of ABC Transporter P-glycoprotein in Three Conformational States. *Sci. Rep.* **9**, 15092 (2019).
238. Zielińska, A. *et al.* Flotillin-mediated membrane fluidity controls peptidoglycan synthesis and MreB movement. *eLife* **9**, e57179 (2020).
239. Gibson, D. G. *et al.* Enzymatic assembly of DNA molecules up to several hundred kilobases. *Nat. Methods* **6**, 343–345 (2009).
240. Green, M. R. & Sambrook, J. *Molecular Cloning: A Laboratory Manual*. (Cold Spring Harbor Laboratory Press, Cold Spring Harbor, N.Y, 2012).
241. Bierman, M. *et al.* Plasmid cloning vectors for the conjugal transfer of DNA from Escherichia coli to Streptomyces spp. *Gene* **116**, 43–49 (1992).
242. Madoń, J. & Hütter, R. Transformation system for Amycolatopsis (Nocardia) mediterranei: direct transformation of mycelium with plasmid DNA. *J. Bacteriol.* **173**, 6325–6331 (1991).
243. Pelzer, S., Reichert, W., Huppert, M., Heckmann, D. & Wohlleben, W. Cloning and analysis of a peptide synthetase gene of the balhimycin producer Amycolatopsis mediterranei DSM5908 and development of a gene disruption/replacement system. *J. Biotechnol.* **56**, 115–128 (1997).
244. Dyballa, N. & Metzger, S. Fast and Sensitive Colloidal Coomassie G-250 Staining for Proteins in Polyacrylamide Gels. *J. Vis. Exp.* (30) e1431 (2009) doi:doi:10.3791/1431.

245. Dietsche, T. *et al.* Structural and Functional Characterization of the Bacterial Type III Secretion Export Apparatus. *PLOS Pathog.* **12**, e1006071 (2016).
246. Bertani, G. Studies on lysogenesis. *J. Bacteriol.* **62**, 293–300 (1951).
247. Hanahan, D. Studies on transformation of *Escherichia coli* with plasmids. *J. Mol. Biol.* **166**, 557–580 (1983).
248. Kieser, T., Bibb, M. J., Buttner, M. J., Chater, K. F. & Hopwood, D. A. *Practical Streptomyces Genetics*. (John Innes Foundation, Norwich Research Park, Colney, Norwich NR4 7UH, UK, 2000).
249. Schupp, T. & Divers, M. Protoplast preparation and regeneration in Nocardia mediterranei. *FEMS Microbiol. Lett.* **36**, 159–162 (1986).
250. Hobbs, G., Frazer, C. M., Gardner, D. C. J., Cullum, J. A. & Oliver, S. G. Dispersed growth of Streptomyces in liquid culture. *Appl. Microbiol. Biotechnol.* **31**, 272–277 (1989).
251. Davis, B. D. & Mingioli, E. S. Mutants of Escherichia coli requiring Methionine or Vitamin B12. *J. Bacteriol.* **60**, 17–28 (1950).
252. Laemmli, U. K. Cleavage of Structural Proteins during the Assembly of the Head of Bacteriophage T4. *Nature* **227**, 680–685 (1970).
253. Zilkenat, S. *et al.* Blue Native PAGE Analysis of Bacterial Secretion Complexes. in *Bacterial Secretion Systems : Methods and Protocols* (eds. Journet, L. & Cascales, E.) 331–362 (Springer US, New York, NY, 2024). doi:10.1007/978-1-0716-3445-5_22.
254. Yanisch-Perron, C., Vieira, J. & Messing, J. Improved M13 phage cloning vectors and host strains: nucleotide sequences of the M13mpl8 and pUC19 vectors. *Gene* **33**, 103–119 (1985).
255. MacNeil, D. J. *et al.* Analysis of Streptomyces avermitilis genes required for avermectin biosynthesis utilizing a novel integration vector. *Gene* **111**, 61–68 (1992).
256. Simon, R., Priefer, U. & Pühler, A. A Broad Host Range Mobilization System for In Vivo Genetic Engineering: Transposon Mutagenesis in Gram Negative Bacteria. *Bio/Technology* **1**, 784–791 (1983).
257. Ansorg, R., H, Z. & R, T. Bedeutung des Nachweises antibakterieller Stoffe im Urin für die bakteriologische Diagnostik und die Kontrolle der Chemotherapie von Harnwegsinfektionen. *Bedeut. Nachweises Antibakterieller Stoffe Im Urin Für Bakteriol. Diagn. Kontrolle Chemother. Von Harnwegsinfekt.* (1975).
258. Muth, G. The pSG5-based thermosensitive vector family for genome editing and gene expression in actinomycetes. *Appl. Microbiol. Biotechnol.* **102**, 9067–9080 (2018).
259. Branon, T. C. *et al.* Efficient proximity labeling in living cells and organisms with TurboID. *Nat. Biotechnol.* **36**, 880–887 (2018).

Spelling and grammar correction

Ich habe KI für Korrekturen der Rechtschreibung und Grammatik genutzt, ohne dass es dabei zu inhaltlich relevanter Textgeneration oder Übersetzungen kam. Das heißt, ich habe von mir verfasste Texte in derselben Sprache korrigieren lassen. Es handelt sich um rein sprachliche Korrekturen, sodass die von mir ursprünglich intendierte Bedeutung nicht wesentlich verändert oder erweitert wurde. Im Zweifelsfall habe ich mich mit meinen Betreuern besprochen. Im Anhang sind alle genutzten Programme mit Versionsnummer in einer Tabelle aufgelistet.

Programme	Version	Application
DeepL Write	Free online version (10/2024-03/2025)	Spelling and grammar
Chat GPT	GPT-4-turbo/GPT-4 (10/2024-03/2025)	Spelling and grammar
Scribbr Free AI Grammar Checker	Free online version (10/2024-03/2025)	Spelling and grammar